Shiny Perspectives of the Pollutant Black Carbon Soot

Submitted in
fulfillment of the requirements for the degree of
Doctor of Philosophy

By
ANUPRIYA SINGH
ID. No. 2013RCY9571

Under the Supervision of
Dr. Sumit Kumar Sonkar

DEPARTMENT OF CHEMISTRY
MALAVIYA NATIONAL INSTITUTE OF TECHNOLOGY JAIPUR

February, 2019

MALAVIYA NATIONAL INSTITUTE OF TECHNOLOGY JAIPUR
(Institute of National Importance under NITs Act, Established by Govt. of India)

DECLARATION

I **Anupriya Singh**, declare that this thesis titled, "**Shiny Perspectives of the Pollutant Black Carbon Soot**" and the work presented in it, are my own. I confirm that:

- This work was done wholly or mainly while in candidature for a research degree at this university.
- Where any part of this thesis has previously been submitted for a degree or any other qualification at this university or any other institution, this has been clearly stated.
- Where I have consulted the published work of others, this is always clearly attributed.
- Where I have quoted from the work of others, the source is always given. With the exception of such quotations, this thesis is entirely my own work.
- I have acknowledged all main sources of help.
- Where the thesis is based on work done by myself, jointly with others, I have made clear exactly what was done by others and what I have contributed myself.

Date: **Anupriya Singh**
                                                                                 ID No. 2013RCY9571

**MALAVIYA NATIONAL INSTITUTE OF TECHNOLOGY
JAIPUR
(Institute of National Importance under NITs Act, Established
by Govt. of India)**

CERTIFICATE

This is to certify that the thesis entitled "**Shiny Perspectives of the Pollutant Black Carbon Soot**" being submitted by **Ms. Anupriya Singh (2013RCY9571)** is a bonafide research work carried out under my supervision and guidance in fulfillment of the requirement for the award of the degree of **Doctor of Philosophy** in the department of Chemistry, Malaviya National Institute of Technology Jaipur, India. The matter embodied in this thesis is original and has not been submitted to any other University or Institute for the award of any other degree.

Place: Jaipur   **Dr. Sumit Kumar Sonkar**
Date: **Assistant Professor**
                                                               Department of Chemistry
                                                                    MNIT Jaipur

ACKNOWLEDGEMENT

research work which always kept me going ahead. I thank him for all the love he has showered upon me and being with me in thicks and thins of life.

*I would like to extend my appreciation to my siblings **Tejasvani Chauhan**, and **Anshul Singh Rathore**, sister-in-law **Dr. Priyanga Singh Hada** and brothers-in law **Mr. Rishi Raj Singh Chauhan** and **Mr. Yudhishthir Singh Hada** for their affection and encouragement. Special thanks to my loving nieces **Yashika** and **Divyanshi** for always cheering me up in life with their beautiful smile.*

*I acknowledge my grandparents **Mr. Ranjit Singh Arun** and **Late. Mrs. Anand Devi**, **Mr. Shivnath Singh Panwar** and **Late. Mrs. Shakuntla Panwar** and uncle **Mr. Jitender Singh Panwar** and **Mr. and Mrs. Praveen Singh Panwar** and all elders of my family with special thanks to **Tarun**, **Nikhil**, **Nupur** and **Chaitanya** for their affection.*

*I thank the **Almighty** for giving me patience, perseverance and determination to work through all these years and indeed, throughout my life.*

Anupriya Singh

ABSTRACT

This thesis describes a simple, low-cost synthetic methodology of the isolations of the non-toxic versions of water soluble graphene nanosheets and carbon nanorods from the pollutant dirty-dangerous black carbon and waste soot of castor oil respectively. The findings presented in this thesis offer a new methodology concerning the environmental application of waste pollutant soot somewhat like utilizing a pollutant material for degrading the other pollutant material. Using the pollutant black carbon and waste soot of castor oil as a freely available carbon source for the isolations of nanocarbons, their 'wet' side potentials are described, towards the photocatalytic dye degradation and sensing applications. Mainly associated with the sunlight-induced photodegradation of the pollutant organic dye even without harming the normal growth of bacterial colonies. In continuation, water soluble graphene nanosheets are being used for the photodegradation of the mixture of dyes followed by the use of the treated wastewater towards the plant growth. Additionally, the sensing applications of water soluble graphene nanosheets and water soluble carbon nanorods have also been investigated, and the new outcomes are presented in the following chapters.

CONTENTS

Chapter 3

Water Soluble Graphene Nanosheets for Visible Light Photodegradation of Pollutant Dye

LIST OF TABLES

LIST OF FIGURES

LIST OF SCHEMES

LIST OF ABBREVIATIONS

Abbreviated Form	Extended Form
Al	Aluminium
As	Arsenic
AA	Ascorbic Acid
AFM	Atomic Force Microscopy
AOP	Advanced Oxidation Process
BC	Black carbon
BET	Brunauer−Emmett−Teller
Cd	Cadmium
CD	Carbon Dots
CND	Carbon Nanodiamonds
CNF	Carbon Nanofibers
CNO	Carbon Nano-Onions
CNR	Carbon Nanorods
CQD	Carbon Quantum Dots
CCl_4	Carbon tetrachloride
CVD	Chemical Vapour Deposition
Cr	Chromium
CFU	Colony Forming Unit
Cu	Copper
CV	Crystal Violet
CV	Cyclic Voltammetry
DI	Deionized water
DNA	Deoxyribose Nucleic Acid
D_2O	Deuterium Oxide
Na_2-EDTA	disodium ethylene diaminetetracetate
DO	Dissolved Oxygen
DA	Dopamine
DMEM	Dulbecco's Modified Eagle's Medium
E. coli	*Escherichia coli*
ECL	Electrogenerated Chemiluminescence
EPR	Electron Paramagnetic Resonance
FeOOH	Ferricoxyhydroxide
$Fe_2(WO_4)_3$	Ferric Tungstate

Abbreviated Form	Extended Form
FESEM	Field Emission Scanning Electronic Microscopy
FRET	Fluorescence Resonance Energy Transfer
FT-IR	Fourier Transform Infrared
GCE	Glassy Carbon Electrode
GNS	Graphene Nanosheets
GO	Graphene Oxide
GQD	Graphene Quantum Dots
C_6Cl_6	Hexachlorobenzene
HeLa	Human Cervical Cancer Cell Line
HOPG	Highly Oriented Pyrolytic Graphite
HRSEM	High-Resolution Scanning Electron Microscopy
h^+	Holes
HOMO	Highest Occupied Molecular Orbital
HRP	Horseradish Peroxidase
HPLC	High Performance Liquid Chromatography
^{1}H NMR	Proton Nuclear Magnetic Resonance Spectroscopy
HRTEM	High-Resolution Transmission Electronic Microscopy
$\bullet$OH	Hydroxyl Radicals
H_2O_2	Hydrogen Peroxide
Fe	Iron
IPA	isopropyl Alcohol
Pb	Lead
LB	Luria-Bertani
LOD	Limit of Detection
Li	Lithium
LUMO	Lowest Unoccupied Molecular Orbitals
Hg	Mercury
MB	Methylene Blue
NIR	Near-Infra Red
Ni	Nickel
HNO_3	Nitric Acid
NBT	Nitro Blue Tetrazolium
N-CNR	Nitrogen Doped CNR
OD	Optical Density
$K_2Cr_2O_7$	Potassium Dichromate

Abbreviated Form	Extended Form
PBS	Phosphate Buffer Saline
p-BZQ	para-Benzoquinone
PCP	Pentachlorophenol
PL	Photoluminescence
PP	Polypropylene
p-XRD	Powder X-ray Diffraction
RhB	Rhodamine B
RNA	Ribose Nucleic Acid
ROS	Reactive Oxygen Species
Ag	Silver
SAED	Single Atom Electron Diffraction
S. aureus	*Staphylococcus aureus*
SD	Standard Deviation
($\pm$SE)	Standard Error
$O_2^{-\bullet}$	Superoxide
SWCNT	Single Walled Carbon Nanotubes
t-BA	tertiary Butyl Alcohol
C_2Cl_4	Tetrachloroethylene
TiO_2	Titanium Dioxide
TEM	Transmission Electronic Microscopy
TGA	Thermogravimetric Analysis
TOC	Total Organic Carbon
UV-Vis	Ultra-Violet Visible Spectroscopy
WEO	Waste Engine Oil
wsCD	Water Soluble Carbon Dots
wsGNS	Water Soluble Graphene Nanosheets
wsCNO	Water Soluble Carbon Nano-Onions
wsCNP	Water Soluble Carbon Nanoparticles
wsCNR	Water Soluble Carbon Nanorods
XPS	X-Ray Photoelectron Spectroscopy
Zn	Zinc
$ZnFe_2O_4$	Zinc Ferrite
ZnO	Zinc Oxide
Z	Zeta potential in mV
δ ppm	Chemical Shift in Parts Per Million
υ cm^{-1}	Wavenumber
λ nm	Wavelength

Chapter-1

Introduction

1.1   Introduction

Currently, the scarcity of safe water is the top concern with the rise in global population and exploitation of water resources. So, protecting the quality of water is crucial for both the human and the ecosystem [1]. Rapid industrialization and unplanned urbanization with exploitation of water resources have decreased the availability of drinking water and broadly contributed to severe water pollution [2]. A number of contaminations including organic dyestuffs, hydrocarbon, organic solvent, metal salts, heavy metal ions, anions, oils, and nanoparticles are entering into water supplies and likely to further worsen substantially [1, 3]. Importantly, the ever-increasing water scarcity is directly associated with a strained global food supply [3]. Although our planet is covered with voluminous fresh water bodies, the misuse and contaminations of water bodies due to human activities have led to unprecedented water scarcity [3]. Constantly increasing concerns related to public and environmental health are focused on novel, secure, and sustainable technologies to serve people worldwide without any additional environmental stress. Recent flurries of activities in technological development of sustainable materials and techniques offer hope in mitigating water contamination with enhanced remediation efficiency. The overarching goal for water remediation is to detect the presence of natural or intentional contaminations to maintain water quality. To achieve these, the accurate and real-time monitoring of contaminations are integral for their selective and safe removal [4]. Monitoring the quality of water is both crucial, and challenging due to highly complex and assorted nature of pollutants at extremely low concentration levels [4]. Currently, the real-time and accurate indications of water quality impairment are potentially significant for both long-term and short-term perspective. In this quest, sensing technologies for monitoring the quality of water are significantly increased [5]. Sensors exhibit sensitivity, detection accuracy, selectivity, and cost effectiveness for practical applications. Conventional sensors are designed to detect total chlorine content, free chlorine, pH, temperature, total organic carbon (TOC), dissolved oxygen (DO), and particle counts [6]. However, challenges associated with accuracy and selectivity often lead to false-negative and false-positive analysis [4, 7]. Hence, development of sustainable and long-term technologies for monitoring water quality is a current need of time.

In this regard, the exploration and adaptation of nanomaterials with advantageous properties has been the focus of the research efforts toward detection and discrimination of diverse pollutant in water. For this, the nanotechnology offers the significant promises in the area of pollutant sensing and its removals by exploiting novel synthetic techniques and properties of nanomaterials [8]. Presently, the most significant requirements for such technological developments are the cost of proposed technology that needs to be very limited. In this respect, low-cost organic materials, industrial, and agriculture waste have been considered for the synthesis of nanomaterials [9]. Particularly, the nanocarbons from renewable and green resources rely on novel nanotechnologies at minimum environmental cost and considerable potential for maximum efficiency [10], and being explored everywhere [11-18]. Nanocarbons [11-18] with unique mechanical, optical, physiochemical, and electronic properties show great prospects in myriad applications such as adsorbents, sensors, energy storage, nanofertilizers, electronic devices, and bio-imaging [11-18]. Nanocarbons have the considerable potentials to be active materials in sensing devices for real-time monitoring at comparatively lower cost and high efficiency [7, 19]. Recently, carbon nanomaterials have been intensely explored in diverse applications for monitoring the quality of air, water and soil [4, 8, 20]. A wide variety of nanocarbons have been used to fabricate high performance sensors for the detection of the contaminants in drinking water at very low concentration levels [21] based on their unique and tunable optical properties for the developments of nanoprobes [7]. Fluorescent nanocarbons such as carbon dots (CD) [11], carbon quantum dots (CQD) [13], graphene quantum dots (GQD) [22], carbon nano-onions (CNO) [23], carbon nanorods (CNR) [24] and water soluble graphene nanosheets (wsGNS) [25] exhibited photoluminescence (PL) emissions that usually red-shifted to a longer excitation wavelength. Until now, most of the nanocarbons sensors are based on fluorescence sensing mechanism [21]. The PL quenching, that is, "turn off" or enhancement assay, that is, "turn on" based nanoprobes have been developed to improve detection accuracy and selectivity. PL changes due to the interaction with target analytes have been directly measured. The PL emissions of nanocarbons can be easily quenched by the addition of an electron acceptor or a donor moiety and quickly restored after the removal of said moiety

[26]. These unique characteristic PL properties of nanocarbons are highly explored for the fabrication of chemosensor to detect pollutant or biological relevant molecules [27, 28].

1.2   Recent Advancements in Sustainable Nanocarbons

Currently, a variety of top-down and bottom-up approaches have been developed for the synthesis of nanocarbons (Figure 1.1) [7, 29]. However, the race is to develop the cost effective facile synthetic techniques that should be environmental friendly, require less energy and chemical inputs, high yield with no harmful by-products [10]. So the researchers have focused on the development of green methodologies for the synthesis of nanocarbons stretching from natural biomass based synthesis route to the waste material and pollutant soot [27, 30]. The cost-quality trade-off is crucial while utilizing raw and waste precursor to avoid frequently existing mismatch between industrial applications with their lab-scale counterparts. Synthesis of nanocarbons is carried out through various synthetic routes, which fall under the criteria of green chemistry principles.
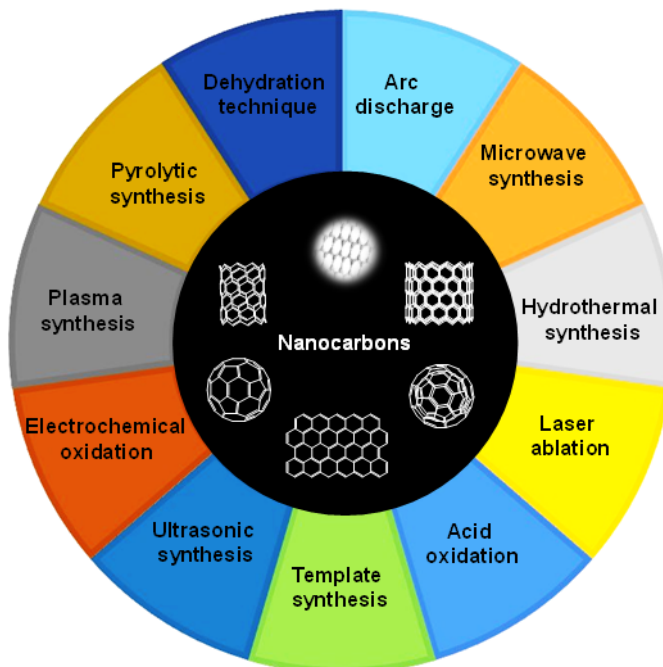
Figure 1.1. A schematic illustration for the synthetic routes of nanocarbons [29].

From the synthetic view point, thermal carbonization is one of the sustainable approaches that is clean and does not require any sophisticated

instruments. Thermal carbonization can be done by traditional techniques using basic laboratory supports or in a furnace under controlled conditions [28, 31]. The drawbacks are the generation of CO_2 and further requirement of acid treatment to convert hydrophobic nanocarbons into hydrophilic. Microwave-assisted technique has created revolutionary developments in recycling wastes, biomass, and nanocarbons owing to green and scalable nature. It provides faster synthesis within minutes but reaction condition cannot be controlled, which is the major limitation of this technique. Hydrothermal synthesis has been preferred as efficient technique for such sustainable nanocarbons synthesis owing to simplicity, faster synthesis, and versatile chemistry of the method [32]. Low specific energy input and control over the morphology and chemical functionalities are the main advantages of this technique [33]. Hydrothermal treatment for carbonization generally increases or changes solubility and accelerates the physical and chemical interaction between reacting components, consequently yielding nanocarbons [33].

1.3   Nanocarbons Derived from Waste

With an increase in the environmental awareness, the utilization of waste materials gained a lot of attention [34]. Recent concerns include treatment of waste produced and development of sustainable routes to recycle wastes to value-added products [35]. Wastes offer valuable raw material for the production of nanocarbons. Development of valuable nanocarbons from renewable waste materials is like hitting two birds with a single stone, that is, waste management and valuable products. Nanocarbons derived from waste materials deserve particular attention from scientific community because they are available in large quantity at almost no costs [9]. The composition, chemical functionality, and physical attributes of precursor materials significantly affected the morphological and chemical behavior of resultant nanocarbons. Waste engine oil (WEO) as most abundant waste material was used as carbon source for carbon nanotubes (CNT) synthesis in an environmentally conscious approach due to highest carbon content among the oils [36]. Thermal chemical vapour deposition (CVD) of WEO at 500 °C and 750 °C in the presence of ferrocene catalyst resulted in quasi-aligned CNT with 18.0 nm to 29.8 nm in diameter. Printed circuit board waste pyrolysis oil was used for second

life applications to synthesize CNT [37], Waste polypropylene (PP) [38], waste plastic [39], and polyethylene-based used plastic [40] were also used as precursor to synthesize CNT. Researchers have been reported the recycling of waste rubber tires into carbonaceous materials as adsorbents or nanocarbons for multifunctional applications [41]. Disposal of waste rubber tires is a serious environmental concern due to continuously increasing number of automobiles worldwide. However, waste-tires derived nanocarbons have been reported as efficient material for the detection and removal of pollutants from wastewater [41]. Waste polystyrene foam was used to synthesize wsCNO with green emissions for cell imaging [34].

Alternatively, in the quest to follow the dictates of sustainable development of biocompatible and environmentally benign nanocarbons, bio-resources have gradually emerged as safe "green" biomaterials. Nature utilizes carbons along with oxygen and hydrogen to provide the basics of life and energy [30]. Direct use of crude natural products provide sustainable alternative for carbon source. In this context, various bio-mass and other waste such as glucose [42], sucrose [43], hemp leaves [44], rice husk [45], wheat straw [46], peanut-shells [47], coconut shells [48], soybean shells [49], waste paper pulp [50], soya-nuggets [51], sugarcane waste [52], kidney bean [53], egg white [11], and so on are frequently used as green precursor for synthesis of nanocarbons [54]. Tripathi *et al.* reported the synthesis of wsCNO via flame pyrolysis of vegetable ghee [28]. Wang *et al.* have reported a sugar-blowing approach for the fabrication of 3D-graphene from glucose where graphitic membranes are tightly connected and supported by robust graphitic microstruts. This 3D-graphene display very high power densities to be used as a supercapacitor [42]. Ruiz-Hitzky *et al.* have prepared graphene like nanomaterial from the natural sources like sucrose (table sugar) and gelatin protein as carbon precursors in absence of oxygen at temperature <800°C. They observed that these graphene like materials display good electrical conductivity [43]. In another report, Wang *et al.* used novel precursor as hemp-bast fibres for the synthesis of interconnected partially graphitic carbon nanosheets via simple hydrothermal carbonization combined with activation and used them as supercapacitors material [44]. Efficient use of rice-husk as precursor for graphene synthesis was reported by Muramatsu *et al.*[45] Similarly,

Chen *et al.* adopted a less expensive method for the synthesis of graphene nanosheets (GNS) from wheat straw using combined hydrothermal and graphitization approach and used them as anode material for Lithium-ion (Li-ion) batteries [46]. Purkait *et al.* used agricultural waste biomass in form of peanut shell using mechanical exfoliation technique fabricated few layer graphene with meso and micropores. These few layer graphene derived from peanut shell possess high specific surface are (2070 m^2 g^{-1}) and high specific capacity (186 F g^{-1}). Further used them for the production of solid-state supercapacitor [47]. Sun *et al.* have used renewable biomass coconut shells for the fabrication of highly porous graphene like nanosheets and used them as electrode material for high power supercapacitors [48]. Similarly, Zhou *et al.* used soybean shells as carbon and nitrogen precursor for the synthesis of nitrogen-doped graphene which show remarkable oxygen reduction performance [49]. Silk cocoon membrane was used for the synthesis of nitrogen-doped graphene that was applied as electrode material for supercapacitor [55, 56].

The direct adaption of agricultural or food-waste for nanocarbons synthesis is another alternative for precursor material. Exploration of bio-waste for nanocarbons synthesis is attractive because these are economic, clean, and easily accessible [8, 54]. In a report, disposable paper cups have been used for the synthesis of graphene using Fe^{+2} as catalyst. It has several promising applications like anode material for Li-ion batteries and for the preparation of graphene supported platinum (Pt) catalyst which displays high catalytic activity for the oxygen reduction reaction in fuel cells [57]. Waste from food industry has been long considered as most fascinating precursor for the synthesis of a wide variety of nanocarbons. Huge amount of bio-mass are discarded as waste from human activities and food industries all over the world. In this milieu, upgrading of this "end-of-pipe" residual bio-waste to value-added products is important from both ecological and economical point of view. Ruan *et al.* synthesized monolayer high quality graphene from six different sources included (cookies, chocolate, roaches, grass, plastics, and dog faeces) [58].
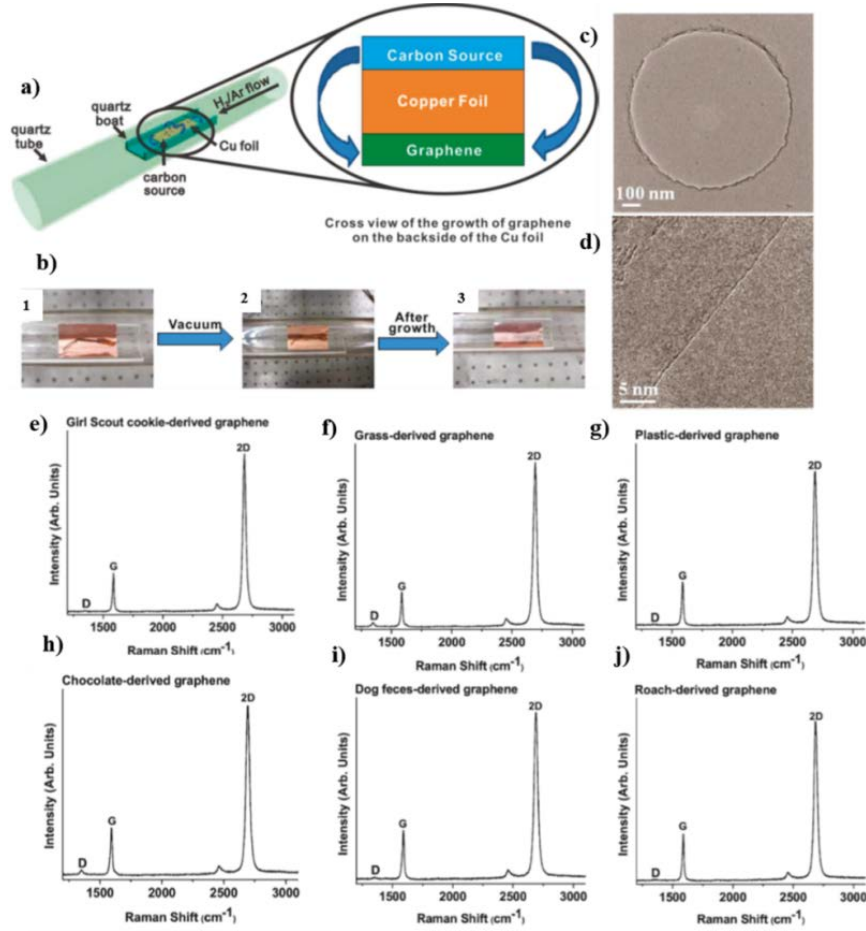
Figure 1.2. (a) Diagram of the experimental equipment for the growth of graphene from insects, food, or waste in a tube furnace. On the left, at the hot zone of a tube furnace, quartz boat contained copper (Cu) foil with the carbon source is placed. The growth is carried at 1050 °C under low pressure with a H_2/Ar gas flow. On the right is a cross view that represents the formation of pristine graphene on the backside of the Cu substrate; (b) Growth of graphene from a roach leg. (1) One roach leg on top of the Cu foil. (2) Roach leg under vacuum. (3) Residue from the roach leg after annealing at 1050 °C for 15 min. The pristine graphene grew on the bottom side of the Cu film. Transmission electron microscopy (TEM) images of the cookie-derived graphene; (c) Suspended graphene film on a 1 μm diameter hole; and (d) the edge of monolayer graphene. Raman spectra of monolayer graphene from six different carbon sources. The Raman spectra graphene were derived from (e) girl scout cookie; (f) grass; (g) plastic (polystyrene petri dish); (h) chocolate; (i) dog feces; and (j) roach leg. There was only a trace D peak in some of the spectra, and the 2D to G peak intensity ratio were ~4, indicating monolayer graphene [58].

The graphene was directly grown on copper foil at 1050°C in the mixture of H_2/Ar flow. The experimental setup is shown in Figure 1.2(a) and different growth conditions in Figure 1.2(b). Graphene was synthesized only on backside of Cu foil and residual particles were deposited on frontside of foil. H_2/Ar flow facilitated the removal of amorphous and other carbon segments during synthesis. Diffusion of a portion of carbon source from slightly bent Cu foil resulted in the deposition of a monolayer graphene film on backside of Cu foil. The TEM image of graphene was shown in Figure 1.2(c) with monolayer edge in Figure 1.2(d). Raman spectra of graphene obtained from all the sources showed intense 2D bands, small or no D peaks and high 2D/G ratio, which confirmed the monolayer nature of graphene. Raman spectra of graphene derived from six sources are shown in Figure 1.2(e-j).

Park *et al.* synthesized CD (4 nm in size) from food-waste at large scale using ultrasound irradiation at room-temperature [59]. Purkayastha *et al.* utilized oil industry waste as spent rapeseed meal for the synthesis of carbon nanoparticles (CNP) having antimicrobial activity [60]. CNR, CNP, and carbon nanodots (CND) were synthesized using similar precursor almond husk, discarded as waste. Morphology was controlled just by tuning pyrolytic temperature from 750 °C, 850 °C to 950 °C for CNR, CNP, and CND synthesis, respectively [31]. Pyrolysis of bio-waste oil palm leaves in inert atmosphere at 500-600 °C led to the synthesis of porous CNP using SiO_2 template without any catalyst [61]. Similarly, wood-wool thrown as waste after its use has been exploited for the synthesis of wsCNO for the application as growth promoter in gram plants [35]. Further, these first generation seeds were used to check the effect of wsCNO on plant metallic micronutrient content and total protein content [18]. The second life use of fullerene waste soot as double walled CNT by arc-discharge technique was reported by Qiu *et al*. [62] Coal combustion fly ash was used as carbon source for the synthesis of industrial grade multiwalled carbon nanotubes (MWCNT) using fluidized bed CVD technique [63]. Dubey *et al.* isolated multipodal junctions (Y, T, and H types) CNT with network structure from waste fullerene soot possessing the integrated interesting magnetic properties [64].

1.4   Nanocarbons for the Sensing of Toxic Metal Ions

Heavy metal ion contamination is one of the most serious concerns to public health because of their highly toxic, carcinogenic nature, and ability to retained by the ecological system [65]. These metal ions are released into environment from their numerous uses in various industrial activities, technologies and combustion of massive quantities of fossil fuels, and coal [66]. Once released into atmosphere, heavy metal ions can enter into aquatic environment by various routes. Heavy metal ions have a great tendency to form a complex with ligands of biological matter and lead to changes in the molecular structure of protein or enzyme inhabitation [66]. However, some of the heavy metal ions such as Cu, zinc (Zn), iron (Fe), aluminium (Al), and chromium (Cr) (III) are nutritionally essential for healthy life and required by some organisms but their higher concentration can lead to toxicity [66]. Heavy metal ions like Cr (VI), lead (Pb), nickel (Ni), arsenic (As), cadmium (Cd), silver (Ag) and mercury (Hg) are the most common non-biodegradable and toxic pollutants in industrial effluents even at trace amounts [65].

To minimize the water pollution, environmentally sound and practically feasible sensors for the detection of heavy metal ions are of great importance to prevent the damaging effects at the very beginning stage. Fluorescent nanocarbons are promising to replace metal-based nanoparticles and organic dyes. Fluorescent nanocarbons such as CD, CNO, and GQD emerged as efficient PL "turn on/turn off" sensors for the recognition of heavy metal ions due to their versatile nature, tunable chemical/ optical properties, low cytotoxicity, chemical inertness, and photo-stability [67]. Previous reports showed that the quenching of PL is mainly attributed to the charge, electron, or energy transfer between nanocarbons and metal ions via selective interactions owing to functional groups and surface traps [67]. The inner filter effect is another reason to contribute in PL quenching and enhance selectivity by absorbers overlap [67]. The selectivity is strongly affected by the surface functionalities, edge structure, size, and morphology of nanocarbons. Therefore, precise control of binding sites and energetics of PL emissions are crucial to develop nanocarbons-based versatile sensors for the detection of heavy metal contaminants in aqueous system. Tan *et al.* synthesized CD using sago industrial waste *via* thermal pyrolysis at different carbonization temperature for the sensing of heavy

metal ions. Most of the tested metal ions exhibited quenching effect toward PL intensity [68].

Hg is one of the most toxic and ubiquitous pollutant and its contamination in water is reported to cause deoxyribose nucleic acid (DNA) damage, permanent damage of central nervous system, mitosis impairment, and mental retardation due to higher reactivity toward sulfhydryl and oxygenous functional groups [69]. Subsequent biotransformation of Hg vapor to more toxic water-soluble Hg(II) are resulting into their environmental accumulation through the food chain [67]. Lu *et al.* described a highly sensitive (0.23 nM detection limit) CNP based sensors for the selective detection of Hg(II) [70]. CNP were synthesized from pomelo peel waste *via* hydrothermal treatment to detect Hg(II) in lake water for showing practical applicability [70]. Likewise, Tripathi *et al.* reported the specific detection of Al(III) using water soluble carbon nano-onions (wsCNO) with 0.77 μM detection limit. CNO were synthesized by a simple technique using wick pyrolysis of flaxseed oil. PL emission of wsCNO was reported to gradually decrease with increasing Al(III) concentration due to the formation of wsCNO-Al(III) complex [71]. Al(III) specifically interact with surface carboxylic groups of wsCNO due to hard acid-hard base interactions resulted in PL quenching as shown in Figure 1.3.
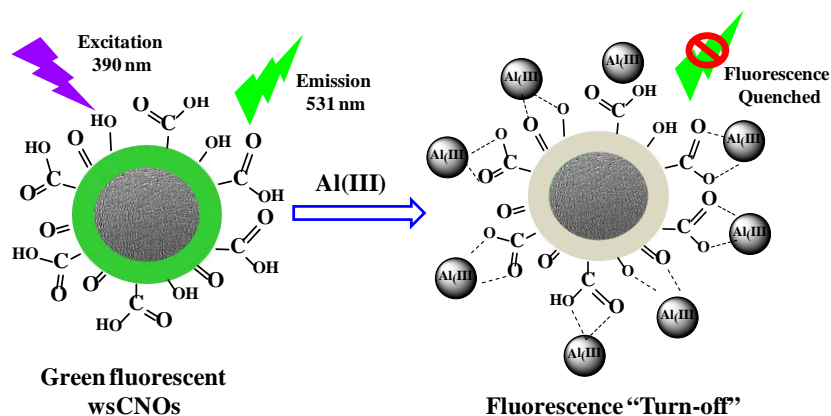
Figure 1.3. Schematic representation of the sensing of Al (III) with wsCNO-based fluorescent probe [71].

Cr is considered as a severe contaminant for natural water brought about by human activities, and various industrial revolutions such as leather-tanning, metal manufacturing, electroplating, textile dyeing, mining, and wood preserving [72]. Cr

in their higher oxidation state as Cr(VI) is highly toxic and exhibits mutagenic and carcinogenic properties even at low abundance. Higher toxicity of Cr(VI) is due to its smaller size, higher oxidation potential, greater tissue penetration ability, and formation of reactive oxygen species (ROS) [73]. Therefore, the concentration of Cr(VI) is strictly monitored and regulated in drinking water [72].

1.5 Nanocarbons for the Sensing of Organic Pollutants

The contamination of water by organic pollutants such as crude oil, petroleum products, hydrocarbons, dyes, aromatic compounds, chlorinated, and other toxic solvents has become a serious concern due to their toxic nature and resistant to biodegradation [74]. Various human activities further induce these hydrocarbons to enter into water systems and consequently water pollution [74]. Phenol being an important chemical is highly used in industries and agriculture [75]. On the other side, phenolic compounds are considerably toxic contaminants in both ground and surface water having adverse impacts on aquatic life and plants [76]. In human consumption of trace amount of phenol can cause coma, nausea, vomiting, paralysis, greenish or smoky colored urine, and death if consume in large amount [76]. Increasing environmental awareness and regulations attract the attention of researcher to monitor and control its contamination in water. High solubility and colorless nature of phenol in water made it monitoring bit difficult. Mohanty *et al.* proposed a simple technique for the removal of phenol from water using nuts of *Terminalia arjuna*, an agricultural waste, derived activated carbons [76]. Sun *et al.* used GQD in presence of horseradish peroxidase (HRP) and hydrogen peroxide (H_2O_2) for the trace analysis of phenol in water by resonance light scattering technique [75]. In a comprehensive study, Li *et al.* reported the detection of highly chlorinated organic compound pentachlorophenol (PCP) with CQD [77]. ECL of CQD attributed to interaction between CQD and $S_2O_8{}^{2-}$ that was quenched by the PCP addition above pH = 7. The schematic illustration of PCP is shown in Figure 1.4. Quenching of PL was attributed to the consumption of excited electron of CQD by PCP [77].
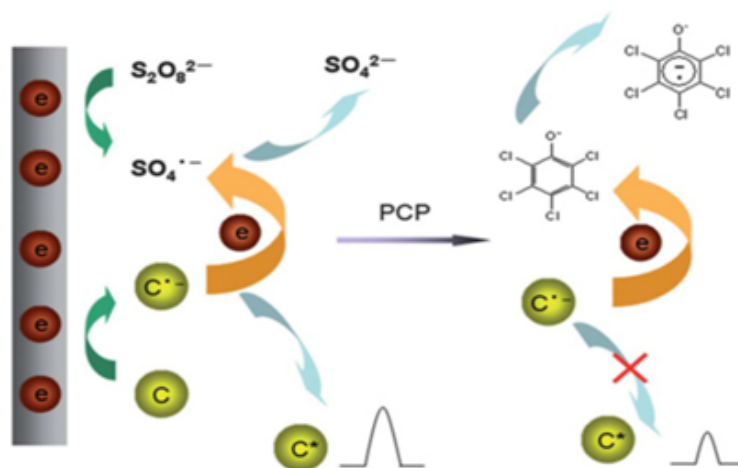
Figure 1.4. Schematic diagram showing the electrogenerated chemiluminiscence (ECL) detection of PCP with CQD in $S_2O_8^{2-}$ solution [77].

1.6   Nanocarbons for the Photocatalytic Degradation of Organic Dyes

Recently, graphene and graphene-based nanocomposites are presently being in used to eliminate the contaminants in water and showed its significant potentials as a photocatalyst nanomaterial [78-81]. The aqueous phase photocatalysis is very attractive and presently in high demand, since it provides a clean, mild and cost-effective method for water purification. The major emphasis for partial or complete aqueous-phase photodegradation of organic dyes were resulted into nontoxic hydrocarbons of low molecular weight [82-84]. So far, several researchers have reported the utilizations of graphene/graphene-based nanocomposites as a successful adsorbent material or photocatalyst material by modifying the graphene. Such as, Under visible light irradiation, WO_3-graphene nanocomposite were used for the photocatalytic degradation of methylene blue (MB) [85]. Zhao *et al.* reported ~96% photocatalytic degradation of MB by 3D Hemin functionalized graphene hydrogel [86]. Similarly, for the decolourization of MB and RhB, GO/chitosan(CS)/Ag nanoparticles were used as shown in Figure 1.5. (a-b) [84] Wei *et al.* reported the effective removal of organic solvents, MB and oil by Ni-doped graphene/carbon cryogels [87]. Similarly, Shen *et al.* fabricated SnO_2-reduced graphene oxide (RGO) core shell structures for the photodegradation of methyl orange under UV light irradiation [88]. For the degradation of pollutant dye like MB, Shanmugam *et al.* synthesized graphene-V_2O_5 nanocomposites under different light conditions [89].

Most of the researchers were focused on the photodegradation of single dye, whereas waste water containing mixture of dyes has been paid a very little consideration [90-93]. The above said materials generally need expensive chemicals and multistep synthesis process [93-95]. Therefore, to synthesize an effective photocatalyst which must be cost-effective, and facile, is still a demanding need.
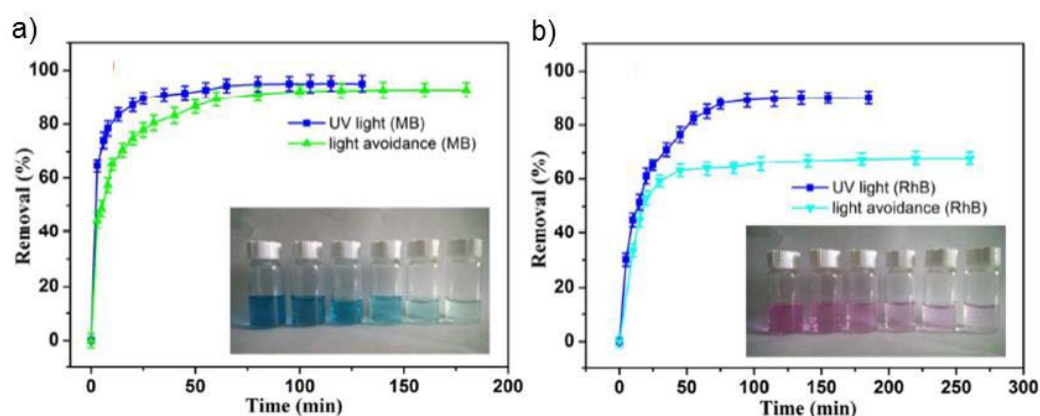
Figure 1.5. Photocatalytic degradation activity of RGO-Chitosan-Ag nanoparticles on the removal of (a) MB; (b) RhB [84].

Apart from all these conventional and non-conventional synthetic route of nanocarbons, is it possible that we do not have to synthesize nanocarbons, we just need to isolate them ?

SECTION A

1.7 Nanocarbons Derived from Black Carbon (BC) Soot

It can be a sustainable approach if we could utilize the nanocarbons derived from the pollutant BC soot. This present work seeks to offer an overview of the technical facets of "sustainable nanocarbons," and assess their benefits as potential material for monitoring and degradation of various contaminants and pollutants in water. Various novel aspects including modifications, and applications of nano-carbons as sensor with special emphasis on sustainability are described. The sustainability credits of nanocarbons as an alternative probe for facile and efficient detection of analytes and the photocatalytic degradation of pollutants are discussed here with some significant examples.

Globally, generated carbon emission-based soot known as BC [96-98] is assumed as potential environmental pollutant produced by incomplete combustion of fossil fuels and biomass and considerable contributors of the greenhouse effect [27]. It has warming impact on climate 460-1500 times stronger than carbon dioxide. The quantity of BC should be decreased to provide a clean environment. Carbon emission soot is composed of hydrophobic carbons, which raise the potential health and environmental concerns [99]. BC emission increases continuously and its disposal in an environment friendly manner is a matter of serious global distress. Alternatively, this BC could be used as freely available carbon precursor for isolation/synthesis of nanocarbons. Their potential use as carbon source is useful in various aspects, since it could reduce the environment pollution especially from urban areas and revalorize as a material for technological applications. Effective use of pollutant soot as renewable precursor follows the dictates of economically feasible and sustainable process. For this, Tripathi *et al.* used the soot from diesel engine exhaust and utilized this for the isolations of CD and its water soluble version as water soluble carbon dots wsCD by oxidation with nitric acid. These wsCD was used as fluorescent probe for cholesterol sensing and imaging of *Escherichia coli* (*E. coli*) cells [27]. Sonkar *et al.* investigated the ferromagnetic behavior of MWCNT generated by anthropogenic indoor activities and trapped in spider web. Recently, few groups have described the presence of graphitic nanoparticles in the pollutant waste soot of diesel [27, 100-102] and petrol engines [103], along with the forecasts of their application [27, 100]. Such as, Uchida *et al.* fabricated typical single walled carbon nanotubes (SWCNT) from diesel soot using a laser vaporization technique [101]. Wang *et al.* reported the isolation of fluorescent wsCNP [100] for the selective sensing of Mn(II). With respect to these findings, there is just a need to use these "freely available carbon precursors" [27, 100-103] for the isolation of nanocarbons from pollutant soot.

The thesis describes the environmental assessment of the BC pollutant soot derived wsGNS as a selective sensor for Cr (VI) ions, imaging of human cervical cancer line (HeLa) cells. And as a nontoxic photocatalytic material for degradation/selective degradation of the organic dyes and the mixture of dyes under the influence of natural sunlight, further the treated wastewater has been used for environmental assessment.

SECTION B

1.8   Carbon Nanorods (CNR)

Apart from the globally generated BC, some other types of nanocarbons can also being isolated from the waste soot such as CNR. CNR belong to a unique class of one-dimensional carbon nanostructures with straight, aligned and graphitic morphology that was discovered very late in 2000 after the discovery of CNT [104] by S. Iijima in the year 1991. These novel CNR were first observed by Liu *et al.* in 2000 formed as a by-product during the purification of CNT fabricated by arc-discharge process using TEM [105]. They found that cavity of nanotubes can be filled with carbon atoms and showed well distributed CNR of diameter 45 nm and length 15-50 nm where graphitic layers are preferentially arranged parallel to the long axis of nanorods. Chen *et al.* in 2001, have used electron-beam induced route for the formation of CNR in situ under high-resolution scanning electron microscopy (HRSEM) [106]. They have observed that when CVD deposited CNT-sample was irradiated with an electron beam under HRSEM, etching and further expansion of nanotubes (particularly near the tips) occur which resulted in the formation of additional nanorods. Structural analysis by TEM observation reveals that typical nanorod was amorphous with diameter of 20 nm [106]. A unique carbon material in form of CNR were first synthesized in 2003 by Chang *et al.* by reacting hexachlorobenzene with Li at 523 K in a pyrex tube sealed under vacuum [107]. They observed rod like morphology with SEM and TEM images with dimensions 0.1-0.5 µm width and 3-15 µm length (Figure 1.6 a-b).
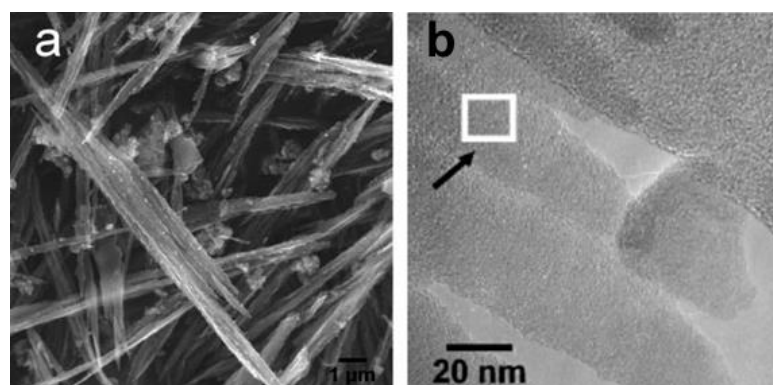
Figure 1.6. (a) SEM and (b) TEM images of CNR synthesized by C_6Cl_6 and Li [8].

1.8.1   Synthesis of CNR

Typical conventional synthetic procedures for the production of CNR are CVD [108-111], arc discharge methods [112], solvothermal synthesis [113, 114], catalytic copyrolysis [115], electrodeposition [116], and soft and hard template assisted synthesis [117-120]. Li *et al.* adopted a facile soft-template method for synthesis of CNR [117]. They used phenolic resol as carbon precursor and tri-block copolymer Pluronic F127 as template and used these as a promising electrode material for supercapacitors [117]. Although CNT due to their unique carbon framework structure have high electrical conductivity but possess less surface area which limit their use in energy storage devices [118]. Porous tubular carbon nanomaterial in form of CNR with high surface area and excellent electrochemical properties were synthesized in large scale *via* template mediated process by Yu *et al.* and used it as active electrode material in supercapacitors. Typical synthesis comprises of the preparation of rod-like nickel-hydrazine complexes in a reverse micelle, further sequential coating of nanorods with a layer of phenolic resin and then silica, further carbonization was done at a high temperature in an inert atmosphere which yield tubular CNR after sequential etching in NaOH and HCl solutions [118]. Orikasa *et al.* synthesized nanorods using anodic aluminium oxide film as template and further used them in electrochemical applications [120]. CNR were produced in high yield ~90% by pyrolysis using C_6H_6 (10 mL) and C_5H_6 (5 mL) together with co-catalyst Fe and Mg and heated in autoclave at 600°C for 12h by Zou *et al.* Dimensions of CNR were found to be 200-350 nm in diameter and length in range 0.8-6 µm [115].

Wang *et al.* synthesized CNR *via* plasma enhanced hot filament CVD system with gold as catalyst [109]. They found that CNR were formed when $CH_4 + N_2 + H_2$ plasma is present. The formation of CNR is primarily a precipitation process. The use of plasma results in the production of different hydrocarbon (CH_3^+, CH_2^+), nitrogenous (NH_3^+ and NH_2^+) and hydrogen ions. These hydrocarbon ions react with hydrogen ions on the surface of gold nanoparticles resulted in rapid delivery of carbon on the surface. When the gold nanoparticles become saturated, carbon precipitates from the nanoparticle at the interface of particle and silicon substrate

leading to formation of rod like morphology [109]. In another report Thien-Nga *et al.* have grown nanorods on BYSCO ($Bi_2Sr_2YCu_2O_8$) substrate *via* CVD process using 80 mL min^{-1} of N_2 and 10 mL min^{-1} of acetylene [111]. They observed that upto 5 min substrate appeared to be disorganized, after 5 min nanorods started to appear and after 30 min of acetylene decomposition substrate was densely covered with nanorods of range 10-40 nm [111]. In another report, Li *et al.* synthesized nanosized CNR by arc discharge of composite electrode made from fullerene soot and iron particles with size range of 30-50 nm [112].

Zhu *et al.* reported facile synthesis of ferricoxyhroxide (FeOOH) rod like nanoparticles via one-pot glucose-mediated hydrothermal method. They found that glucose aid in formation of FeOOH nanorods along with deposition of glucose derived carbon rich polysaccharide overlayer on FeOOH nanorods. Further these GCP coated FeOOH nanorods on carbonization results in formation of carbon coated magnetite nanocomposite (Fe_3O_4@C) which possess good cycling performance for lithium storage used as anode material in lithium ion batteries [114]. Wang *et al.* used solvothermal method a novel route for the synthesis of CNR by using C_2Cl_4 and potassium as reducing agent at low temperature of 200°C [113]. Further the freshly reduced free C_2 in form of one dimension carbon chain clusters can assemble into nanorods in presence of Ag as catalyst. The diameter and length of nanorod was found to be 70 nm and 1000 nm respectively [113]. Highly nitrogenated CNR were fabricated by Wan *et al.* from an acetonitrile solution of dicyandimide by electrochemical method [116]. However, all these above mentioned synthesis methods require complex methodologies, high temperature synthetic conditions, metallic particles, expensive chemicals and are not cost-efficient which restrict their economic viability. Therefore, it could be a promising approach if there is development of some economically viable and metal catalyst free or template free synthesis of CNR.

1.8.2 Applications of CNR

Among all the nano forms of carbon, like MWCNT/SWCNT [104, 121], fullerenes [122, 123], CNR [105, 106], CNO [23, 28, 34, 124, 125], carbon nanofibres (CNF) [126], graphene [127, 128], GQD [22, 129], CD [13, 14, 51, 130]

CND [131, 132], CNR are the least explored nanocarbon due to lack of simple and reproducible method of synthesis. As their synthesis require sophisticated instruments, multistep production techniques, and expensive chemicals. Morphologically CNR are more straight, aligned graphitic inter-planar structures than CNT, exhibits remarkable electrical, thermal and mechanical properties thus used in various potential applications such as energy storage devices [117, 118], field emission devices [133], Li-ion batteries [114], composite materials [134], electrochemical applications [118, 120, 135, 136], catalyst [137, 138], water-oxidation/splitting [139,140], supercapacitors [141,142]. For example, Yuan *et al.* observed the electrochemical performance of nitrogen doped CNR (N-CNR) as ultrasensitive electrochemical sensor for dopamine (DA) as shown in Figure 1.7 [143]. Figure 1.7 (a) shows the cyclic voltammetry (CV) performance of phosphate buffer saline (PBS), ascorbic acid (AA) and DA on bare glassy carbon electrode (GCE) where there is broad oxidation peak for AA with absence of reduction peak. DA displays couple of asymmetrical redox peaks while there is no faradic current in case of PBS. Figure 1.7 (b) shows Nafion/GCE, CV performance results which were same as bare GCE. Figure 1.7 (c) exhibits the role of N-CNR showing well-defined redox peaks of DA with enhanced anodic peak current compared to bare GCE. This reveals that N-CNR-Nafion/GCE increased the selectivity of DA and AA with enhanced sensitivity for DA [143].
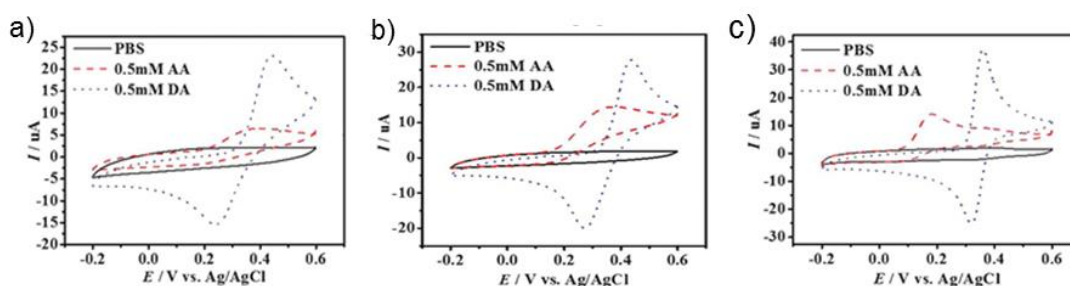
Figure 1.7. CV performance of (a) bare GCE; (b) Nafion/GCE; and (c) N-CNR-Nafion/GCE in 0.1 M PBS, 0.5 mM AA + 0.1 M PBS and 0.5 mM DA + 0.1 M PBS solutions, respectively [143].

Herein this thesis, CNR were being synthesized in the quantitative yield just by simple pyrolysing the castor oil without using of any metal catalyst or template. The water-soluble version of graphitic hollow CNR showed excitation-dependent

multicoloured PL emission from the green to red region of the visible spectrum and extending to the near infra-red (NIR) region. The application of wsCNR describes into two sections first relates to the light-induced photochemical degradation of MB. The second relates to the PL behaviour, used to produce a fluorescent turn-off/turn-on sensor for the specific, sensitive and rapid detection of DNA.

1.9   Scope of the Work

Since the discovery of graphene and CNR, various synthetic approaches relevant to produce graphene and CNR have been reported. The present thesis describes a straightforward, cost-effective approach towards the isolations of the water-soluble version of graphene and CNR from the BC and the waste soot of castor oil respectively as a freely available carbon precursor. The potential 'wet' side applications of the wsGNS and wsCNR, towards the photocatalytic dye degradation applications, have been examined and the results are discussed. Especially the sunlight-induced selective photodegradation of the dye without harming the ecological balance and the photodegradation of the different dyes and its mixture followed by the significant usage of the wastewater towards the plant growth. The method is being described for the environmental appeal of pollutant soot somewhat like utilizing a pollutant material for degrading the other pollutant material. Additionally, the sensing applications of wsGNS and wsCNR have also been explored, and the new outcomes are presented in the following chapters.

1.10   References

1. Shannon, M. A.; Bohn, P. W.; Elimelech, M.; Georgiadis, J. G.; Mariñas, B. J.; Mayes, A. M., Science and Technology for Water Purification in the Coming Decades. *Nature* **2008**, *452*, 301-310.

2. Sui, Z.; Meng, Q.; Zhang, X.; Ma, R.; Cao, B., Green Synthesis of Carbon Nanotube-Graphene Hybrid Aerogels and Their Use as Versatile Agents for Water Purification. *J. Mater. Chem.* **2012**, *22*, 8767-8771.

3. Lee, A.; Elam, J. W.; Darling, S. B., Membrane Materials for Water Purification: Design, Development, and Application. *Environ. Sci.: Water Res. Technol.* **2016**, *2*, 17-42.

4. Qu, X.; Brame, J.; Li, Q.; Alvarez, P. J. J., Nanotechnology for a Safe and Sustainable Water Supply: Enabling Integrated Water Treatment and Reuse. *Acc. Chem. Res.* **2013**, *46*, 834-843.

5. Pellerin, B. A.; Stauffer, B. A.; Young, D. A.; Sullivan, D. J.; Bricker, S. B.; Walbridge, M. R.; Clyde, G. A.; Shaw, D. M., Emerging Tools for Continuous Nutrient Monitoring Networks: Sensors Advancing Science and Water Resources Protection. *J. Am. Water Resour. Assoc.* **2016**, *52*, 993-1008.

6. Yang, Y. J.; Haught, R. C.; Goodrich, J. A., Real-Time Contaminant Detection and Classification in a Drinking Water Pipe Using Conventional Water Quality Sensors: Techniques and Experimental Results. *J. Environ. Manage.* **2009**, *90*, 2494-2506.

7. Baptista, F. R.; Belhout, S. A.; Giordani, S.; Quinn, S. J., Recent Developments in Carbon Nanomaterial Sensors. *Chem. Soc. Rev.* **2015**, *44*, 4433-4453.

8. Ng, S. M., Sustainable Alternative in Environmental Monitoring Using Carbon Nanoparticles as Optical Probes. *Trend Anal. Chem.* **2014**, *3-4*, 36-42.

9. Magnacca, G.; Allera, A.; Montoneri, E.; Celi, L.; Benito, D. E.; Gagliardi, L. G.; Gonzalez, M. C.; Mártire, D. O.; Carlos, L., Novel Magnetite Nanoparticles Coated with Waste-Sourced Biobased Substances as Sustainable and Renewable Adsorbing Materials. *ACS Sustainable Chem. Eng.* **2014**, *2*, 1518-1524.

10. Bazaka, K.; Jacob, M. V.; Ostrikov, K., Sustainable Life Cycles of Natural-Precursor-Derived Nanocarbons. *Chem. Rev.* **2016**, *116*, 163-214.

11. Zhang, Z.; Sun, W.; Wu, P., Highly Photoluminescent Carbon Dots Derived from Egg White: Facile and Green Synthesis, Photoluminescence Properties, and Multiple Applications. *ACS Sustainable Chem. Eng.* **2015**, *3*, 1412-1418.

12. Dai, H., Carbon Nanotubes: Synthesis, Integration, and Properties. *Acc. Chem. Res.* **2002**, *35*, 1035-1044.

13. Luo, P. G.; Sahu, S.; Yang, S.-T.; Sonkar, S. K.; Wang, J.; Wang, H.; LeCroy, G. E.; Cao, L.; Sun, Y.-P., Carbon "Quantum" Dots for Optical Bioimaging. *J. Mater. Chem. B* **2013**, *1*, 2116-2127.

14. Babar, D. G.; Sonkar, S. K.; Tripathi, K. M.; Sarkar, S., P_2O_5 Assisted Green Synthesis of Multicolor Fluorescent Water Soluble Carbon Dots. *J. Nanosci. Nanotechnol.* **2014**, *14*, 2334-2342.

15. Tripathi, K. M.; Begum, A.; Sonkar, S. K.; Sarkar, S., Nanospheres of Copper(III) 1,2-dicarbomethoxy-1,2-dithiolate and its Composite with Water Soluble Carbon Nanotubes. *New J. Chem.* **2013**, *37*, 2708-2715.

16. Tyagi, A.; Tripathi, K. M.; Gupta, R. K., Recent Progress in Micro-Scale Energy Storage Devices and Future Aspects. *J. Mater. Chem. A.* **2015**, *3*, 22507-22541.

17. Tripathi, K. M.; Vincent, F.; Castro, M.; Feller, J. F., Flax Fibers - Epoxy with Embedded Nanocomposite Sensors to Design Lightweight Smart Bio-Composites. *Nanocomposites* **2016**, *2*, 125-134.

18. Tripathi, K. M.; Bhati, A.; Singh, A.; Sonker, A. K.; Sarkar, S.; Sonkar, S. K., Sustainable Changes in the Contents of Metallic Micronutrients in First Generation Gram Seeds Imposed by Carbon Nano-Onions: Life Cycle Seed to Seed Study. *ACS Sustainable Chem. Eng.* **2017**, *5*, 2906-2916.

19. Tripathi, K. M.; Kim, T.; Losic, D.; Tung, T. T., Recent Advances in Engineered Graphene and Composites for Detection of Volatile Organic Compounds (VOCs) and Non-Invasive Diseases Diagnosis. *Carbon* **2016**, *110*, 97-129.

20.   Gupta, S. S.; Sreeprasad, T. S.; Maliyekkal, S. M.; Das, S. K.; Pradeep, T., Graphene from Sugar and Its Application in Water Purification. *ACS Appl. Mater. Interfaces* **2012**, *4*, 4156-4163.

21.   Costas-Mora, I.; Romero, V.; Lavilla, I.; Bendicho, C., Luminescent Assays Based on Carbon Dots for Inorganic Trace Analysis. *Rev. Anal. Chem.* **2015**, *34*, 61-76.

22.   Shen, J.; Zhu, Y.; Yang, X.; Li, C., Graphene Quantum Dots: Emergent Nanolights for Bioimaging, Sensors, Catalysis and Photovoltaic Devices. *Chem. Commun.* **2012**, *48*, 3686-3699.

23.   Sonkar, S. K.; Ghosh, M.; Roy, M.; Begum, A.; Sarkar, S., Carbon Nano-Onions as Nontoxic and High-Fluorescence Bioimaging Agent in Food Chain-an *in vivo* Study from Unicellular *E. coli* to Multicellular *C. elegans*. *Mater. Express* **2012**, *2*, 105-114.

24.   Tripathi, K. M.; Sonker, A. K.; Bhati, A.; Bhuyan, J.; Singh, A.; Singh, A.; Sarkar, S.; Sonkar, S. K., Large-Scale Synthesis of Soluble Graphitic Hollow Carbon Nanorods with Tunable Photoluminescence for the Selective Fluorescent Detection of DNA. *New J. Chem.* **2016**, *40*, 1571-1579.

25.   Tripathi, K. M.; Singh, A.; Bhati, A.; Sarkar, S.; Sonkar, S. K., Sustainable Feasibility of the Environmental Pollutant Soot to Few-Layer Photoluminescent Graphene Nanosheets for Multifunctional Applications. *ACS Sustainable Chem. Eng.* **2016**, *4*, 6399-6408.

26.   Basu, A.; Suryawanshi, A.; Kumawat, B.; Dandia, A.; Guin, D.; Ogale, S. B., Starch (*Tapioca*) to Carbon Dots: An Efficient Green Approach to an on-off-on Photoluminescence Probe for Fluoride Ion Sensing. *Analyst* **2015**, *140*, 1837-1841.

27.   Tripathi, K. M.; Sonker, A. K.; Sonkar, S. K.; Sarkar, S., Pollutant Soot of Diesel Engine Exhaust Transformed to Carbon Dots for Multicoloured Imaging of *E. coli* and Sensing Cholesterol. *RSC Adv.* **2014**, *4*, 30100-30107.

28.   Tripathi, K. M.; Bhati, A.; Singh, A.; Gupta, N. R.; Verma, S.; Sarkar, S.; Sonkar, S. K., From the Traditional Way of Pyrolysis to Tunable Photoluminescent Water Soluble Carbon Nano-Onions for Cell Imaging and Selective Sensing of Glucose. *RSC Adv.* **2016**, *6*, 37319-37329.

29. Tripathi, K. M.; Singh, A.; Myung, Y.; Kim, T.; Sonkar, S. K., Sustainable Nanocarbons as Potential Sensor for Safe Water. *In Nanotechnology for Sustainable Water Resources*, **2018**, 141-176.

30. Titirici, M.-M.; White, R. J.; Brun, N.; Budarin, V. L.; Su, D. S.; del Monte, F.; Clark, J. H.; MacLachlan, M. J., Sustainable Carbon Materials. *Chem. Soc. Rev.* **2015,** *44*, 250-290.

31. Tripathi, K. M.; Tyagi, A.; Ashfaq, M.; Gupta, R. K., Temperature Dependent, Shape Variant Synthesis of Photoluminescent and Biocompatible Carbon Nanostructures from Almond Husk for Applications in Dye Removal. *RSC Adv.* **2016**, *6* , 29545-29553.

32. Titirici, M. M.; Antonietti, M., Chemistry and Materials Options of Sustainable Carbon Materials Made by Hydrothermal Carbonization. *Chem. Soc. Rev.* **2010**, *39*, 103-116.

33. Hu, B.; Wang, K.; Wu, L.; Yu, S. H.; Antonietti, M.; Titirici, M. M., Engineering Carbon Materials from the Hydrothermal Carbonization Process of Biomass. *Adv. Mater.* **2010**, *22*, 813-828.

34. Dubey, P.; Tripathi, K. M.; Sonkar, S. K., Gram Scale Synthesis of Green Fluorescent Water-Soluble Onion-Like Carbon Nanoparticles from Camphor and Polystyrene Foam. *RSC Adv.* **2014**, *4* , 5838-5844.

35. Sonkar, S. K.; Roy, M.; Babar, D. G.; Sarkar, S., Water Soluble Carbon Nano-Onions from Wood Wool as Growth Promoters for Gram Plants. *Nanoscale* **2012**, *4*, 7670-7675.

36. Suriani, A. B.; Alfarisa, S.; Mohamed, A.; Isa, I. M.; Kamari, A.; Hashim, N.; Mamat, M. H.; Mohamed, A. R.; Rusop, M., Quasi-Aligned Carbon Nanotubes Synthesised from Waste Engine Oil. *Mater. Lett.* **2015**, *139*, 220-223.

37. Quan, C.; Li, A.; Gao, N., Synthesis of Carbon Nanotubes and Porous Carbons from Printed Circuit Board Waste Pyrolysis Oil. *J. Hazard. Mater.* **2010**, *179*, 911-917.

38. Mishra, N.; Das, G.; Ansaldo, A.; Genovese, A.; Malerba, M.; Povia, M.; Ricci, D.; Fabrizio, E. D.; Zitti, E. D.; Sharon, M.; Sharon, M., Pyrolysis of Waste Polypropylene for the Synthesis of Carbon Nanotubes. *J. Analytic. Appl. Pyrolysis* **2012**, *94*, 91-98.

39. Wu, C.; Nahil, M. A.; Miskolczi, N.; Huang, J.; Williams, P. T., Processing Real-World Waste Plastics by Pyrolysis-Reforming for Hydrogen and High-Value Carbon Nanotubes. *Environ. Sci. Technol.* **2014**, *48*, 819-826.

40. Pol, V. G.; Thiyagarajan, P., Remediating Plastic Waste into Carbon Nanotubes. *J. Environ. Monit.* **2010**, *12*, 455-459.

41. Saleh, T. A.; Gupta, V. K., Processing Methods, Characteristics and Adsorption Behavior of Tire Derived Carbons: A Review. *Adv. Colloid Interface Sci.* **2014**, *211*, 93-101.

42. Wang, X.; Zhang, Y.; Zhi, C.; Wang, X.; Tang, D.; Xu, Y.; Weng, Q.; Jiang, X.; Mitome, M.; Golberg, D.; Bando, Y., Three-Dimensional Strutted Graphene Grown by Substrate-Free Sugar Blowing for High-Power-Density Supercapacitors. *Nat. Commun.* **2013**, *4*, 2905.

43. Ruiz-Hitzky, E.; Darder, M.; Fernandes, F. M.; Zatile, E.; Palomares, F. J.; Aranda, P., Supported Graphene from Natural Resources: Easy Preparation and Applications. *Adv. Mater.* **2011**, *23*, 5250-5255.

44. Wang, H.; Xu, Z.; Kohandehghan, A.; Li, Z.; Cui, K.; Tan, X.; Stephenson, T. J.; King'ondu, C. K.; Holt, C. M. B.; Olsen, B. C.; Tak, J. K.; Harfield, D.; Anyia, A. O.; Mitlin, D., Interconnected Carbon Nanosheets Derived from Hemp for Ultrafast Supercapacitors with High Energy. *ACS Nano* **2013**, *7*, 5131-5141.

45. Muramatsu, H.; Kim, Y. A.; Yang, K. S.; Cruz-Silva, R.; Toda, I.; Yamada, T.; Terrones, M.; Endo, M.; Hayashi, T.; Saitoh, H., Rice Husk-Derived Graphene with Nano-Sized Domains and Clean Edges. *Small* **2014**, *10*, 2766-2770.

46. Chen, F.; Yang, J.; Bai, T.; Long, B.; Zhou, X., Facile Synthesis of Few-Layer Graphene from Biomass Waste and its Application in Lithium Ion Batteries. *J. Electroanal. Chem.* **2016**, *768*, 18-26.

47. Purkait, T.; Singh, G.; Singh, M.; Kumar, D.; Dey, R. S., Large Area Few-Layer Graphene with Scalable Preparation from Waste Biomass for High-Performance Supercapacitor. *Sci. Rep.* **2017**, *7*, 15239.

24

48. Sun, L.; Tian, C.; Li, M.; Meng, X.; Wang, L.; Wang, R.; Yin, J.; Fu, H., From Coconut Shell to Porous Graphene-Like Nanosheets for High-Power Supercapacitors. *J. Mater. Chem. A* **2013**, *1*, 6462-6470.

49. Zhou, H.; Zhang, J.; Amiinu, I. S.; Zhang, C.; Liu, X.; Tu, W.; Pan, M.; Mu, S., Transforming Waste Biomass with an Intrinsically Porous Network Structure into Porous Nitrogen-Doped Graphene for Highly Efficient Oxygen Reduction. *Phys. Chem. Chem. Phys.* **2016**, *18*, 10392-10399.

50. Kumar, S.; Singh, V. P.; Vaish, R. Waste Paper Pulp Derived Reduced Graphene Oxide for Antimicrobial Cement Composites, *J. Electron. Mater.* **2018**, *47*, 6862-6867.

51. Dubey, P.; Tripathi, K. M.; Mishra, R.; Bhati, A.; Singh, A.; Sonkar, S. K., A Simple One-Step Hydrothermal Route Towards Water Solubilization of Carbon Quantum Dots from Soya-Nuggets for Imaging Applications. *RSC Adv.* **2015**, *5*, 87528-87534.

52. Babu, D. B.; Ramesha, K., Melamine Assisted Liquid Exfoliation Approach for the Synthesis of Nitrogen Doped Graphene-Like Carbon Nano Sheets from Bio-Waste Bagasse Material and its Application towards High Areal Density Li-S batteries. *Carbon* **2019**, *144*, 582-590.

53. Tripathi, K. M.; Tran, T. S.; Tung, T. T.; Losic, D.; Kim, T., Water Soluble Fluorescent Carbon Nanodots from Biosource for Cells Imaging. *J. Nanomater.* **2017**, *2017*, 7029731.

54. Raghavan, N.; Thangavel, S.; Venugopal, G., A Short Review on Preparation of Graphene from Waste and Bioprecursors. *Appl. Mater. Today* **2017**, *7*, 246-254.

55. Sahu, V.; Grover, S.; Tulachan, B.; Sharma, M.; Srivastava, G.; Roy, M.; Saxena, M.; Sethy, N.; Bhargava, K.; Philip, D.; Kim, H.; Singh, G.; Singh, S. K.; Das, M.; Sharma, R. K., Heavily Nitrogen Doped, Graphene Supercapacitor from Silk Cocoon. *Electrochim. Acta.* **2015**, *160*, 244-253.

56. Roy, M.; Dubey, A.; Singh, S. K.; Bhargava, K.; Sethy, N. K.; Philip, D.; Sarkar, S.; Bajpai, A.; Das, M., Soft Magnetic Memory of Silk Cocoon Membrane. *Sci. Rep.* **2016**, *6*, 29214.

57. Zhao, H.; Zhao, T. S., Graphene Sheets Fabricated from Disposable Paper Cups as a Catalyst Support Material for Fuel Cells. *J. Mater. Chem. A* **2013**, *1*, 183-187.

58. Ruan, G.; Sun, Z.; Peng, Z.; Tour, J. M., Growth of Graphene from Food, Insects, and Waste. *ACS Nano* **2011**, *5*, 7601-7607.

59. Park, S. Y.; Lee, H. U.; Park, E. S.; Lee, S. C.; Lee, J.-W.; Jeong, S. W.; Kim, C. H.; Lee, Y.-C.; Huh, Y. S.; Lee, J., Photoluminescent Green Carbon Nanodots from Food-Waste-Derived Sources: Large-Scale Synthesis, Properties, and Biomedical Applications. *ACS Appl Mater Interfaces* **2014**, *6*, 3365-3370.

60. Purkayastha, M. D.; Manhar, A. K.; Mandal, M.; Mahanta, C. L., Industrial Waste-Derived Nanoparticles and Microspheres Can Be Potent Antimicrobial and Functional Ingredients. *J. Appl. Chem.* **2014**, *2014*, 171427.

61. Kumar, A.; Hegde, G.; Manaf, S. A. B. A.; Ngainic, Z.; Sharma, K. V., Catalyst Free Silica Templated Porous Carbon Nanoparticles from Bio-Waste Materials. *Chem. Commun.* **2014**, *50*, 12702-12705.

62. Qiu, J.; Chen, G.; Li, Z.; Zhao, Z., Preparation of Double-Walled Carbon Nano-Tubes from Fullerene Waste Soot by Arc-Discharge. *Carbon* **2010**, *48*, 1312-1315.

63. Dunens, O. M.; MacKenzie, K. J.; Harris, A. T., Synthesis of Multiwalled Carbon Nanotubes on Fly Ash Derived Catalysts. *Environ. Sci. Technol.* **2009**, *43*, 7889-7894.

64. Dubey, P.; Sonkar, S. K.; Majumder, S.; Tripathi, K. M.; Sarkar, S., Isolation of Water Soluble Carbon Nanotubes with Network Structure Possessing Multipodal Junctions and Its Magnetic Property. *RSC Adv.* **2013**, *3*, 7306-7312.

65. Tang, J.; Mu, B.; Zheng, M.; Wang, A., One-Step Calcination of the Spent Bleaching Earth for the Efficient Removal of Heavy Metal Ions. *ACS Sustainable Chem. Eng.* **2015**, *3*, 1125-1135.

66. Aragay, G.; Pons, J.; Merkoçi, A., Recent Trends in Macro-, Micro-, and Nanomaterial-Based Tools and Strategies for Heavy-Metal Detection. *Chem. Rev.* **2011**, *111*, 3433-3458.

67. Guo, Y.; Zhang, L.; Zhang, S.; Yang, Y.; Chen, X.; Zhang, M., Fluorescent Carbon Nanoparticles for the Fluorescent Detection of Metal Ions. *Biosens. Bioelectron.* **2015**, *63*, 61-71.

68. Tan, X. W.; Romainor, A. N. B.; Chin, S. F.; Ng, S. M., Carbon Dots Production *via* Pyrolysis of Sago Waste as Potential Probe for Metal Ions Sensing. *Anal. Appl. Pyrolysis* **2014**, *105*, 157-165.

69. Tchounwou, P. B.; Ayensu, W. K.; Ninashvili, N.; Sutton, D., Environmental Exposure to Mercury and Its Toxicopathologic Implications for Public Health. *Environ. Toxicol.* **2003**, *18*, 149-175.

70. Lu, W.; Qin, X.; Liu, S.; Chang, G.; Zhang, Y.; Luo, Y.; Asiri, A. M.; Al-Youbi, A. O.; Sun, X., Economical, Green Synthesis of Fluorescent Carbon Nanoparticles and their use as Probes for Sensitive and Selective Detection of Mercury(II) Ions. *Anal. Chem.* **2012**, *84*, 5351-5357.

71. Tripathi, K. M.; Tran, T. S.; Kim, Y. J.; Kim, T., Green Fluorescent Onion-Like Carbon Nanoparticles from Flaxseed Oil for Visible Light Induced Photocatalytic Applications and Label-Free Detection of Al(III) Ions. *ACS Sustainable Chem. Eng.* **2017**, *5*, 3982-3992.

72. Tyagi, A.; Tripathi, K. M.; Singh, N.; Choudhary, S.; Gupta, R. K., Green Synthesis of Carbon Quantum Dots from Lemon Peel Waste: Applications in Sensing and Photocatalysis. *RSC Adv.* **2016**, *6*, 72423-72432.

73. Zhitkovich, A., Chromium in Drinking Water: Sources, Metabolism, and Cancer Risks. *Chem. Res. Toxicol.* **2011**, *24*, 1617-1629.

74. Pejcic, B.; Myers, M.; Ross, A., Mid-Infrared Sensing of Organic Pollutants in Aqueous Environments. *Sensors* **2009**, *9*, 6232-6253.

75. Sun, R.; Wang, Y.; Ni, Y.; Kokot, S., Graphene Quantum Dots and the Resonance Light Scattering Technique for Trace Analysis of Phenol in Different Water Samples. *Talanta* **2014**, *125*, 341-346.

76. Mohanty, K.; Jha, M.; Meikap, B. C.; Biswas, M. N., Preparation and Characterization of Activated Carbons from *Terminalia arjuna* Nut with Zinc Chloride Activation for the Removal of Phenol from Wastewater. *Ind. Eng. Chem. Res.* **2005**, *44*, 4128-4138.

77. Li, J.; Wang, N.; Tran.T, T.; Huang, C.; Chen, L.; Yuan, L.; Zhou, L.; Shen, R.; Cai, Q., Electrogenerated Chemiluminescence Detection of Trace Level Pentachlorophenol Using Carbon Quantum Dots. *Analyst* **2013**, *138*, 2038-2043.

78. Putri, L. K.; Ong, W.-J.; Chang, W. S.; Chai, S.-P., Heteroatom Doped Graphene in Photocatalysis: A Review. *Appl. Surf. Sci.* **2015**, *358*, 2-14.

79. Zhang, J.; Xiong, Z.; Zhao, X. S., Graphene-Metal-Oxide Composites for the Degradation of Dyes under Visible Light Irradiation. *J. Mater. Chem.* **2011**, *21*, 3634-3640.

80. Boruah, P. K.; Szunerits, S.; Boukherroub, R.; Das, M. R., Magnetic $Fe_3O_4@V_2O_5$/RGO Nanocomposite as a Recyclable Photocatalyst for Dye Molecules Degradation under Direct Sunlight Irradiation. *Chemosphere* **2018**, *191*, 503-513.

81. Tang, B.; Chen, H.; Peng, H.; Wang, Z.; Huang, W., Graphene Modified TiO_2 Composite Photocatalysts: Mechanism, Progress and Perspective. *Nanomaterials* **2018**, *8*, 105.

82. Gayathri, S.; Jayabal, P.; Kottaisamy, M.; Ramakrishnan, V., Synthesis of the Graphene-$ZnTiO_3$ Nanocomposite for Solar Light Assisted Photodegradation of Methylene Blue. *J. Phys. D: Appl. Phys.* **2015**, *48*, 415305-415315

83. Umrao, S.; Sharma, P.; Bansal, A.; Sinha, R.; Singh, R. K.; Srivastva, A., Multi-Layered Graphene Quantum Dots Derived Photodegradation Mechanism of Methylene Blue. *RSC Adv.* **2015**, *5*, 51790-51798.

84. Jiao, T.-F.; Zhao, H.; Zhou, J.; Zhang, Q.; Luo, X.; Hu, J.; Peng, Q.; Yan, X., The Self-Assembly Reduced Graphene Oxide Nanosheet Hydrogel Fabrication by Anchorage of Chitosan/Silver and Its Potential Efficient Application toward Dyes Degradation for Wastewater Treatments. *ACS Sustainable Chem. Eng.* **2015**, *3*, 3130-3139.

85. Gan, L.; Xu, L.; Shang, S.; Zhou, X.; Meng, L., Visible Light Induced Methylene Blue Dye Degradation Photo-Catalyzed by WO$_3$/Graphene Nanocomposites and the Mechanism. *Ceram. Int.* **2016**, *42*, 15235-15241.

86. Zhao, Y.; Zhang, Y.; Liu, A.; Wei, Z.; Liu, S., Construction of Three-Dimensional Hemin-Functionalized Graphene Hydrogel with High Mechanical Stability and Adsorption Capacity for Enhancing Photodegradation of Methylene Blue. *ACS Appl. Mater. Interfaces* **2017**, *9*, 4006-4014.

87. Wei, G.; Miao, Y.-E.; Zhang, C.; Yang, Z.; Liu, Z.; Tjiu, W. W.; Liu, T., Ni-Doped Graphene/Carbon Cryogels and Their Applications as Versatile Candidates for Water Purification. *ACS Appl Mater Interfaces* **2013**, *14*, 7584-7591.

88. Shen, H.; Zhao, X.; Duan, L.; Liu, R.; Wu, H.; Hou, T.; Jiang, X.; Gao, H., Influence of Interface Combination of RGO-Photosensitized SnO$_2$@RGO Core-Shell Structures on their Photocatalytic Performance. *Appl. Surf. Sci.* **2017**, *391*, 627-634.

89. Shanmugam, M.; Alsalme, A.; Alghamdi, A.; Jayavel, R., Photocatalytic Properties of Graphene-SnO$_2$-PMMA Nanocomposite in the Degradation of Methylene Blue Dye under Direct Sunlight Irradiation. *Mater. Express* **2015**, *5*, 319-326.

90. Gupta, A. K.; Pal, A.; Sahoo, C., Photocatalytic Degradation of a Mixture of Crystal Violet (Basic Violet 3) and Methyl Red Dye in Aqueous Suspensions Using Ag$^+$ Doped TiO$_2$. *Dyes Pigm.* **2006**, *69*, 224-232.

91. Sahoo, P. K.; Thakur, D.; Bahadur, D.; Panigrahy, B., Highly Efficient and Simultaneous Catalytic Reduction of Multiple Dyes Using Recyclable RGO/Co Dendritic Nanocomposites as Catalyst for Wastewater Treatment. *RSC Adv.* **2016**, *6*, 106723-106731.

92. Mosleh, S.; Rahimi, M. R.; Ghaedi, M.; Dashtian, K.; Hajati, S., Photocatalytic Degradation of Binary Mixture of Toxic Dyes by HKUST-1 MOF and HKUST-1-SBA-15 in a Rotating Packed Bed Reactor under Blue Led Illumination: Central Composite Design Optimization. *RSC Adv.* **2016**, *6*, 17204-17214.

93. Moitra, D.; Chandel, M.; Ghosh, B. K.; Jani, R. K.; Patra, M. K.; Vadera, S. R.; Ghosh, N. N., A Simple 'in situ' Co-Precipitation Method for the Preparation of Multifunctional $CoFe_2O_4$-Reduced Graphene Oxide Nanocomposites: Excellent Microwave Absorber and Highly Efficient Magnetically Separable Recyclable Photocatalyst for Dye Degradation. *RSC Adv.* **2016**, *6*, 76759-76772.

94. Gao, L.; Wang, Y.; Yan, T.; Cui, L.; Hu, L.; Yan, L.; Wei, Q.; Du, B., A Novel Magnetic Polysaccharide-Graphene Oxide Composite for Removal of Cationic Dyes from Aqueous Solution. *New J. Chem.* **2015**, *39*, 2908-2916.

95. Guo, R.; Jiao, T.; Li, R.; Chen, Y.; Guo, W.; Zhang, L.; Zhou, J.; Zhang, Q.; Peng, Q., Sandwiched Fe_3O_4/Carboxylate Graphene Oxide Nanostructures Constructed by Layer-by-Layer Assembly for Highly Efficient and Magnetically Recyclable Dye Removal. *ACS Sustainable Chem. Eng.* **2018**, *6*, 1279-1288.

96. Jacobson, M. Z., Control of Fossil-Fuel Particulate Black Carbon and Organic Matter, Possibly the Most Effective Method of Slowing Global Warming. *J. Geophys. Res.* **2002**, *107*, 4410-4431.

97. Ramanathan, V.; Carmichael, G., Global and Regional Climate Changes Due to Black Carbon. *Nat. Geosci.* **2008**, *1*, 221-227.

98. Kopp, R. E.; Mauzerall, D. L., Assessing the Climatic Benefits of Black Carbon Mitigation. *PNAS* **2010**, *107*, 11703-11708.

99. Kelly, F. J.; Fussell, J. C., Air Pollution and Public Health: Emerging Hazards and Improved Understanding of Risk. Environ. *Geochem. Health* **2015**, *37*, 631-649.

100. Wang, Q.; Zhang, S. R., Size Separation of Carbon Nanoparticles from Diesel Soot for Mn(II) Sensing. *J. Lumin.* **2014**, *146*, 37-41.

101. Uchida, T.; Ohashi, O.; Kawamoto, H.; Yoshimura, H.; Kobayashi, K.; Tanimura, M.; Fujikawa, N.; Nishimoto, T.; Awata, K.; Tachibana, M.; Kojima, K., Synthesis of Single-Wall Carbon Nanotubes from Diesel Soot. *Jpn. J. Appl. Phys.* **2006**, *45*, 8027-8029.

102. Tripathi, K. M.; Gupta, N. R.; Sonkar, S. K., Nano-Carbons from Pollutant Soot: A Cleaner Approach toward Clean Environment. In *Smart Materials for Waste Water Applications*, **2016**, *1*, 127-153.

103. Lee, T. H.; Yao, N.; Chen, T. J.; Hsu, W. K., Fullerene-Like Carbon Particles in Petrol Soot. *Carbon* **2002**, *40*, 2275-2279.

104. Iijima, S., Helical Microtubules of Graphitic Carbon. *Nature* **1991**, *354*, 56-58.

105. Liu, Y.; Hu, W.; Wang, X.; Long, C.; Zhang, J.; Zhu, D.; Tang, D.; Xie, S., Carbon Nanorods. *Chem. Phys. Lett.* **2000**, *331*, 31-34.

106. Chen, K. H.; Wu, C. T.; Hwang, J. S.; Wen, C. Y.; Chen, L. C.; Wang, C. T.; Ma, K. J., Electron Beam Induced Formation of Carbon Nanorods. *J. Phys. Chem. Solids* **2001**, *62*, 1561-1565.

107. Chang, Y.-H.; Chiu, H.-T.; Wang, L.-S.; Wan, C.-Y.; Peng, C.-W.; Lee, C.-Y., Synthesis of sp^2 Carbon Nano- and Microrods with Novel Structure and Morphology. *J. Mater. Chem.* **2003**, *13*, 981-982.

108. Woo, Y. S.; Jeon, D. Y.; Han, I. T.; Park, Y. J.; Kim, H. J.; Jung, J. E.; Kim, J. M.; Lee, N. S., Structural Characteristics of Carbon Nanorods and Nanotubes Grown Using Electron Cyclotron Resonance Chemical Vapor Deposition. *J. Appl. Phys.* **2003**, *94*, 6789-6795.

109. Wang, B. B.; Ostrikov, K.; van der Laan, T.; Zheng, K.; Wang, J. J.; Yan, Y. P.; Quan, X. J., Carbon Nanorods and Graphene-Like Nanosheets by Hot Filament CVD: Growth Mechanisms and Electron Field Emission. *J. Mater. Chem. C.* **2013**, *1*, 7703-7708.

110. Ritikos, R.; Rahman, S. A.; Gani, S. M. A.; Muhamad, M. R.; Yap, Y. K., Catalyst-Free Formation of Vertically-Aligned Carbon Nanorods as Induced by Nitrogen Incorporation. *Carbon* **2011**, *49*, 1842-1848.

111. Thiên-Nga, L.; Hernadi, K.; Forró, L., Catalytic Growth of Carbon Nanorods on a High-Tc Substrate. *Adv. Mater.* **2001**, *13*, 148-150.

112. Li, Y.; Qiu, J.; Wang, Y.; Zhang, H., Novel Iron-Decorated Carbon Nanorods from Fullerene Soot. *Chem. Commun.* **2004**, 656-657.

113. Wang, X.; Lu, J.; Xie, Y.; Du, G.; Guo, Q.; Zhang, S., A Novel Route to Multiwalled Carbon Nanotubes and Carbon Nanorods at Low Temperature. *J. Phys. Chem. B* **2002**, *106*, 933-937.

114. Zhu, T.; Chen, J. S.; Lou, X. W., Glucose-Assisted One-Pot Synthesis of FeOOH Nanorods and Their Transformation to Fe_3O_4@Carbon Nanorods for Application in Lithium Ion Batteries. *J. Phys. Chem. C* **2011**, *115*, 9814-9820.

115. Zou, G.; Lu, J.; Wang, D.; Xu, L.; Qian, Y., High-Yield Carbon Nanorods Obtained by a Catalytic Copyrolysis Process. *Inorg. Chem.* **2004**, *43*, 5432-5435.

116. Wan, S.; Wang, L.; Xue, Q., Electrodeposition of Nitrogenated Carbon Nanorods by a Facile Electrochemical Method: Microstructure and the Growing Process. *Electrochem. Solid-State Lett.* **2010**, *13*, K89-K92.

117. Li, M.; Xue, J., Ordered Mesoporous Carbon Nanoparticles with Well-Controlled Morphologies from Sphere to Rod *via* a Soft-Template Route. *J Colloid and Interface Sci.* **2012**, *377*, 169-175.

118. Yu, H.; Zhang, Q.; Joo, J. B.; Li, N.; Moon, G. D.; Tao, S.; Wang, L.; Yin, Y., Porous Tubular Carbon Nanorods with Excellent Electrochemical Properties. *J. Mater. Chem. A* **2013**, *1*, 12198-12205.

119. Xia, Y.; Yang, Z.; Mokaya, R., Simultaneous Control of Morphology and Porosity in Nanoporous Carbon: Graphitic Mesoporous Carbon Nanorods and Nanotubules with Tunable Pore Size. *Chem. Mater.* **2006**, *18*, 140-148.

120. Orikasa, H.; Akahane, T.; Okada, M.; Tong, Y.; Ozaki, J.-i.; Kyotani, T., Electrochemical Behavior of Carbon Nanorod Arrays Having Different Graphene Orientations and Crystallinity. *J. Mater. Chem.* **2009**, *19*, 4615-4621.

121. Iijima, S.; Ichihashi, T., Single-Shell Carbon Nanotubes of 1-nm Diameter. *Nature* **1993**, *363*, 603-605.

122. Kroto, H. W.; Sheath, J. R.; O'Brien, S. C.; Curl, R. F.; Smalley, R. E., C_{60} - Buckminsterfullerene. *Nature* **1985**, *318*, 162-163.

123. Guldi, D. M.; Illescas, B. M.; Atienza, C. M.; Wielopolski, M.; Martin, N., Fullerene for Organic Electronics. *Chem. Soc. Rev.* **2009**, *38*, 1587-1597.

124. Ugarte, D., Curling and Closure of Graphitic Networks under Electron-Beam Irradiation. *Nature* **1992**, *359*, 707-709.

125. Ghosh, M.; Sonkar, S. K.; Saxena, M.; Sarkar, S., Carbon Nano-Onions for Imaging the Life Cycle of *Drosophila melanogaster. Small* **2011**, *7*, 3170-3177.

126. Jiang, J.; Zhu, J.; Ai, W.; Fan, Z.; Shen, X.; Zou, C.; Liu, J.; Zhang, H.; Yu, T., Evolution of Disposable Bamboo Chopsticks into Uniform Carbon Fibers: A Smart Strategy to Fabricate Sustainable Anodes for Li-Ion Batteries. *Energy Environ. Sci.* **2014**, *7*, 2670-2679.

127. Novoselov, K. S.; Geim, A. K.; Morozov, S. V.; Jiang, D.; Zhang, Y.; Dubonos, S. V.; Grigorieva, I. V.; Firsov, A. A., Electric Field Effect in Atomically Thin Carbon Films. *Science* **2004**, *306*, 666-669.

128. Geim, A. K., Graphene: Status and Prospects. *Science* **2009**, *324*, 1530-1534.

129. Zhang, Z.; Zhang, J.; Chen, N.; Qu, L., Graphene Quantum Dots: An Emerging Material for Energy-Related Applications and Beyond. *Energy Environ. Sci.* **2012**, *5*, 8869-8890.

130. Sun, Y.-P.; Zhou, B.; Lin, Y.; Wang, W.; Fernando, K. A. S.; Pathak, P.; Meziani, M. J.; Harruff, B. A.; Wang, X.; Wang, H.; Luo, P. G.; Yang, H.; Kose, M. E.; Chen, B.; Veca, L. M.; Xie, S.-Y., Quantum-Sized Carbon Dots for Bright and Colorful Photoluminescence. *J. Am. Chem. Soc.* **2006**, *128*, 7756-7757.

131. Chang, Y.-R.; Lee, H.-Y.; Chen, K.; Chang, C.-C.; Tsai, D.-S.; Fu, C.-C.; Lim, T.-S.; Tzeng, Y.-K.; Fang, C.-Y.; Han, C.-C.; Chang, H.-C.; Fann, W., Mass Production and Dynamic Imaging of Fluorescent Nanodiamonds. *Nat. Nanotechnol.* **2008**, *3*, 284-288.

132. Mochalin, V. N.; Shenderova, O.; Ho, D.; Gogotsi, Y., The Properties and Applications of Nanodiamonds. *Nat. Nanotechnol.* **2011**, *7*, 11-23.

133. Che, R.; Takeguchi, M.; Shimojo, M.; Furuya, K., Field Electron Emission from Single Carbon Nanorod Fabricated by Electron Beam Induced Deposition. *J. Phys. Conf. Ser.* **2007**, *61*, 200-204.

134. Wong, E. W.; Sheehan, P. E.; Lieber, C. M., Nanobeam Mechanics: Elasticity, Strength, and Toughness of Nanorods and Nanotubes. *Science* **1997**, *277*, 1971-1975.

135. Bo, X.; Zhu, L.; Wang, G.; Guo, L., Template-Free Synthesis of Rectangular Mesoporous Carbon Nanorods and Their Application as a Support for Pt Electrocatalysts. *J. Mater. Chem.* **2012**, *22*, 5758-5763.

136. Wang, N.; Hei, Y.; Liu, J.; Sun, M.; Sha, T.; Hassan, M.; Bo, X.; Guo, Y.; Zhou, M., Low-cost and Environment-Friendly Synthesis of Carbon Nanorods Assembled Hierarchical Meso-macroporous Carbons Networks Aerogels from Natural Apples for the Electrochemical Determination of Ascorbic Acid and Hydrogen Peroxide. *Analytica. Chimica. Acta.* **2019**, *1047*, 36-44.

137. Liu, X.; Pang, F.; Ge, J., Synthesis of N-Doped Mesoporous Carbon Nanorods through Nano-Confined Reaction: High-Performance Catalyst Support for Hydrogenation of Phenol Derivatives. *Chem. Asian J.* **2018**, *13*, 822-829.

138. Amiinu, I. S.; Liu, X.; Pu, Z.; Li, W.; Li, Q.; Zhang, J.; Tang, H.; Zhang, H.; Mu, S., From 3D ZIF Nanocrystals to Co-Nx/C Nanorod Array Electrocatalysts for ORR, OER, and Zn-Air Batteries. *Adv. Funct. Mater.* **2018**, *28*, 1704638.

139. Liu, G.; Yao, R.; Zhao, Y.; Wang, M.; Li, N.; Li, Y.; Bo, X.; Li, J.; Zhao, C., Encapsulation of Ni/Fe$_3$O$_4$ Heterostructures inside Onion-like N-doped Carbon Nanorods Enables Synergistic Electrocatalysis for Water Oxidation. *Nanoscale*, **2018**, *10*, 3997-4003.

140. Amiinu, I. S.; Pu, Z.; He, D.; Monestel, H.G.R.; Mu, S., Scalable Cellulose-Sponsored Functionalized Carbon Nanorods Induced by Cobalt for Efficient Overall Water Splitting. *Carbon*, **2018**, *137*, 274-281.

141. Yang, Y. W.; Liu, X.-H.; Gao, E.-P.; Feng, T.-T.; Jiang, W.-J.; Wu, J.; Jiang, H.; Sun, B., Self-template Construction of Nanoporous Carbon Nanorods from a Metal-Organic Framework for Supercapacitor Electrodes. *RSC Adv.*, **2018**, *8*, 20655-20660.

142.   Wang, Z.; Perera, W. A.; Perananthan, S.; Ferraris, J. P.; Balkus, Jr. K. J., Lanthanum Hydroxide Nanorod-Templated Graphitic Hollow Carbon Nanorods for Supercapacitors. *ACS Omega*, **2018**, *3*, 13913-13918.

143.   Yuan, D.; Yuan, X.; Zhou, S.; Zou, W.; Zhou, T., N-Doped Carbon Nanorods as Ultrasensitive Electrochemical Sensors for the Determination of Dopamine. *RSC Adv.* **2012**, *2*, 8157-8163.

Chapter – 2

Pollutant Soot derived Water Soluble Graphene Nanosheets for Sensing and Imaging Application
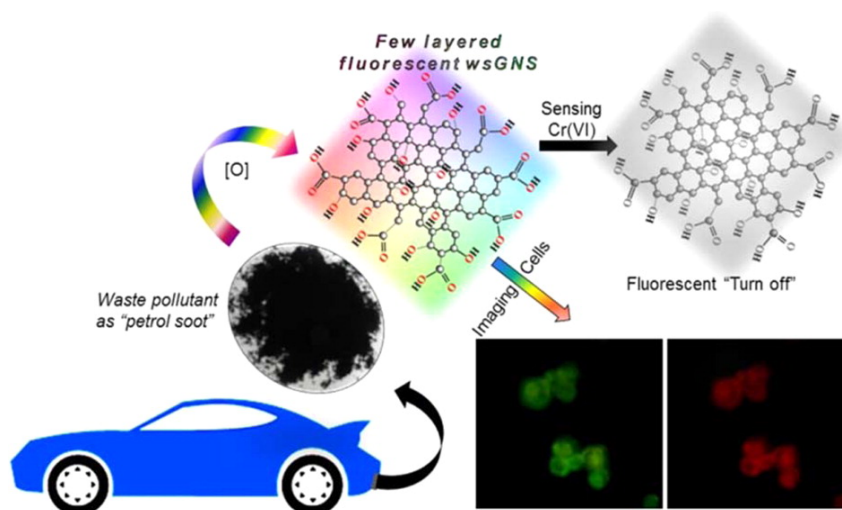
2.1   Introduction

Globally generated black particulate matter, known as BC, is recognized as a major air pollutant. Alternatively, this BC holds significant potential to be used as a free carbon precursor for the synthesis of valuable nanocarbons [1-3]. Considerable efforts and evidence of the role of air pollution caused by BC and its adverse impacts on the radiation budget of Earth have been documented [4]. To prevent its negative impacts, the quantity of BC should be decreased alternatively by its utilization in value-added products. To provide a clean environment along with some economic benefits, waste management of BC and identifying its second-life uses can be a possible approach to the synthesis of well-developed nanocarbons [5-7]. Recently, a few groups reported the presence of graphitic nanoparticles in the pollutant waste soot of diesel [5, 6, 8, 9] and petrol engines [7], along with the prospects of its application [5, 6, 9]. For example, Uchida *et al.* synthesized SWCNT from diesel soot using a laser vaporization technique [9]. Tripathi *et al.* used diesel soot for the practical isolation of multiemissive wsCD [5] for multicolored imaging of *E.coli* and sensing cholesterol. Wang *et al.* reported the synthesis of fluorescent wsCNP [6] for the selective sensing of Mn(II). Remarkably, Tripathi *et al.* [5] and Wang *et al.* [6] did not synthesize any nanocarbons. In contrast, they synthesized only the soluble version of nanocarbons that was routinely manufactured during the burning process inside the engine chambers and discharged globally into the atmosphere as BC [6, 9, 10]. On the basis of these findings, we need to use these "freely available carbon precursors" [5-9] for the isolation of nanocarbons from pollutant soot. A few reports about the structural or nanostructural characterization of pollutant soot are also available [7, 11, 12]. The burning process in a diesel engine is very much similar to the burning of conventional hydrocarbon flames, whereas petrol engines typically need a "spark" for the ignition of fuel, which is premixed with atmospheric air [7]. Therefore, differences in morphologies of synthesized nanocarbons are expected [5, 6, 8]. Like diesel soot particulates, petrol soot particulates also cause environmental pollution [10, 13], but in comparison to diesel particulates, petrol soot particulates are a bit less harmful when they interact with the proteins of the cell membranes [10] but still cause several cardiopulmonary diseases [14].

The findings presented in this paper are associated with the isolation of GNS from the petrol soot to provide some commercial and environmental benefits. GNS are imperative and constitute a new two-dimensional (2D) macromolecule [15] that has unique and novel intrinsic properties [16]. The intrinsic atomic characteristics of GNS such as edges, stacking order, lateral size, defects [17-19], and quantum confinement effects [20] make them suitable candidates for various potential optoelectronic and biological applications such as batteries, solar cell supercapacitors [21], chemical sensors [22, 23], biological sensors [24], nanocomposites [25, 26], hydrogen storage systems [16], electromechanical resonators [27], and quantum electrical devices [28]. With regard to their synthesis, both top-down and bottom-up techniques such as CVD [29], reduction of GO [30], epitaxial growth on silicon carbide [31], exfoliation of graphite crystals [32], and, recently, microwave-assisted synthesis [33] have been exclusively developed. All existing approaches typically required multistep fabrication protocols, expensive instruments, high temperatures, toxic chemical processing steps, and sophisticated processing techniques. Other important issue restricting their long-term use are their aggregation [34] that can be overcome *via* surface modification and/or functionalization [35]. In contrast to GO, graphene did not show any PL properties unless their optical band gap can be different from zero. Either by cutting its forms into ribbons [36] or dots [37] or by destroying the integral π system *via* some chemical or physical modification [38], we used a simple oxidative treatment for implanting the high degree of surface functionalization that imparts aqueous stability along with tunable PL properties. Fluorescence-based sensing is in great demand at present, because of its operational simplicity, fast response, high sensitivity, effectiveness, and real-time monitoring potential [39, 40]. Tunable PL properties with red to NIR emissions and high quantum yields are highly desirable for the exploitation in further applications in bioimaging. Emissions in the NIR region make an advantageous "biological window" over the blue-green region of the visible spectrum because of the absence of autofluorescence, deep-tissue penetration ability, and negligible damage to healthy tissues [41].

The specific objective of this chapter is simple and economical one-step large-scale isolation and synthesis of water soluble graphene nanosheets (wsGNS) by a simple oxidative treatment of dirty dangerous pollutant petrol soot. Our specific approach is simply to isolate the nanosized crystalline graphene nanosheets (GNS) and synthesize its water-soluble version. Tunable photoluminescence properties of wsGNS was used as a fluorescence-based sensor for the selective sensing of carcinogenic Cr(VI) and imaging of HeLa cells.

Sensing of Cr(VI) is very important for both the environment and human health [42]. Deviation of Cr(VI) concentrations from normal levels increases the risk of maturity-onset diabetes, cardiovascular diseases, autoimmune diseases, and genotoxicity [43-45]. Ingestion of Cr(VI) increases the risk for stomach and respiratory cancer and tumors in the alimentary tract [45]. In addition, Cr(VI) is also responsible for mutations and chromosomal breaks that result in DNA damage, in particular Cr-DNA adducts [45]. Traditionally used detection techniques such as inductively coupled plasma mass spectrometry [46], electrochemical detection [47], and atomic absorption/emission spectroscopy [48] required expensive instruments, complicated and tedious sample preparation procedures, and large amounts of time. Identifying a simple, selective, and highly sensitive sensor for Cr(VI) detection in aqueous media at low concentrations remains a challenge. A few reports of the detection of Cr(III) by using nanocarbons as a fluorescent probe are available [49], and there is a need to explore processes for more toxic Cr(VI) ions. Among all nanocarbons, graphene/GNS could show promise as a fluorescence-based sensor because of their excellent fluorescence resonance energy transfer (FRET) capability [50]. To the best of our knowledge, there has been no report on the use of wsGNS as a fluorescence probe in an aqueous medium for the sensitive and selective detection of carcinogenic Cr(VI).

2.2   Experimental Section

2.2.1   Materials and Reagents

Petrol engine soot was collected from the exhaust gas pipes of the engines of local automobile of Jaipur, India. Acetonitrile was procured from Merck, India, nitric acid (HNO_3), pet ether and acetone from Rankem, India. Phosphate buffer

saline (PBS), paraformaldehyde, fetal bovine serum, glutamine, Dulbecco's Modified Eagle's Medium (DMEM), potassium dichromate ($K_2Cr_2O_7$), ferrous nitrate, cadmium nitrate, cobalt nitrate, lead nitrate, copper nitrate, manganese nitrate, nickel nirate, zinc nitrate, barium chloride, sodium arsenate from S. D. fine Chemicals, India. All chemicals and solvents were of analytical grade and used as obtained. All experiments and measurements were conducted in water purified through a Millipore system. All anion samples were metal nitrate salts except barium chloride, sodium arsenate, and potassium dichromate and prepared in aqueous solutions. The Cr(VI) solution was prepared from $K_2Cr_2O_7$, and other metal ions were prepared from their respective salts. HeLa cells were procured from Biological Sciences and Bioengineering Lab, IIT Kanpur, India.

2.2.2 Instrumentation

The morphology of the synthesized GNS was analyzed with a Tecnai G^2 20 (FEI) HRTEM operating at 200 kV. Samples were prepared by drying the droplet of an aqueous solution of wsGNS on a 400 mesh carbon-coated copper grid under a 100 W table lamp. FESEM in high-vacuum mode on a SUPRA 40VP FESEM (Carl Zeiss NTS GmbH, Oberkochen, Germany) microscope operated at an accelerating voltage of 10kV. The topology and thickness of wsGNS were analyzed by using a Pico SPM (Molecular Imaging) atomic force microscope. Room-temperature Raman spectra were recorded by using a WITEC model Raman spectrometer with an Ar^+ laser at an excitation wavelength of 532 nm. Thermogravimetric analysis (TGA) measurements were recorded on a Mettler thermal analyzer under an inert atmosphere at a heating rate of 10°C min^{-1}. Infrared spectra were recorded on a Bruker fourier transform infra-red (FT-IR) spectrometer (Vector, model 22) with pressed KBr pellets. Ultraviolet-visible (UV-Vis) and PL spectrometry analyses in aqueous solutions were conducted at room temperature with PerkinElmer Lamda 35 and PerkinElmer LS55 instruments, respectively. XPS was conducted in an omicron multiprobe system. The optical images of wsGNS and HeLa cells were acquired with a Leica inverted microscope (Leica DM 2500, Leica microscopy system Ltd.) under 488 nm and 532 nm band-pass filter. Powdered X-ray diffraction (p-XRD) spectra of Soxhlet-purified soot and wsGNS were recorded at room temperature (Cu

Kα radiation, scan rate of 3° min^{-1}) and recorded on a Bruker D8 Advance Series 2 powder X-ray diffractometer. Zeta potential (ζ) measurements were carried out on a Beckman Coulter Delsa Nano in aqueous medium.

2.2.3   Synthesis of wsGNS

Soxhlet-purified petrol soot was used as a free carbon precursor material to produce wsGNS. Soxhlet purification was conducted as reported previously [5] by stepwise purification from boiling solvents (acetonitrile, pet ether, and acetone sequentially) to remove unburnt organic impurities. To transform insoluble Soxhlet-purified pollutant soot into wsGNS, we adopted the primary oxidative approach using concentrated nitric acid. In a typical synthetic procedure [5], Soxhlet-purified petrol soot (∼2 g) was refluxed in concentrated nitric acid (100 mL) for 10 h, followed by a high-speed centrifugation of the resultant solution to remove the acid residues. The centrifugate was transferred for repeated evaporation on the water bath after the addition of a small amount of water (approximately seven or eight times) for the removal of traces of the nitric acid residue. The final residue was dried to obtain wsGNS in almost quantitative yield (∼81%) based on the carbon used for the oxidative treatment.

2.2.4   Detection of Hexavalent Chromium Ions

Cr(VI) detection was performed in an aqueous solution at room temperature under ambient conditions. In a typical run for the detection of metal ion, 10 μL (1 × 10^{-2} M) solutions of different metal ions were added to a 2 mL aqueous solution of wsGNS (4 × 10^{-5} g mL^{-1}). The fluorescence intensity was measured at an excitation wavelength (λ_{ex}) of 460 nm. The fluorescence intensity was recorded immediately after the addition of metal ions. The exciting slit and emission slit both were kept at 15 nm during all measurements. The sensitivity and selectivity for Cr(VI) were analyzed in triplicate.

2.2.5   Cell Imaging

HeLa cells were grown according to previously reported protocols [51, 52]. In brief, HeLa cells were seeded in a culture flask (25 cm^2) in a humidified incubator containing 5% CO_2 at 37 °C. HeLa cells were supplemented with 10% (v/v) fetal

bovine serum and 4×10^{-3} M L^{-1} glutamine in DMEM. Fresh medium containing wsGNS at a concentration of 0.25 mg mL^{-1} was added to the flask and the mixture incubated for 2 h [51]. Then, the cells were washed with PBS solution and fixed with 4 wt% paraformaldehyde followed by repeated PBS washing. Cell imaging was performed with a Leica inverted microscope under 488 nm and 532 nm band-pass filters.

2.3.   Results and Discussion

Being carbon, petrol soot (a part of BC) possesses almost the same composition as other forms of nanocarbons. The basic principle is the same, high-temperature pyrolytic carbonization, where petrol is acting as a source of carbon. Premixing of atmospheric air before burning the fuel (at a high temperature within a short period of time) leads to the fabrication of GNS. Oxidative treatment of Soxhlet-purified soot was performed under refluxing conditions for ∼10 h [5] to achieve aqueous solubility via the introduction of negative surface functionalities in the form of hydrophilic carboxylic and hydroxyl type groups [53, 54]. Moreover, the polar negative group immobilized on the surface and edge of wsGNS through stable covalent interactions causes the reduction of the level of π-π stacking between individual wsGNS due to electrostatic repulsion and leads to the aqueous stability of GNS without showing agglomeration. No sign of precipitation or coagulation appeared even after one year. Zeta potential measurements for the analysis of the surface charge that show a negative value of approximately -30 mV are known to be sufficient for the mutual repulsion between wsGNS to ensure their aqueous stability [34].

2.3.1   Absorbance, FT-IR, Raman, XPS, TGA and XRD Analysis

The aqueous solution of wsGNS displays absorption at 254 nm with a continuous decrease up to 1000 nm, which is attributed to π conjugation within the graphene sheet as described in the legend of Figure 2.1(a) [34]. The aqueous solution of wsGNS appears grayish yellow in color (inset of Figure 2.1(b), left) in daylight and displays a fluorescent green color under UV light illumination (Figure 2.1(b), right). In contrast to those produced by the previously reported methods [33], our wsGNS have aqueous stability for a longer period of time without using any

surfactants or stabilizers. In addition, the derivatization of wsGNS in terms of the degree of structural disorder (negative surface functionalities) in graphitic carbon domains, clustering of the sp^2 phases, and the number of graphene layers and edge structure was further elaborated via Raman, FT-IR, XPS, and HRTEM analysis [30, 55].
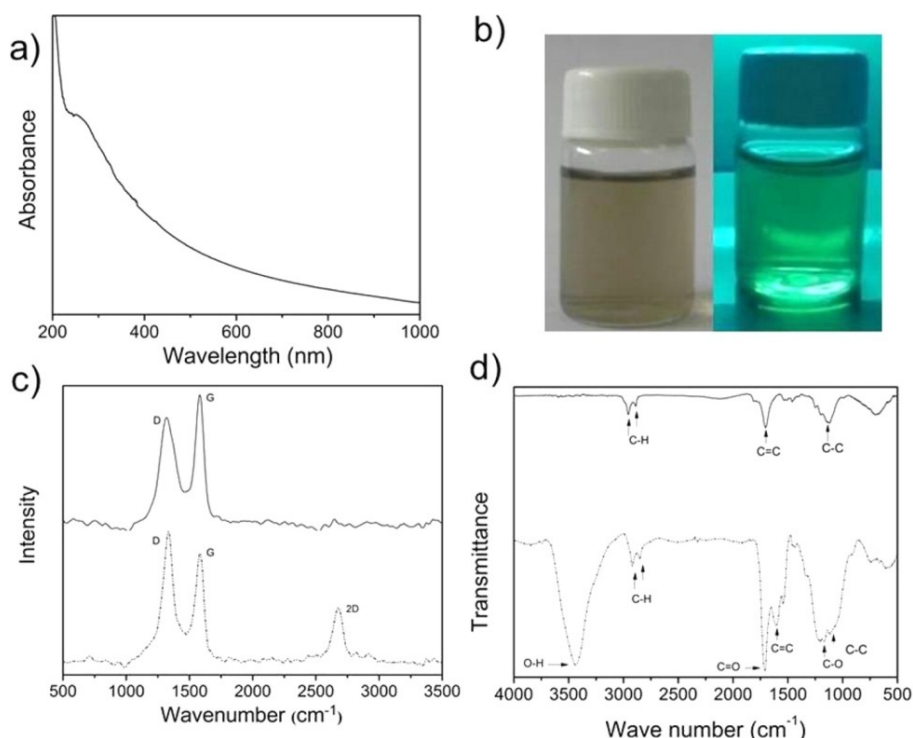
Figure 2.1. (a) Absorption spectrum of an aqueous solution of wsGNS; (b) Digital photograph showing the emission of wsGNS irradiated under daylight (left) and UV light excitation (right), after solubilization for three weeks; (c) Raman; and (d) FT-IR spectra of Soxhlet-purified petrol soot (solid line) and wsGNS (dash line).

Raman spectra of Soxhlet-purified soot (solid line) and its water-soluble version (dash line) are illustrated in Figure 2.1(c). The solid line in Figure 2.1(c) reveals the presence of two prominent characteristic peaks for graphene-based materials. G bands arise due to zone center E_{2g} mode of sp^2-hybridized carbon ($\sim$1587 cm^{-1}), and the D band is usually termed the disorder band and results from the breathing mode of κ point photons of A_{1g} symmetry for sp^3-hybridized carbon ($\sim$1336 cm^{-1}). After oxidative treatment [56], D and G bands were exaggerated and were a bit narrower in comparison to those of Soxhlet-purified soot (Figure 2.1(c), dashed line). Also, the peak intensities of the D band to those of the G band revert,

indicating the increase in the density of defects during the oxidation process. wsGNS exhibit an R value (the ratio of the integrated intensity of the D band to the integrated intensity of the G band) of 1.44, higher in comparison to that of Soxhlet-purified soot (1.31), revealing the increase in the number of sp^3 carbons in terms of surface defects as a result of oxidation-induced defects. wsGNS show the emergence of a sharp and intense 2D band at ∼2678 cm^{-1} with an intensity that significantly increases after oxidative treatment, confirming the efficient removal of amorphous type carbons and cleaning of the 2D wsGNS with high crsytallinity. Moreover, the presence of a sharp and intense 2D band at ∼2678 cm^{-1} strongly supports the growth of high-crsytallinity 2D graphene domains. The 2D bands represent an excitation energy-dependent, double-resonance-activated second-order two-photon process and are characteristic of graphitic sp^2 materials [57, 58]. The shape, peak position, and relative intensity of the 2D band are sensitive probes for the development of structural and electronic characteristics of graphene-based nanomaterials such as the number of layers, interlayer stacking, and the number of defects. The intensity of the 2D band strongly depends upon the perturbation of the electronic and photonic structure of graphene. Four successive transitions (excitation of the electron-hole pair, scattering and backscattering of the excited electron by two phonons, and electron-hole pair recombination) as a combination lead to the generation of the 2D band. With the addition of an additional layer to graphene, the number of double-resonance scattering processes increases, due to π electron interaction under interlayer stacking, and eventually the line shape becomes wider [57, 58]. The I_{2D}/I_G ratio and full width at half-maximum were ∼1.4 and ∼87, respectively. This indicated that wsGNS consisted of few layers (more than two but lesser than ten) [58-60]. These results are further confirmed by high-magnification HRTEM and AFM analysis studies described in section 2.3.2.

FT-IR results are in accordance with Raman data that support the high-density surface functionalization evidenced in comparisons to Soxhlet purified petrol soot (insoluble GNS). Figure 2.1(d) (solid line) is the FT-IR spectrum of the Soxhlet purified petrol soot that have the characteristic peaks of insoluble graphitic carbon, −C-H (doublet), −C=C, and −C-C at 2921 cm^{-1} and 2853 cm^{-1}, 1632 cm^{-1}, and 1051 cm^{-1}, respectively. Comparing to that of Soxhlet purified petrol soot, the

FT-IR spectrum of wsGNS (dashed line in Figure 2.1(d)) shows a broad absorption band at 3435 cm^{-1} attributed to the presence of −O-H stretching vibrations. A sharp absorption peak at 1712 cm^{-1} for -C=O stretching and a sharp peak at 1604 cm^{-1} indicated the presence of –C=C stretching; peaks at 1206 cm^{-1} and 1166 cm^{-1} are responsible for the −C-O and −C-C stretching vibrations, respectively. XPS analysis was used for the further investigation of these negative surface functionalities.

Figure 2.2 describes the XPS survey scan of the Soxhlet-purified petrol soot and wsGNS that support the FT-IR and Raman data. Panels (a-c) of Figure 2.2 represent the full survey scan of soxhlet purified petrol soot and its corresponding short scan for the presence of the C_{1s} peak at ∼284.3 eV and the O_{1s} peak at ∼531.7 eV. After deconvulation, a short scan survey of carbon shows the presence of C=C (284.2 eV) and a small amount of C-O (285.2 eV), and the O_{1s} short scan illustrates the C-O peak (532.2 eV). Similarly, panels (d-f) of Figure 2.2 interpret the survey scan of wsGNS, and the corresponding short scan of wsGNS confirms the presence of the C_{1s} peak at ∼284.4 eV and the O_{1s} peak at ∼532.7 eV, in the form of negative surface functionalities of wsGNS. As determined by deconvulation of the C_{1s} short scan, XPS data can easily differentiate among the different modes of carbon binding with oxygen in three distinct ways as C=C- (284 eV), −C-O- (284.8 eV), and -C=O (288.4 eV). Likewise, for O_{1s} peak, the deconvulated short scan shows the binding of oxygen with carbon as −C-O- (531.6 eV), −C=O (532.8 eV), and COO^{-} (533.7 eV) [61]. The changes in the thermal stability and composition of Soxhlet-purified soot and its water-soluble version were investigated via TGA [62].
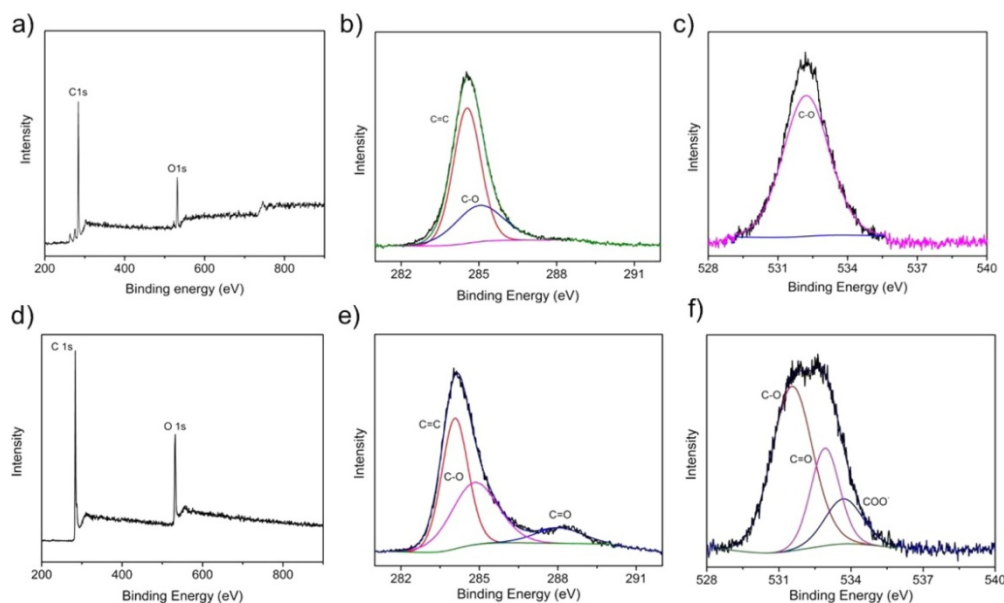
Figure 2.2. (a) XPS full scan of Soxhlet-purified petrol soot and its corresponding; (b) C_{1s} short scan; and (c) O_{1s} short scan; (d) XPS full scan of wsGNS and its corresponding; (e) C_{1s} short scan; and (f) O_{1s} short scan.

  The thermal decomposition curves for both Soxhlet-purified soot (solid line) and wsGNS (dash line) are displayed in Figure 2.3(a). The mass loss of Soxhlet-purified soot (~32.5 wt %) was smaller than that of wsGNS (~45.6 wt %) under a nitrogen atmosphere at 1400°C. The incorporation of a thermally labile oxygen functional group into wsGNS reduces their thermal stability as would be expected from acid oxidation [61]. The TGA curve clearly demonstrates the thermal stability of wsGNS; even at 1400 °C, it lost only ~45.6% of its total weight. As per our understanding, the graphene materials are conducting in nature [62]. A thin film (~10 μm) of wsGNS was prepared on a petri dish (plastic) by the evaporation of an aqueous solution of wsGNS and dried overnight at 80°C.
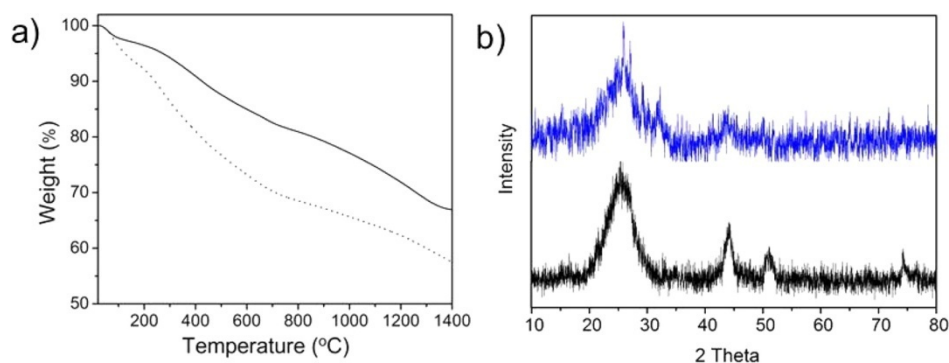
Figure 2.3. (a) TGA of Soxhlet-purified petrol soot (solid) and wsGNS (dash line); (b) Powder XRD of Soxhlet-purified petrol soot (blue) and wsGNS (black).

45

The electrical conductivity of the wsGNS film with a meaning height of 10 μm (1 cm^2) was analyzed by measuring the electrical resistivity at room temperature with a Keithley model 6517A multimeter by a two-probe method [59]. The electrical conductivity (σ) was calculated by the following equation

$$\sigma = 1/\rho$$

where ρ is the volume resistivity.

The conductivity of the wsGNS film was as high as 200 S/m without any further surface modification or doping and implies the presence of a highly conjugated network of sp^2 carbons even after the incorporation of negative surface groups.

The XRD pattern (Figure 2.3(b)) of wsGNS exhibits a slightly broad, high-intensity diffraction peak at 2θ = 25° corresponding to the (002) diffraction plane of the hexagonal lattice of sp^2 domains of few-layer graphene sheets with an interlayer spacing of 0.36 nm, which is larger than that of pristine graphite because of the intercalation of oxide functional groups and depicts the high degree of oxidation that took place and these additional small peaks at 2θ = 44°, 51°, and 74.5° that are ascribed to (100), (004), and (110) diffractions, respectively, of the hexagonal phase [63]. The diffraction peaks at 2θ = 25° and 51° were identified as characteristics of the parallel graphene layers demonstrating the crystalline nature of the compound and/or graphene sheets due to efficient removal of amorphous type carbon and formation of wsGNS with high crsytallinity, and peaks at 2θ = 44° and 74.5° correspond to the 2D in-plane symmetry along the graphene sheets [63].

2.3.2 Microscopic Studies

Morphological characterization and structural characterization of wsGNS were conducted by TEM and HRTEM. Low-resolution TEM images as shown in panels (a and b) of Figure 2.4 confirmed the presence of wsGNS with many folds and corrugations. These corrugations have an advantage with regard to the increasing surface area to volume ratio [62]. The HRTEM image shown in Figure 2.4(c) revealed the interlayer crystalline nature of wsGNS and edge showing approximately four-layer graphene sheets with the single atom electron diffraction

(SAED) pattern (inset). The HRTEM image depicted in Figure 2.4(c) also shows surface defects of wsGNS (marked with black arrows) and its interlayer d spacing, which is found to be 0.36 nm as indicated by white lines [64,65].

Panels (d-f) of Figure 2.4 show the high-magnification atomic force microscopy (AFM) images of wsGNS on a silicon substrate with its corresponding line profile image (green line in a black box) illustrating that the Z-axis depth (marked by a black bracket in Figure 2.4(e)) is ∼1.5 nm, which corresponds to the presence of approximately four layers of graphene in wsGNS. FESEM image of wsGNS Figure 2.5(a) and the lateral size distribution statistics of wsGNS were evaluated *via* FESEM as shown in Figure 2.5(b)
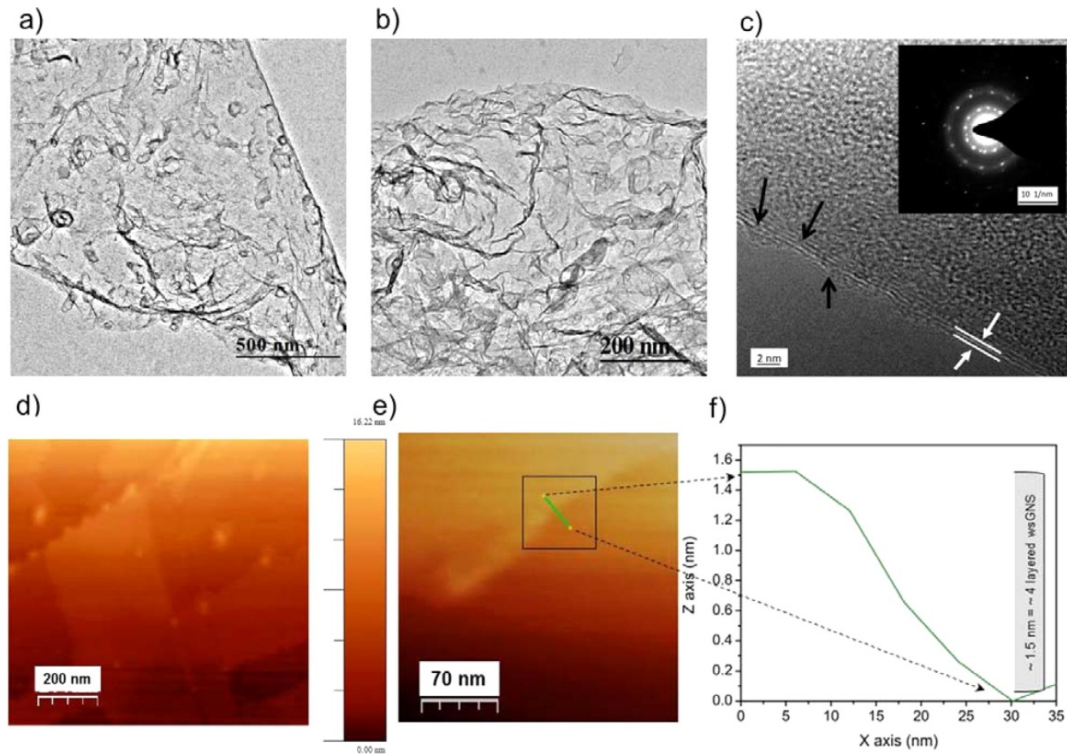
Figure 2.4. (a and b) Low-magnification TEM images of wsGNS showing the clear edges; (c) HRTEM image showing the number of graphitic sheets in wsGNS by focusing on its edge. Surface defects are denoted with black arrows, and white marks denote the interlayer distance of 0.36 nm (white arrows) along with the SAED pattern that displays its crystalline nature; (d and e) High-magnification AFM images; (f) Line profile AFM image of wsGNS (inset in a black box) illustrating the presence of approximately four layers in wsGNS.
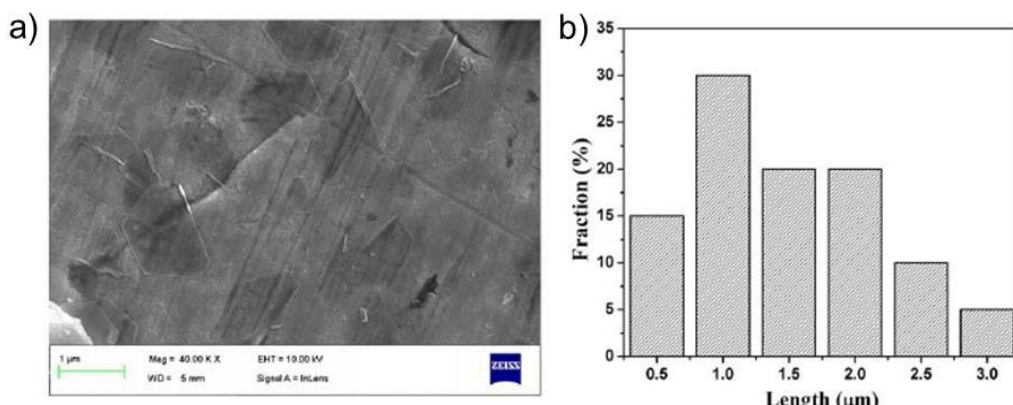
Figure 2.5. (a) FESEM image of wsGNS; (b) Lateral size distribution histogram of wsGNS.

2.3.3 Photoluminescence Emission-Excitation Study

Oxidative treatment imparts the fabricated "self-passivated" wsGNS with tunable PL properties without using any external passivation agent, such as polymers or quantum dots. In addition, the introduced solubility and long-term stability in an aqueous medium prevent irreversible agglomeration, as well [66]. Tunable PL properties were studied in detail with different excitation (λ_{ex}) wavelengths ranging from 400 nm to 660 nm within an increment of 20 nm toward the right. The series of PL emissions with a change in excitation lines are illustrated in Figure 2.6(a). In contrast to previously published reports, wsGNS exhibit tunable PL emissions (λ_{em}) emitted over a broad range of the visible region (green/red) to the NIR (Figure 2.6(b)), which is a characteristic generic feature of nanoparticles possessing a carbogenic core [15]. wsGNS show two PL excitation bands, 391 nm (3.17 eV) and 476 nm (2.64 eV), as shown in Figure 2.6(c), confirming the presence of multiple types of emitting centers located over the wsGNS. Significantly, the aqueous solution of wsGNS exhibits a high photostability as illustrated in Figure 2.6(d) the photobleaching experiment was performed for 5 h under continuous 460 nm irradiation (λ_{ex}). The PL properties and appearance of wsGNS remain unaffected without any distinct decrease in fluorescence intensity even after one year upon being stored at room temperature in a closed vessel.

Harsh oxidation generated the surface energy traps of different energy levels because the degree of oxidation is expected to be different on the basis of the

graphite arrangements of lattices and differential hybridized configurations of carbon. With respect to the excitation, these energy traps became emissive when they are excited with different wavelengths. Fluorescence microphotographs of an aqueous solution of wsGNS on the glass slide (after evaporation) under λ_{ex} of 488 nm and 532 nm excitations are shown in panels (e and f) of Figure 2.6, respectively. The most plausible mechanism for the tuning of the PL emissions with changing excitations (λ_{ex}) can be ascribed on the basis of a general photophysical mechanism based upon recombination of the electron hole [67] in association with emissive surface energy traps with properties very much similar to the PL properties of soluble carbon dots [68]. The electronic coupling between six-membered ring arrays having an oxygenous functional group and the nearby atoms of the wsGNS was responsible for the fluorescence. The tunable emissions can be ascribed on the basis of the variation of the conjugated length of the six-membered ring array, which resulted in different types of energy gaps from a ground state to an excited state. However, the exact mechanism of fluorescence emission of graphene is still a matter of discussion and needs thorough prospective investigations.
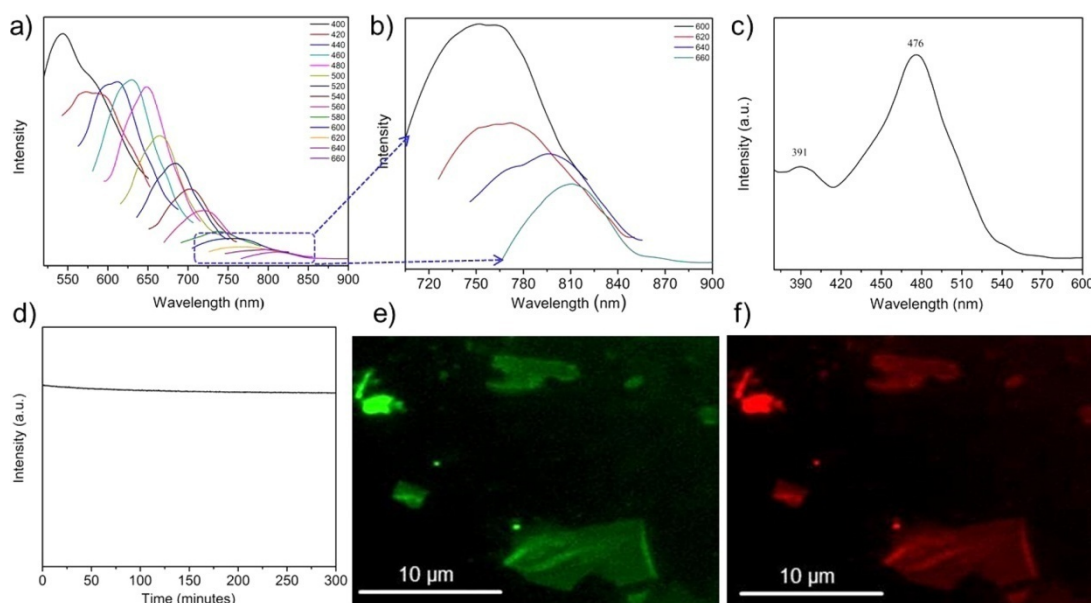
Figure 2.6. PL properties of wsGNS. (a) PL spectra recorded for λ_{ex} values from 400 to 660 nm in 20 nm continuous increments; (b) An enlarged PL spectrum in the NIR region from 600 to 660 nm; (c) PL excitation spectra at 630 nm emission; (d) PL spectrum of wsGNS at a λ_{ex} of 460 nm for 5 h; Fluorescence images of wsGNS at (e) a λ_{ex} of 488 nm; and (f) a λ_{ex} of 532 nm after evaporation of an aqueous solution on a glass slide.

Pramanik *et al.* suggested the local reorganization of the photoexcited state, intramolecular transfer of protons from hydroxyl to carboxylate anions, can be possible from two different hydroxyl moieties over the surface [69]. Few groups suggested the contribution of surface-functionalized groups and surface defects (oxidized sp^3) to the fluorescence of GNS. As a consequence, the PL properties were mainly attributed to the sp^3 domain in sp^2 matrices that are formed because of the large number of carbon atoms bonded with oxygen-containing functional groups exacting the large number of disorder-induced localized states. In carbon materials containing a mixture of sp^2 and sp^3 bonding, the transition between π and π^* states of the sp^2 sites, which lie within the σ-σ^* gap, is mainly responsible for PL as π bonding is weaker and has a lower formation energy [67,69-71].

2.3.4 Sensing of Cr(VI) Ions

The PL properties of wsGNS were further explored to determine if they could be a fluorescent probe of the selective and efficient sensing of Cr(VI). The fluorescence intensity of wsGNS at 460 nm excitation decreases gradually by the stepwise addition of Cr(VI) and was almost quenched to its maximum, the "turn off" (Figure 2.7(a)), upon addition of 100 μL of a $K_2Cr_2O_7$ [Cr(VI)] solution without altering the emission wavelength. Figure 2.7(b) describes the effect of fluorescence quenching of a wsGNS solution with different concentrations of Cr(VI), and Figure 2.7(c) shows the curve of fluorescence quenching. It also demonstrates the PL data *versus* the concentration of Cr(VI) ions in a linear correlation ($R^2 = 0.99$) over the concentration range of 0-20 mM. The detection limit based on a 3δ/slope was found to be as low as 0.51 μM in comparison with the previously reported values as shown in Table 2.1 [40, 72-77].

The selectivity of Cr(VI) ions for fluorescence quenching in comparison with those of other metal ions was evaluated. The assay response of the different metal ions (Na^+, Ba^{2+}, Mn^{2+}, Cd^{2+}, Fe^{2+}, Fe^{3+}, As^{3+}, Ni^{2+}, Pb^{2+}, Co^{2+}, Cu^{2+}, and Zn^{2+}) at the same concentration (1×10^{-2} M) under the same experimental conditions that were used for wsGNS was tested individually. Remarkably, no apparent changes in fluorescence intensity were observed with most of the metal ions; only a minor decrease in fluorescence intensity was observed with Ba^{2+} and Pb^{2+}. Figure 2.7(d) clearly demonstrates the selectivity of Cr(VI) ions. It quenches the fluorescence

emissions more sensitively that other metal ions do. With regard to the selectivity and PL quenching by transition metal ions, diverse investigations have been performed. Cr(VI) can promote the recombination of the electron-hole pair on the surface of wsGNS in a nonradiative way. Because Cr(VI) ions have low-lying d-d transition states and low redox potentials due to their paramagnetic nature, Cr(VI) ions hence efficiently quench PL emission [78-80]. Selectivity can be explained on the basis of the higher thermodynamic affinity of Cr(VI), and surface functional groups also make some contribution.
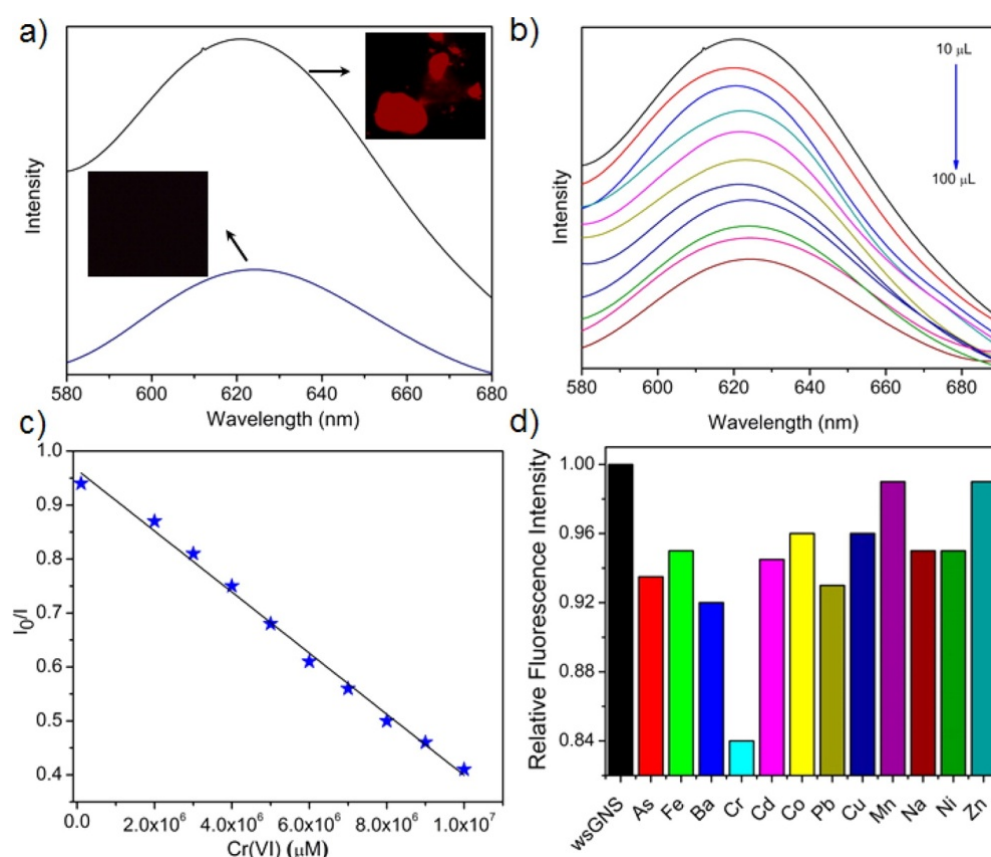
Figure 2.7. (a) Fluorescence spectra of wsGNS before (black) and after (blue) addition of Cr(VI) ions (100 μL, 1×10^{-2} M); The right inset shows the fluorescence image of wsGNS before addition of Cr(VI) ions, and the left inset shows the fluorescence image of wsGNS after the addition of Cr(VI) ions; (b) Fluorescence emission responses of wsGNS with increasing concentrations of Cr(VI); (c) Curve of the fluorescence quenching values (I_o/I) *versus* Cr(VI) concentration; (d) Histogram showing the changes in fluorescence emission of wsGNS at 460 nm upon addition of different heavy metal ions.

Table 2.1. Performance comparison between various fluorescence sensors towards Cr (VI).

Methods	Response Time	Detection Limit	Ref.
Rhodamine derivatives	NA	0.14 ppb	[40]
P(NIPAM-co-RhBUA)-nanogel	NA	2.2×10^{-7} M	[72]
Rhodamine derivatives	5 min	1.6×10^{-8} mol L^{-1}	[73]
DTNBA-Au nanoparticles	30 min	93.6 ppb	[74]
GSH-CdTe quantum dots	30 min	8×10^{-3} µg mL^{-1}	[75]
tris(1,10-phenanthroline)Ru(II)	10 min	66×10^{-3} µM	[76]
Rhodamine B hydrazide	10 min	5.5×10^{-9} mol L^{-1}	[77]
wsGNS	Immediate	0.51 µM	Present study

2.3.5 Fluorescence Imaging of HeLa Cells

After the successful evaluation of sensing properties of wsGNS for Cr(VI), luminescence properties were further explored for fluorescence cell labeling. wsGNS were mixed with cell culture medium, and after being incubated for 2 h, cells were washed with PBS and imaged under a fluorescence microscope. Figure 2.8 illustrates the fluorescence microscopic images of HeLa cells after incubation with wsGNS. Strong green fluorescence and red fluorescence were observed from wsGNS-labeled HeLa cells at excitation wavelengths of 488 nm and 532 nm, respectively ((panels a and b) of Figure 2.8, respectively). The wsGNS with NIR emitting properties may be used in the future as efficient imaging probes.
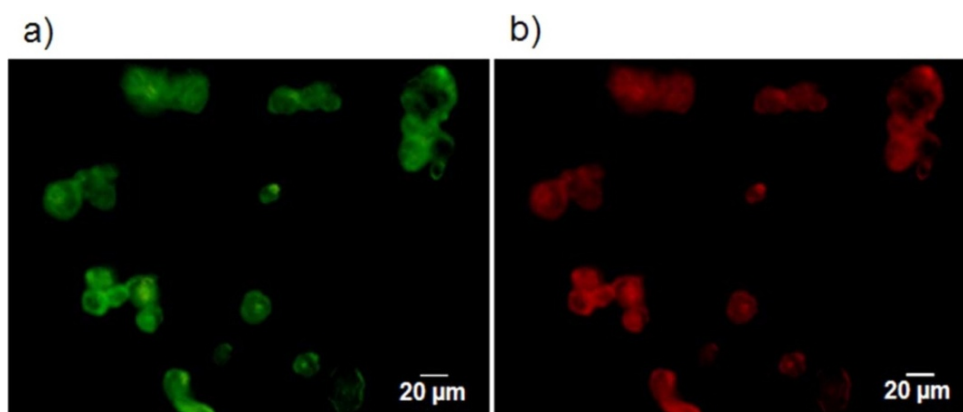
Figure 2.8. Fluorescence microscopic images of HeLa cells with (a) 488 and (b) 532 nm band-pass filters.

2.4   Conclusion

The environmental feasibility and utility of pollutant petrol soot for the fabrication of tunable photoluminescent wsGNS were investigated to decrease the level of environmental pollution. The simple oxidation of Soxhlet-purified petrol soot (carbon) provides a convenient method for the large-scale synthesis of few-layer wsGNS with tunable PL emissions covering the green and red regions with a slight extension in the NIR region of the spectrum. A high degree of passivation via negative surface functionalities imparts the aqueous solubility with excellent stability for long-term imaging purposes. The PL properties of the waste-derived wsGNS were further explored to determine the fitness of wsGNS as fluorescence nanoprobes for the selective and sensitive detection of Cr(VI) in an aqueous solution with a detection limit of 0.51 μM and for the imaging of HeLa cells. A fluorescence-based sensor can be effectively used to detect the quality of the microenvironment in water bodies.

2.5. References

1. Jacobson, M. Z., Control of Fossil-Fuel Particulate Black Carbon and Organic Matter, Possibly the Most Effective Method of Slowing Global Warming. *J. Geophys. Res. Atmos.* **2002**, *107*, ACH 16-1-ACH 16-22.

2. Ramanathan, V.; Ramana, M. V.; Roberts, G.; Kim, D.; Corrigan, C.; Chung, C.; Winker, D., Warming Trends in Asia Amplified by Brown Cloud Solar Absorption. *Nature* **2007**, *448*, 575-579.

3. Ramanathan, V.; Carmichael, G., Global and Regional Climate Changes Due to Black Carbon. *Nat. Geosci.* **2008**, *1*, 221-227.

4. Ramanathan, V.; Li, F.; Ramana, M. V.; Praveen, P. S.; Kim, D.; Corrigan, C. E.; Nguyen, H.; Stone, E. A.; Schauer, J. J.; Carmichael, G. R.; Adhikary, B.; Yoon, S. C., Atmospheric Brown Clouds: Hemispherical and Regional Variations in Long-Range Transport, Absorption, and Radiative Forcing. *J. Geophys. Res.* **2007**, *112*, D22S21.

5. Tripathi, K. M.; Sonker, A. K.; Sonkar, S. K.; Sarkar, S., Pollutant Soot of Diesel Engine Exhaust Transformed to Carbon Dots for Multicoloured Imaging of *E. coli* and Sensing Cholesterol. *RSC Adv.* **2014**, *4*, 30100-30107.

6. Wang, Q.; Zhang, S. R., Size Separation of Carbon Nanoparticles from Diesel Soot for Mn (II) Sensing. *J. Lumin.* **2014**, *146*, 37-41.

7. Lee, T. H.; Yao, N.; Chen, T. J.; Hsu, W. K., Fullerene-Like Carbon Particles in Petrol Soot. *Carbon* **2002**, *40*, 2275-2279.

8. Tripathi, K. M.; Gupta, N. R.; Sonkar, S. K., Nano-Carbons from Pollutant Soot: A Cleaner Approach toward Clean Environment. In *Smart Materials For Waste Water Applications*, **2016**, 127-153.

9. Uchida, T.; Ohashi, O.; Kawamoto, H.; Yoshimura, H.; Kobayashi, K.; Tanimura, M.; Fujikawa, N.; Nishimoto, T.; Awata, K.; Tachibana, M.; Kojima, K., Synthesis of Single-Wall Carbon Nanotubes from Diesel Soot. *Jpn. J. Appl. Phys.* **2006**, *45*, 8027-8029.

10. Bolton, C. H.; Hopton, M. I.; Rogers, W.; Slade, R. R.; Evershed, R. P.; Carter, J. F.; Hartog, M., Reaction of Proteins with Vehicle Exhaust Soot. *Biochem. Soc. Trans.* **1996**, *24*, 179S.

11. Vander Wal, R. L.; Yezerets, A.; Currier, N. W.; Kim, D. H.; Wang, C. M., HRTEM Study of Diesel Soot Collected from Diesel Particulate Filters. *Carbon* **2007**, *45*, 70-77.

12. Sonkar, S. K.; Tripathi, S.; Sarkar, S., Activation of Aerial Oxygen to Superoxide Radical by Carbon Nano Tube of Aerosol Trapped in Indoor Spider Web. *Curr. Sci.* **2009**, *97*, 1227-1230.

13. Bunger, J.; Krahl, J.; Baum, K.; Schroder, O.; Muller, M.; Westphal, G.; Ruhnau, P.; Schulz, T. G.; Hallier, E., Cytotoxic and Mutagenic Effects, Particle Size and Concentration Analysis of Diesel Engine Emissions Using Biodiesel and Petrol Diesel as Fuel. *Arch. Toxicol.* **2000**, *74*, 490-498.

14. Salvi, S.; Blomberg, A.; Rudell, B.; Kelly, F.; Sandstrom, T.; Holgate, S. T.; Frew, A., Acute Inflammatory Responses in the Airways and Peripheral Blood after Short-Term Exposure to Diesel Exhaust in Healthy Human Volunteers. *Am. J. Resp. Crit. Care Med.* **1999**, *159*, 702-709.

15. Novoselov, K. S.; Geim, A. K.; Morozov, S. V.; Jiang, D.; Zhang, Y.; Dubonos, S. V.; Grigorieva, I. V.; Firsov, A. A., Electric Field Effect in Atomically Thin Carbon Films. *Science* **2004**, *306*, 666-669.

16. Geim, A. K.; Novoselov, K. S., The Rise of Graphene. *Nat. Mater.* **2007**, *6*, 183-191.

17. Liu, K.; Zhang, J.-J.; Cheng, F.-F.; Zheng, T.-T.; Wang, C.; Zhu, J.-J., Green and Facile Synthesis of Highly Biocompatible Graphene Nanosheets and Its Application for Cellular Imaging and Drug Delivery. *J. Mater. Chem.* **2011**, *21*, 12034-12040.

18. Wu, Q.; Xu, Y.; Yao, Z.; Liu, A.; Shi, G., Supercapacitors Based on Flexible Graphene/Polyaniline Nanofiber Composite Films. *ACS Nano* **2010**, *4*, 1963-1970.

19. Xia, F.; Farmer, D. B.; Lin, Y.-m.; Avouris, P., Graphene Field-Effect Transistors with High on/off Current Ratio and Large Transport Band Gap at Room Temperature. *Nano Lett.* **2010**, *10*, 715-718.

20. Pan, D.; Zhang, J.; Li, Z.; Wu, M., Hydrothermal Route for Cutting Graphene Sheets into Blue-Luminescent Graphene Quantum Dots. *Adv. Mater.* **2010**, *22*, 734-738.

21. Novoselov, K. S.; Falko, V. I.; Colombo, L.; Gellert, P. R.; Schwab, M. G.; Kim, K., A Roadmap for Graphene. *Nature* **2012**, *490*, 192-200.

22. Tripathi, K. M.; Kim, T. Y.; Losic, D.; Tung, T. T., Recent Advances in Engineered Graphene and Composites for Detection of Volatile Organic Compounds (VOCs) and Non-Invasive Diseases Diagnosis. *Carbon* **2016**, *110*, 97-129.

23. Tung, T. T.; Castro, M.; Pillin, I.; Kim, T. Y.; Suh, K. S.; Feller, J.-F., Graphene-Fe$_3$O$_4$/Pil-Pedot for the Design of Sensitive and Stable Quantum Chemo-Resistive VOC Sensors. *Carbon* **2014**, *74*, 104-112.

24. Seo, D. H.; Rider, A. E.; Kumar, S.; Randeniya, L. K.; Ostrikov, K., Vertical Graphene Gas- and Bio-Sensors via Catalyst-Free, Reactive Plasma Reforming of Natural Honey. *Carbon* **2013**, *60*, 221-228.

25. Kumar, S. K.; Castro, M.; Saiter, A.; Delbreilh, L.; Feller, J. F.; Thomas, S.; Grohens, Y., Development of Poly(Isobutylene-Co-Isoprene)/Reduced Graphene Oxide Nanocomposites for Barrier, Dielectric and Sensing Applications. *Mater. Lett.* **2013**, *96*, 109-112.

26. Li, D.; Kaner, R. B., Graphene-Based Materials. *Science* **2008**, *320*, 1170-1171.

27. Bunch, J. S.; van der Zande, A. M.; Verbridge, S. S.; Frank, I. W.; Tanenbaum, D. M.; Parpia, J. M.; Craighead, H. G.; McEuen, P. L., Electromechanical Resonators from Graphene Sheets. *Science* **2007**, *315*, 490-493.

28. Xia, J.; Chen, F.; Li, J.; Tao, N., Measurement of the Quantum Capacitance of Graphene. *Nat. Nanotechnol.* **2009**, *4*, 505-509.

29. Reina, A.; Jia, X.; Ho, J.; Nezich, D.; Son, H.; Bulovic, V.; Dresselhaus, M. S.; Kong, J., Large Area, Few-Layer Graphene Films on Arbitrary Substrates by Chemical Vapor Deposition. *Nano Lett.* **2009**, *9*, 30-35.

30. Stankovich, S.; Dikin, D. A.; Piner, R. D.; Kohlhaas, K. A.; Kleinhammes, A.; Jia, Y.; Wu, Y.; Nguyen, S. T.; Ruoff, R. S., Synthesis of Graphene-Based Nanosheets Via Chemical Reduction of Exfoliated Graphite Oxide. *Carbon* **2007**, *45*, 1558-1565.

31.   Emtsev, K. V.; Bostwick, A.; Horn, K.; Jobst, J.; Kellogg, G. L.; Ley, L.; McChesney, J. L.; Ohta, T.; Reshanov, S. A.; Rohrl, J.; Rotenberg, E.; Schmid, A. K.; Waldmann, D.; Weber, H. B.; Seyller, T., Towards Wafer-Size Graphene Layers by Atmospheric Pressure Graphitization of Silicon Carbide. *Nat. Mater.* **2009**, *8*, 203-207.

32.   Lotya, M.; Hernandez, Y.; King, P. J.; Smith, R. J.; Nicolosi, V.; Karlsson, L. S.; Blighe, F. M.; De, S.; Wang, Z.; McGovern, I. T.; Duesberg, G. S.; Coleman, J. N., Liquid Phase Production of Graphene by Exfoliation of Graphite in Surfactant/Water Solutions. *J. Am. Chem. Soc.* **2009**, *131*, 3611-3620.

33.   Patel, M. A.; Yang, H.; Chiu, P. L.; Mastrogiovanni, D. D. T.; Flach, C. R.; Savaram, K.; Gomez, L.; Hemnarine, A.; Mendelsohn, R.; Garfunkel, E.; Jiang, H.; He, H., Direct Production of Graphene Nanosheets for near Infrared Photoacoustic Imaging. *ACS Nano* **2013**, *7*, 8147-8157.

34.   Li, D.; Müller, M. B.; Gilje, S.; Kaner, R. B.; Wallace, G. G., Processable Aqueous Dispersions of Graphene Nanosheets. *Nat. Nanotechnol.* **2008**, *3*, 101-105.

35.   Niyogi, S.; Bekyarova, E.; Itkis, M. E.; McWilliams, J. L.; Hamon, M. A.; Haddon, R. C., Solution Properties of Graphite and Graphene. *J. Am. Chem. Soc.* **2006**, *128*, 7720-7721.

36.   Li, X.; Wang, X.; Zhang, L.; Lee, S.; Dai, H., Chemically Derived, Ultrasmooth Graphene Nanoribbon Semiconductors. *Science* **2008**, *319*, 1229-1232.

37.   Ponomarenko, L. A.; Schedin, F.; Katsnelson, M. I.; Yang, R.; Hill, E. W.; Novoselov, K. S.; Geim, A. K., Chaotic Dirac Billiard in Graphene Quantum Dots. *Science* **2008**, *320*, 356-358.

38.   Park, S.; Ruoff, R. S., Chemical Methods for the Production of Graphenes. *Nat. Nanotechnol.* **2009**, *4*, 217-224.

39.   Amiot, C.; Xu, S.; Liang, S.; Pan, L.; Zhao, J., Near-Infrared Fluorescent Materials for Sensing of Biological Targets. *Sensors* **2008**, *8*, 3082-3105.

40. Mahato, P.; Saha, S.; Suresh, E.; Di Liddo, R.; Parnigotto, P. P.; Conconi, M. T.; Kesharwani, M. K.; Ganguly, B.; Das, A., Ratiometric Detection of Cr^{3+} and Hg^{2+} by a Naphthalimide-Rhodamine Based Fluorescent Probe. *Inorg. Chem.* **2012**, *51*, 1769-1777.

41. Wang, R.; Zhang, F., NIR Luminescent Nanomaterials for Biomedical Imaging. *J. Mater. Chem. B* **2014**, *2*, 2422-2443.

42. Zheng, M.; Xie, Z.; Qu, D.; Li, D.; Du, P.; Jing, X.; Sun, Z., On-Off-on Fluorescent Carbon Dot Nanosensor for Recognition of Chromium(VI) and Ascorbic Acid Based on the Inner Filter Effect. *ACS Appl. Mater. Interfaces* **2013**, *5*, 13242-13247.

43. Vincent, J. B., Quest for the Molecular Mechanism of Chromium Action and Its Relationship to Diabetes. *Nutr. Rev.* **2000**, *58*, 67-72.

44. Pagano, G.; Manini, P.; Bagchi, D., Oxidative Stress-Related Mechanisms Are Associated with Xenobiotics Exerting Excess Toxicity to Fanconi Anemia Cells. *Environ. Health Perspect.* **2003**, *111*, 1699-1703.

45. Zhitkovich, A., Chromium in Drinking Water: Sources, Metabolism, and Cancer Risks. *Chem. Res.Toxicol.* **2011**, *24*, 1617-1629.

46. Menegario, A. A.; Smichowski, P.; Tonello, P. S.; Polla, G.; Oliveira, E. P.; Santelli, R. E., On-Line Redox Speciation Analysis of Antimony Using L-Proline Immobilized on Controlled Pore Glass and Hydride Generation Inductively Coupled Plasma Optical Emission Spectrometry for Detection. *Anal. Chim. Acta.* **2008**, *625*, 131-136.

47. Metters, J. P.; Kadara, R. O.; Banks, C. E., Electroanalytical Sensing of Chromium(III) and (VI) Utilising Gold Screen Printed Macro Electrodes. *Analyst* **2012**, *137*, 896-902.

48. Bai, X.; Fan, Z., Determination of Chromium (III) in Natural Water Samples Utilizing Capillary Micro-Extraction on Nanometre Zirconium Phosphate Coating Coupled to Electrothermal Atomic Absorbance Spectrometry. *J. Environ. Monit.* **2009**, *11*, 326-329.

49. Abbaspour, A.; Izadyar, A., Carbon Nanotube Composite Coated Platinum Electrode for Detection of Cr(III) in Real Samples. *Talanta* **2007**, *71*, 887-892.

50. Lee, J. S.; Joung, H.-A.; Kim, M.-G.; Park, C. B., Graphene-Based Chemiluminescence Resonance Energy Transfer for Homogeneous Immunoassay. *ACS Nano* **2012**, *6*, 2978-2983.

51. Cui, T.; Zhang, C.; Sun, L.; Hu, Z.; Liu, X., Simple and Efficient Synthesis of Strongly Green Fluorescent Carbon Dots with Upconversion Property for Direct Cell Imaging. *Part. Part. Sys. Charact.* **2015**, *32*, 542-546.

52. Bhunia, S. K.; Saha, A.; Maity, A. R.; Ray, S. C.; Jana, N. R., Carbon Nanoparticle-Based Fluorescent Bioimaging Probes. *Sci. Rep.* **2013**, *3*, 1473-1479.

53. Dubey, P.; Tripathi, K. M.; Mishra, R.; Bhati, A.; Singh, A.; Sonkar, S. K., A Simple One-Step Hydrothermal Route Towards Water Solubilization of Carbon Quantum Dots from Soya-Nuggets for Imaging Applications. *RSC Adv.* **2015**, *5*, 87528-87534.

54. Tripathi, K. M.; Sonker, A. K.; Bhati, A.; Bhuyan, J.; Singh, A.; Singh, A.; Sarkar, S.; Sonkar, S. K., Large-Scale Synthesis of Soluble Graphitic Hollow Carbon Nanorods with Tunable Photoluminescence for the Selective Fluorescent Detection of DNA. *New J. Chem.* **2016**, *40*, 1571-1579.

55. Lin, S. F.; Liu, F. X.; Chen, G. H., Effective Production of Nano-Sized Graphene via Straight-Forward Exfoliation of Microcrystalline Graphite. *RSC Adv.* **2014**, *4*, 45885-45889.

56. Malard, L. M.; Pimenta, M. A.; Dresselhaus, G.; Dresselhaus, M. S., Raman Spectroscopy in Graphene. *Phys. Rep.* **2009**, *473*, 51-87.

57. Dresselhaus, M. S.; Jorio, A.; Hofmann, M.; Dresselhaus, G.; Saito, R., Perspectives on Carbon Nanotubes and Graphene Raman Spectroscopy. *Nano Lett.* **2010**, *10*, 751-758.

58. Tran, T. S.; Park, S. J.; Yoo, S. S.; Lee, T.-R.; Kim, T., High Shear-Induced Exfoliation of Graphite into High Quality Graphene by Taylor-Couette Flow. *RSC Adv.* **2016**, *6*, 12003-12008.

59. Primo, A.; Atienzar, P.; Sanchez, E.; Delgado, J. M.; Garcia, H., From Biomass Wastes to Large-Area, High-Quality, N-Doped Graphene: Catalyst-Free Carbonization of Chitosan Coatings on Arbitrary Substrates. *Chem. Commun.* **2012**, *48*, 9254-9256.

59

60. Cançado, L. G.; Jorio, A.; Ferreira, E. H. M.; Stavale, F.; Achete, C. A.; Capaz, R. B.; Moutinho, M. V. O.; Lombardo, A.; Kulmala, T. S.; Ferrari, A. C., Quantifying Defects in Graphene *via* Raman Spectroscopy at Different Excitation Energies. *Nano Lett.* **2011**, *11*, 3190-3196.

61. Tripathi, K. M.; Bhati, A.; Singh, A.; Gupta, N. R.; Verma, S.; Sarkar, S.; Sonkar, S. K., From the Traditional Way of Pyrolysis to Tunable Photoluminescent Water Soluble Carbon Nano-Onions for Cells Imaging and Selective Sensing of Glucose. . *RSC Adv.* **2016**, *6*, 37319-37329.

62. Choucair, M.; Thordarson, P.; Stride, J. A., Gram-Scale Production of Graphene Based on Solvothermal Synthesis and Sonication. *Nat. Nanotechnol.* **2008**, *4*, 30-33.

63. Dervishi, E.; Li, Z.; Watanabe, F.; Biswas, A.; Xu, Y.; Biris, A. R.; Saini, V.; Biris, A. S., Large-Scale Graphene Production by Rf-cCVD Method. *Chem. Commun.* **2009**, *27*, 4061-4063.

64. Gollavelli, G.; Chang, C.-C.; Ling, Y.-C., Facile Synthesis of Smart Magnetic Graphene for Safe Drinking Water: Heavy Metal Removal and Disinfection Control. *ACS Sustainable Chem. Eng.* **2013**, *1*, 462-472.

65. Zhang, Q.; Qian, X.; Thebo, K. H.; Cheng, H.-M.; Ren, W., Controlling Reduction Degree of Graphene Oxide Membranes for Improved Water Permeance. *Sci. Bull.* **2018**, *63*, 788-794.

66. Hu, S. H.; Chen, Y. W.; Hung, W. T.; Chen, I. W.; Chen, S. Y., Quantum-Dot-Tagged Reduced Graphene Oxide Nanocomposites for Bright Fluorescence Bioimaging and Photothermal Therapy Monitored *in situ*. *Adv. Mater.* **2012**, *24*, 1748-1754.

67. Shang, J.; Ma, L.; Li, J.; Ai, W.; Yu, T.; Gurzadyan, G. G., The Origin of Fluorescence from Graphene Oxide. *Sci. Rep.* **2012**, *2*, 792-799.

68. Momper, R.; Steinbrecher, J.; Dorn, M.; Rörich, I.; Bretschneider, S.; Tonigold, M.; Ramanan, C.; Ritz, S.; Mailänder, V.; Landfester, K.; Bannwarth, M. B. Enhanced Photoluminescence Properties of a Carbon Dot System through Surface Interaction with Polymeric Nanoparticles. *J. Colloid Interface Sci.* **2018**, *518*, 11-20.

69. Pramanik, A.; Fan, Z.; Chavva, S. R.; Sinha, S. S.; Ray, P. C., Highly Efficient and Excitation Tunable Two-Photon Luminescence Platform for Targeted Multi-Color MDRB Imaging Using Graphene Oxide. *Sci. Rep.* **2014**, *4*, 6090-6095.

70. Loh, K. P.; Bao, Q.; Eda, G.; Chhowalla, M., Graphene Oxide as a Chemically Tunable Platform for Optical Applications. *Nat. Chem.* **2010**, *2*, 1015-1024.

71. Chien, C. T.; Li, S. -S.; Lai, W. -J.; Yeh, Y. -C.; Chen, H. -A.; Chen, I. -S.; Chen, L. -C.; Chen, K. -H.; Nemoto, T.; Isoda, S.; Chen, M.; Fujita, T.; Eda, G.; Yamaguchi, H.; Chhowalla, M.; Chen, C.-W., Tunable Photoluminescence from Graphene Oxide. *Angew. Chem.* **2012**, *124*, 6766-6770.

72. Wan, X.; Liu, H.; Yao, S.; Liu, T.; Yao, Y., A Stimuli-Responsive Nanogel-Based Sensitive and Selective Fluorescent Sensor for Cr^{3+} with Thermo-Induced Tunable Detection Sensitivity. *Macromol. Rapid Commun.* **2014**, *35*, 323-329.

73. Mao, J.; He, Q.; Liu, W., An "off-on" Fluorescence Probe for Chromium(III) Ion Determination in Aqueous Solution. *Anal. Bioanal. Chem.* **2010**, *396*, 1197-1203.

74. Dang, Y.-Q.; Li, H.-W.; Wang, B.; Li, L.; Wu, Y., Selective Detection of Trace Cr^{3+} in Aqueous Solution by using 5,5′-Dithiobis (2-Nitrobenzoic Acid)-Modified Gold Nanoparticles. *ACS Appl. Mater. Interfaces* **2009**, *1*, 1533-1538.

75. Zhang, L.; Xu, C.; Li, B., Simple and Sensitive Detection Method for Chromium(VI) in Water Using Glutathione-Capped CdTe Quantum Dots as Fluorescent Probes. *Microchim. Acta.* **2009**, *166*, 61-68.

76. Wang, J.-N.; Qi, Q.; Zhang, L.; Li, S.-H., Turn-on Luminescent Sensing of Metal Cations via Quencher Displacement: Rational Design of a Highly Selective Chemosensor for Chromium(III). *Inorg. Chem.* **2012**, *51*, 13103-13107.

77. Xiang, Y.; Mei, L.; Li, N.; Tong, A., Sensitive and Selective Spectrofluorimetric Determination of Chromium(VI) in Water by Fluorescence Enhancement. *Anal. Chim. Acta.* **2007**, *581*, 132-136.

78.   Huang, H.; Liao, L.; Xu, X.; Zou, M.; Liu, F.; Li, N., The Electron-Transfer Based Interaction between Transition Metal Ions and Photoluminescent Graphene Quantum Dots (GQDs): A Platform for Metal Ion Sensing. *Talanta* **2013**, *117*, 152-157.

79.   Hu, Q.; Li, T.; Gao, L.; Gong, X.; Rao, S.; Fang, W.; Gu, R.; Yang, Z. Ultrafast and Energy-saving Synthesis of Nitrogen and Chlorine Co-doped Carbon Nanodots via Neutralization Heat for Selective Detection of Cr(VI) in Aqueous Phase. *Sensors* **2018**, *18*, 3416-3429.

80.   Wang, H.; Liu, S.; Xie, Y.; Bi, J.; Li, Y.; Song, Y.; Cheng, S.; Li, D.; Tan, M. Facile One-Step Synthesis of Highly Luminescent N-Doped Carbon Dots as an Efficient Fluorescent Probe for Chromium(VI) Detection Based on the Inner Filter Effect. *New J. Chem.* **2018**, *42*, 3729-3735.

Chapter - 3

Water Soluble Graphene Nanosheets for Visible Light Photodegradation of Pollutant Dye
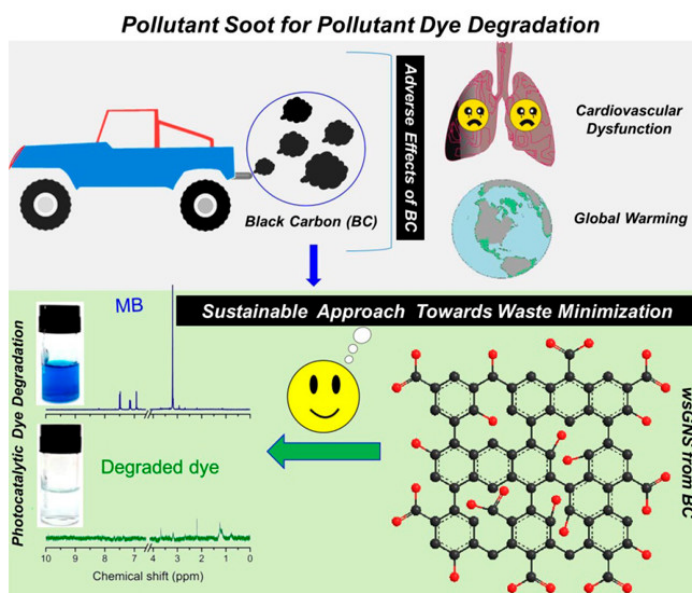
3.1 Introduction

The globally generated black particulate matter BC soot has, at present, shown dramatic negative impacts on human and environmental health. These include cancer [1], dysfunctions of heart and lungs [2], and mental retardation that are consequently responsible for the loss of millions of lives every year as well as significantly contributing toward global warming [3]. Similarly, like BC for air pollution, the contamination of water bodies arising from the discharge of water-soluble organic dyes [4] from various textiles and printing industries has also become a crucial environmental issue due to the fast growth in industrialization [5]. The considerable sources of nonaesthetic pollutants in water are potentially damaging the aquatic biota and life [6]. In reaction to the overall concern related to water pollution [7], different techniques (adsorption, advanced oxidation process, flocculation, ultrafiltration, coagulation by chemical agents, etc.) have been employed in the past [8], for the remediation of soluble toxic dyes [9]. From all the techniques, photocatalysis is very attractive and currently in high demand, since it provides a clean and cost-effective method for water purification. Additionally, visible light driven photocatalysis employs renewable and abundant energy to promote dye degradation under mild conditions. It can be a sustainable approach if we could utilize the nanocarbons derived from the pollutant BC [10-15] for the photocatalytic removal of organic dyes from wastewater via a single step that resolves two contaminant issues at the same time. The idea is very simple and purely based on the age-old practice of using carbon for water filtration because of its high adsorption efficiency [16]. The scientific insights about the conversion of pollutant soots into nanocarbons could open a new sustainable and potential window to mitigate climate change to some extent. Few groups have already been reported [11-15] the isolation (*via* the simplest processes from the bulk) of nanocarbons of different shapes from BC as CD, SWCNT, and GNS for their multiple applications in the field of bioimaging [11, 15], sensing of heavy metal ions [13], and sensing biomolecules [11]. Composition-wise (graphitic/ amorphous structures) nanocarbons isolated from BC [11-15] and from other black charred carbonaceous materials [17-22] are similar to the nanocarbons fabricated from sophisticated instruments [23-27].

From all the allotropic forms of nanocarbons, graphene is the most innovative two-dimensional carbon nanomaterials, owing to its higher surface activities [28] and remarkable biocompatibility [29, 30]. Recently, fresh scientific insights about graphene and graphene-based nanocomposites to eliminate the contaminants in water showed its significant potentials as a photocatalyst nanomaterial [31-47]. So far, several groups have reported the utilizations of graphene/graphene-based nanocomposites as a successful adsorbent material or photocatalyst by modifying the graphene *via* the step of chemical surface functionalization [38]. As such, hydrothermally synthesized 3D Hemin functionalized graphene hydrogel (Hem/GH) was explored for the almost complete (~96%) photocatalytic degradation of MB under sunlight [31]. Gan *et al*. synthesized WO_3-graphene nanocomposite (WO_3/G) for the highest degradation efficiency of MB under the visible light [32]. Ai *et al*. reported the GNS based GNS-magnetite (Fe_3O_4) composites for the removal of MB from aqueous solution [33]. Self-assembled composites based on GO/chitosan (CS)/silver nanoparticles were used for the removal of MB and rhodamine (RhB) dye [34]. Hou *et al*. reported the synthesis of P25 (TiO_2)-graphene hydrogels for the decomposition of MB [35]. Wei *et al*. used Ni-doped graphene/carbon cryogels for efficient removal of oil, organic solvents, and MB [36]. Shanmugam *et al*. fabricated graphene-V_2O_5 nanocomposites for the degradation of MB under UV, visible light, and direct sunlight [37]. However, most of the above-stated reports utilize GNS and metal-based GNS nanocomposites for dye degradations. Metal-based nanocomposites [48, 49] are a bit better option for photocatalysis applications owing to their efficiencies. But great concern has been expressed regarding their negative impacts in biological systems. Additionally, these materials generally require a sophisticated synthesis process and use of expensive chemicals. Hence, it is still a challenging task to develop a low-cost, facile, and effective photocatalyst for the degradation of organic dyes.

For this, what could be the possibilities if graphene need not be synthesized at all, and would be free from the all processing issues related to metallic contaminations? GNS were isolated from the waste (petrol soot) and were used with surface modifications (as surface defects in the form of high degree

functionalizations) for dye degradation applications with the expectation that wsGNS can perform the same or bit better result than the reported studies on graphene and other graphitic materials [17,25,27,50-53]. To the best of our knowledge MB degradation in ~90 min (with soluble wsGNS only) is comparatively better than many other earlier reports, using metal-based GNS nanocomposites [31-37,41,43,44,46].

3.2   Experimental Section

3.2.1   Materials and Reagents

Petrol engine soot was collected from Jaipur motors, Jaipur, India, a local automobile workshop from the exhaust pipe of opened engine. MB and Deuterium oxide (D_2O) was purchased from Sigma-Aldrich, US. The chemicals, like HNO_3, HCl, acetone, methanol and iso-propyl alcohol (i-PA) from Rankem, India, used in the experiments were of analytical grade and used as such without any modification. All the experiments were performed using deionized (DI) water.

3.2.2   Instrumentation

Structural analysis was done through TEM and HRTEM images were acquired with a Tecnai G^2 20 high-resolution TEM operating at a voltage of 200 kV. Samples for TEM were prepared by casting droplets of an aqueous solution of wsGNS onto a 400 mesh carbon-coated copper grid, followed by drying under 100 W tungsten bulb for 12 h. XPS measurements was recorded in ESCA$^+$ Omicron Nanotechnology Oxford instrument. Raman spectra were obtained with a WITEC Raman spectrometer at 532 nm with Ar$^+$ laser excitation. Solid state FT-IR spectra were taken with pressed KBr pellets on a BRUKER Vector22 IR spectrometer. The UV-Vis absorption spectra of wsGNS were analyzed at room temperature with PerkinElmer Lambda 35 spectrometer. The PL analysis of wsGNS in aqueous phase was performed at room temperature by PerkinElmer LS55 instruments. ^{1}H NMR measurements were recorded on a JEOL ECS-400 (operating at 400 MHz, in D_2O solvent). High performance liquid chromatography (HPLC) analyses were performed using HPLC instrument (Agilent technologies 1260 infinity) equipped with Zorbax Eclipse plus C 18 (250 × 4.6 mm) column with 5 μm particle size. Mobile phase consisted of methanol/water (10:90), and the flow rate was set 1.0 mL

min^{-1}. Approximately 25 μL volume of samples was injected in the column and the effluent was monitored at 663 nm.

3.2.3   Synthesis of wsGNS

wsGNS was prepared by a slightly modified method as reported earlier [15]. Pristine carbon-based waste material, petrol soot was collected by scrubbing off petrol engine exhaust pipe through brush, was isolated and characterized as GNS. Pristine material was modified by successive treatment of Soxhlet purification solvents such as acetone followed by oxidative treatment in order to convert GNS into water-soluble GNS. The unburned organic impurities present in GNS (∼1 g) were removed by Soxhlet purification using only acetone as a solvent. Next, for oxidative treatment step, insoluble Soxhlet purified GNS (∼1 g) was refluxed in 500 mL round bottom-flask with water and nitric acid (100 mL) in ratio 40:60 at temperature of 50°C for 10 h [15]. After oxidative treatment, the refluxed solution was centrifuged at 7000 rpm repetitively for 30 min. Further, the centrifuged supernatant solution was evaporated on the water bath for the several times after the addition of deionized water (approximately seven or eight times) to remove the residual nitrate. Further, nitrate test was done by using sulfanilic acid and zinc dust, no appearance of pink color justifies there are no more nitrate to be reduced. The final nitrate free residue obtained after centrifugation was vacuum-dried and called as wsGNS with almost quantitative yield (∼80-85%) which varied from batch to batch.

3.2.4   Photocatalytic Activity Measurement

The photocatalytic activities of GNS and wsGNS samples were determined by the degradation of MB, a heteropolyaromatic dye, in aqueous solution under direct visible light illumination. A stock solution of MB of concentration 16 mg L^{-1} was prepared in DI water for photocatalytic degradation experiment. In a typical process, 10 mg of GNS and wsGNS were added separately in 50 mL of prepared MB solution and both the solutions were stirred for 30 min in the dark to reach the adsorption and desorption equilibration. The solutions were then sealed in a glass vial and exposed to visible light illumination placed at 25 cm away under 60 W tungsten bulb. During the photocatalytic tests, fixed amount of photoreacted solution

were taken at a time interval of 10 min. The collected solution was centrifuged, and the supernatant was collected in a quartz cuvette for determining MB concentration in the supernatant by using UV-Vis absorbance spectroscopy at wavelength 663 nm. For further characterization of the photodegraded products of MB by wsGNS, the samples MB-wsGNS were collected after 2 and 4 h time period. Further, these samples were centrifuged and supernatant was collected and dried to carry out the analysis by nuclear magnetic resonance (NMR), HPLC, Raman, and FT-IR spectroscopy to distinguish the degraded products formed.

3.2.5. Regeneration Analysis

The recovered wsGNS was regenerated with 0.01 M HCl solution repeatedly over ~10-12 times followed by washing of distilled water until the pH of the effluent become neutral. The regenerated sample after washing dried in the oven at 80 °C for the further use.

3.3   Results and Discussion

wsGNS were fabricated by the simple method of the oxidation [15] of soot with nitric acid with a slight modification to minimize the use of excessive solvents as an environmental concern. Nitric acid oxidized GNS are highly soluble in water because of the presence of high-density surface carboxylation [15, 20, 21]. The incorporation of carboxylic acid groups has the advantages of creating water-soluble wsGNS with more active sites.

3.3.1   Structural Characterization

Structural analyses were executed by TEM and HRTEM microscopy, showing the presence of high-density surface defects [15, 21, 22]. Figure 3.1(a-b) shows the presence of low-resolution TEM images of wsGNS with its corresponding diffraction pattern confirming the graphitic character (inset of Figure 3.1(b)). The HRTEM image as displayed in Figure 3.1(c) shows the presence of 3-5 layered graphene sheets marked with white arrows showing the graphitic interlayer (0.34 nm) along with high density surface defects (yellow box) as the surface functionalizations. Figure 3.1(d) displayed the zoomed image of Figure 3.1(c) (yellow box), showing the presence of different sized graphitic patches (encircled by

the yellow color), organized differently on the surface of wsGNS (marked with white arrows). HRTEM images shown in Figure 3.1(c-d) are simply advocating the presence of the various emissive centers/sites [15] in the form of surface defects. These high-density emissive centers/sites impart multicolored emissive properties to these wsGNS which can be utilized for imaging and sensing purposes [15, 54].
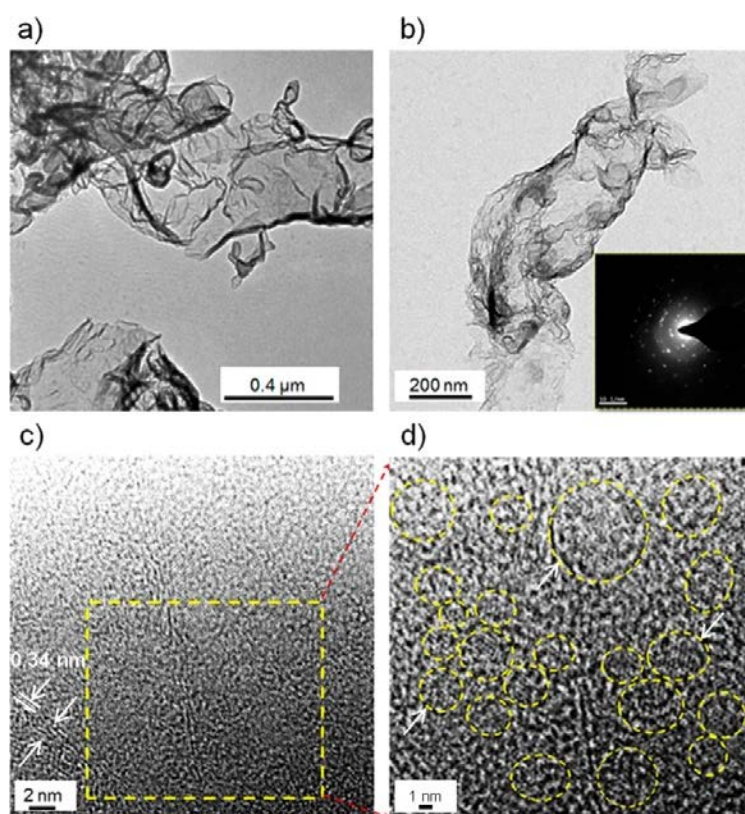
Figure 3.1. (a, b) Low resolution TEM images of wsGNS; (c) HRTEM image of wsGNS revealing well-defined layers of multilayered graphene sheets; (d) Presence of graphitic centers with different shapes (marked by yellow circles).

3.3.2 XPS Analysis

The detailed analysis of the surface functionalization with negative hydrophilic moieties on wsGNS as the surface defects [15] was performed by XPS analysis. Figure 3.2 displayed a comparative XPS analysis of GNS *versus* wsGNS. Figure 3.2(a) displayed an XPS survey scan of GNS shows the presence of two prominent peaks for C_{1s} and O_{1s} at 283.0 eV and 531.5 eV respectively. Over the elemental quantification, this indicates the surface of GNS was composed of carbon (~91%) and oxygen (~9%). High-resolution peak fitting of C_{1s} (Figure 3.2(b)) of GNS shows three different binding states of surface carbon ascribed to C=C, C-C,

and C-O at 283.7 eV, 284.0 eV, and 285.6 eV, respectively. Contrary to the different carbon (C_{1s}) bindings of GNS, the high-resolution peak fitting of O_{1s} (Figure 3.2(c)) shows only a single binding state of oxygen with carbon as C-O at 531.4 eV. As expected, after the surface functionalizations [15], there is a significant increase in the degree of oxygen functionalities in wsGNS as seen in the survey scan of Figure 3.2(d). High-resolution peak fitting of C_{1s} of wsGNS shows the appearance of two newer binding sites for surface carbon (Figure 3.2(e)) compared to the insoluble GNS. As C=O at 286.4 eV, COO$^-$ at 288.3 eV along with the C=C at 283.5 eV, C-C at 284.2 eV, and C-O at 285.3 eV. Likewise, the O_{1s} high-resolution scan (Figure 3.2(f)) of wsGNS also showed the increased in the binding sites of oxygen with carbon corresponding to C-O, C=O, and COO$^-$ at 531.2 eV, 532.7 eV, and 535.9 eV, respectively. The emergence of newer moieties in wsGNS compared to GNS clearly defined the high-density surface modification by negative functional groups. That consequently increases the percentage of oxygen from ∼9% to ∼23% in wsGNS (Figure 3.2(a and d)). These high-density surface defects in form of high-density surface functionalizations are further used for the degradations of MB under the influence of visible light.
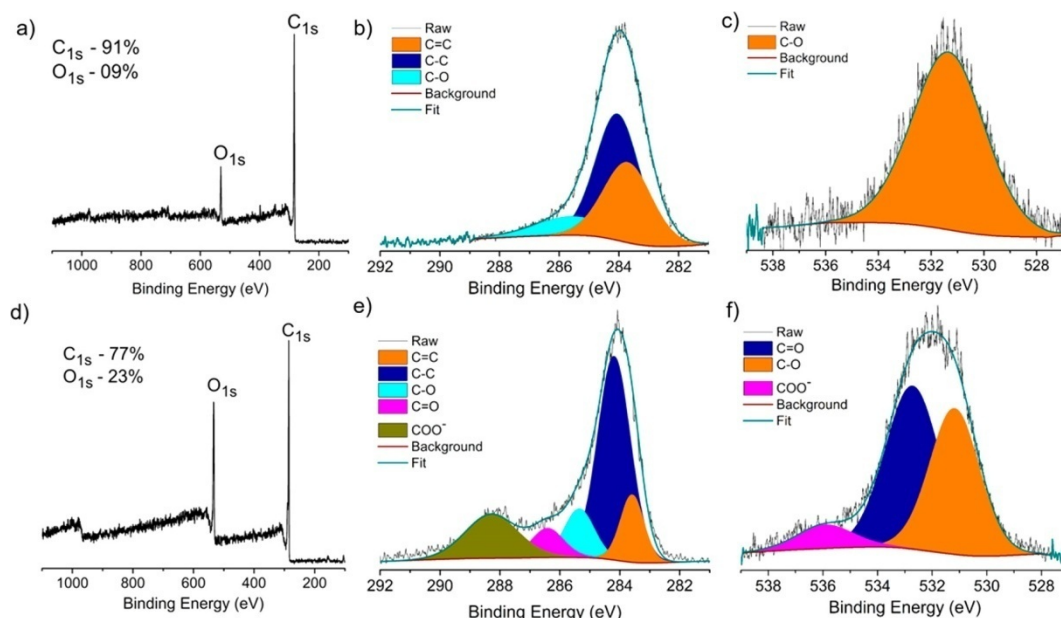
Figure 3.2. (a) Full scan XPS analysis of GNS along with its corresponding; (b) C_{1s}; and (c) O_{1s} short scans; (d) Full scan XPS analysis of wsGNS with its corresponding (e) C_{1s}; and (f) O_{1s} short scans.

3.3.3   **Absorbance and Photoluminescence Study**

The UV-visible absorption spectrum of wsGNS as shown in Figure 3.3(a) displayed an absorption band at 265 nm, which can be attributed to the n−π* transition of the C-O/C=O bonds. The optical digital images of the aqueous solution of wsGNS under the ordinary (Figure 3.3(b)) light illumination. Over the exposure of UV light irradiation of the sample showed a fluorescent green color (Figure 3.3(c)). As described earlier [15], a high degree of oxidative treatments of the graphitic materials can readily impart the tunable PL properties along with the high solubility in the aqueous phase. In the case of wsGNS, a wide range of PL emissions were observed (Figure 3.3(d) spread over a vast range of visible spectra including a smaller portion of NIR spectrum (Figure 3.3(e)). Figure 3.3(d) shows the PL emissions obtained with continuous change in excitation (λ_{ex} from 420 nm to 600 nm) wavelengths with an increment of 20 nm toward the higher wavelength. Concerning the possible mechanism for tunable PL emission, from the graphene like materials are most probably because of the intramolecular proton transfer over the surface of wsGNS between the carboxylate anions/hydroxyl group and in between the hydroxyl/hydroxyl moieties. As well the contributions of high surface functionalizations (Figure 3.2 (d-f)) impart the tunable multiemissive properties to wsGNS, and depending on the degree of functionalizations, the PL properties can easily be tuned. During the process of surface functionalization, the formations of many sp^3 domains within the sp^2 matrices cause formations of newer graphitic structures having disorder-mediated localized emissive states [15]. The surface defects of wsGNS as high-density surface functionalities can trap the photoexcited electrons during the visible light irradiation, which will be used for the photodegradation of MB in the next section.
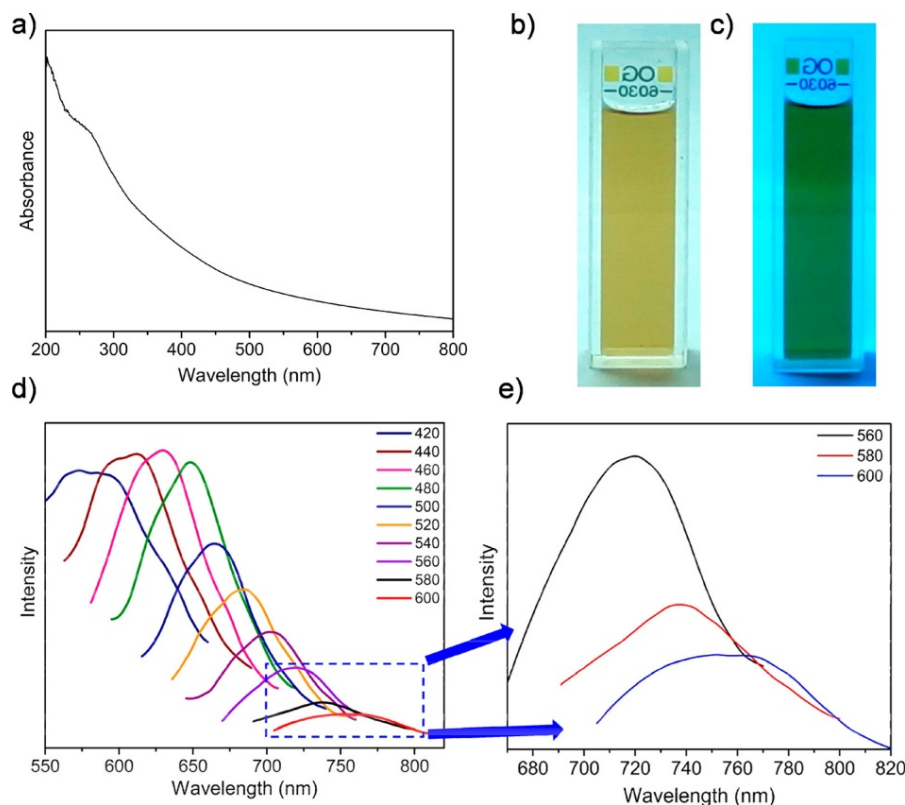
Figure 3.3. (a) UV-Visible absorption spectrum of wsGNS in aqueous solution; (b) Digital camera photograph of the wsGNS under visible light; and (c) UV light irradiation; (d and e) Tunable PL emission spectra of wsGNS recorded with different excitations (λ_{ex} from 420 nm to 600 nm) with an increment of 20 nm toward the higher wavelength; (e) Zoomed spectra of part d (blue box) showing the NIR emissions.

3.3.4 Photocatalytic Dye Degradation under Visible-Light Irradiation

In detailed the photocatalytic degradation behavior of insoluble GNS *versus* wsGNS on the extensively used organic dye as MB under the visible light irradiation using a 60 W tungsten bulb was studied. The background test for wsGNS in the dark for the initial 30 min (green line) showed the adsorption of ~ 9 %. Afterward, ~ 99 % of the photodegradation of MB was achieved within 90 min. Based on the continuous decrease in characteristic absorbance peak of MB at 663 nm as shown in Figure 3.4.
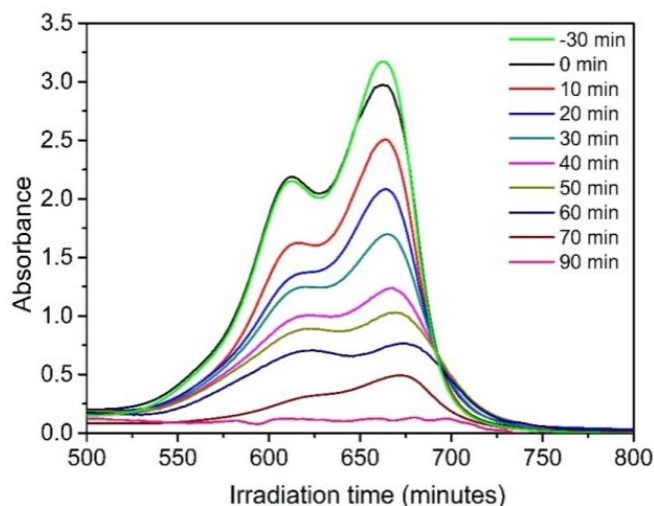
Figure 3.4. UV-Vis absorbance spectra of MB in the presence of wsGNS.

Figure 3.5(a-(i)) represents the relative change in the concentration of the MB solution as a function of time under visible light irradiation. UV-Vis absorbance spectroscopy continuously monitored the change in the concentration of MB, based on the gradual decrease in the absorption intensity of MB with time (at 663 nm). As a control test, MB showed a very high stability in light without the presence of GNS/wsGNS. Under the presence of visible light irradiation, GNS showed the incomplete degradation of MB ($\sim$19.6%) from its initial measured concentration. On the other side, the substantial influence of water solubilizations in wsGNS showed the highest performance among all the tested materials. In the presence of wsGNS initially within the 70 min of visible light irradiation, $\sim$77% of MB gets degraded which was further degraded completely ($\sim$96%) in 90 min as presented in Figure 3.5(a-(i)). In the presence of visible light the apparent rate constant of wsGNS was 0.0313 min^{-1}, which was $\sim$11 times higher than that of GNS (0.0028 min^{-1}). Moreover, the rate constants of wsGNS and GNS in the absence of visible light follow similar trends as shown in Figure 3.5(a-ii). Figure 3.5(b-(i)) shows the schematic diagram of MB photodegradation under visible light irradiation by wsGNS. The degradation efficiency with respect to time for our pollutant waste derived wsGNS is compared with other graphitic and metals-based graphitic nanocomposites [31, 32, 37, 39, 41, 43, 46, 47] and given in Table 3.1. As shown in Table 3.1., most of the documented reports describe metal doping of graphitic (CD [55], GQD) [45] /graphene (r-GO, GO) [31-37, 39, 41, 43-47] material for the

improvement of its photodegradation efficiency. Significantly, compared to metal doped graphitic materials, wsGNS derived from pollutant soot shows complete degradation of MB within 90 min.
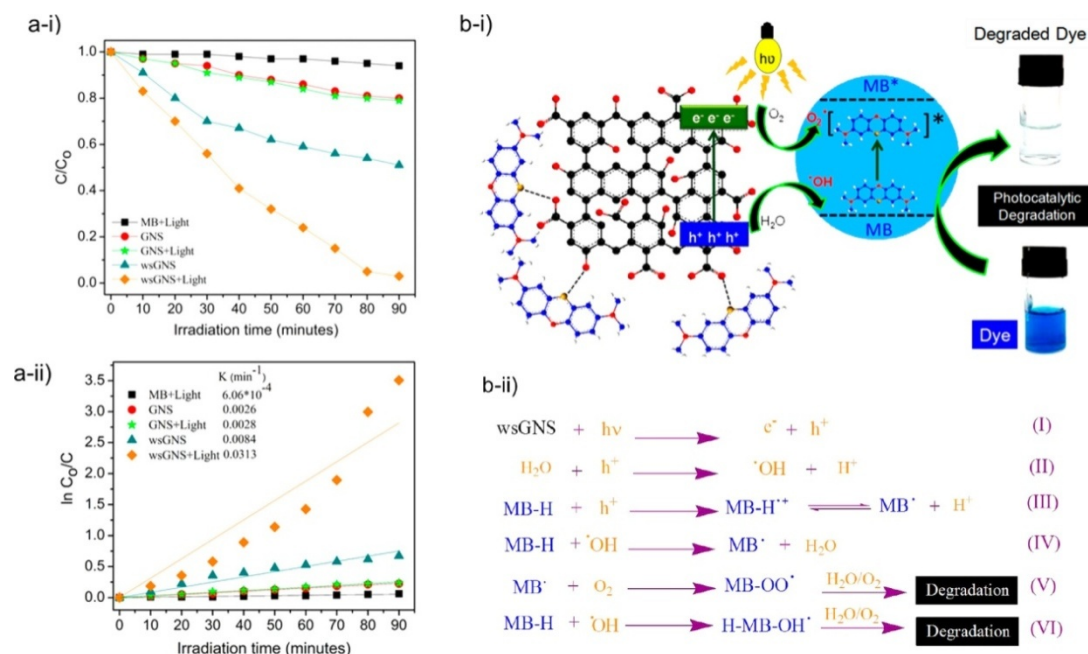
Figure 3.5. Extent of (a-i) plot of (C/C_o); and (a-ii) plot of $\ln(C_o/C)$ for MB photodegradation by different sample; (b-i) Schematic diagram showing MB photodegradation; and (b-ii) its possible mechanism for photocatalytic degradation of MB by wsGNS under visible light irradiation.

Concerning the possible explanation for the enhanced photocatalytic activity of wsGNS can be attributed to the utilizations of high-density surface defects (different sized graphitic patches shown in Figure 3.1(d). Planar nanostructures and high aspect ratio of graphene can facilitate the generation of more active surface sites for the catalysis [56]. A plausible scheme and degradation mechanism has been demonstrated in Figure 3.5(b-(i)) and 3.5(b-(ii)) respectively. The surface adsorption/interactions of MB on wsGNS can be toward the higher side (compared to GNS). That significantly owes the accelerated bonding interactions [11] of MB with surface carboxylic acid groups (as illustrated in Figure 3.5(b-(i)), via the process of initial adsorption [57] which is the primary condition for the initiation of the photodegradation process. Moreover, the high-density functionalization of wsGNS with negative charges leads to enhanced spatial separation between highest

occupied molecular orbital (HOMO)- lowest unoccupied molecular orbital (LUMO) along with generation of oxygen radicals and consequently improving the efficiency of photocatalytic degradation of organic dyes [40].

Table 3.1. Comparative Study Related to the Photodegradation Performance of Different Graphitic Materials

S. No.	Sample	Degradation (%)	Degradation time (minutes)	Ref.
1.	Hemin-functionalized graphene hydrogel	96	180	[31]
2.	WO_3/graphene nanocomposite	99	480	[32]
3.	r-GO/ chitosan/ silver nanoparticles hydrogel	99	70	[34]
4.	P25 (TiO_2)-graphene hydrogels	96	55	[35]
5.	Graphene-V_2O_5 nanocomposite	99	90	[37]
6.	TiO_2- graphene based composites	99	300	[39]
7.	Multilayered GQDs	93.3	60	[40]
8.	Reduced-GO/CdS	94	180	[41]
9.	Graphitic carbon nitride	99	120	[42]
10.	WO_3 nanorods on graphene nanosheets	80	300	[43]
11.	reduced graphene/Manganese oxide hybrid	66	5	[44]
12.	Zinc porphyrin functionalized GQD	95	60	[45]
13.	Mn_3O_4 decorated graphene oxide	99	200	[46]
14.	TiO_2-Graphene	90	150	[47]
15.	wsGNS	96[a] 99.9[b]	90[a] 120[b]	Present study

[a]Based on the UV-Visible absorption spectroscopy as described in Figure 3.5.

[b]Based on NMR, HPLC, and Raman results as described in Figures 3.7. and 3.8.

Surface defects in wsGNS trapped the photoexcited electrons, which further frees up the oxidative valence hole (equation I) for the decomposition of MB as shown in the schematic diagram (Figure 3.5(b-(ii)). Under visible light illumination, photoexcitation of electrons in wsGNS and retarded electron-hole pair recombination generate the reactive oxygen radicals as reaction intermediates on the

surface of wsGNS (equation II) [34, 37]. MB molecules also react with holes and form excited MB species (equation III) Surface adsorbed MB molecules (blue vial in Figure 3.5(b-(i)) react with active oxygen species (hydroxyl radicals $^\bullet$OH) as shown in equations IV−VI (transparent vial in Figure 3.5(b-(i)) which leads to the degradation of MB molecules into smaller hydrocarbons and could finally into CO_2 and H_2O molecules [34, 40, 41, 44, 46]. To further confirm the presence of reactive species as $^\bullet$OH, we performed a separate trap experiment based on the scavenging property of isopropyl alcohol (IPA) for hydroxyl radicals [58]. In the trapping experiment, the different concentrations of IPA on the photodegradation rate of MB was checked and showed them in Figure 3.6, which shows evidence for the role of hydroxyl radicals in the photodegradation of MB.

The trap experiment includes the different concentrations of IPA(Figure 3.6), which showed that the increase in concentrations of IPA significantly reduces the photodegradation efficiency of MB by wsGNS [58-62]. Although ~96% degradation of MB confirmed by absorption spectra (determined from UV-Visible analysis) as shown in Figure 3.5(a) took place within 90 min, the photocatalytic experiment was extended to 2 h and 4 h and collected the supernatant at respective time intervals. With the expectations that the prolonged exposure of MB with wsGNS in the presence of visible light would result in the breakage of the overall aromatic system of MB and reported the same in Figures 3.7 and 3.8.
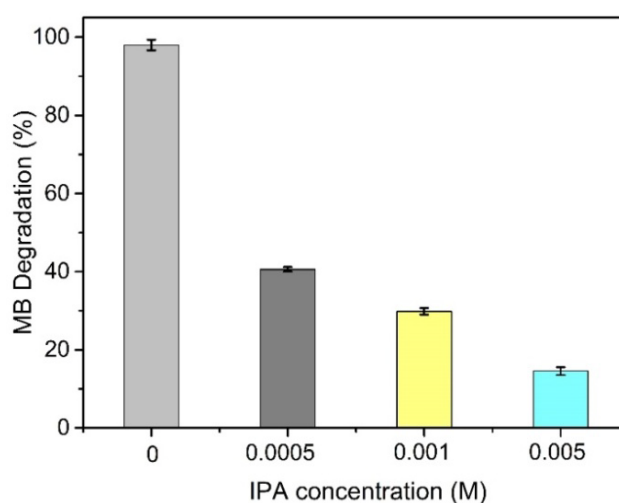
Figure 3.6. A trap experiment showing the presence of $^\bullet$OH radicals based on the scavenging property of IPA for $^\bullet$OH radicals.

3.3.5   NMR Investigation of Degraded Products

Contrary to the former reports limited to the decolorization of MB only 35-37, 39, 42, 43, 47], except a few [31, 32, 45], herein, we present a detailed analysis based on several spectroscopic methods and a discussion for the possible degradation of MB into its smaller constituents by wsGNS under the influence of visible light. Figure 3.7(a) shows the chemical structure of MB with different protons labeled on it. We have performed a comparative ^{1}H NMR analysis of the aqueous phase photodegraded products of MB (Figure 3.7(b)).
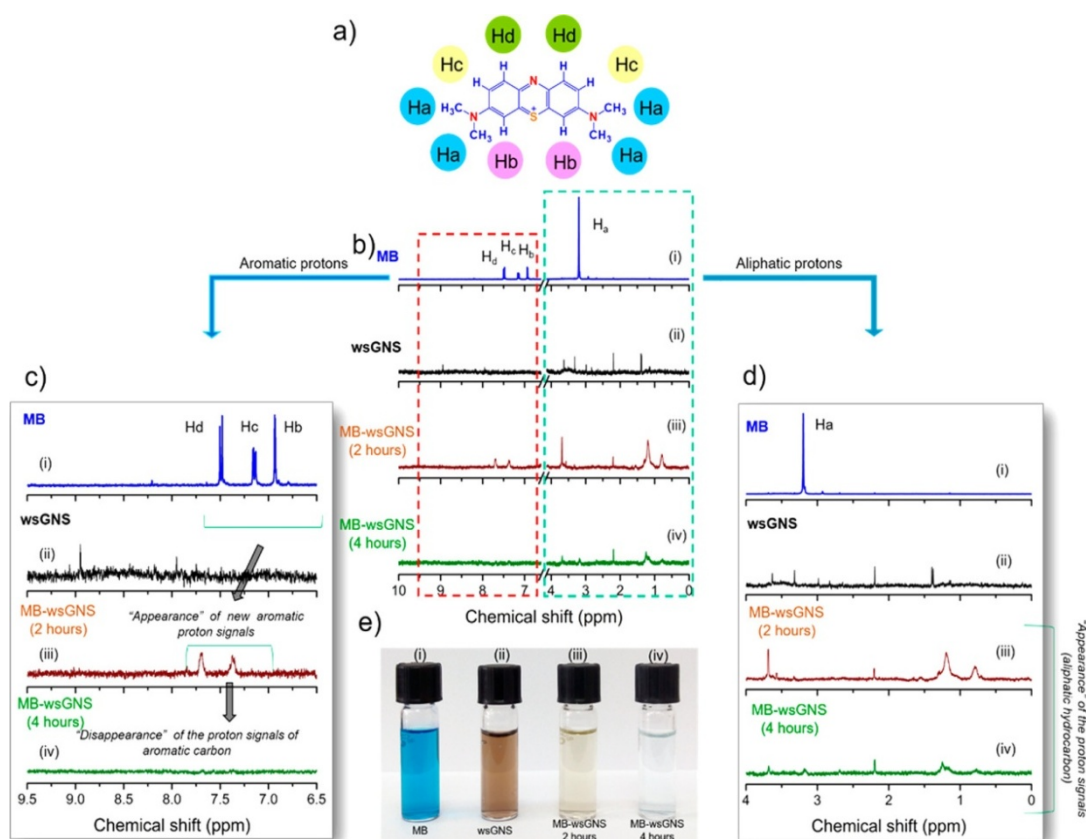
Figure 3.7. (a) Chemical structure of MB. (b) ^{1}H NMR spectra of the photodegradation of MB with time by wsGNS; (i) MB; (ii) wsGNS; (iii) MB-wsGNS after 2 h (wine line); and (iv) MB-wsGNS after 4 h (olive line) under visible light irradiation. (c) Zoomed image of the aromatic region (between 9.5 and 6.5 ppm) of part (b) showing changes in the spectrum of MB while interacting with wsGNS. (d) Zoomed image of the aliphatic region (between 4 and 0 ppm) of part b showing the changes in the specific region of MB while interacting with wsGNS. (e) Photograph of vials of (i) MB solution, (ii) wsGNS, MB-wsGNS (iii) after 2 h, and (iv) after 4 h of the photocatalytic experiment.

The ^{1}H NMR spectra of MB (i (blue line)), wsGNS (ii (black line)), MB-wsGNS (degraded products of MB in the supernatant) were collected from the pool of the MB-wsGNS system. After the respective time intervals, visible light irradiation, 2 h (iii (wine line)) and 4 h (iv (olive line)) is demonstrated in Figure 3.7(b-d), respectively. The proton signals from the MB were seen in two regions of the spectra: aliphatic (for 12 protons (Ha)) and aromatic (for six protons (Hb, Hc, and Hd) as shown in Figure 3.7(b-(i)). The aromatic region shows three prominent signals for six aromatic protons (Hb, Hc, and Hd), in three different environments.

Two protons marked as Hb gives a doublet (d) at 6.92-6.94 ppm, two protons marked as Hc gives double doublet (dd) at 7.13-7.16 ppm, and the other two aromatic protons (Hd) disclosed their signal at 7.48 to 7.50 ppm. In the aliphatic region, MB displayed only a single singlet (s) peak for all the 12 methyl protons (Ha) at 3.2 ppm. Compared to MB, the proton spectrum shown in Figure 3.7(b-(ii)) of wsGNS shows signals ranging from 1.1 to 2.9 ppm (at 1.1 (dd), 1.38 (dd), 2.2 (s) 2.9 (s), and 3.3 (s) ppm) which corresponds to the aliphatic protons and a sharp signal at 3.6 ppm which relates to the presence of ether type organic moieties. Along with this, the proton signal that originated at 8.9 ppm corresponds to the presence of an aldehydic proton. Over the interactions of MB-wsGNS in the presence of visible light, significant changes in both of the important regions of the ^{1}H NMR spectrum; aromatic (Figure 3.7(c)) and aliphatic (Figure 3.7(d)) was observed. For the initial 2 h of interaction of MB-wsGNS, the proton signals of the aromatic region of MB (Figure 3.7(c-(iii))) displayed broadening and shifting in deshielded region. Importantly, the disappearance of one of the aromatic signals (Figure 3.7(c-(iii))) at 6.98 ppm (d), and the shifting and broadening of the signal [63] at 7.37 (s) and 7.69 (s) ppm peaks, respectively, toward the deshielded region confirms the significant interaction between MB-wsGNS. As well the aliphatic proton signals shown in (Figure 3.7(d-(iii))) showed the origin of a few additional and new broad signals in the upfield region at 0.79 (s) and 1.18 (s) ppm indicating the formation of small aliphatic hydrocarbon compounds [64] as the degraded products of MB. Moreover, on increasing the exposure time of visible light to MB-wsGNS conjugates for 4 h, we have observed the complete disappearance of proton signals in the aromatic

region (Figure 3.7(b-(iv)) and Figure 3.7(c-(iv))) indicating a loss in aromaticity of MB (photodegradation of the MB skeleton). On the other side, the origins of newer proton peaks in the aliphatic region (Figure 3.7(b-(iv)) and Figure 3.7(d-(iv))) are due to degradation in the organic skeleton of MB into its smaller aliphatic hydrocarbon. The signal at 1.24 (s), 2.21 (s), 3.17 (s), and 3.68 (s) ppm, confirms the formations of smaller aliphatic hydrocarbons as the photodegraded products of the MB. (Figure 3.7(e) displays photographs of vials of (i) MB solution, (ii) wsGNS, (iii) MB-wsGNS after 2 h, and (iv) MB-wsGNS after 4 h of photocatalytic experiment.

3.3.6   HPLC, Raman, and FT-IR Investigation of Degraded Products

^{1}H NMR results (Figure 3.7) confirming the photodegradation of MB were further supported by the comparative analysis based on the HPLC, Raman, and FT-IR analysis as displayed in Figure 3.8(a-c). A comparative HPLC [65] chromatograms of (i) MB, (ii) wsGNS, MB-wsGNS (iii) 2 h and (iv) 4 h samples (Figure 3.8(a)). Chromatogram of MB shows a sharp peak at the retention time of 20.51 min. In the same panel, we did not find any characteristic peak in the chromatogram of wsGNS. After the 2 h of the irradiation of visible light on MB-wsGNS. It shows the decrement of the main peak intensity of MB molecules up to ~98%. Addition to the reduction in the peak intensity of MB, two newer peaks were seen at the retention time of 9.18 min and 32.64 min attributing to the initial degradation of the MB. After the 4 h of analysis, we did not notice any peak related to the MB, suggesting the complete degradation of the organic aromatic skeleton of MB.

Raman spectra of MB as shown in Figure 3.8(b-(i)) shows the most intense band at 1623 cm^{-1} which is assigned to sp^2 hybridized aromatic υ(C-C) ring stretching [66]. Furthermore, two neighboring bands at 1394 cm^{-1}and 1439 cm^{-1} corresponds to υ_{sym}(C-N) stretching and υ_{asym}(C-N) stretching, respectively [67]. Likewise in the same panel wsGNS (Figure 3.8(b-(ii))) shows the characteristic disordered (D-band) and graphitic (G-band) at 1337 cm^{-1} and 1566 cm^{-1}, respectively. Along with a characteristic sharp 2D band at 2679 cm^{-1}, confirming the presence of graphene like material [15]. After the interactions of MB-wsGNS for 2 h

(Figure 3.8(b-(iii))) we have observed the weakening of the sharp band at 1623 cm^{-1} and the other signature bands from ~400 cm^{-1} to 650 cm^{-1} of the MB. However, these bands were further completely disappeared in 4 h of interactions in MB-wsGNS (Figure 3.8(b-(iv))) in visible light, which strongly verify that no traces of the aromatic structure are left behind in the aqueous phase.
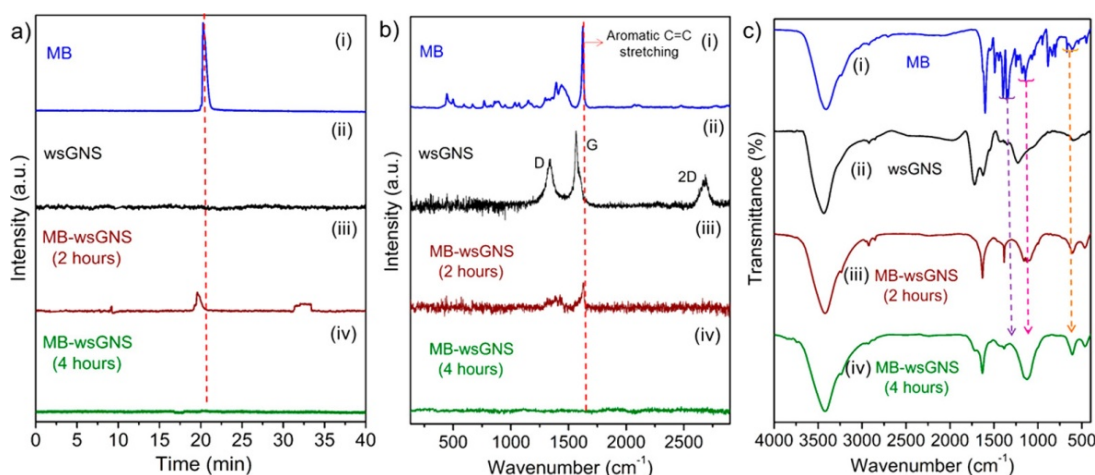
Figure 3.8. Comparative (a) HPLC chromatogram; (b) Raman; and (c) FT-IR analysis of (i) MB; (ii) wsGNS; and photodegraded products of MB-wsGNS (iii) after 2 h and (iv) after 4 h, respectively.

Similarly, a comparative FT-IR spectra are shown in Figure 3.8(c) contains the signature peaks of MB [68, 69] (as highlighted) (Figure 3.8(c-(i)) at 1597 cm^{-1} which is associated with the stretching vibration of C=C group. The peaks at 1353 cm^{-1} and 1339 cm^{-1} relates to the C-N(CH$_3$)$_2$ and C=S$^+$ stretching modes. Peaks at 1142 cm^{-1} and 1064 cm^{-1} attribute to the C-N bending and C-S-C stretching peaks in MB molecule. While in case of wsGNS, (Figure 3.8(c-(ii)) broad absorption O-H stretching was observed around 3300 cm^{-1}. A sharp peak at 1724 cm^{-1} and 1628 cm^{-1} indicate the presence of -C=O stretching and C=C stretching. Furthermore, additional peak at 1232 cm^{-1} relates to C-O stretching. Over the interactions of MB-wsGNS after 2 h, in (Figure 3.8(c-(iii)). All the sharp and characteristic peaks of MB disappear/weakens as highlighted by arrows affirming the significant degradation of MB. Along with this there is emergence of new peaks at 1161 cm^{-1} and 1122 cm^{-1} which can relates to the asymmetric and symmetric stretching of S, O bonds.[69] On continuing the experiment for 4 h, no more signature peaks of MB in supernatant water were observed in Figure 3.8(c-(iv)). Thus, absorbance (Figure 3.4(a) and

3.5(a)), ^{1}H NMR (Figure 3.7), HPLC (Figure 3.8(a)) and the weakening of signature Raman bands (Figure 3.8(b)) and FT-IR peaks (Figure 3.8(c)) are in support of the breaking down of the aromatic skeleton of MB by wsGNS into the smaller hydrocarbons under the influence of visible light [69, 70].

3.3.7 Regeneration Recycling Study

Apart from the photodegradation study [71-73], the recycling ability of a photocatalyst [74-77] is an important characteristic feature that would decide the overall sustainability of newer finding. Figure 3.9 shows the photodegradation efficiency of MB with a five number of cycles. After three cycles there is a negligible loss of degradation efficiency (below ~10%) while after five cycles the degradation efficiency reached 75%.
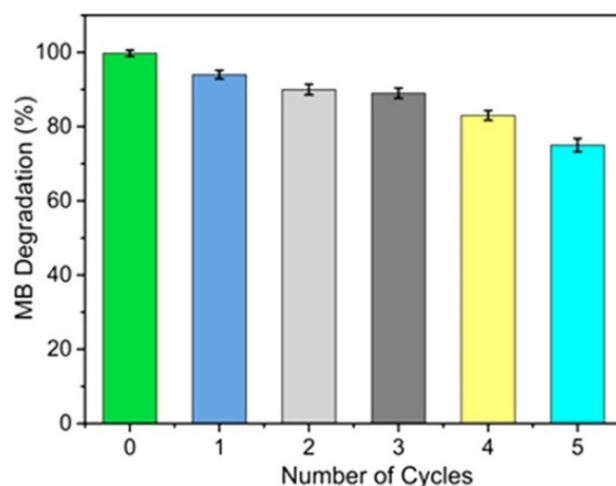
Figure 3.9. Photodegradation activity of wsGNS after five cycles of recycling testing.

3.4   Conclusion

The significant potential of hazardous pollutant soot as an efficient material for water remediation is explored here. The simplistic isolation of wsGNS from the free of cost available pollutant petrol soot showed enormous potential for the photocatalysis. wsGNS are successfully used for the visible-light-induced photodegradation of organic pollutant dye, owing to the presence of high-density surface defects as surface functionalization. More significantly wsGNS exhibited a higher rate of photocatalytic activity toward MB degradation, in contrast to GNS

firmly advocated the strong influence of water solubilizations which is the only prime difference between GNS and wsGNS. The higher solubility related to the high degree of surface functionalizations, which can directly relates to the broad availability of active sites, which promptly facilitates for the utilization of BC as wsGNS toward MB degradation. On the other hand, the successful utilization of wsGNS for multiple applications can be expected to reduce environmental stress. Additionally, higher in stability, recoverability, and reusability made this pollutant soot derived wsGNS as a future alternative material that could be further employed in real world applications.

3.5   References

1.   Janssen, N. A. H.; Hoek, G.; Simic-Lawson, M.; Fischer, P.; Bree, L. V.; Brink, H. T.; Keuken, M.; Atkinson, R. W.; Anderson, H. R.; Brunekreef, B.; Cassee, F. R., Black Carbon as an Additional Indicator of the Adverse Health Effects of Airborne Particles Compared with PM_{10} and $PM_{2.5}$ *Environ. Health Perspect.* **2011**, *119*, 1691-1699.

2.   Kelly, F. J.; Fussell, J. C., Air Pollution and Public Health: Emerging Hazards and Improved Understanding of Risk. Environ. *Geochem. Health.* **2015**, *37*, 631-649.

3.   Kopp, R. E.; Mauzerall, D. L., Assessing the Climatic Benefits of Black Carbon Mitigation. *Proc. Natl. Acad. Sci.* **2010**, *107*, 11703-11708.

4.   Carmen, Z.; Daniela, S., Textile Organic Dyes - Characteristics, Polluting Effects and Separation/Elimination Procedures from Industrial Effluents - a Critical Overview, In *Organic Pollutants Ten Years after the Stockholm Convention - Environmental and Analytical Update*, **2012**, 33.

5.   Teng, Y.; Yang, J.; Zuo, R.; Wang, J., Impact of Urbanization and Industrialization Upon Surface Water Quality: A Pilot Study of Panzhihua Mining Town. *J. Earth Sci.* **2011**, *22*, 658-668.

6.   Ali, M.; Sreekrishnan, T. R., Aquatic Toxicity from Pulp and Paper Mill Effluents: A Review. *Adv. Environ. Res.* **2001**, *5*, 175-196.

7.   Aksu, Z., Application of Biosorption for the Removal of Organic Pollutants: A Review. *Process Biochem.* **2005**, *40*, 997-1026.

8.   Robinson, T.; McMullan, G.; Marchant, R.; Nigam, P., Remediation of Dyes in Textile Effluent: A Critical Review on Current Treatment Technologies with a Proposed Alternative. *Bioresour. Technol.* **2001**, *77*, 247-255.

9.   Tripathi, K. M.; Tyagi, A.; Sonker, A. K.; Sonkar, S. K., Waste-Derived Nanocarbons: A Cleaner Approach Towards Water Remediation. In *Nanomaterials for Water Remediation: Carbon-Based Materials*, **2016**, *1*, 135-160.

10.   Tripathi, K. M.; Gupta, N. R.; Sonkar, S. K., Nano-Carbons from Pollutant Soot: A Cleaner Approach toward Clean Environment. In *Smart Materials For Waste Water Applications*, **2016**, *1*, 127-153.

11. Tripathi, K. M.; Sonker, A. K.; Sonkar, S. K.; Sarkar, S., Pollutant Soot of Diesel Engine Exhaust Transformed to Carbon Dots for Multicoloured Imaging of *E. coli* and Sensing Cholesterol. *RSC Adv.* **2014**, *4*, 30100-30107.

12. Uchida, T.; Ohashi, O.; Kawamoto, H.; Yoshimura, H.; Kobayashi, K.; Tanimura, M.; Fujikawa, N.; Nishimoto, T.; Awata, K.; Tachibana, M.; Kojima, K., Synthesis of Single-Wall Carbon Nanotubes from Diesel Soot. *Jpn. J. Appl. Phys.* **2006**, *45*, 8027-8029.

13. Wang, Q.; Zhang, S. R., Size Separation of Carbon Nanoparticles from Diesel Soot for Mn (II) Sensing. *J. Lumin.* **2014**, *146*, 37-41.

14. Lee, T. H.; Yao, N.; Chen, T. J.; Hsu, W. K., Fullerene-Like Carbon Particles in Petrol Soot. *Carbon* **2002**, *40*, 2275-2279.

15. Tripathi, K. M.; Singh, A.; Bhati, A.; Sarkar, S.; Sonkar, S. K., Sustainable Feasibility of the Environmental Pollutant Soot to Few-Layer Photoluminescent Graphene Nanosheets for Multifunctional Applications. *ACS Sustainable Chem. Eng.* **2016**, *4*, 6399-6408.

16. Otowa, T.; Nojima, Y.; Miyazaki, T., Development of Koh Activated High Surface Area Carbon and Its Application to Drinking Water Purification. *Carbon* **1997**, *35*, 1315-1319.

17. Tripathi, K. M.; Sonker, A. K.; Bhati, A.; Bhuyan, J.; Singh, A.; Singh, A.; Sarkar, S.; Sonkar, S. K., Large-Scale Synthesis of Soluble Graphitic Hollow Carbon Nanorods with Tunable Photoluminescence for the Selective Fluorescent Detection of DNA. *New J. Chem.* **2016**, *40*, 1571-1579.

18. Sonkar, S. K.; Tripathi, K. M.; Sarkar, S., Ferromagnetic Behaviour of Anthropogenic Multi-Walled Carbon Nanotubes Trapped in Spider Web Indoor. *J. Nanosci. Nanotechnol.* **2014**, *14*, 2532-2538.

19. Tripathi, K. M.; Bhati, A.; Singh, A.; Gupta, N. R.; Verma, S.; Sarkar, S.; Sonkar, S. K., From the Traditional Way of Pyrolysis to Tunable Photoluminescent Water Soluble Carbon Nano-Onions for Cells Imaging and Selective Sensing of Glucose. *RSC Adv.* **2016**, *6*, 37319-37329.

20. Tripathi, K. M.; Bhati, A.; Singh, A.; Sonker, A. K.; Sarkar, S.; Sonkar, S. K., Sustainable Changes in the Contents of Metallic Micronutrients in First Generation Gram Seeds Imposed by Carbon Nano-Onions: Life Cycle Seed to Seed Study. *ACS Sustainable Chem. Eng.* **2017**, *5*, 2906-2916.

21.   Tripathi, K. M.; Tran, T. S.; Kim, Y. J.; Kim, T. Y., Green Fluorescent Onion-Like Carbon Nanoparticles from Flaxseed Oil for Visible Light Induced Photocatalytic Applications and Label-Free Detection of Al(III) Ions. *ACS Sustainable Chem. Eng.* **2017**, *5*, 3982-3992.

22.   Ghosh, M.; Sonkar, S. K.; Saxena, M.; Sarkar, S., Carbon Nano-Onions for Imaging the Life Cycle of *Drosophila melanogaster*. *Small* **2011**, *7*, 3170-3177.

23.   Aqel, A.; M.M., K.; El-Nour, A.; Ammar, R. A. A.; Al-Warthan, A., Carbon Nanotubes, Science and Technology Part (I) Structure, Synthesis and Characterisation *Arab. J. Chem.* **2012**, *5*, 1-23.

24.   Baker, S. N.; Baker, G. A., Luminescent Carbon Nanodots: Emergent Nanolights. *Angew. Chem. Int. Ed.* **2010**, *49*, 6726-6744.

25.   Dubey, P.; Tripathi, K. M.; Mishra, R.; Bhati, A.; Singh, A.; Sonkar, S. K., A Simple One-Step Hydrothermal Route Towards Water Solubilization of Carbon Quantum Dots from Soya-Nuggets for Imaging Applications. *RSC Adv.* **2015**, *5*, 87528-87534.

26.   H. Lange ; Sioda, M.; Huczko, A.; Zhu, Y. Q.; Kroto, H. W.; Walton, D. R. M., Nanocarbon Production by Arc Discharge in Water. *Carbon* **2003**, *41*,1617-1623.

27.   Jaiswal, A.; Ghosh, S. S.; Chattopadhyay, A., One Step Synthesis of C-Dots by Microwave Mediated Caramelization of Poly(Ethylene Glycol). *Chem. Commun.* **2012**, *48*, 407-409.

28.   Geim, A. K., Graphene: Status and Prospects. *Science* **2009**, *324*, 1530-1534.

29.   Zhang, B.; Wang, Y.; Zhai, G., Biomedical Applications of the Graphene-Based Materials. *Mater Sci Eng: C* **2016**, *61*, 953-964.

30.   Yang, Y.; Asiri, A. M.; Tang, Z.; Du, D.; Lin, Y., Graphene Based Materials for Biomedical Applications. *Mater. Today* **2013**, *16*, 365-373.

31.   Zhao, Y.; Zhang, Y.; Liu, A.; Wei, Z.; Liu, S., Construction of Three-Dimensional Hemin-Functionalized Graphene Hydrogel with High Mechanical Stability and Adsorption Capacity for Enhancing Photodegradation of Methylene Blue. *ACS Appl. Mater. Interfaces* **2017**, *9*, 4006-4014.

32. Gan, L.; Xu, L.; Shang, S.; Zhou, X.; Meng, L., Visible Light Induced Methylene Blue Dye Degradation Photo-Catalyzed by WO$_3$/Graphene Nanocomposites and the Mechanism. *Ceram. Int.* **2016**, *42*, 15235-15241.

33. Ai, L.; Zhang, C.; Chen, Z., Removal of Methylene Blue from Aqueous Solution by a Solvothermal-Synthesized Graphene/Magnetite Composite. *J. Hazard. Mater.* **2011**, *192*, 1515-1524.

34. Jiao, T.-F.; Zhao, H.; Zhou, J.; Zhang, Q.; Luo, X.; Hu, J.; Peng, Q.; Yan, X., The Self-Assembly Reduced Graphene Oxide Nanosheet Hydrogel Fabrication by Anchorage of Chitosan/Silver and Its Potential Efficient Application toward Dyes Degradation for Wastewater Treatments. *ACS Sustainable Chem. Eng.* **2015**, *3*, 3130-3139.

35. Hou, C.; Zhang, Q.; Li, Y.; Wang, H., P25-Graphene Hydrogels: Room-Temperature Synthesis and Application for Removal of Methylene Blue from Aqueous Solution. *J. Hazard. Mater.* **2012**, *205-206*, 229-235.

36. Wei, G.; Miao, Y.-E.; Zhang, C.; Yang, Z.; Liu, Z.; Tjiu, W. W.; Liu, T., Ni-Doped Graphene/Carbon Cryogels and Their Applications as Versatile Candidates for Water Purification. *ACS Appl Mater Interfaces* **2013**, *14*, 7584-7591.

37. Shanmugam, M.; Alsalme, A.; Alghamdi, A.; Jayavel, R., Enhanced Photocatalytic Performance of the Graphene-V$_2$O$_5$ Nanocomposite in the Degradation of Methylene Blue Dye under Direct Sunlight. *ACS Appl. Mater. Interfaces* **2015**, *7*, 14905-14911.

38. Shen, Y.; Chen, B., Sulfonated Graphene Nanosheets as a Superb Adsorbent for Various Environmental Pollutants in Water. *Environ. Sci. Technol.* **2015**, *49*, 7364-7372.

39. Umrao, S.; Abraham, S.; Theil, F.; Pandey, S.; Ciobota, V.; Shukla, P. K.; Rupp, C. J.; Chakraborty, S.; Ahuja, R.; Popp, J.; Dietzek, B.; Srivastava, A., A Possible Mechanism for the Emergence of Additional Band Gap Due to Ti-O-C Bond in TiO$_2$-Graphene Hybrid System for Enhanced Photodegradation of Methylene Blue under Visible Light. *RSC Adv.* **2014**, *4*, 59890-59901.

40. Umrao, S.; Sharma, P.; Bansal, A.; Sinha, R.; Singh, R. K.; Srivastva, A., Multi-Layered Graphene Quantum Dots Derived Photodegradation Mechanism of Methylene Blue. *RSC Adv.* **2015**, *5*, 51790-51798.

41. Wang, X.; Tian, H.; Yang, Y.; Wang, H.; Wang, S.; Zheng, W.; Liu, Y., Reduced Graphene Oxide/CdS for Efficiently Photocatalytic Degradation of Methylene Blue. *J. Alloy. Compd.* **2012**, *524*, 5-12.

42. Liu, J.; Zhang, T.; Wang, Z.; Dawson, G.; Chen, W., Simple Pyrolysis of Urea into Graphitic Carbon Nitride with Recyclable Adsorption and Photocatalytic Activity. *J. Mater. Chem.* **2011**, *21*, 14398-14401.

43. Khan, M. E.; Khan, M. M.; Cho, M. H., Fabrication of WO_3 Nanorods on Graphene Nanosheets for Improved Visible Light-Induced Photocapacitive and Photocatalytic Performance. *RSC Adv.* **2016**, *6*, 20824-20833.

44. Qu, J.; Shi, L.; He, C.; Gao, F.; Li, B.; Zhou, Q.; Hu, H.; Shao, G.; Wang, X.; Qiu, J., Highly Efficient Synthesis of Graphene/MnO_2 Hybrids and Their Application for Ultrafast Oxidative Decomposition of Methylene Blue. *Carbon* **2014**, *66*, 485-492.

45. Lu, Q.; Zhang, Y.; Liu, S., Graphene Quantum Dots Enhanced Photocatalytic Activity of Zinc Porphyrin toward the Degradation of Methylene Blue under Visible-Light Irradiation. *J. Mater. Chem. A.* **2015**, *3*, 8552-8558.

46. Li, Y.; Qu, J.; Gao, F.; Lv, S.; Shi, L.; He, C., In Situ Fabrication of Mn3o4 Decorated Graphene Oxide as a Synergistic Catalyst for Degradation of Methylene Blue. *Applied Catal. B. Environ.* **2015**, *162*, 268-274.

47. Yang, N.; Liu, Y.; Wen, H.; Tang, Z.; Zhao, H.; Li, Y.; Wang, D., Photocatalytic Properties of Graphdiyne and Graphene Modified TiO_2: From Theory to Experiment. *ACS Nano* **2013**, *7*, 1504-1512.

48. Reimer, T.; Paulowicz, I.; Röder, R.; Kaps, S. r.; Lupan, O.; Chemnitz, S.; Benecke, W.; Ronning, C.; Adelung, R.; Mishra, Y. K., Single Step Integration of ZnO Nano- and Microneedles in Si Trenches by Novel Flame Transport Approach: Whispering Gallery Modes and Photocatalytic Properties. *ACS Appl. Mater. Interfaces* **2014**, *6*, 7806-7815.

49.   Mishra, Y. K.; Modi, G.; Cretu, V.; Postica, V.; Lupan, O.; Reimer, T.; Paulowicz, I.; Hrkac, V.; Benecke, W.; Kienle, L.; Adelung, R., Direct Growth of Freestanding ZnO Tetrapod Networks for Multifunctional Applications in Photocatalysis, UV Photodetection and Gas Sensing. *ACS Appl. Mater. Interfaces* **2015**, *7*, 14303-14316.

50.   Ray, S. C.; Saha, A.; Jana, N. R.; Sarkar, R., Fluorescent Carbon Nanoparticles: Synthesis, Characterization, and Bioimaging Application. *J. Phys. Chem. C* **2009**, *113*, 18546-18551.

51.   Zhang, Z.; Mu, S.; Zhang, B.; Tao, L.; Huang, S.; Huang, Y.; Gao, F.; Zhao, Y., A Novel Synthesis of Carbon Nanotubes Directly from an Indecomposable Solid Carbon Source for Electrochemical Applications. *J. Mater. Chem. A.* **2016**, *4*, 2137-2146

52.   Bhuyan, M. S. A.; Uddin, M. N.; Islam, M. M.; Bipasha, F. A.; Hossain, S. S., Synthesis of Graphene. *Int. Nano Lett.* **2016**, *6*, 65-83.

53.   Sonkar, S. K.; Ghosh, M.; Roy, M.; Begum, A.; Sarkar, S., Carbon Nano-Onions as Nontoxic and High-Fluorescence Bioimaging Agent in Food Chain-an *in vivo* Study from Unicellular *E. coli* to Multicellular *C. elegans*. *Mater. Express* **2012**, *2*, 105-114.

54.   Bahadır, E. B.; Sezginturk, M. K., Applications of Graphene in Electrochemical Sensing and Biosensing. *Trends Analyt. Chem.* **2016**, *76*, 1-14.

55.   Martins, N. C. T.; Angelo, J.; Girao, A. V.; Trindade, T.; Andrade, L.; Mendes, A., N-Doped Carbon Quantum Dots/TiO$_2$ Composite with Improved Photocatalytic Activity. *Appl. Catal. B* **2016**, *193*, 67-74.

56.   Tripathi, K. M.; Kim, T. Y.; Losic, D.; Tung, T. T., Recent Advances in Engineered Graphene and Composites for Detection of Volatile Organic Compounds (VOCs) and Non-Invasive Diseases Diagnosis. *Carbon* **2016**, *110*, 97-129.

57.   Gao, Y.; Pu, X.; Zhang, D.; Ding, G.; Shao, X.; Ma, J., Combustion Synthesis of Graphene Oxide-TiO$_2$ Hybrid Materials for Photodegradation of Methyl Orange. *Carbon* **2012**, *50*, 4093-4101.

58. Zhang, B.; Zhang, D.; Xi, Z.; Wang, P.; Pu, X.; Shao, X.; Yao, S., Synthesis of $Ag_2O/NaNbO_3$ P-N Junction Photocatalysts with Improved Visible Light Photocatalytic Activities. *Sep. Purif. Technol.* **2017**, *178*, 130-137.

59. Tao, T.-X.; Dai, J.-S.; Yang, R.-C.; Xu, J.-B.; Chu, W.; Wu, Z.-C., Synthesis, Characterization and Photocatalytic Properties of BiOBr/ Amidoxime Fiber Composites. *Mater. Sci. Semicond. Process* **2015**, *40*, 344-350.

60. Najam Khan, M.; Al-Hinai, M.; Al-Hinai, A.; Dutta, J., Visible Light Photocatalysis of Mixed Phase Zinc Stannate/Zinc Oxide Nanostructures Precipitated at Room Temperature in Aqueous Media. *Ceram. Int.* **2014**, *40*, 8743-8752.

61. Yu, J.; Lin, W.-F.; Leng, L.-H.; Bao, S.-K.; Zou, J.-P.; Luo, X.-B.; Chen, D.-Z.; Luo, S.-L.; Au, C.-T., Adsorption-Degradation Synergetic Effects on Removal of Methylene Blue over Heterostructured $TiO_2/Co_4S_{4.23}Se_{3.77}$ Composites. *J. Mol. Catal. A: Chem.* **2014**, *394*, 121-128.

62. Xu, Y.; Xu, S.; Wang, S.; Zhang, Y.; Li, G., Citric Acid Modulated Electrochemical Synthesis and Photocatalytic Behavior of BiOCl Nanoplates with Exposed {001} Facets. *Dalton Trans.* **2014**, *43*, 479-485.

63. Moreno-Villoslada, I.; Torres, C.; Gonza ́lez, F.; Shibue, T.; Nishide, H., Binding of Methylene Blue to Polyelectrolytes Containing Sulfonate Groups. *Macromol. Chem. Phys.* **2009**, *210*, 1167-1175.

64. Hafshejani, M. K.; Ogugbue, C. J.; Morad, N., Application of Response Surface Methodology for Optimization of Decolorization and Mineralization of Triazo Dye Direct Blue 71 by *Pseudomonas aeruginosa*. *3 Biotech* **2014**, *4*, 605-619.

65. Zuo, R.; Du, G.; Zhang, W.; Liu, L.; Liu, Y.; Mei, L.; Li, Z., Photocatalytic Degradation of Methylene Blue Using TiO_2 Impregnated Diatomite. *Adv. Mater. Sci. Eng.* **2014**, 2014 (170148).

66. Li, C.; Huang, Y.; Lai, K.; Rasco, B. A.; Fan, Y., Analysis of Trace Methylene Blue in Fish Muscles Using Ultra-Sensitive Surface-Enhanced Raman Spectroscopy. *Food Control* **2016**, *65*, 99-105.

67. Lazaro, D. A.; Caldeira, C. L.; Dantas, M. S. S.; Mansur, M. B.; Oliveira, L. S.; Franca, A. S., Adsorption of Methylene Blue onto Carbons Made of Residues from the Biodiesel Industry. *Int. J. Sus. Dev. Plann.* **2012**, *7*, 446-456.

68. Cabrera, L. I.; Martinez, M.; Reyman, D.; Crespo, P.; Morales, M. P.; Herrasti, P., One Single-Step Synthesis of Multifunctional Methylene Blue-Coated Magnetite Nanoparticles. *J. Nanopart. Res.* **2011**, *13*, 6931-6939.

69. Xu, P.; Xu, T.; Lu, J.; Gao, S.; Hosmane, N. S.; Huang, B.; Dai, Y.; Wang, a. Y., Visible-Light-Driven Photocatalytic S- and C-Codoped Meso/ Nanoporous TiO_2. *Energy Environ. Sci.* **2010**, *3*, 1128-1134.

70. Hassena, H., Photocatalytic Degradation of Methylene Blue by Using Al_2O_3/Fe_2O_3 Nano Composite under Visible Light. *Mod. Chem. Appl.* **2016**, *4*, 176-180.

71. Lonkar, S. P.; Pillai, V. V.; Alhassan, S. M., Facile and Scalable Production of Heterostructured ZnS-ZnO/Graphene Nano-Photocatalysts for Environmental Remediation. *Sci. Rep.* **2018**, *8*, 13401.

72. Si, Y.-H.; Xia, Y.; Shang, S.-K.; Xiong, X.-B.; Zeng, X.-R.; Zhou, J.; Li, Y.-Y. Enhanced Visible Light Driven Photocatalytic Behavior of $BiFeO_3/$ Reduced Graphene Oxide Composites. *Nanomaterials* **2018**, *8*, 526.

73. Medidi, S.; Markapurapu, S.; Kotupalli, M. S.; Chinnam, R. K. R.; Susarla, V. M.; Gandham, H. B.; Sanasi, P.D. Visible Light Photocatalytic Degradation of Methylene Blue and Malachite Green Dyes with $CuWO_4$-GO Nano Composite. *Mod. Res. Catal.* **2018**, *7*, 17-34.

74. Neena D.; Kondamareddy, K. K.; Bin, H.; Lu, D.; Kumar, P.; Dwivedi, R. K.; Pelenovich, V. O.; Zhao, X.-Z.; Gao, W.; Fu, D. Enhanced Visible Light Photodegradation Activity of RhB/MB from Aqueous Solution using Nanosized Novel Fe-Cd co-Modified ZnO. *Sci. Rep.* **2018**, *8*, 10691.

75. Mushtaq, F.; Chen, X.; Hoop, M.; Torlakcik, H.; Pellicer, E.; Sort, J.; Gattinoni, C.; Nelson, B. J.; Pane, S. Piezoelectrically Enhanced Photocatalysis with $BiFeO_3$ Nanostructures for Efficient Water Remediation. *iScience* **2018**, *4*, 236-246.

76. Reheman, A.; Tursun, Y.; Dilinuer, T.; Halidan, M.; Kadeer, K.; Abulizi, A. Facile One-Step Sonochemical Synthesis and Photocatalytic Properties of Graphene/Ag3PO4 Quantum Dots Composites. *Nanoscale Res. Lett.* **2018**, *13*, 70-79.

77. Peter, C. N.; Anku, W. W.; Sharma, R.; Joshi, G. M.; Shukla, S. K.; Govender, P. P. N-doped ZnO/Graphene Oxide: a Photostable Photocatalyst for Improved Mineralization and Photodegradation of Organic Dye under Visible Light. *Ionics* **2018**, *25*, 327-339.

Chapter - 4

Non-toxic Water Soluble Graphene Nanosheets for Selective Photodegradation of Methylene Blue under the Presence of Sunlight

4.1   Introduction

Advances in the field of light-induced photocatalysis [1, 2], particularly in aqueous-phase photocatalytic degradation [3, 4] of various toxic and hazardous water-soluble organic pollutant dyes have shown tremendous development [5, 6]. The prime focus for the aqueous-phase photodegradation of organic dyes is associated with their partial or complete degradation to relatively nontoxic constituents such as low molecular weight hydrocarbons that can ultimately end up to carbon dioxide and water [7-10]. Moreover, the use of sunlight as a freely available renewable light source under the natural conditions can offer an additional advantage for searching the newer sustainable alternatives of water remediation [11, 12]. In the recent past years, the extent of the use of pollutant dyes like MB in different industrial applications [13, 14] followed by their subsequent discharge as a waste in water stream is continuously increasing. Once released into the water bodies as contaminants, these were causing serious issues for both humans and the environment such as heart disease, lung and urinary bladder cancer, chromosomal fractures, mutagenesis, and respiratory toxicity in humans [15-18]. From the environmental perspective, organic dyes are well-known for their ability to significantly damage the aquatic biota of the water system [19]. So tremendous effort for the photodegradation of these pollutant dyes [20], especially using metal-based nanomaterials, are gained a lot attention [21-23] because of their higher photodegradation efficiencies. However, being metallic in nature, metal-based nanomaterials have always been a great concern regarding their toxicity [24]. The toxicity issues can be resolved or minimized via the utilization of long known carbon materials. At present, nanocarbons and functionalized nanocarbons are being explored widely for the wastewater treatment [9, 25-27]. Among all the nanocarbons, graphene [28-31] and graphene-based nanocomposites [7, 8, 32-49] are presently in high demand for photocatalytic/aqueous-phase photocatalytic applications because of its higher surface activities [43, 45].

Herein the present outcomes are concerned with the sustainability of the overall process. In this context, the environmental assessment of the pollutant soot [26, 27, 50] derived wsGNS as a nontoxic photocatalytic material for

degradation/selective degradation of the organic dye is described. Compared to an earlier report [51], sunlight-induced photodegradation of MB by wsGNS shows a higher rate of photodegradation and therefore takes relatively less time (~75 min) for the almost complete degradation (~98%), concerning the decolorization of MB (based on the UV-Vis studies at the wavelength of 663 nm). Furthermore, ^{1}H NMR studies showed the almost complete degradation (~99.9%).

Further, nontoxic wsGNS are being used here precisely for the selective degradation of MB without affecting the growth of two tested bacterial strains, Gram-negative *E. coli* and Gram-positive *Staphylococcus aureus* (*S. aureus*). Additionally, the reaction mechanism and identifications of reactive species involved in photocatalytic degradation of MB are being explored for the sustainable applications of pollutant soot. The nontoxic photodegradation of MB in bacterial cultures can be explained on the basis of the high degree of surface functionalization [51] and simplest trap experiments [51]. Up to now, to the best of our understanding, there is no report available related to the assessments of the waste derived nontoxic wsGNS concerning the evaluation of its environmental applicability for the selective degradation of pollutant dye.

4.2 Experimental Section

4.2.1 Materials and Reagents

Petrol soot was collected from a motor car repair workshop, localized in Jaipur, Rajasthan, India. The different analytical grade reagents like MB, and D_2O, were procured from Sigma-Aldrich, US. HNO_3, acetone, tertiary- butyl alcohol (t-BA), disodium ethylene diaminetetracetate (Na_2-EDTA) were procured from Rankem, India and para-benzoquinone (p-BZQ) from Acros Organics, US. The stock solution of MB was prepared in DI water. All the chemicals were of analytical grade and used as such. Microorganism strains of gram negative bacteria *E. coli* K-12 and gram positive bacteria *S. aureus* RN4220 strains used in the bacteriological test were obtained from Department of Materials Science and Engineering Lab, IIT Kanpur, India.

4.2.2 Photocatalytic Activity Measurement

The photocatalytic experiment was performed using MB (16 mg L^{-1}) as model dye and wsGNS (0.2 g L^{-1}) as photocatalyst under sunlight irradiation. For comparison, photocatalytic experiments using wsGNS were performed using sunlight *versus* artificial light (60 W tungsten bulb). Prior to the start of photodegradation experiment, different photocatalyst materials (GNS and wsGNS) were mixed with MB solution and stirred in dark for 30 min to reach adsorption/desorption equilibration. The respective solutions were put in glass vials and irradiated under sunlight and at fixed interval of time, samples were collected and centrifuged for determining MB concentration in supernatant solution using UV-Vis spectroscopy analyzed at room temperature with PerkinElmer Lambda 35 spectrometer (at wavelength of 663 nm). For detailed analysis of degraded products, photodegradation process was extended up to 8 h, and the collected supernatant sample was analyzed by ^{1}H NMR spectroscopy. Regeneration analysis was performed to confirm the reusable property of wsGNS which was examined by collection of residual wsGNS, followed by the repeated washing with 0.01 M HCl solution ~10-12 times and then washed with distilled water until the pH of the effluent became neutral. The regenerated sample was repeatedly washed and dried in the oven at 80°C to reuse for multiple cycles.

4.2.3 Instrumentation

Microscopic analysis was done through FESEM (Zeiss SUPRA 4A), TEM and HRTEM analysis were performed with a Tecnai G^{2} 20 high-resolution TEM operating at a voltage of 200 kV. Samples for SEM and TEM were prepared by dropping aqueous solution of wsGNS on a brass stub and on a 400 mesh carbon-coated copper grid, respectively, followed by drying under 100 W table lamp. BET surface area for wsGNS was determined using Quantachrome Autosorb iQ. Solid state FT-IR spectra were recorded on a BRUKER Vector22 IR spectrometer. XPS measurements were measured on ESCA^{+} omicron nanotechnology oxford instruments. ^{1}H NMR measurements was performed on a JEOL ECS-400 (operating at 400 MHz, in D$_{2}$O solvent). UV-Vis DRS recorded on a PerkinElmer UV-Vis

(NIR) spectrometer to measure the optical properties of the samples with $BaSO_4$ as internal reflectance standard.

4.2.4 Antibacterial Activity in the Presence and Absence of Sunlight

To measure the antibacterial activity, samples were sterilized in an autoclave and then added to 1 mL of LB media (Himedia) in a 20 mL conical flask. The amount of sample was fixed at 20 μL per mL of media, while the final concentration was varied from 0.1 to 0.3 mg mL^{-1}. The sample and media were then inoculated with 200 μL of overnight culture of *E. coli* and *S. aureus* and incubated at 37°C (75 rpm) for 8 h in a dark incubator shaker. For antibacterial activity in the presence of sunlight, the inoculated samples were kept under the same condition as mentioned above, and the temperature of conical flask was maintained at ~40°C by continuously flowing water. After 8 h, the optical density of the both the media was measured at 600 nm against the respective control sample.

4.2.5 Procedure for Selective Dye Degradation Tests

For ecological study, *E. coli* and *S. aureus* were grown overnight in LB media in an incubator shaker at 37°C and at 75 rpm. Then, 2 mL of *E. coli* and *S. aureus* enriched LB media was added to 50 mL of PBS containing 0.2 mg mL^{-1} particle and 16 mg L^{-1} MB dye. The sample was mixed well and incubated under sunlight for 90 min. Readings were taken at time interval of 30 min. Furthermore, to prevent a surge in the sample temperature, the whole assembly was placed in a waterbath, and water was changed periodically to check that the temperature does not rise beyond 40°C. For bacterial viability test, samples were diluted and plated on luria-bertani (LB) agar plates and allowed to grow at 37°C overnight. Colony forming unit (CFU) count was measured to calculate bacterial viability. Sample aliquots were then centrifuged at 13,500 rpm for 10 min, and supernatant absorbance was measured at 663 nm against appropriate controls.

4.3 Results and Discussion

The straightforward methodology presented here has a significant advantage toward the concomitant reductions in the quantity of two different pollutant materials by countering one with another. Scheme 4.1 illustrated the utilization of

wsGNS as nontoxic photocatalytic nanomaterial for the sunlight-induced photodegradation of MB. As well showing the potential assessment of wsGNS regarding the selective degradation of MB without harming the bacterial growth with two different bacterial strains (*E. coli and S. aureus*).
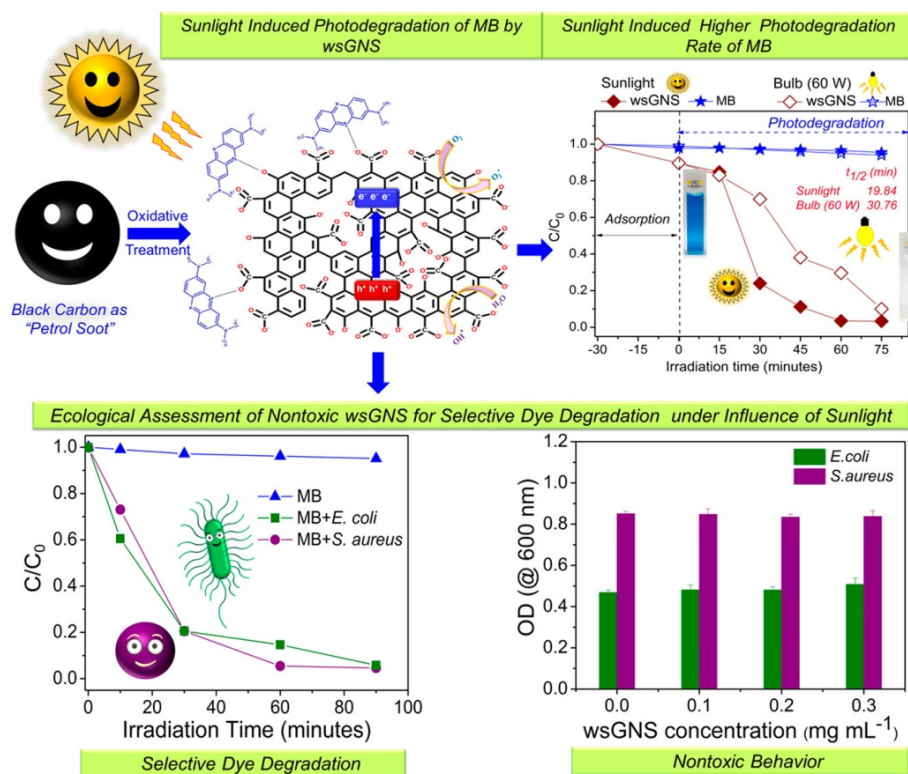
Scheme 4.1. Schematic representation illustrated the synthesis and application of nontoxic wsGNS for the sunlight induced selective photodegradation of MB.

4.3.1 Microscopic Analysis of wsGNS

Low-resolution SEM image of the wsGNS (Figure 4.1(a)) shows the sheet like morphology rolled one top on another. The high-resolution SEM image in Figure 4.1 (b) shows the crumpled nature of graphitic wsGNS. Furthermore, TEM and HRTEM provided the detailed internal structural analysis. Low-resolution TEM image in Figure 4.1(c) confirms the presence of corrugated structures of multilayered graphene sheets. The HRTEM images show that wsGNS consisted of 4-5 layers of graphene sheets (Figure 4.1(d)). Figure 4.1(e-f) indicate the presence of surface defects in the shape of different sized graphitic patches as encircled with the red color. The presence of such small graphitic patches (~2-3 nm in diameter) in the form of the surface defects/active centers on the wsGNS provides active catalytic sites [51] for the aqueous-phase photodegradation of pollutant dyes [51].
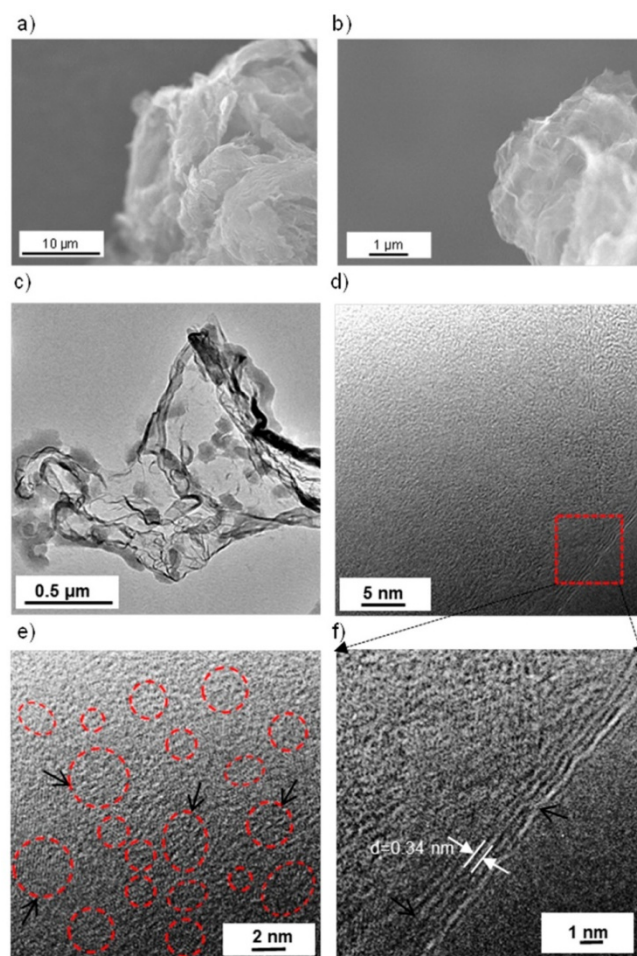
Figure 4.1. (a) Low-resolution; and (b) High-resolution SEM image of wsGNS; (c) Low-resolution TEM image; (d) HRTEM image of wsGNS; (e) Presence of different shaped graphitic patches (marked by red circles); and (f) Few-layer graphene sheets with interlayer spacing of 0.34 nm.

4.3.2 Spectroscopic Analysis of wsGNS: FT-IR and XPS Analysis

The presence of negative surface functionalities on wsGNS was confirmed by FT-IR and XPS analysis. FT-IR spectrum in Figure 4.2 (a) shows broad absorption band at ∼3438 cm^{-1} for the stretching vibrations of −OH, which indicates the presence of hydroxyl groups. The two small, weak bands at 2924 cm^{-1} and 2853 cm^{-1} (doublet) correspond to the C-H stretching. The sharp, intense split peaks observed at 1713 cm^{-1} and 1615 cm^{-1} correspond to a C=O carbonyl functional group and a C=C stretching of aromatic hydrocarbons, respectively. Two intense peaks of C-O and C-C stretching vibrations were observed at 1241 cm^{-1} and 1093 cm^{-1}, respectively.

XPS further supported the negative surface functionalities, showing the different binding sites of carbon with oxygen. A complete survey scan of wsGNS (Figure 4.2(b)) shows two characteristic peaks for C_{1s} and O_{1s} at 284.5 eV and 532.0 eV respectively. The elemental composition of carbon and oxygen was ∼80% and ∼20%. The deconvulated short scan spectra of C_{1s} and O_{1s} are presented in Figure 4.2 (c,d) respectively. The deconvulated C_{1s} short scan spectra (Figure 4.2 (c)) shows five different types of carbon binding in wsGNS, presented in the form of groups such as C=C (283.6 eV), C-C (284.9 eV), C-O (285.6 eV), C=O (286.9 eV), and COO$^-$ (288.7 eV). Similarly, Figure 4.2 (d) shows the deconvulated spectra of the O_{1s} short scan, composed of three different types of binding moieties related to oxygen and carbon as C-O, C=O, and COO$^-$ at 530.8 eV, 532.2 eV, and 533.8 eV, respectively [52, 53]. The presence of surface defects in the form of high density hydrophilic groups because of the oxidative treatment are responsible for imparting the water solubilizations [51] and the excellent optical properties in the form of tunable PL properties as described earlier [51, 54].
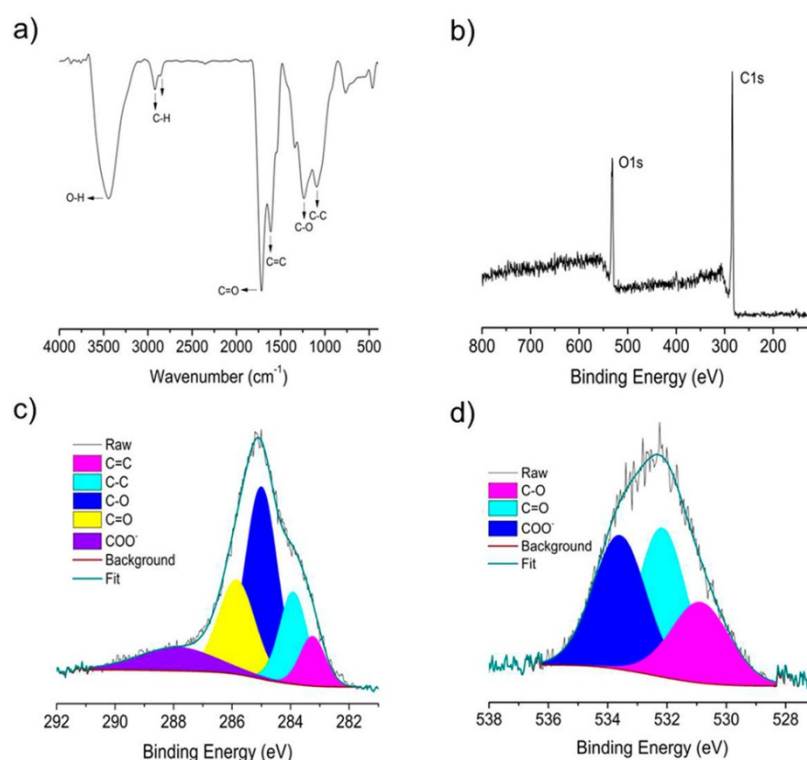
Figure 4.2. (a) FT-IR spectrum of wsGNS; (b) XPS full scan spectra of wsGNS and its corresponding (c) C_{1s} short scan and (d) O_{1s} short scan.

4.3.3 Photocatalytic Dye Degradation under Sunlight Illumination

Figure 4.3 (a) also includes the adsorption-desorption equilibrium achieved initially in 30 min before the start of photodegradation process. Approximately 9% adsorption of MB is obtained with wsGNS, which can be attributed to the surface adsorption, and could be related to the lower values of Brunauer-Emmett-Teller (BET) surface area [55, 56] (23 m^2 g^{-1}), and total pore volume is $\sim$0.168 cc g^{-1}. In absence of photocatalyst wsGNS, a negligible change in MB concentration was observed as shown in Figure 4.3 (a). Furthermore, a detailed aqueous-phase photodegradation study of MB [51] under sunlight irradiation with wsGNS and GNS are shown in Figure 4.3 (a), carried out in different conditions for the comparison purpose. The continuous change in the concentration (concerning the decolorization) of MB by GNS and wsGNS (Figure 4.3 (a)) in sunlight was observed at different time intervals using the UV-Vis absorbance spectroscopy. The rate constant data were evaluated from the corresponding experimental data Figure 4.3 (a) by assuming pseudo first-order kinetics and the linear fitting of pseudo first-order kinetics is shown in Figure 4.3 (b).
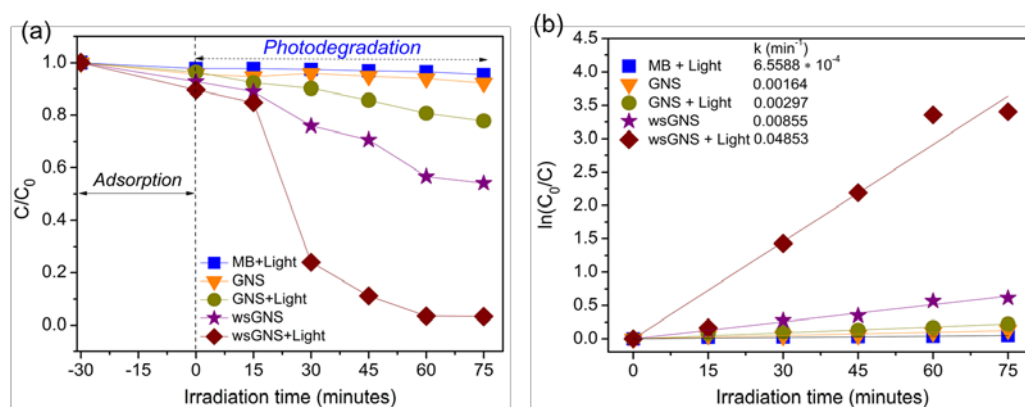
Figure 4.3. Extent of (a) Plot of C/C_o for MB photodegradation by wsGNS under sunlight irradiation with adsorption as background tests; (b) Plot of $\ln(C_o/C)$ for MB photodegradation by different samples.

A comparative photodegradation study was performed experimentally in the aqueous-phase using natural sunlight *versus* 60 W tungsten bulb (as a source of initiative step for the photocatalytic reaction). Figure 4.4 (a) shows a comparative photodegradation study of MB using wsGNS as photocatalyst, in the presence of

sunlight and 60 W tungsten bulb [51], with the variation of C/C_o of the aqueous samples of MB-wsGNS with different time interval using UV-Vis spectroscopy at 663 nm [51, 57]. The data demonstrate the higher degradation efficiency in the case of sunlight (achieved ~97%) for the initial 60 min of exposure compared to that of 60 W bulb (~77%).

UV-Vis analysis (decolorization of MB) data confirms that using wsGNS in the presence of sunlight shows the highest degradation efficiency (~98%) observed within the 75 min. For the faster rate of photodegradation under sunlight by wsGNS, the high level of surface functionalization is the only principal difference between GNS and wsGNS and can be responsible for the increased in the photodegradation efficiencies of MB. Almost ~97% MB was photodegraded (decolorized) within the initial 60 min and starts degrading completely (~99.9%), based on the ^{1}H NMR analysis described in next section.
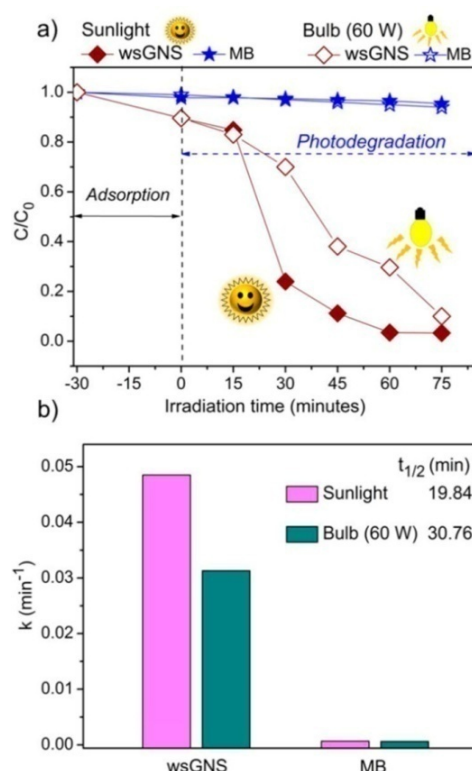
Figure 4.4. (a) Influence of sunlight over 60 W bulb light for photodegradation of MB using wsGNS; (b) Comparative data of pseudo-first-order rate constant and half-life ($t_{1/2}$) in minutes obtained from experimental data in panel (a).

Figure 4.3 (b) shows the higher rate constant (0.04853 min^{-1}) for wsGNS in the presence of sunlight which is ~1.5 times greater compared to that with 60 W bulb (0.0313 min^{-1}), indicating the significant influence of natural sunlight. The results suggest that the presence of natural sunlight quickly activates the different emitting centers of wsGNS for the degradation study as corroborated with $t_{1/2}$ data shown in Figure 4.4 (b), degrading 50% of initial MB concentration even in a shorter period of time. These rate constant data were evaluated from the corresponding experimental data Figure 4.3 (a) by assuming pseudo-first-order kinetics, and the linear fitting of pseudo-first-order kinetics is shown in Figure 4.3 (b). In the presence of sunlight, the photodegradation rate constant for wsGNS was 0.04853 min^{-1} compared to 0.00297 min^{-1} for GNS indicating the increased photocatalytic efficiency was up to ~16 times higher in wsGNS than the GNS.

Also, the photodegradation efficiency and the rate constant of wsGNS are compared with those of the other photocatalyst materials under the presence of sunlight, shown in Table 4.1. The data obtained for the photodegradation efficiency of wsGNS in the present study are found to be higher compared to those of the other studies [7, 10, 32-34, 38, 42, 58].

Furthermore, UV-Vis diffuse reflectance spectroscopy (DRS) [43, 44, 59] was performed to better understand the influence of different light sources on wsGNS. wsGNS shows a strong absorption in UV region (Figure 4.5 (a)) that shows a near edge absorption at ~243 nm which corresponds to the bandgap of wsGNS. Similarly, to understand the influence of different light sources, a comparative analysis was performed with wsGNS irradiated with different light sources such as 60 W bulb and sunlight. The Tauc plots in Figure 4.5 (b) ((αhυ)^2 vs hυ (where hυ is photon energy)) show the measured bandgap for wsGNS which was 4.0 eV. While this value was found to decrease when irradiated with 60 W bulb light (3.8 eV) and sunlight (3.3 eV) [60]. The experimental observation based on diffuse reflectance are consistent with the photodegradation rate constant and $t_{1/2}$ values as shown in Figure 4.3 (b) and Figure 4.4 (b), respectively.

Table 4.1. Comparative table showing degradation of MB under direct sunlight by different graphene/r-GO composites and present study

S. No	Sample	Degradation (%)	Degradation time (minutes)	Rate	Ref.
1.	Graphene-ZnTiO$_3$ nanocomposite	>95%	60 min	-	[7]
2.	ZnO-RGO/RuO$_2$ nanocomposites 10 mg L^{-1}	99%	60 min	-	[10]
3.	Graphene-SnO$_2$-PMMA nanocomposite 0.01 mM	99%	60 min	0.0488 min^{-1}	[32]
4.	ZnFe$_2$O$_4$/ZnO nanocomposites on graphene 10 mg L^{-1}	99%	120 min	0.0330 min^{-1}	[33]
5.	Graphene-V$_2$O$_5$ nanocomposite	99%	90 min	0.0366 min^{-1}	[34]
6.	Hemin-functionalized graphene hydrogel 50 mg L^{-1}	96 %	180 min	0.017 min^{-1}	[38]
7.	ZnO flower/reduced GO composite 15 mg L^{-1}	97%	150 min	0.0395 min^{-1}	[42]
8.	Graphene-SnO$_2$ composites 2.7*10^{-5} M	99%	5 min	-	[58]
9.	wsGNS	98%	75 min	0.04853 min^{-1}	Present study
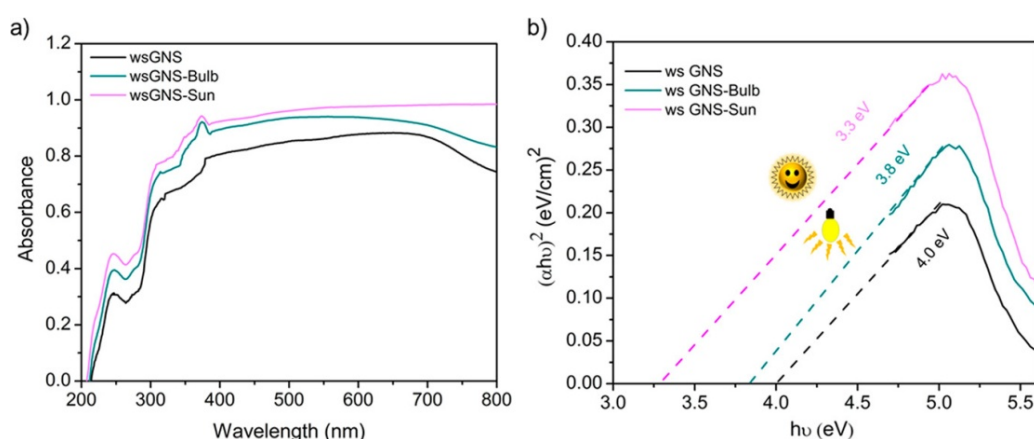
Figure 4.5. (a) UV-Vis DRS spectra; and (b) Tauc plot of (αhυ)^2 *versus* hυ of wsGNS under different light sources.

The most plausible mechanism responsible for the increase in the efficiency of photodegradation by wsGNS in sunlight is shown in Figure 4.6 (a-b). This was attributed to the presence of high-density surface defects that can provide enhanced active surface sites for the photocatalytic process. The presence of negative moieties (hydroxyl and carboxyl groups) as the high-density functionalization of wsGNS enhanced the spatial separation between HOMO-LUMO as shown in Figure 4.6 (a-b) equation (i) [9] A high degree of the generated holes reacted with water molecules, oxygenated functional groups, and generated the reactive oxygen groups Figure 4.6 (b), equation (ii). Moreover, surface functionalization retarded the recombination of electron-hole pairs via the trapping of electrons as active species on surface defects [51, 61].

As well, the planar morphology of wsGNS could enhances the electron transfer between wsGNS and photoexcited dye molecules Figure 4.6 (b), equation (iii), very similar to graphene which is acting as an excellent photocatalytic material. Figure 4.6 (b), equation (iv-vi), show the reaction of active radical species with surface-adsorbed MB molecules leading to degradation of MB into possible nontoxic products, like smaller hydrocarbons and can ultimately convert to the carbon dioxide and water [7, 10, 33].

The generation of active-reactive species in photocatalytic reaction responsible for the degradations of MB and the insight of photodegradation mechanism were further explored by performing trap experiments separately as shown in Figure 4.6 (c-f). On the basis of the use of the different types of scavengers like t-BA for the trapping of $^{\bullet}OH$, Na_2-EDTA for the trapping of surface generated holes (h^+), and the p-BZQ for the trapping of superoxide ($O_2^{-\bullet}$) scavengers Figure 4.6 (c-e). Such scavengers are widely used and reported in trapping the different radicals in literatures [51, 62-69]. The molar concentration of different scavengers varies from 0.5 mM to 10 mM in aqueous system of MB-wsGNS. Figure 4.6 (c) shows that the photodegradation activity was significantly reduced from 97% to 82% in the presence of 0.5 mM of t-BA. In the same Figure 4.6 (c), the photocatalytic efficiency of wsGNS toward MB was completely reduced up to 4% when t-BA molar concentration was increased by ~20 times of 0.5 mM

concentration, implying the strong influence of hydroxyl radicals in the process of photodegradation in the presence of sunlight. A similar trend was observed when Na_2-EDTA was added into aqueous system of MB-wsGNS Figure 4.6 (d).
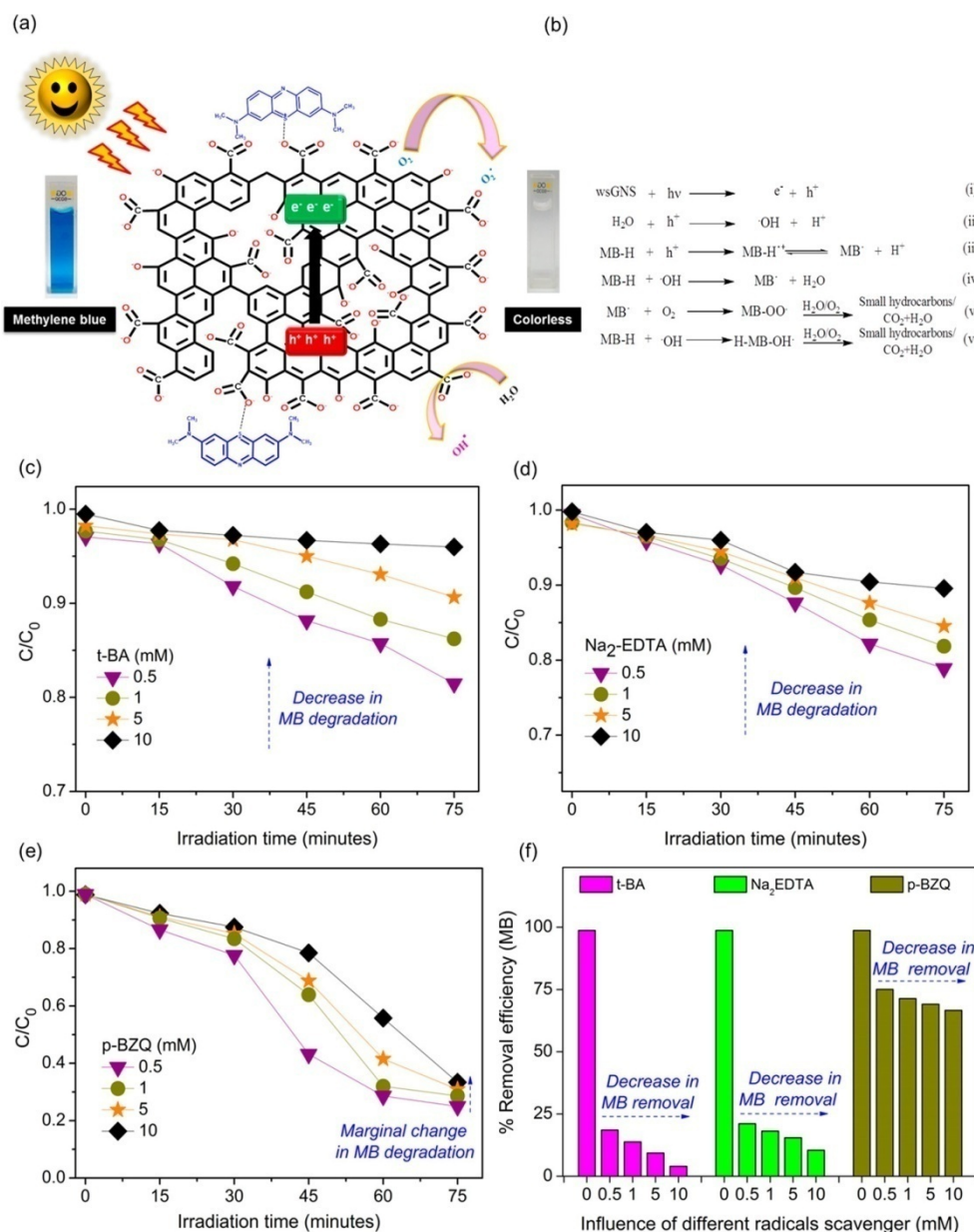
Figure 4.6. (a, b) Plausible mechanism of photodegradation of MB by wsGNS in sunlight; Effect of different scavengers on photodegradation efficiency of MB using wsGNS: (c) t-BA for hydroxyl radicals; (d) Na_2-EDTA for holes; (e) p-BZQ for superoxide radicals. (f) Comparative influence of different scavengers in photocatalytic activity of different reactive species for MB degradation.

The photocatalytic degradation efficiency was reduced up to ~10% at higher concentration of Na$_2$-EDTA (10 mM) which is acting as scavengers for holes, although the influence of holes scavenger on the MB degradation was relatively lower than that of $^•$OH radical scavenger. Contrary to the hydroxyl and holes scavengers, marginal changes in photodegradation efficiency were observed for O$_2^{-•}$ radicals as shown in Figure 4.6 (e). Figure 4.6 (f) shows a comparative influence of all three plausible reactive species that are responsible for the photocatalytic degradation efficiency of MB in MB-wsGNS system. The trap experiments clearly suggest that out of three reactive species, only hydroxyl and holes have the strong influence toward the photodegradation of MB. The recycling ability and potential utility of the material as wsGNS used for the photodegradation is the crucial character that can decide the overall feasibility of the process. Figure 4.7 indicates the loss of ~17% in degradation efficiency of wsGNS as a photocatalyst material after 4 cycles of use in photodegradation of MB.
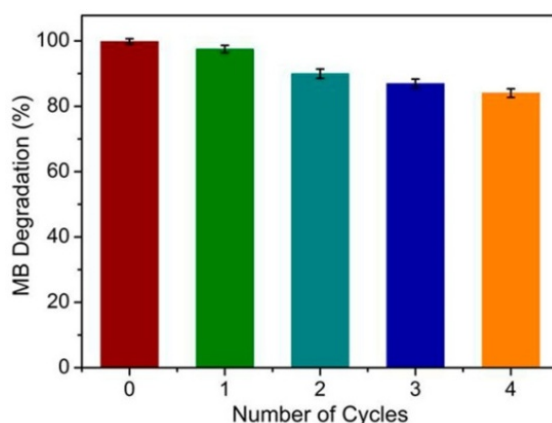
Figure 4.7. Photocatalytic performance of wsGNS with 4 cycles of recycling testing.

4.3.4 Insights of the Photodegradation Analysis by ^{1}H NMR Spectroscopy

Comparative ^{1}H NMR was performed (Figure 4.8) to analyze the degraded products of MB in aqueous-phase before and after the degradation process. Figure 4.8 (a) shows the chemical structure of MB (with numbers labeled on chemically different protons). Figure 4.8 (b) shows the photocatalytic effect of wsGNS on the MB (blue solution in left cuvette) in the presence of sunlight which makes it colorless (transparent solution in right cuvette). ^{1}H NMR spectra of (i) MB, (ii) MB-wsGNS (degraded dye after 4 h), and (iii) after 8 h are shown in Figure 4.8 (c-(i-iii)), respectively, in the presence of sunlight. Photodegraded samples were collected

from the pool of MB-wsGNS system after 4 and 8 h time periods, and the as-collected samples were further centrifuged and supernatant collected and dried on a waterbath for the ^{1}H NMR analysis. Figure 4.8 (c-(i)) shows the ^{1}H NMR spectrum of MB which shows a sharp singlet at δ1H 2.96 ppm assigned to aliphatic protons and three doublet signals from δ1H 6.56 to 7.0 ppm associated with the presence of aromatic protons.
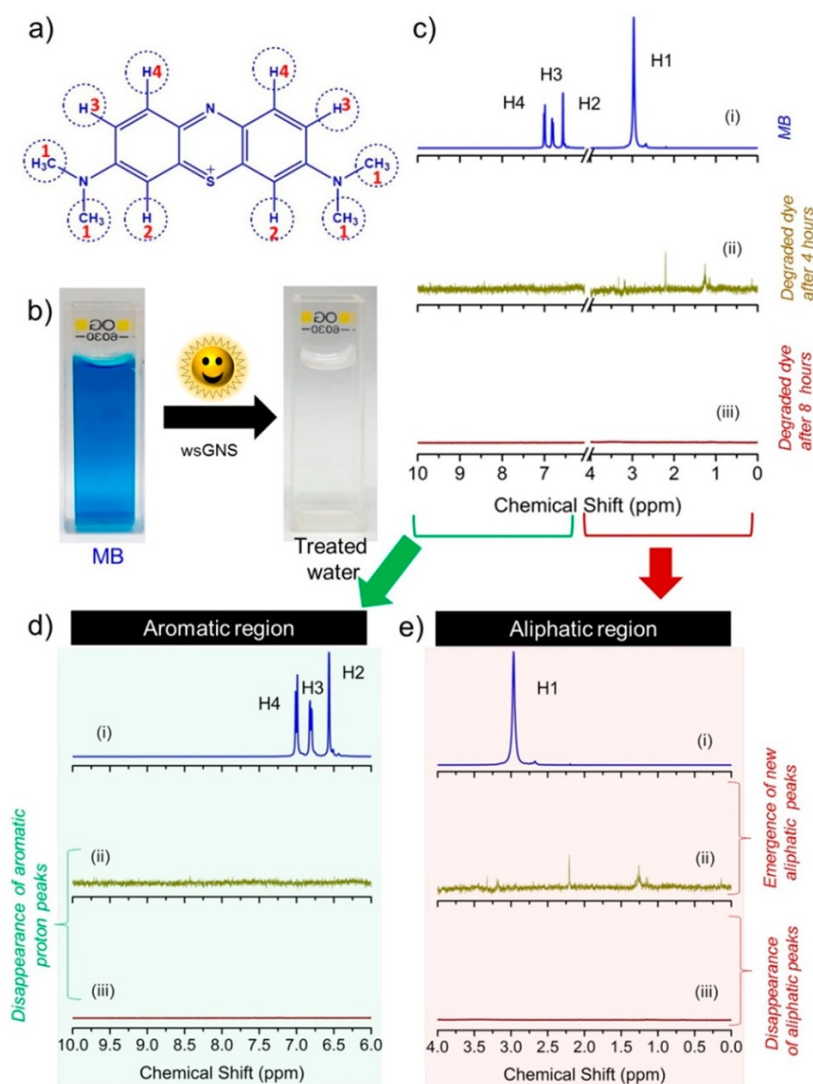
Figure 4.8. (a) Chemical structure of MB; (b) Effect of wsGNS in sunlight on MB (blue solution in left cuvette) to colorless (transparent solution in right cuvette); (c) ^{1}H NMR spectra of the photodegradation of MB while interaction with wsGNS over different time intervals: (i) ^{1}H NMR of MB; (ii) ^{1}H NMR of MB with wsGNS after 4 h; and (iii) ^{1}H NMR of MB with wsGNS after 8 h of sunlight irradiation. (d) Zoomed image of panel c Aromatic region (between 10 ppm to 6 ppm); (e) Aliphatic region (between 4 ppm to 0 ppm).

The aromatic region shows six chemically different aromatic protons which give their doublets (signals at δ1H 6.56, 6.80, and 7.0 ppm representing H2-H4, respectively) are shown in Figure 4.8 (d-(i)). Compared to control (MB), after photocatalytic treatment of dye with wsGNS, the proton spectrum of the degraded dye after 4 h and 8 h shows the disappearance of signals in the aromatic region (Figure 4.8 (d-(ii)) and Figure 4.8 (d-(iii)) respectively) indicating loss of the aromaticity. The aliphatic region Figure 4.8 (e) shows a sharp singlet (δ1H 2.96 ppm) assigned to H1 indicates the presence of methyl groups of MB as in Figure 4.8 (e-(i)). After 4 h of photocatalytic degradation, the sharp peak related to 12 methyl protons disappears, and an emergence of newer aliphatic peaks in the more shielded region is observed (at 1.44, 2.2, and 3.33 ppm) corresponding to the formation of small aliphatic hydrocarbons as shown in Figure 4.8 (e-(ii)) which further disappeared after 8 h of photodegradation Figure 4.8 (e-(iii)). Overall, ^{1}H NMR study as indicated by the Figure 4.8 (d-(iii)) and (e-(iii)) displaying the complete disappearance of all the protons in aromatic and aliphatic regions confirms the complete degradation of the MB molecules.

4.3.5 Nontoxic Effects of wsGNS Exposure to the Bacterial Cells: *E. coli* and *S. aureus*

The ease of water solubilization of wsGNS, which is the most important parameter for the biological applications, is further used here for analyzing its nontoxic behavior toward the two different types of bacterial strains that is Gram negative bacteria *E. coli* and Gram positive *S. aureus*. Bacteriological tests evaluating the nontoxicity of wsGNS on *E. coli* and *S. aureus* cells were performed in aqueous LB media in a 20 mL conical flask. The growth of bacterial culture was determined by measuring the optical density (OD) at fixed wavelength of 600 nm (OD$_{600}$) in LB media complemented with four different concentrations of wsGNS, including (i) the control, 0 mg mL^{-1}, (ii) 0.1 mg mL^{-1}, (iii) 0.2 mg mL^{-1}, and (iv) 0.3 mg mL^{-1} in 20 mL of LB media, respectively, under both dark (Figure 4.9 (a,c)) and sunlight (Figure 4.9 (b,d)) conditions. All four concentrations of wsGNS were checked for OD$_{600}$ to assess the nontoxic behavior of wsGNS. The dye photodegradation test of MB was performed for the concentration of 0.2 mg mL^{-1} of wsGNS. To confirm a wider level of tolerance, a higher level of wsGNS 0.3 mg mL^{-}

[1] was also studied. After the 8 h incubation period, wsGNS did not show any toxic characteristics toward the growth of the *E. coli* and *S. aureus* (Figure 4.9). The nontoxic bacteriological test was performed in triplicate, and results are shown in Figure 4.9 (a-d) with ±SE. Compared to earlier reports [70-71], herein the biocompatibility can be described concerning the nontoxic behavior (Figure 4.9) based on our earlier findings, describing the nontoxic behavior because of the heavily derivatization of nanocarbons on various model, such as *E. coli* [72], *Caenorhabditis elegans* [73], *Drosophila melanogaster* [74], and on plants (gram plants [75] and wheat [76]). Similarly, highly functionalized wsGNS carrying the same nontoxic behavior along with the additional ability to efficiently photodegrade the pollutant dye in sunlight.
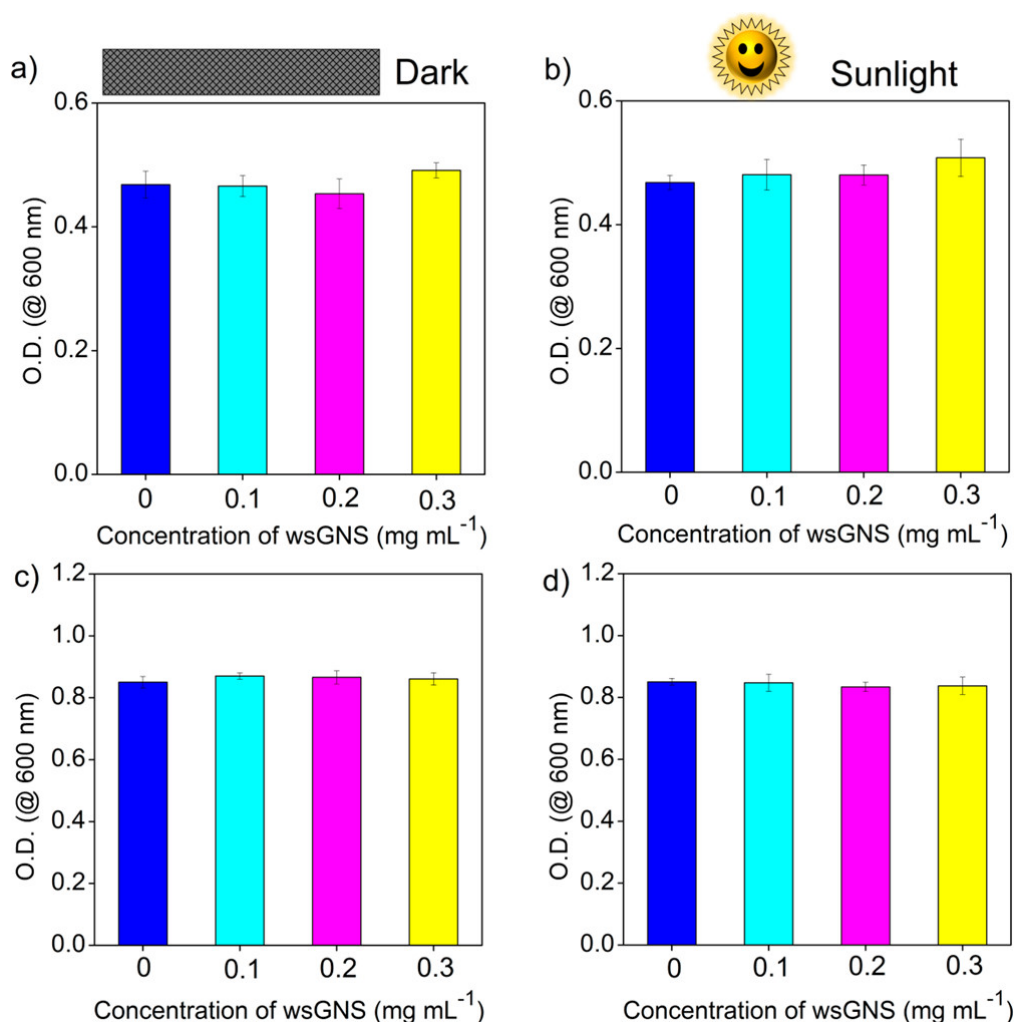
Figure 4.9. Growth bars based on OD_{600} in dark; (a) *E. coli*; and (c) *S. aureus* compared to the OD_{600} in the presence of sunlight for (b) *E. coli*; and (d) *S. aureus* inoculated in LB media having the different concentration of wsGNS with ±SE.

4.3.6   Selective Dye Degradation Test

Concerning the ecological sustainability of the overall process, we have extended the dye degradation experiments in bacterial cell culture with a positive hope for the selective degradation of MB without harming the routine biological growth of *E. coli* and *S. aureus* by wsGNS. Introducing nontoxic wsGNS in the bacterial cells grown within the MB solution with wsGNS in dark and in the presence of sunlight conditions showed the remarkable results in the form of a capability to selectively degrade the MB. Figure 4.10 (a,d) includes a cartoon illustration showing the experimental setup used for sunlight-induced selective degradation of MB within the bacterial culture of *E. coli* and *S. aureus* cell. Figure 4.10 (b,e) show the nontoxic behavior of wsGNS.

The nontoxic behavior is further confirmed by CFU counts, as shown in Figure 4.10 (c,f) before and after photodegradation of MB. Figure 4.10 (g,h) show the degradation curves of MB (selectively degraded the MB only) from the pool of *E. coli* and *S. aureus* respectively in the presence of sunlight along with its corresponding degradation rate constants in Figure 4.10 (i,j) respectively. In the presence of *E. coli* and *S. aureus* a marginal interference in degradation efficiency of MB by wsGNS was observed, as shown by the same Figure 4.10 (i,j).
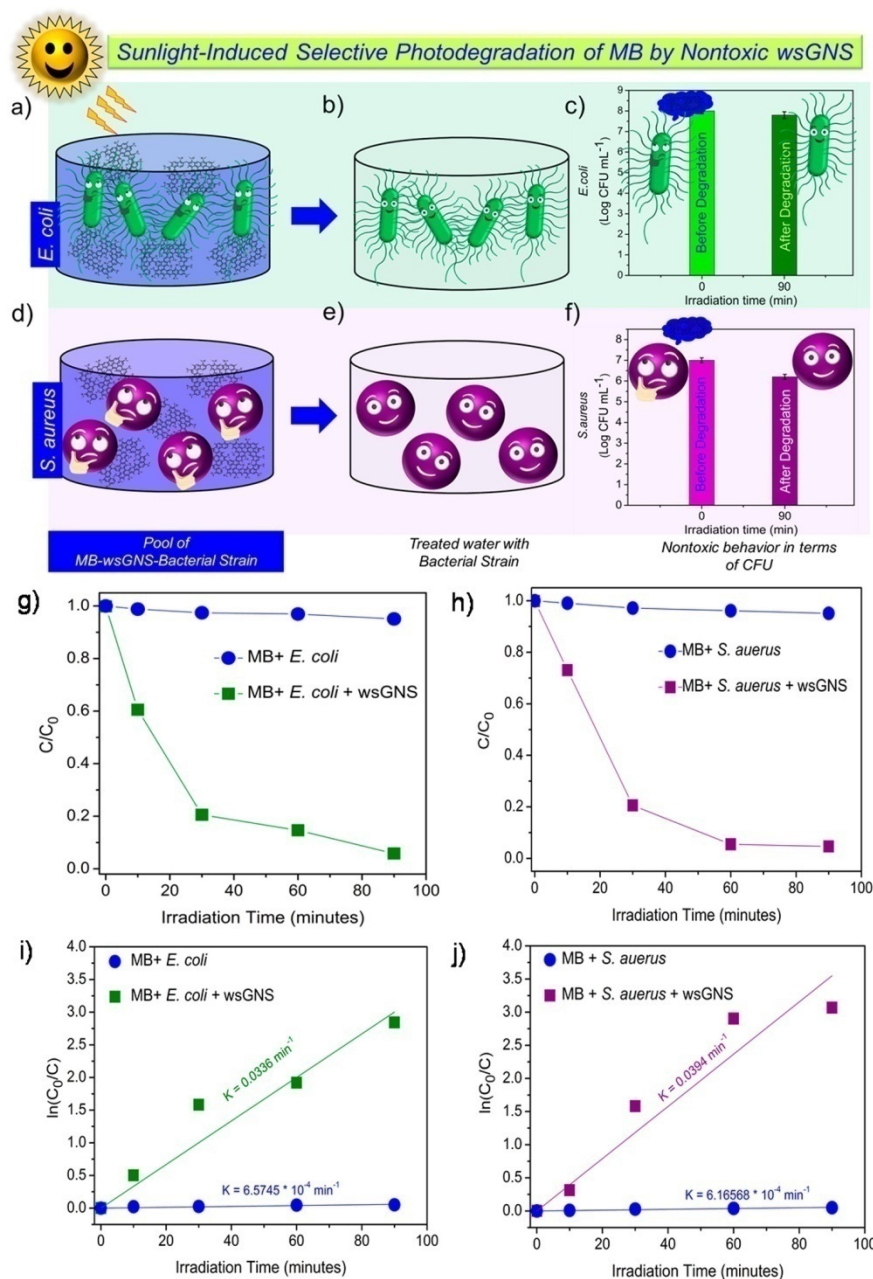
Figure 4.10. Cartoon illustration describing the simplest approach used in the sunlight-induced selective dye degradation *via* wsGNS. Pool of MB-wsGNS-bacterial strain in the presence of sunlight: (a) *E. coli*; and (d) *S. aureus*; where wsGNS selectively degraded MB without harming bacterial colonies, (b) *E. coli*; and (e) *S. aureus*; Along with bacterial viability test in the form of CFU before and after MB degradation for (c) *E. coli*; and (f) *S. aureus*; The extent of the plot of C/C_o for the selective photodegradation of MB by wsGNS under the influence of sunlight in the bacterial LB media of (g) *E. coli*; and (h) *S. aureus*; Plot of $\ln(C_o/C)$ with apparent rate constant for the selective photodegradation by wsGNS in sunlight within the bacterial culture of (i) *E. coli*; and (j) *S. aureus*.

4.4   Conclusion

The present finding has introduced a facile and sustainable approach for the usage of pollutant soot (wsGNS) for the complete photodegradation of MB in a very cost efficient and simpler way at ambient conditions. wsGNS are nontoxic on the tested *E. coli* and *S. aureus* cells. The successful utilization of the most sustainable energy source as sunlight is being explored here, and the most important wsGNS are being used here for the selective photodegradation of pollutant dye without harming the bacterial balance which would sustain the environmental prospect and the sustainability of the overall described procedure. wsGNS degrade the complex organic framework of MB molecules into smaller nontoxic constituents with a higher rate in the presence of sunlight compared to that of 60 W tungsten bulb. The reported method can be easily scaled up, which can directly relate to the reduction in the extent of pollutant soot and pollutant dye (photodegradation of soluble organic dye). Nontoxicity along with photocatalytic properties makes wsGNS a potential material, which could be utilized thoroughly as a photocatalytic material for the photodegradation purposes, and the high degree of water solubility could be used in the area of biomedical and biological applications.

4.5   References

1.   Yoon, T. P.; Ischay, M. A.; Du, J., Visible Light Photocatalysis as a Greener Approach to Photochemical Synthesis. *Nat. Chem.* **2010**, *2*, 527-532.

2.   Likodimos, V.; Dionysiou, D. D.; Falaras, P., Clean Water: Water Detoxification Using Innovative Photocatalysts. *Rev. Environ. Sci. Biotechnol.* **2010**, *9*, 87-94.

3.   Kabra, K.; Chaudhary, R.; Sawhney, R. L., Treatment of Hazardous Organic and Inorganic Compounds through Aqueous-Phase Photocatalysis: A Review. *Ind. Eng. Chem. Res.* **2004**, *43*, 7683-7696.

4.   Herrmann, J.-M., Heterogeneous Photocatalysis: Fundamentals and Applications to the Removal of Various Types of Aqueous Pollutants. *Catal. Today* **1999**, *53*, 115-129.

5.   Berberidou, C.; Poulios, I.; Xekoukoulotakis, N. P.; Mantzavinos, D., Sonolytic, Photocatalytic and Sonophotocatalytic Degradation of Malachite Green in Aqueous Solutions. *Appl. Catal. B.* **2007**, *74*, 63-72.

6.   Lachheb, H.; Puzenat, E.; Houas, A.; Ksibi, M.; Elaloui, E.; Guillard, C.; Herrmann, J.-M., Photocatalytic Degradation of Various Types of Dyes (Alizarin S, Crocein Orange G, Methyl Red, Congo Red, Methylene Blue) in Water by UV-Irradiated Titania. *Appl. Catal., B.* **2002**, *39*, 75-90.

7.   Gayathri, S.; Jayabal, P.; Kottaisamy, M.; Ramakrishnan, V., Synthesis of the Graphene-ZnTiO$_3$ Nanocomposite for Solar Light Assisted Photodegradation of Methylene Blue. *J. Phys. D: Appl. Phys* **2015**, *48*, 415305-415315.

8.   Jiao, T.-F.; Zhao, H.; Zhou, J.; Zhang, Q.; Luo, X.; Hu, J.; Peng, Q.; Yan, X., The Self-Assembly Reduced Graphene Oxide Nanosheet Hydrogel Fabrication by Anchorage of Chitosan/Silver and Its Potential Efficient Application toward Dyes Degradation for Wastewater Treatments. *ACS Sustainable Chem. Eng.* **2015**, *3*, 3130-3139.

9.   Umrao, S.; Sharma, P.; Bansal, A.; Sinha, R.; Singh, R. K.; Srivastva, A., Multi-Layered Graphene Quantum Dots Derived Photodegradation Mechanism of Methylene Blue. *RSC Adv.* **2015**, *5*, 51790-51798.

10. Reddy, D. A.; Ma, R.; Kim, T. K., Efficient Photocatalytic Degradation of Methylene Blue by Heterostructured ZnO-RGO/RuO$_2$ Nanocomposite under the Simulated Sunlight Irradiation. *Ceram Int.* **2015**, *41*, 6999-7009.

11. Malato, S.; Fernandez-Ibanez, P.; Maldonado, M. I.; Blanco, J.; Gernjak, W., Decontamination and Disinfection of Water by Solar Photocatalysis: Recent Overview and Trends. *Catal. Today.* **2009**, *147*, 1-59.

12. Ravelli, D.; Dondi, D.; Fagnonia, M.; Albini, A., Photocatalysis. A Multi-Faceted Concept for Green Chemistry. *Chem. Soc. Rev.* **2009**, *38*, 1999-2011.

13. Khan, S.; Malik, A., Environmental and Health Effects of Textile Industry Wastewater. *In Environmental Deterioration and Human Health: Natural and anthropogenic determinants*, **2014**, 55-71.

14. Carmen, Z.; Daniela, S., Textile Organic Dyes - Characteristics, Polluting Effects and Separation/Elimination Procedures from Industrial Effluents - a Critical Overview, In: *Organic Pollutants Ten Years after the Stockholm Convention - Environmental and Analytical Update.* **2012**, 55-86.

15. Clarke, E. A.; Anliker, R., Organic Dyes and Pigments. In: *Anthropogenic Compounds*, *The Handbook of Environmental Chemistry,* **1980**, *3*, 181-215.

16. Vanhulle, S.; Trovaslet, M.; Enaud, E.; Lucas, M.; Taghavi, S.; Lelie, D. V. D.; Aken, B. V.; Foret, M.; Onderwater, R. C. A.; Wesenberg, D.; Agathos, S. N.; Schneider, Y.-J.; Corbisier, A.-M., Decolorization, Cytotoxicity, and Genotoxicity Reduction During a Combined Ozonation/Fungal Treatment of Dye-Contaminated Wastewater. *Environ. Sci. Technol.* **2008**, *42*, 584-589.

17. Brown, M. A.; Vito, S. C. D., Predicting Azo Dye Toxicity. *Crit. Rev. Environ. Sci. Technol.* **1993**, *23*, 249-324.

18. Weisburger, J. H., Comments on the History and Importance of Aromatic and Heterocyclic Amines in Public Health. *Mutat. Res.* **2002**, *506-507*, 9-20.

19. Ali, M.; Sreekrishnan, T. R., Aquatic Toxicity from Pulp and Paper Mill Effluents: A Review. *Adv. Environ. Res.* **2001**, *5*, 175-196.

20. Luo, B.; Liu, G.; Wang, L., Recent Advances in 2 D Materials for Photocatalysis. *Nanoscale* **2016**, *8*, 6904-6920.

21. Mishra, Y. K.; Modi, G.; Cretu, V.; Postica, V.; Lupan, O.; Reimer, T.; Paulowicz, I.; Hrkac, V.; Benecke, W.; Kienle, L.; Adelung, R., Direct Growth of Freestanding ZnO Tetrapod Networks for Multifunctional Applications in Photocatalysis, UV Photodetection and Gas Sensing. *ACS Appl. Mater. Interfaces* **2015**, *7*, 14303-14316.

22. Reimer, T.; Paulowicz, I.; Röder, R.; Kaps, S. r.; Lupan, O.; Chemnitz, S.; Benecke, W.; Ronning, C.; Adelung, R.; Mishra, Y. K., Single Step Integration of ZnO Nano- and Microneedles in Si Trenches by Novel Flame Transport Approach: Whispering Gallery Modes and Photocatalytic Properties. *ACS Appl. Mater. Interfaces* **2014**, *6*, 7806-7815.

23. Gröttrup, J.; Schütt, F.; Smazna, D.; Lupan, O.; Adelung, R.; Mishra, Y. K., Porous Ceramics Based on Hybrid Inorganic Tetrapodal Networks for Efficient Photocatalysis and Water Purification. *Ceram. Int.* **2017**, *43*, 14915-14922.

24. He, W.; Kim, H.-K.; Wamer, W. G.; Melka, D.; Callahan, J. H.; Yin, J.-J., Photogenerated Charge Carriers and Reactive Oxygen Species in ZnO/Au Hybrid Nanostructures with Enhanced Photocatalytic and Antibacterial Activity. *J. Am. Chem. Soc.* **2014**, *136*, 750-757.

25. Bhati, A.; Singh, A.; Tripathi, K. M.; Sonkar, S. K., Sunlight-Induced Photochemical Degradation of Methylene Blue by Water-Soluble Carbon Nanorods. *Int. J. Photoenergy* **2016**, *2016*, 2583821.

26. Tripathi, K. M.; Gupta, N. R.; Sonkar, S. K., Nano-Carbons from Pollutant Soot: A Cleaner Approach toward Clean Environment. In: *Smart Materials For Waste Water Applications*, **2016**, *1*, 127-153.

27. Tripathi, K. M.; Tyagi, A.; Sonker, A. K.; Sonkar, S. K., Waste-Derived Nanocarbons: A Cleaner Approach Towards Water Remediation. In: *Nanomaterials for Water Remediation: Carbon-Based Materials*, **2016**, *1*, 135-160.

28. Quan, Q.; Lin, X.; Zhang, N.; Xu, Y.-J., Graphene and Its Derivatives as Versatile Templates for Materials Synthesis and Functional Applications. *Nanoscale* **2017**, *9*, 2398-2416.

29.   Sreeprasad, T. S.; Pradeep, T., Graphene for Environmental and Biological Applications. *Int. J. Mod. Phys. B* **2012**, *26*, 1242001-1242026.

30.   Shen, Y.; Chen, B., Sulfonated Graphene Nanosheets as a Superb Adsorbent for Various Environmental Pollutants in Water. *Environ. Sci. Technol.* **2015**, *49*, 7364-7372.

31.   Han, C.; Zhang, N.; Xu, Y.-J., Structural Diversity of Graphene Materials and Their Multifarious Roles in Heterogeneous Photocatalysis. *Nano Today* **2016**, *11*, 351-372.

32.   Shanmugam, M.; Alsalme, A.; Alghamdi, A.; Jayavel, R., Photocatalytic Properties of Graphene-SnO$_2$-PMMA Nanocomposite in the Degradation of Methylene Blue Dye under Direct Sunlight Irradiation. *Mater. Express* **2015**, *5*, 319-326.

33.   Sun, L.; Shao, R.; Tang, L.; Chen, Z., Synthesis of ZnFe$_2$O$_4$/ZnO Nanocomposites Immobilized on Graphene with Enhanced Photocatalytic Activity under Solar Light Irradiation. *J. Alloys Compd.* **2013**, *564*, 55-62.

34.   Shanmugam, M.; Alsalme, A.; Alghamdi, A.; Jayavel, R., Enhanced Photocatalytic Performance of the Graphene-V$_2$O$_5$ Nanocomposite in the Degradation of Methylene Blue Dye under Direct Sunlight. *ACS Appl. Mater. Interfaces* **2015**, *7*, 14905-14911.

35.   Wei, G.; Miao, Y.-E.; Zhang, C.; Yang, Z.; Liu, Z.; Tjiu, W. W.; Liu, T., Ni-Doped Graphene/Carbon Cryogels and Their Applications as Versatile Candidates for Water Purification. *ACS Appl. Mater. Interfaces* **2013**, *14*, 7584-7591.

36.   Xiong, Z.; Zhang, L. L.; Ma, J.; Zhao, X. S., Photocatalytic Degradation of Dyes over Graphene-Gold Nanocomposites under Visible Light Irradiation. *Chem. Commun.* **2010**, *46*, 6099-6101.

37.   Khan, M. E.; Khan, M. M.; Cho, M. H., Fabrication of WO$_3$ Nanorods on Graphene Nanosheets for Improved Visible Light-Induced Photocapacitive and Photocatalytic Performance. *RSC Adv.* **2016**, *6*, 20824-20833.

38.   Zhao, Y.; Zhang, Y.; Liu, A.; Wei, Z.; Liu, S., Construction of Three-Dimensional Hemin-Functionalized Graphene Hydrogel with High Mechanical Stability and Adsorption Capacity for Enhancing Photodegradation of Methylene Blue. *ACS Appl. Mater. Interfaces* **2017**, *9*, 4006-4014.

39.   Umrao, S.; Abraham, S.; Theil, F.; Pandey, S.; Ciobota, V.; Shukla, P. K.; Rupp, C. J.; Chakraborty, S.; Ahuja, R.; Popp, J.; Dietzek, B.; Srivastava, A., A Possible Mechanism for the Emergence of Additional Band Gap Due to Ti-O-C Bond in TiO_2 -Graphene Hybrid System for Enhanced Photodegradation of Methylene Blue under Visible Light. *RSC Adv.* **2014**, *4*, 59890-59901.

40.   Lu, Q.; Zhang, Y.; Liu, S., Graphene Quantum Dots Enhanced Photocatalytic Activity of Zinc Porphyrin toward the Degradation of Methylene Blue under Visible-Light Irradiation. *J. Mater. Chem. A.* **2015**, *3*, 8552-8558.

41.   Qu, J.; Shi, L.; He, C.; Gao, F.; Li, B.; Zhou, Q.; Hu, H.; Shao, G.; Wang, X.; Qiu, J., Highly Efficient Synthesis of Graphene/MnO_2 Hybrids and Their Application for Ultrafast Oxidative Decomposition of Methylene Blue. *Carbon* **2014**, *66*, 485-492.

42.   Xu, S.; Fu, L.; Pham, T. S. H.; Yu, A.; Han, F.; Chen, L., Preparation of ZnO Flower/Reduced Graphene Oxide Composite with Enhanced Photocatalytic Performance under Sunlight. *Ceram. Int.* **2015**, *41*, 4007-4013.

43.   Yang, M.-Q.; Han, C.; Zhang, N.; Xu, Y.-J., Precursor Chemistry Matters in Boosting Photoredox Activity of Graphene/Semiconductor Composites. *Nanoscale* **2015**, *7*, 18062-18070.

44.   Lu, K.-Q.; Zhang, N.; Han, C.; Li, F.; Chen, Z.; Xu, Y.-J., Insight into the Origin of Boosted Photosensitive Efficiency of Graphene from the Cooperative Experiment and Theory Study. *J. Phys. Chem. C* **2016**, *120*, 27091-27103.

45.   Putri, L. K.; Ong, W.-J.; Chang, W. S.; Chai, S.-P., Heteroatom Doped Graphene in Photocatalysis: A Review. *Appl. Surf. Sci.* **2015**, *358*, 2-14.

46.   Luo, W.; Zafeiratos, S., A Brief Review of the Synthesis and Catalytic Applications of Graphene-Coated Oxides. Chem. *Cat. Chem.* **2017**, *9*, 2432-2442.

47.   Khurana, I.; Saxena, A.; Bharti; Khurana, J. M.; Rai, P. K., Removal of Dyes Using Graphene-Based Composites: A Review. *Water Air Soil Pollut.* **2017**, *228*, 180-196.

48. Khan, A.; Wang, J.; Li, J.; Wang, X.; Chen, Z.; Alsaedi, A.; Hayat, T.; Chen, Y.; Wang, X. The Role of Graphene Oxide and Graphene Oxide-Based Nanomaterials in the Removal of Pharmaceuticals from Aqueous Media: A Review. *Environ. Sci. Pollut. Res.* **2017**, *24*, 7938-7958

49. Xiang, Q.; Yu, J.; Jaroniec, M., Graphene-Based Semiconductor Photocatalysts. *Chem. Soc. Rev.* **2012**, *41*, 782-796.

50. Tripathi, K. M.; Sonker, A. K.; Sonkar, S. K.; Sarkar, S., Pollutant Soot of Diesel Engine Exhaust Transformed to Carbon Dots for Multicoloured Imaging of *E. coli* and Sensing Cholesterol. *RSC Adv.* **2014**, *4*, 30100-30107.

51. Singh, A.; Khare, P.; Verma, S.; Bhati, A.; Sonker, A. K.; Tripathi, K. M.; Sonkar, S. K., Pollutant Soot for Pollutant Dye Degradation: Soluble Graphene Nanosheets for Visible Light Induced Photodegradation of Methylene Blue. *ACS Sustainable Chem. Eng.* **2017**, *5*, 8860−8869.

52. Ray, S. C.; Saha, A.; Jana, N. R.; Sarkar, R., Fluorescent Carbon Nanoparticle: Synthesis, Characterization and Bio-Imaging Application. *J. Phys. Chem. C* **2009**, *113*, 18546-18551.

53. Zhang, Y.; Sun, Z.; Wang, H.; Wang, Y.; Liang, M.; Xue, S., Nitrogen-Doped Graphene as a Cathode Material for Dye-Sensitized Solar Cells: Effects of Hydrothermal Reaction and Annealing on Electrocatalytic Performance. *RSC Adv.* **2015**, *5*, 10430-10439.

54. Tripathi, K. M.; Singh, A.; Bhati, A.; Sarkar, S.; Sonkar, S. K., Sustainable Feasibility of the Environmental Pollutant Soot to Few-Layer Photoluminescent Graphene Nanosheets for Multifunctional Applications. *ACS Sustainable Chem. Eng.* **2016**, *4*, 6399-6408.

55. Wang, S.; Tristan, F.; Minami, D.; Fujimori, T.; Cruz-Silva, R.; Terrones, M.; Takeuchi, K.; Teshima, K.; Rodrıguez-Reinoso, F.; Endo, M.; Kaneko, K., Activation Routes for High Surface Area Graphene Monoliths from Graphene Oxide Colloids. *Carbon* **2014**, *76*, 220-231.

56. Li, C.; Shi, G., Three-Dimensional Graphene Architectures. *Nanoscale* **2012**, *4*, 5549-5563.

57. Tripathi, K. M.; Tran, T. S.; Kim, Y. J.; Kim, T., Green Fluorescent Onion-Like Carbon Nanoparticles from Flaxseed Oil for Visible Light Induced Photocatalytic Applications and Label-Free Detection of Al(III) Ions. *ACS Sustainable Chem. Eng.* **2017**, *5*, 3982-3992.

58. Seema, H.; Kemp, K. C.; Chandra, V.; Kim, K. S., Graphene-SnO_2 Composites for Highly Efficient Photocatalytic Degradation of Methylene Blue under Sunlight. *Nanotechnology* **2012**, *23*, 355705-355713.

59. Hsu, H.-C.; Shown, I.; Wei, H.-Y.; Chang, Y.-C.; Du, H.-Y.; Lin, Y.-G.; Tseng, C.-A.; Wang, C.-H.; Chen, L.-C.; Lin, Y.-C.; Chen, K.-H., Graphene Oxide as a Promising Photocatalyst for CO_2 to Methanol Conversion. *Nanoscale* **2013**, *5*, 262-268.

60. Yu, H.; Irie, H.; Hashimoto, K., Conduction Band Energy Level Control of Titanium Dioxide: Toward an Efficient Visible-Light-Sensitive Photocatalyst. *J. Am. Chem. Soc.* **2010**, *132*, 6898-6899.

61. Tripathi, K. M.; Bhati, A.; Singh, A.; Sonker, A. K.; Sarkar, S.; Sonkar, S. K., Sustainable Changes in the Contents of Metallic Micronutrients in First Generation Gram Seeds Imposed by Carbon Nano-Onions: Life Cycle Seed to Seed Study. *ACS Sustainable Chem. Eng.* **2017**, *5*, 2906-2916.

62. Zhang, B.; Zhang, D.; Xi, Z.; Wang, P.; Pu, X.; Shao, X.; Yao, S., Synthesis of Ag_2O/$NaNbO_3$ P-N Junction Photocatalysts with Improved Visible Light Photocatalytic Activities. *Sep. Purif. Technol.* **2017**, *178*, 130-137.

63. Li, F.-T.; Wang, Q.; Ran, J.; Hao, Y.-J.; Wang, X.-J.; Zhao, D.; Qiao, S. Z., Ionic Liquid Self-Combustion Synthesis of $BiOBr$/$Bi_{24}O_{31}Br_{10}$ Heterojunctions with Exceptional Visible-Light Photocatalytic Performances. *Nanoscale* **2015**, *7*, 1116-1126.

64. Bibi, R.; Shen, Q.; Wei, L.; Hao, D.; Li, N.; Zhou, J. Hybrid $BiOBr$/UiO-66-NH_2 Composite with Enhanced Visible-Light Driven Photocatalytic Activity toward RhB Dye Degradation. *RSC Adv.* **2018**, *8*, 2048-2058.

65. Reheman, A.; Tursun, Y.; Dilinuer, T.; Halidan, M.; Kadeer, K.; Abulizi, A. Facile One-Step Sonochemical Synthesis and Photocatalytic Properties of Graphene/Ag_3PO_4 Quantum Dots Composites. *Nanoscale Res. Lett.* **2018**, *13*, 70-79.

66.   Bhati, A.; Anand, S. R.; Gunture, Garg, A. K.; Khare, P.; Sonkar, S. K. Sunlight-Induced Photocatalytic Degradation of Pollutant Dye by Highly Fluorescent Red-Emitting Mg-N-Embedded Carbon Dots. *ACS Sustainable Chem. Eng.* **2018**, *6*, 9246-9256.

67.   Garg, S.; Yadav, M.; Chandra, A.; Sapra, S.; Gahlawat, S.; Ingole, P. P.; Todea, M.; Bardos, E.; Pap, Z.; Hernadi, K., Facile Green Synthesis of BiOBr Nanostructures with Superior Visible-Light-Driven Photocatalytic Activity. *Materials* **2018**, *11*, 1273.

68.   Rajendran, R., Varadharajan, K., Jayaraman, V.; Singaram, B.; Jeyaram, J., Photocatalytic Degradation of Metronidazole and Methylene Blue by PVA-Assisted Bi_2WO_6-CdS Nanocomposite Film under Visible Light Irradiation *Appl. Nanosci.* **2018**, *8*, 61.

69.   Ramacharyulu, P. V. R. K.; Abbas, S. J.; Sahoo, S. R.; Ke, S.-C., Mechanistic Insights into 4-Nitrophenol Degradation and Benzyl Alcohol Oxidation Pathways over MgO/g-C_3N_4 Model Catalyst Systems. *Catal. Sci. Technol.* **2018**, *8*, 2825-2834.

70.   Kang, S.; Herzberg, M.; Rodrigues, D. F.; Elimelech, M., Antibacterial Effects of Carbon Nanotubes: Size Does Matter! *Langmuir* **2008**, *24*, 6409-6413.

71.   Lyon, D. Y.; Adams, L. K.; Falkner, J. C.; Alvarez, P. J. J., Antibacterial Activity of Fullerene Water Suspensions: Effects of Preparation Method and Particle Size. *Environ. Sci. Technol.* **2006**, *40*, 4360-4366.

72.   Roy, M.; Sonkar, S. K.; Tripathi, S.; Saxena, M.; Sarkar, S., Non-Toxicity of Water Soluble Multi-Walled Carbon Nanotube on *Escherichia-coli* Colonies. *J. Nanosci. Nanotechnol.* **2012**, *12*, 1754-1759.

73.   Sonkar, S. K.; Ghosh, M.; Roy, M.; Begum, A.; Sarkar, S., Carbon Nano-Onions as Nontoxic and High-Fluorescence Bioimaging Agent in Food Chain-an *in vivo* Study from Unicellular *E. coli* to Multicellular *C. elegans*. *Mater. Express* **2012**, *2*, 105-114.

74.   Ghosh, M.; Sonkar, S. K.; Saxena, M.; Sarkar, S., Carbon Nano-Onions for Imaging the Life Cycle of *Drosophila melanogaster*. *Small* **2011**, *7*, 3170-3177.

75. Tripathi, S.; Sonkar, S. K.; Sarkar, S., Growth Stimulation of Gram (*Cicer arietinum*) Plant by Water Soluble Carbon Nanotubes. *Nanoscale* **2011**, *3*, 1176-1181.

76. Saxena, M.; Maity, S.; Sarkar, S., Carbon Nanoparticles in 'Biochar' Boost Wheat (*Triticum aestivum*) Plant Growth. *RSC Adv.* **2014**, *4*, 39948-39954.

Chapter - 5

Soluble Graphene Nanosheets for the Sunlight-Induced Photodegradation of the Mixture of Dyes and its Environmental Assessment
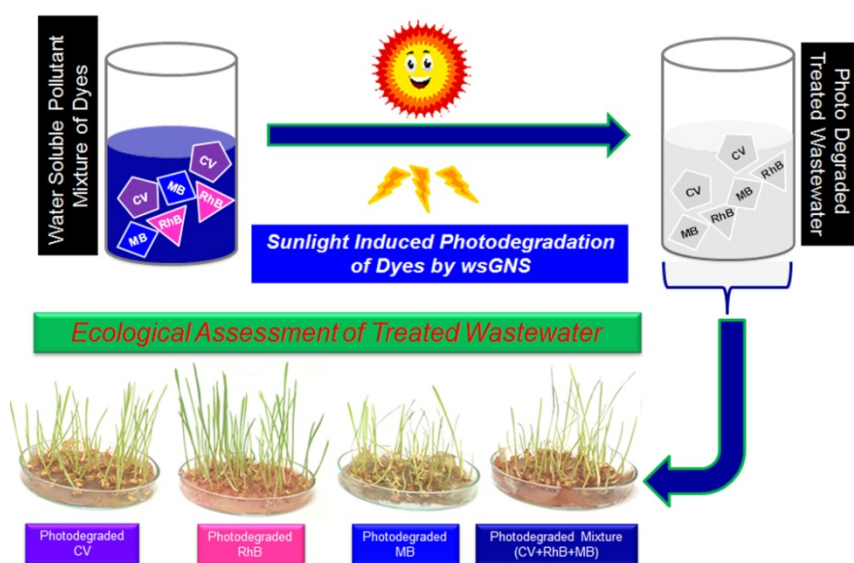
5.1   Introduction

The ever-growing desire to improve the quality of human lifestyle significantly promoted the rapid industrialization and urbanization [1-3]. Primarily, associated with the accelerating advancement of the automotive industrialization, which can directly link to the release of pollutant soot as BC [4-7] particulate matter in the environment. BC is closely related with global warming and at present is continuously deteriorating the environmental and human health [7, 8]. Along with air pollutions, industrialization have also brought the another important concern related to the water pollutions [9]. So, the most demanding aggravated concerns of the present world is to significantly reuse the waste products (it could also be the dangerous-dirty-BC)[10] and the treatment of wastewater [11], From the standpoint of the overall environmental health, the discharge of the BC [7] in air and the effluents of industrial wastewater [12-14] (containing hazardous, carcinogenic and non-biodegradable organic dyes) in the water-bodies are unceasingly deteriorating the ecological balance [15, 16], and causes many serious diseases [17-19].

At present, few groups have explored the recent-promising approaches related to the adaptation of pollutant soot as freely available carbon precursor for the synthesis/isolations of the value-added nanocarbons [20-26]. Such as CD [22], GNS [23, 24, 26], SWCNT [25], CNP [21] for the diverse applications [21, 22, 26] including the photodegradation of the pollutant dyes [23, 24]. In the same context, the visible-light photocatalysis using the nanocarbons, metal-based carbon nanomaterials [27-31] and its composites [28, 32-40] has attracted the widespread attention, because of its interesting applicative prospects in the field of the water remediation [37, 38, 41]. Sunlight-induced dye degradation exhibits high efficiency along with the ability to use the most renewable and sustainable source of energy as sunlight [42], hence can offers a feasible approach to overcome the degree of water pollutions.

Presently, the graphene [43, 44] and graphene-based nanostructures [34, 39] have drawn more and more attention due to their advantageous many features like high optical absorption, fast charge carrier mobility, high conductivity, non-toxicity, corrosion resistance, the unique surface properties and environmental acceptability

[45]. Although a few milestones have already been documented for enhancing photocatalytic efficiency of the graphene based nanostructures for the degradation of organic pollutant [46-48], but their fabrications methods inevitably include the tedious, and complex process [41, 49-51]. Along with this to tune the band-gap of graphene based nanostructures, these were further require the additional strategies such as metal/heteroatom doping, composite fabrication and surface functionalization [28, 37, 46, 52]. Additionally, the above mentioned most of the reports were mostly deals with the photodegradation of the single components of organic dyes [29, 38, 41, 46, 53-56]. As per the general consideration, the effluents of industrial wastewater are being composed of the complex system, containing the combination of dyes. But only a little attention has been paid to remediate wastewater containing a mixture of dyes [57-62].

For this, the exploration of a facile, cost-effective and sustainable approach for the synthesis of graphene-based nanostructures having the desirable light response is very much crucial for the application of photocatalysis. As they require a superior charge separation efficiency and a broad photoresponsive range [63]. Under the presence of sunlight, the same can be provided by the wsGNS, isolated from the BC possessing the advantageous efficiency to work as a photocatalytic material [23, 24]. Based on the few reports posing the controversies regarding the observance of acute toxicity due to generation of toxic byproducts even after complete degradation of dyes [64-67]. The present times demands a strong requirement of environmental assessment of the whole process to rule out the possible risk and maintain the ecological balance and being smoothly used for the real life applications.

Herein, the present chapter describes a simple and feasible approach related to the utilization of the almost free of cost available photocatalytic materials (wsGNS) for the complete photodegradation of three individual dyes like crystal violet (CV), rhodamine B (RhB), and methylene blue (MB) and their mixture (CV+RhB+MB) under the sunlight irradiation. A plausible photocatalytic mechanism is proposed based upon the trapping of active-reactive species and analysis of the photodegraded products with the ^{1}H NMR spectroscopy. The potentials of the wsGNS were further investigated under the presence of common

interfering ions/substances. In continuation of earlier studies, the work described here is based on the simple idea, related to the photodegradation of the pollutant material (for the degradation of mixture of the dyes) from the pollutant material (BC). Importantly, addition to the aqueous phase photocatalysis only. The treated wastewater is being utilized for the germination of wheat plants related to the environmental risk assessment for the treated wastewater. Initial results are in favor that treated wastewater can be used for growing the plants that can maintain the ecological balance of the required water. In this context, growths of wheat (*Triticum aestivum*) plants were assessed with the dye-polluted water before and after photocatalytic degradation, including the control to evaluate the environmental applicability of the treated wastewater.

5.2 Experimental Section

5.2.1 Materials and Reagents

Petrol engine soot was collected locally from the Jaipur city, Rajasthan, India. MB was purchased from Sigma Aldrich, USA. CV and RhB was purchased from LobaChem, Mumbai, India. HNO_3, acetone, t-BA, Na_2-EDTA were procured from Rankem, India and p-BZQ from Acros Organics, USA. Other chemicals used in the study such as $CaCl_2$, $FeCl_3$, Na_2SO_4, Na_2HPO_4, $NaNO_3$, and KCl from Rankem India. All the reagents were of analytical grade and used as such. All the experiments were performed using DI water. Wheat seeds were purchased from local market, Jaipur, Rajasthan.

5.2.2 Instrumentation

Structural characterization was performed through TEM and HRTEM analysis with a Tecnai G^2 20 high-resolution TEM operating at a voltage of 200 kV. Samples for TEM/HRTEM analysis were prepared by casting droplets of an aqueous solution of wsGNS onto a 400 mesh carbon-coated copper grid, followed by drying under 100 W table lamp for 12 h. The UV-Vis absorption analysis were done at room temperature with Perkin Elmer Lambda 35 spectrometer. XPS measurements was recorded in ESCA$^+$ omicron nanotechnology oxford instrument. ^{1}H NMR measurements were recorded on a JEOL ECS-400 (operating at 400 MHz, in D_2O solvent). Remi magnetic stirrer was used during the experiment.

5.2.3   Photocatalytic Experimental Procedure

Three different types of dyes and their corresponding mixture were taken to examine the photocatalytic activity of wsGNS under direct sunlight illumination. All the photocatalytic experiments were carried out in Jaipur, India in the month of May 2018. In a typical process stock solution of CV, RhB and MB of concentration, 20 ppm was prepared in DI water along with this the concentrations of all the three dyes in mixture maintained to 20 ppm in a 100 mL conical flask for the photocatalytic degradation [58, 60-62]. 0.3 mg mL^{-1} of wsGNS added separately to all the dyes solution (individual dyes as CV,RhB and MB and their corresponding mixture) and the solutions stirred for 30 min in the dark to reach the adsorption and desorption equilibration. During the photocatalytic experiments, fixed amount of photoreacted solution was taken at regular time intervals. The collected solution was centrifuged and the supernatant was collected in a quartz cuvette for determining the dye concentration by using UV-Vis absorbance spectroscopy at wavelength 589 nm, 554 nm, and 663 nm for CV, RhB, and MB dyes respectively. For further characterization of the photodegraded products of different dyes by wsGNS, the complete photodegraded samples were collected and centrifuged, further the as collected supernatant was dried and dissolved in D_2O to perform the ^1H NMR analysis.

5.2.4   Germination

Wheat seeds (*Triticum aestivum*) were washed with DI water and further soaked in tap water for the one day for germination.

5.2.5   Seeds

Soaked moist seeds were placed in wet cotton cloth for one day. One-day-old sprouted wheat seeds were used for monitoring the growth under the controlled conditions (DI water and in wsGNS); in polluted dyes and their mixture *versus* the treated wastewater (water contained after the photocatalysis by wsGNS in the presence of sunlight). For the growth of the plants; one day germinated seeds were placed in petri dish containing the almost similar cotton sheets soaked with the equal amount (~10 ml for the first day) of (i) DI water; (ii) wsGNS solution; (iii) dyes and their mixture; and (iv) with their the respective treated wastewater. All the

experiments were performed thrice for the 15 days, including the daily additions of ~ 3 ml of the each solution to check the growth of wheat plants.

5.2.6 Regeneration Analysis

The recovered wsGNS after photodegradation was regenerated with 0.01 M HCl solution repeatedly over ~ 10-12 times followed by washing of DI water until the pH of the effluent become neutral. The regenerated sample after washing dried in the oven at 80° C for the further use.

5.3 Results and Discussion

At present, most of the photocatalytic materials are showing their selectivity toward the photodegradation of the specific dyes only. Therefore, for the practical applicative prospects just target the single pollutant dye has not been a sufficient feasible approach. For the same, the photocatalytic performance of the wsGNS [23, 24] was extended concerning the photocatalytic degradation of the three different individual model dyes as CV, RhB, MB and their mixture (CV+RhB+MB) under the influence of the natural sunlight. A simpler methodology described in scheme 1, illustrates the significant usage of BC derived wsGNS as a photocatalytic material under the influence of natural sunlight for the photodegradation of three different dyes as CV, RhB, MB and their mixture (CV+RhB+MB). As well, includes the sustainability of the overall process, concerning the reuse of the treated wastewater for growing the wheat plants.
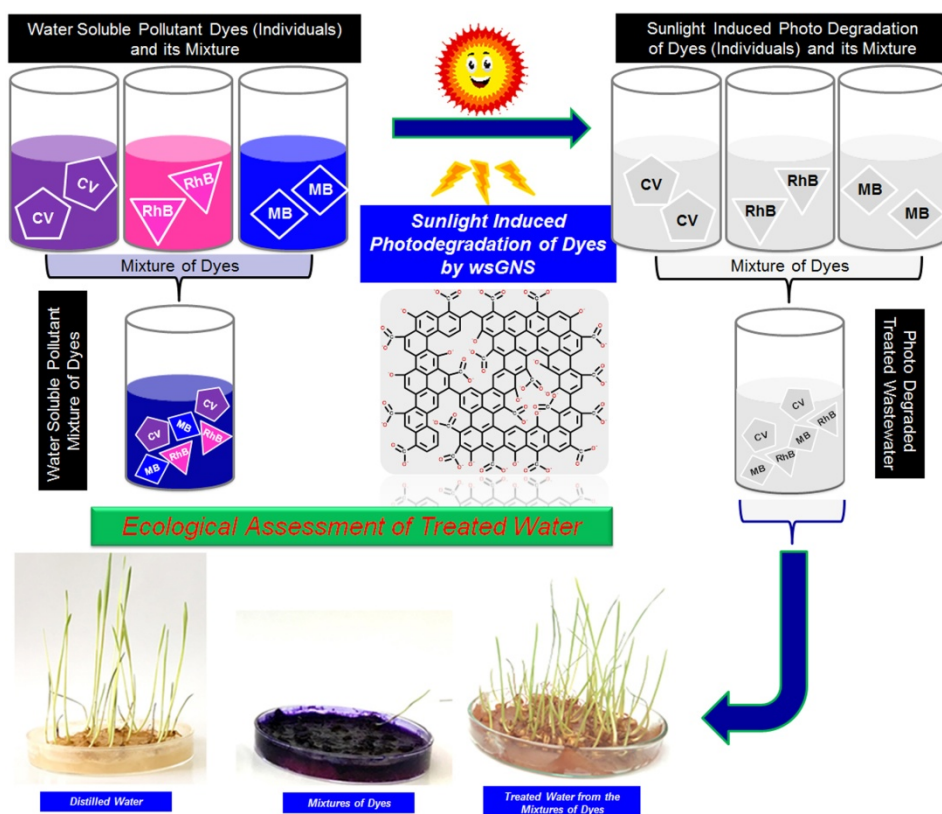
Scheme 5.1: Schematic representation illustrating the application of the wsGNS for the photodegradation of the three different dyes and their mixture under the presence of sunlight. Further, the treated wastewater was being employed for growing the wheat plants.

5.3.1 Microscopic and Spectroscopic Characterization

TEM was used to analyze the morphology of wsGNS (Figure 5.1 (a)), which displays the randomly oriented layers of wsGNS with a lot wrinkled and crumpled surface morphology. HRTEM image (Figure 5.1 (b)) showed the existence of mutil-layered wsGNS. Randomly oriented surface dents and graphitic patches are also evident in HRTEM images (Figure 5.1 (c), which are attributed to high-density surface functionalization [26] of wsGNS. The morphological insights of the wsGNS is shown in Figure 5.1 (c) confirm the lattice fringes, existence of multi-layers graphene (black arrows showing ~ 5 layers) in wsGNS and the presence of differentially oriented graphitic patches (marked by red circles). The interplanar spacing of ~ 0.36 nm as shown in Figure 5.1 (c) could be assigned to the (002) plane of the few-layer wsGNS.

XPS measurements were describing the surface elemental composition and the nature of surface functional groups on the surface [23]. XPS spectrum (Figure 5.1 (d)) of wsGNS shows the two characteristics prominent peaks at ~ 284.4 eV and ~ 532.1 eV for the C_{1s} and O_{1s} respectively. The high resolution C_{1s} XPS spectrum (Figure 5.1 (e)) was deconvoluted into five states of C_{1s} as C=C, C-C, C-O, C=O, and COO^- corresponding to the binding energy of 284.2 eV, 284.8 eV, 285.6 eV, 286.7 eV and 288.8 eV respectively. Figure 5.1(f), shows the high resolution O_{1s} XPS spectrum, which exhibits the presence of three peaks at 531.3 eV, 532.5 eV and 533.7 eV corresponding to C-O, C=O, and COO^- respectively. The elemental composition analysis of wsGNS by XPS shows the presence of ~ 80 % carbon and ~20% oxygen.

Higher oxygen content confirms the incorporation of high-degree of the negative organic functional moieties as hydroxyl and carboxyl groups over the surface of wsGNS as the surface defects. The high-density surface-defects have the strong ability to facilitate the photocatalytic efficiencies of the wsGNS, for the photodegradation of the dyes and their mixture in the influence of sunlight.
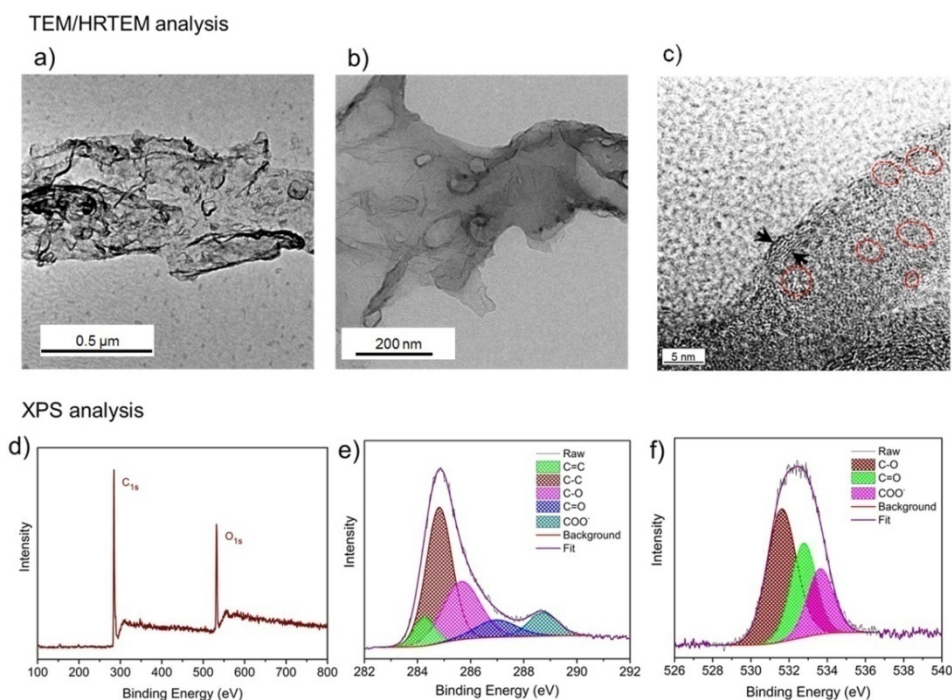
Figure 5.1. (a, b) Low-resolution TEM images of wsGNS; (c) HRTEM image of wsGNS show existence of few-layered graphene sheets with surface defects; (d) A full survey scan XPS analysis of wsGNS along with its corresponding short scan; (e) C_{1s}; and (f) O_{1s}.

5.3.2   Photocatalytic Dye Degradation under Sunlight Irradiation

A detailed UV-Vis absorption study as shown in Figure 5.2 (a-e) shows the relative change in concentration of respective dye and its mixture (decrease in the color intensity) as a function of time under the presence of sunlight. Figure 5.2 (a-c) shows that there is a gradual decrement in absorption maxima with time at 589 nm for CV, 554 nm for RhB and at 663 nm for MB. Figure 5.2 (d) shows the absorption spectra of the mixture of dyes (CV+RhB+MB) which can be easily differentiated based on the three separate individual peaks in the mixture because of absorbance associated with CV, RhB, and MB with inset showing violet curve for CV, pink curve for RhB and blue curve for MB. Figure 5.2 (e) shows the gradual decrease in absorption maxima for different dyes in the mixture by wsGNS under sunlight irradiation and within 225 min mixture of dyes has been decolorized as observed by UV-Vis absorbance study.
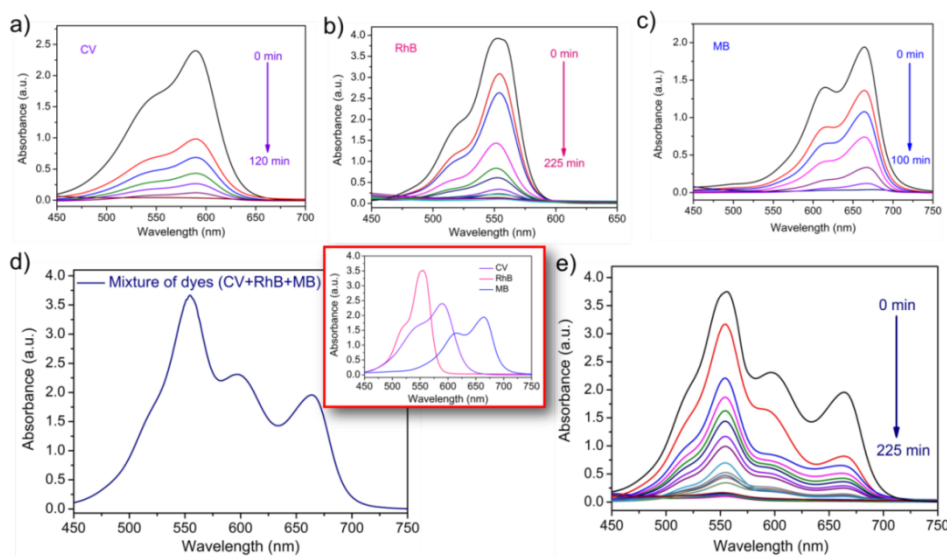
Figure 5.2. UV-Visible absorption spectra of (a) CV; (b) RhB; and (c) MB with time; (d) mixture of dyes (CV+RhB+MB) with inset showing violet curve for CV, pink curve for RhB and blue curve for MB; (e) UV-Visible absorption spectra of mixture of dyes with time by wsGNS under sunlight irradiation.

The photocatalytic degradation efficiency of wsGNS displayed in Figure 5.3 for the freshly prepared three different dyes and their mixture (all the individual dyes are having the concentration of 20 ppm and for the mixture it contains the 20 ppm of the each dye) [58, 60-62]. An adsorption-de-adsorption balance was attained

between the wsGNS and dyes (CV, RhB, MB) and their mixture (CV+RhB+MB) for the initial time of 30 min *via* the stirring. In the dark at the same experimental conditions, prior to the process of the photocatalytic degradation. It was observed that ~ 11 % CV, ~10 % RhB, ~ 11 % MB and ~ 12 % of their mixture (CV+RhB+MB) were adsorbed on the wsGNS in 30 min.

The photocatalytic degradation of dyes was accessed by monitoring the relative change in concentration with time, concerning the rate of decolorization. The change in intensity of characteristic peaks using UV-Vis absorption spectroscopy was recorded for CV, RhB, and MB at 589 nm, 554 nm, and 663 nm respectively. As expected, the different rate constant for the photodegradation of different dyes could be attributed to their difference in the chemical structures. In the presence of wsGNS, MB shows the fastest photodegradation ~ 99 % within 100 min, CV shows ~ 99% within the 120 min, while the RhB takes a bit longer time ~ 225 min (might be because of the complex organic framework of CV and RhB in comparison with MB) to shows ~ 99% of its photodegradation as shown in Figure 5.3 (a). In the same panel, Figure 5.3 (b) shows the apparent rate constant related to the photodegradation of MB, CV and RhB as 0.0512 min^{-1}, 0.0263 min^{-1} and 0.0109 min^{-1} respectively. Concerning the photocatalytic degradation of the mixture of dyes (CV+RhB+MB), the absorption spectrum shows the appearance of three different peaks (589 nm, 554 nm, and 663 nm) related to their respective three different dyes as CV, RhB, and MB respectively. The clarity in differing the three peaks is very much advantageous for the present study.

The photodegradation efficiency (illustrated in Figure 5.3 (c)) of respective dyes from the mixture (CV+RhB+MB) was being analyzed based on their respective absorbance value (λ_{max} values of 589 nm, 554 nm, and 663 nm). Similar to the individual dyes, the mixture of dyes displays the progressive decrease in its concentration by wsGNS under the presence of sunlight Figure 5.3 (c). The degradation rates of dyes in mixture were found to be 180 min for the MB, and for the case of CV, and RhB it is ~ 225 min. The rate constant for CV, RhB, and MB was observed 0.0145 min^{-1}, 0.0124 min^{-1} and 0.0226 min^{-1} respectively based on their photodegradation efficiency observed at their respective λ_{max} values. The

decrease in rate constant in the mixture of dyes, compared to the individual dyes can be because of the competitive occupancy of optically active centers in-between the photodegradation process over the surface of the wsGNS. Concerning the control test for the photocatalytic degradation of the respective dyes and its mixture in the absence of wsGNS could almost be overlooked (as shown in the inset of the Figure 5.3 (a and c), which confirms the high photostability of dyes under the presence of sunlight.
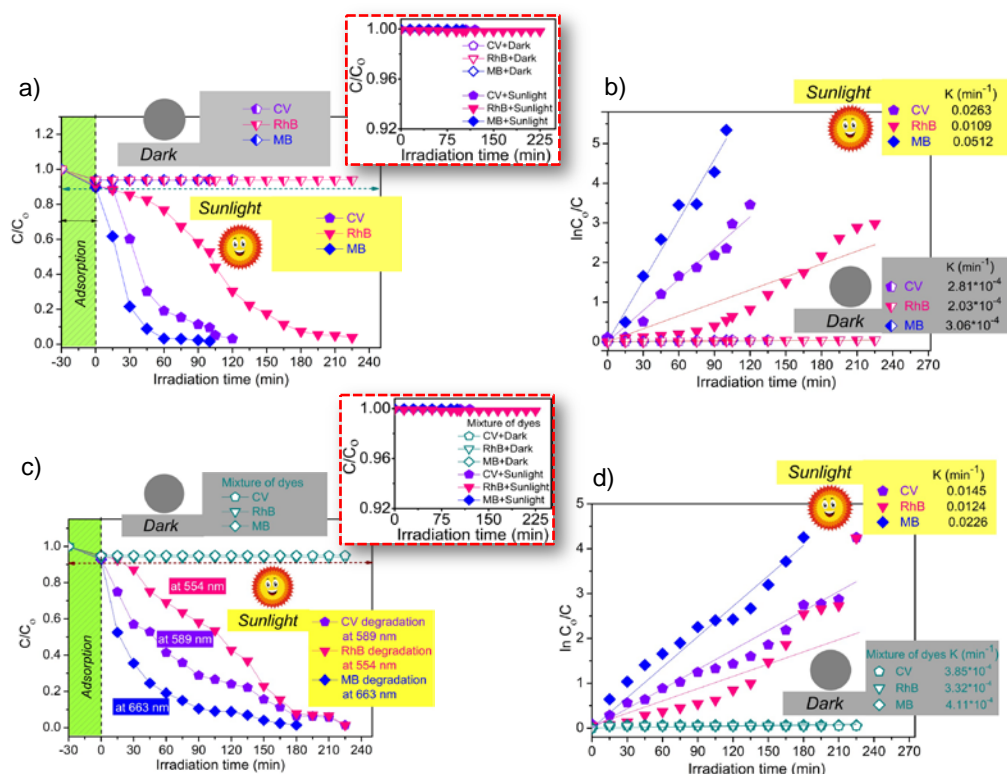
Figure 5.3. (a) Extent of plot of (C/C$_o$) (with inset showing photocatalytic degradation of the respective dyes in the absence of wsGNS) ; with their (b) respective plot of ln(C$_o$/C) for the individual dyes (CV, RhB and MB); (c) Extent of plot of (C/C$_o$) (with inset showing photocatalytic degradation of the mixture of dyes in the absence of wsGNS) of a mixture of dyes; with their (d) respective plot of ln(C$_o$/C) for the mixture of dyes; under dark and sunlight condition.

5.3.3 Trap Study

To explore the active moieties involved in photocatalytic degradation of dyes [31, 68-79] under direct sunlight irradiation radical scavengers were introduced to trap specific reactive species. A simpler trap experiment has been performed based on the scavenging properties of Na$_2$-EDTA for trapping of the surface generated h$^+$,

t-BA for trapping •OH radicals, and p-BZQ for the trapping of $O_2^{-\bullet}$ radicals. In all the cases, concentrations of scavengers were fixed at 1 mM, and their effects were observed in the change in concentration of dyes (in terms of C/Co) as displayed in Figure 5.4 (a-c) for CV, RhB, and MB respectively. As perceived in Figure 5.4 (a-c) the photodegradation process in comparison to control where no scavengers were used considerably inhibited in the presence of t-BA and Na_2-EDTA implying that •OH radicals and h^+ are significantly participating in the process of the photodegradation. The degradation efficiencies of dyes, on the addition of t-BA decrease from 99% to 13%, 99% to 12% % and 99% to 11 % for CV, RhB, and MB respectively. Similarly, the addition of Na_2-EDTA reduces the degradation efficiency from 99% to 21%, 99% to 20 % and 99% to 21 % for CV, RhB, and MB respectively. Contrary to additions of t-BA and Na_2-EDTA, a very slight decrease in the photodegradation efficiency of dyes observed with the addition of p-BZQ, supporting that $O_2^{-\bullet}$ are not actively participating in photodegradation process. Almost similar trends were observed for the mixture (CV+RhB+MB) of dyes Figure 5.4 (d).
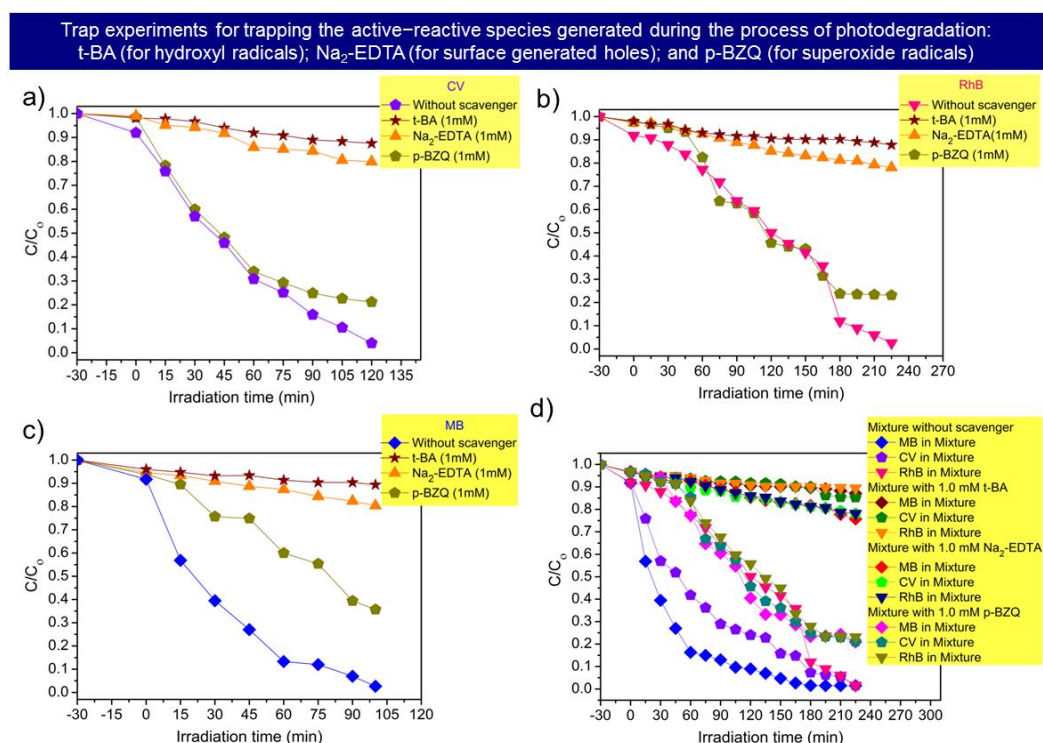
Figure 5.4. Effect of scavengers t-BA, Na_2-EDTA, and p-BZQ for •OH, h^+, and $O_2^{-\bullet}$ radicals respectively on the degradation performance of (a) CV; (b) RhB; and (c) MB; (d) on the mixture of dyes.

Based on the results from the trapping experiments, a schematic of the possible mechanism for the photocatalytic degradation of the dyes and their mixture by wsGNS under the direct sunlight irradiation is proposed in Scheme 5.2. The high-degree of the surface functional groups as surface defects on wsGNS made a considerable contribution for the energy absorption and the photocatalytic activity. wsGNS get photosensitized during the irradiation of sunlight, and the electron-hole pairs are generated (equation 1 and equation 2 from scheme 5.2). The trapped photoexcited electrons were lead to higher charge transfer and electron-hole pair separation efficiency, while the photo-induced holes accumulated on the surface adsorbed water molecule would initiate the generation of hydroxyl radical which might directly react with dyes (equation 3,4 from scheme 5.2). Hydroxyl radical, as the predominant species attacked on dye molecules and contribute towards the effective photodegradation of respective dyes and its mixture (equation 5-7 from scheme 5.2).
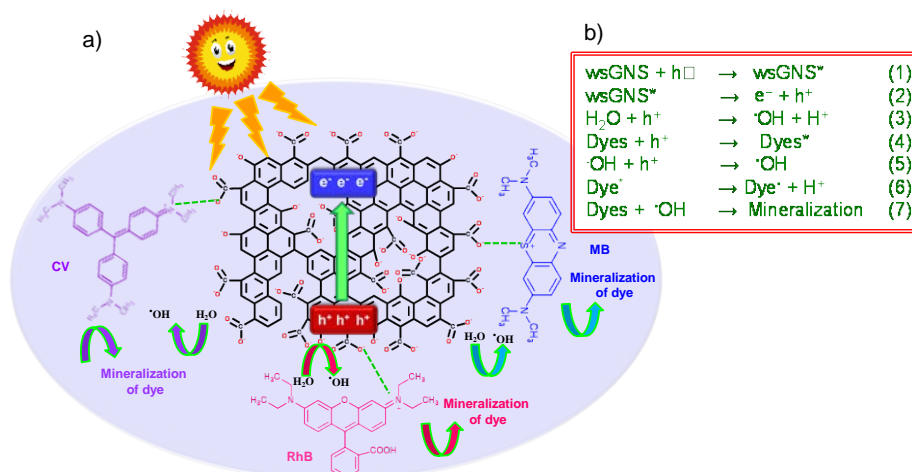
Scheme 5.2. (a) Schematic illustration showing degradation of different dyes using wsGNS under sunlight irradiation; (b) with their respective suggested pathways.

5.3.4. ^{1}H NMR Investigation of Degraded Products of CV, RhB and MB and its Mixture (CV+RhB+MB)

Concerning about the formation of the smaller fragments of the respective dyes during the process of the photodegradation. A straightforward comparative ^{1}H NMR analysis was carried out for the control sample (individual dye and its mixture) *versus* the photodegraded products of respective dyes and their mixture (CV+RhB+MB). Figure 5.5 (a-d) shows the comparative aqueous phase ^{1}H NMR analysis of the control dyes and their mixture (CV+RhB+MB) with their respective

photodegraded products. The ^{1}H NMR spectra of CV, RhB, and MB (Figure 5.5 (a-c)) were taken before and after the photodegradation of dyes (sample collected from the supernatant from the pool of dye-wsGNS system was being dried and dissolved in D_2O for the ^{1}H NMR analysis). After the time interval of the four hours of sunlight irradiations; the samples were collected for all CV, RhB, MB and their mixture (CV+RhB+MB), for NMR analysis.

Figure 5.5 (a), shows the proton peaks associated with the aliphatic and aromatic region of the CV. ^{1}H NMR (400 MH$_Z$, D_2O): δ (ppm) 3.03 (s, 18H), 6.50 (d, J=7.6H$_Z$, 6H), 6.87 (d, J=7.6H$_Z$, 6H). Over a comparative analysis after photodegradation experiment for four hours of sunlight irradiation on the pool of CV-wsGNS mixture, it shows the breakage of the complete aromatic framework of the used dye (disappearance of the signals associated with the aromatic protons). As well, the ^{1}H NMR spectrum of the photodegraded CV showed the appearance of new smaller aliphatic peaks at δ 2.15-3.28 ppm (m, fragmented hydrocarbons), which can be directly related to the disintegration/mineralization of the original aromatic organic framework of CV molecules into the smaller aliphatic fragments. Similarly, for the other two dyes (RhB and MB), the same has been observed.

The proton signals from the RhB (Figure 5.5 (b)) were divided into the two regions; ^{1}H NMR (400 MH$_Z$, D_2O): δ (ppm) 1.12 (t, J=7.2, 12H), 3.39-3.50 (m, 8H), 6.55 (d, J=2H$_Z$, 2H), 6.74 (dd, J=2H$_Z$, J=9.6H$_Z$, 2H), 6.69 (d, J=9.6H$_Z$, 2H), 7.29 (d, J=7.2H$_Z$, 2H), 7.71-7.79 (m, H,H), 8.12 (d, J=8, 1H). After the photodegradation, signature proton signals from RhB does not appear as before degradation, as well as almost the disappearance of the intense aromatic signals and the emergence of the few aliphatic protons δ 1.23-3.31 ppm (m, fragmented hydrocarbons) is in support of the disintegration of the complex organic framework of the RhB molecules into smaller aliphatic components.

Likewise, in the case of MB, before photodegradation following peaks appear in ^{1}H NMR spectra (Figure 5.5 (c)), ^{1}H NMR (400 MH$_Z$, D_2O): δ (ppm) 2.97 (s, 12H), 6.57 (s, 2H), 6.82 (d, J=8.8H, 2H), 7.01(d, J=8.8H$_Z$, 2H), and after the photodegradation, showed its dissociation into the smaller hydrocarbons (δ 2.19 ppm to 3.31 ppm) in the aliphatic region and the aromatic signals were disappeared

entirely. Similar to the individual dyes, the photodegradation of the mixture of dyes (CV+RhB+MB) has also been analyzed by ^{1}H NMR.
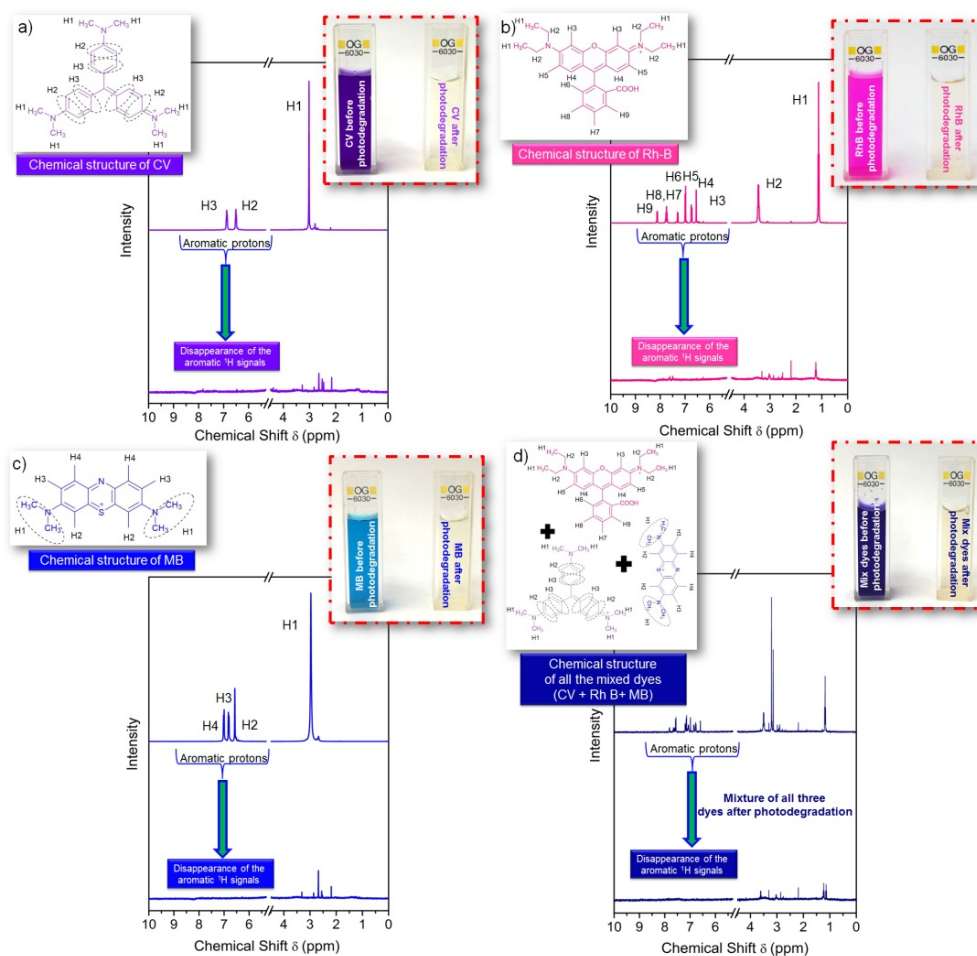
Figure 5.5. The chemical structure of (a) CV; (b) RhB; (c) MB; and (d) Mixture of dyes; including with their respective ^{1}H NMR spectra, before and after their photodegradation by wsGNS. Inset of all figure (a-d), shows the digital images of respective dye (a-c); and their mixture (d) before and after the photodegradation.

A similar result was observed for the mixture of dyes in Figure 5.5 (d), which shows a comparative ^{1}H NMR spectrum of the mixture of dyes; before and after the photodegradation experiment. The proton signals associated with the mixture is of now becomes a complex system of the organic molecule, so the individual assigning of the proton signals is being excluded here. But after the photodegradation (Figure 5.5 (d)), a complete change in the proton signals; before and after the photodegradation is being observed. After the photodegradation, the disappearance of aromatic protons has strongly advocated the disintegrations of the complex organic frameworks of the mixture of dyes. ^{1}H NMR analysis as described

above shows the strong influence of wsGNS under the presence of sunlight for the photodegradation applications of the pollutant dyes and their mixture (CV+RhB+MB).

5.3.5. Regeneration Recycling Study

In addition to the photodegradation efficiency, the recycling ability of a photocatalyst is an important parameter to define the sustainability of the new proposed process. The reusability performance of the wsGNS employed up to the four cycles under sunlight irradiation towards a mixed dye solution as shown in Figure 5.6 After the four cycles, there is the only loss of ∼ 22 % in the degradation efficiency. The decrease in efficiency could be attributed to loss of material during recycling. Due to higher stability, recoverability, and reusability, the pollutant soot derived wsGNS could be used as an efficient material for the photodegradation of the mixture of the pollutant organic dyes in the real samples also.
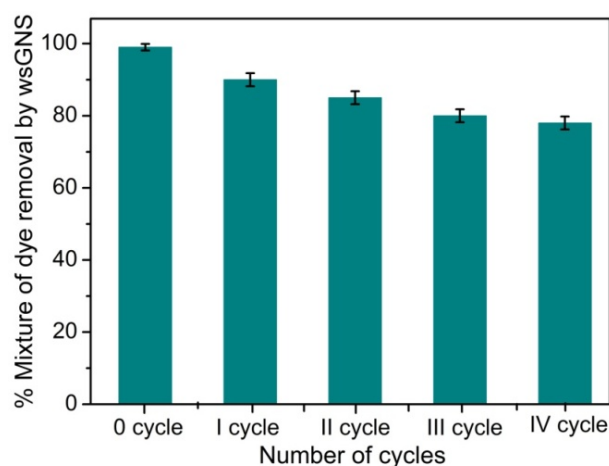
Figure 5.6. Photodegradation activity of wsGNS after the four cycles of recycling testing in the case of the mixture of dyes.

5.3.6. Effects of Interfering Substances

To check its possible potentials for the practical-applications, the photodegradation efficiency of wsGNS was further been examined in the presence of various interfering ions [59]. Different interfering ions were mixed separately into separate dye solution and their photodegradation were carried out at same experimental conditions as discussed above. Figure 5.7 (a-c) displayed the photodegradation efficiency of wsGNS towards CV, RhB, and MB in the presence of diverse interfering ions (100 ppm of Ca^{2+}, Fe^{3+}, SO_4^{2-}, HPO_4^{2-}, NO_3^-, Cl^-), suggesting that the photodegradation efficiency of wsGNS was not significantly

affected even in the presence of many interfering ions. Only few ions were observed to affect the photocatalytic efficiency.
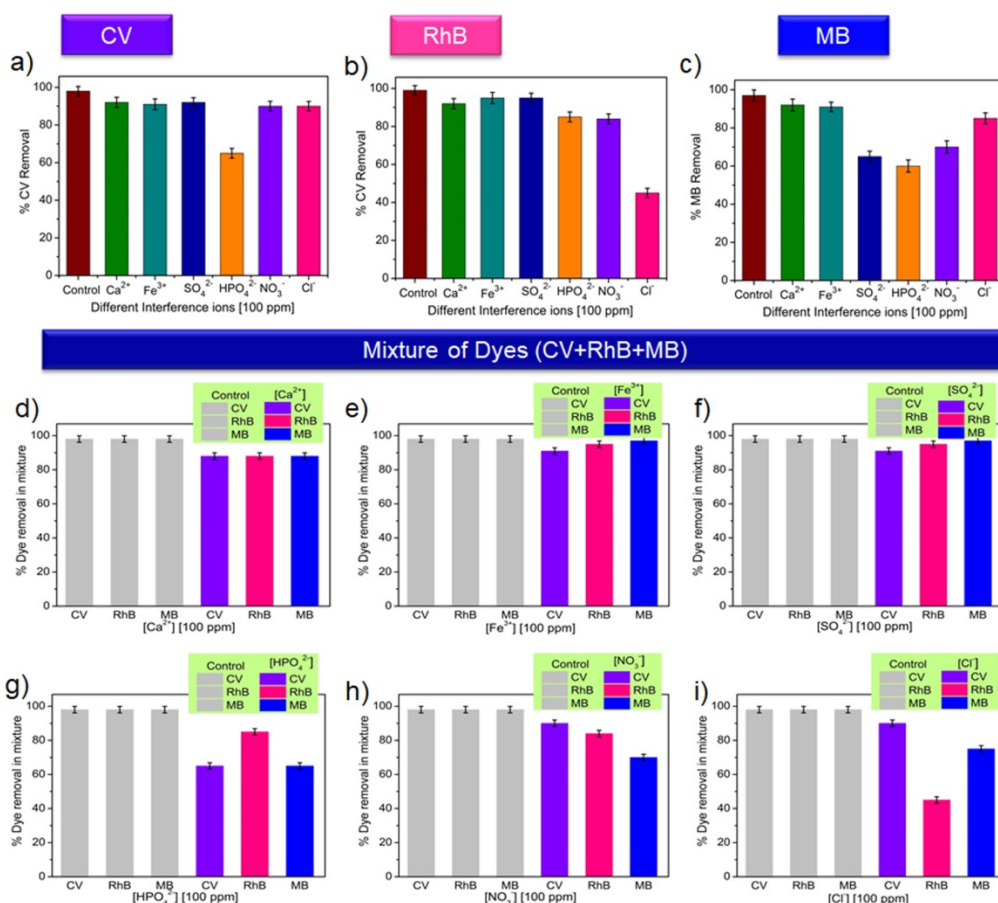
Figure 5.7. Effect of different interfering ions Ca^{2+}, Fe^{3+}, SO_4^{2-}, HPO_4^{2-}, NO_3^-, and Cl^- ions (100 ppm) on the decolorization efficiency of (a) CV (b) RhB, and (c) MB separately by wsGNS with respect to control; (d-i) Effect of different interfering ions Ca^{2+}, Fe^{3+}, SO_4^{2-}, HPO_4^{2-}, NO_3^-, and Cl^- ions (100 ppm) on the decolorization of mixture of dyes with respect to control.

Such as in the case of CV, only HPO_4^{2-} intervened a bit, while in case of RhB dye it is only Cl^- ions and in the case of MB, the SO_4^{2-}, HPO_4^{2-}, and NO_3^- ions are being interfered for its photodegradation. Similarly, for the mixture of the dyes (CV+RhB+MB) the effects of these interfering ions on the percentage degradation are shown separately in Figure 5.7 (d-i). The dye degradations were monitored separately at their respective λ_{max} values of 589 nm, 554 nm, and 663 nm for CV, RhB, and MB respectively. In the described range the degradation of CV and MB in the mixture of dyes was not affected by most of the ions except for HPO_4^{2-} while in

135

case of RhB, Cl⁻ ions affected the degradation of RhB in the mixture of dyes. The delay in photodegradation of dyes in the presence of SO_4^{2-}, HPO_4^{2-}, NO_3^- and Cl⁻ might be because of reaction of positive holes with these negative ions. Like there may be competition of negative ions with negative surface groups of wsGNS for the photodegradation of cationic dye molecules [59].

5.3.7. Treated Wastewater for the Growth of Wheat Plants

A simple eco-toxicological bioassay like the growth of plants from the germinated seeds was performed to check suitability and sustainability of overall photocatalytic process, related to the possible reuse of the treated waste water [80]. Influence of dyes and their mixtures before and after the photodegradation with control and with wsGNS (only DI water and in wsGNS) were investigated on the growth of wheat plants as one of the most sensitive and fast growing plants. One day germinated wheat seeds were grown with pollutant water containing dyes, their mixtures and photodegraded treated wastewater and growth were observed after the 15 days of germination as shown in Figure 5.8. The solutions of dyes and their mixtures before degradation showed a very-strong inhibition in the growth of wheat plants (Figure 5.8 (a)). However, the wheat plants were grown with photodegraded water showed the almost similar manner of growth compared to the control plants (treated with DI water and in wsGNS) (Figure 5.8 (b,c)).
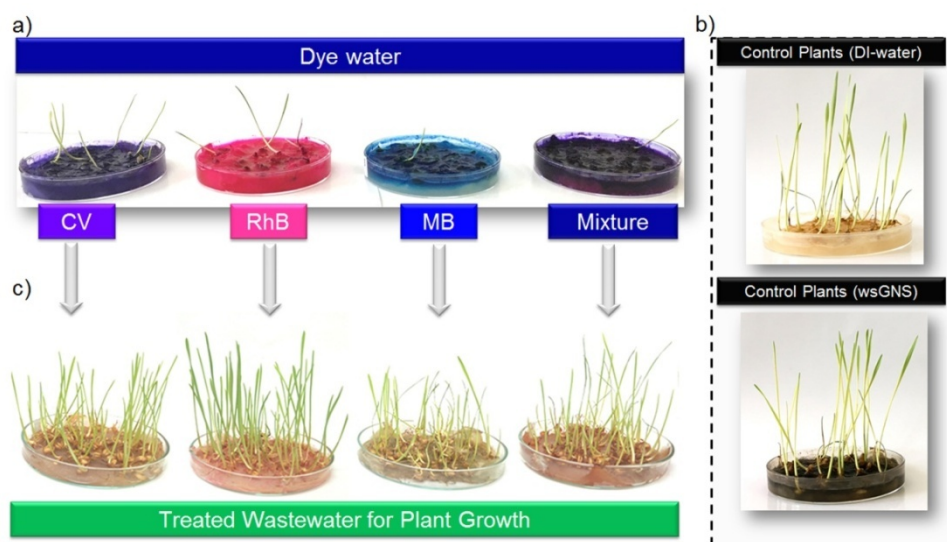
Figure 5.8. The effect of dyes, their mixture *versus* treated wastewater on the wheat plant was tested for the 15 days of germination; Seeds treated with (a) dyes water and their mixture (CV+RhB+MB); (b) Control (as in DI water and in wsGNS solution); *versus* the (c) Treated wastewater of dyes and their mixture.

The growth observed in the case of wsGNS strongly advocated the non-toxic [23] behavior towards the plant growth. The obtained results are in the favor concerning the safe uses of the treated wastewater. But for the edible plants, more précised and the thorough studies need to be taken care. Indeed, this practice can further lessen the overexploitation of natural water and could promote the reuse of treated wastewater to at least irrigate the playgrounds, parks, and gardens.

5.4   Conclusion

Environmentally benign isolations, cost-economic factors, and the utilization of the dangerous BC derived wsGNS as an advanced photocatalytic material is being explored here. For the almost complete photodegradation of the three chosen different organic dyes and their mixtures under the presence of natural sunlight. The complete photodegradation of the mixture of dyes was achieved within ~ 225 min of the sunlight exposure. The reactive oxygen species were responsible for the photodegradation processes identified as holes and hydroxyl radicals *via* the simplest radical trapping experiments. ^{1}H NMR investigations of the photodegraded products after the degradation of dyes are confirming the breaking of the organic complex aromatic framework of the dyes into their smaller non-toxic versions. Further to sustain the overall sustainability of the whole process the photodegraded wastewater from the pollutant dyes is being used for growth of wheat plants, which shows the remarkable results compared to the dye treated plants. Further, the use of wastewater for growing the wheat plants could relate to with the practical sustainability of the treated water for its use in real-life applications.

5.5   References

1. Teng, Y.; Yang, J.; Zuo, R.; Wang, J., Impact of Urbanization and Industrialization Upon Surface Water Quality: A Pilot Study of Panzhihua Mining Town. *J. Earth Sci.* **2011**, *22*, 658-668.

2. Metz, B.; Davidson, O.; Bosch, P.; Dave, R.; Meyer, L., Climate Change 2007: Mitigation of Climate Change. Working Group III Contribution to the Fourth Assessment Report of the Intergovernmental Panel on Climate Change. *Cambridge University Press*, NY, USA., **2007**.

3. Jiang, Z.; Lin, B., China's Energy Demand and Its Characteristics in the Industrialization and Urbanization Process. *Energy Policy* **2012**, *49*, 608-615.

4. Reddy, M. S.; Venkataraman, C., Direct Radiative Forcing from Anthropogenic Carbonaceous Aerosols over India. *Current Sci.* **1999**, *76*, 1,005-1,011.

5. Menon, S.; Hansen, J.; Nazarenko, L.; Luo, Y., Climate Effects of Black Carbon Aerosols in China and India. *Science* **2002**, *297*, 2250-2253.

6. Chandrappa, R.; Gupta, S.; Kulshrestha, U. C., Industrial Revolutions, Climate Change and Asia. *In Coping with Climate Change: Principles and Asian Context*, **2011**, 27-43.

7. Ramanathan, V.; Carmichael, G., Global and Regional Climate Changes Due to Black Carbon. *Nat. Geosci.* **2008**, *1*, 221-227.

8. Nichols, J. L.; Owens, E. O.; Dutton, S. J.; Luben, T. J., Systematic Review of the Effects of Black Carbon on Cardiovascular Disease among Individuals with Pre-Existing Disease. *Int. J. Public Health* **2013**, *58*, 707-724.

9. Reddy, D. H. K.; Lee, S. M., Water Pollution and Treatment Technologies. *J Environ Anal Toxicol.* **2012**, *2*, e103.

10. Sonkar, S. K.; Tripathi, K. M.; Sarkar, S., Ferromagnetic Behaviour of Anthropogenic Multi-Walled Carbon Nanotubes Trapped in Spider Web Indoor. *J. Nanosci. Nanotechnol.* **2014**, *14*, 2532-2538.

11. Theron, J.; Walker, J. A.; Cloete, T. E., Nanotechnology and Water Treatment: Applications and Emerging Opportunities. *Crit. Rev. Microbiol.* **2008**, *34*, 43-69.

12. Wang, C.; Yediler, A.; Lienert, D.; Wang, Z.; Kettrup, A., Toxicity Evaluation of Reactive Dyestuffs, Auxiliaries and Selected Effluents in Textile Finishing Industry to Luminescent Bacteria *Vibrio fischeri*. *Chemosphere* **2002**, *46*, 339-344.

13. Zollinger, H., Color Chemistry: Syntheses, Properties, and Applications of Organic Dyes and Pigments. *Verlag Helvetica Chimica Acta Wiley* VCH , **2003**, 637.

14. Claxton, L. D.; Houk, V. S.; Hughes, T. J., Genotoxicity of Industrial Wastes and Effluents. *Mutat. Res. Rev. Mutat. Res.* **1998**, *410*, 237-243.

15. Anliker, R., Color Chemistry and the Environment. *Ecotoxicol. Environ. Saf.* **1977**, *1*, 211-237.

16. Au, W.; Pathak, S.; Collie, C. J.; Hsu, T. C., Cytogenetic Toxicity of Gentian Violet and Crystal Violet on Mammalian Cells *in vitro*. *Mutat. Res.* **1978**, *58*, 269-276.

17. Golka, K.; Kopps, S.; Myslak, Z. W., Carcinogenicity of Azo Colorants: Influence of Solubility and Bioavailability. *Toxicol. Let.* **2004**, *151*, 203-210.

18. Akarslan, F.; Demiralay, H., Effects of Textile Materials Harmful to Human Health. *Acta Phys. Pol. A* **2015**, *128*, B-407.

19. Khan, S.; Malik, A., Environmental and Health Effects of Textile Industry Wastewater. In *Environmental Deterioration and Human Health: Natural and anthropogenic determinants*, *Springer*, **2014**, 55-71.

20. Lee, T. H.; Yao, N.; Chen, T. J.; Hsu, W. K., Fullerene-Like Carbon Particles in Petrol Soot. *Carbon* **2002**, *40*, 2275-2279.

21. Wang, Q.; Zhang, S. R., Size Separation of Carbon Nanoparticles from Diesel Soot for Mn (II) Sensing. *J. Lumin.* **2014**, *146*, 37-41.

22. Tripathi, K. M.; Sonker, A. K.; Sonkar, S. K.; Sarkar, S., Pollutant Soot of Diesel Engine Exhaust Transformed to Carbon Dots for Multicoloured Imaging of *E. coli* and Sensing Cholesterol. *RSC Adv.* **2014**, *4*, 30100-30107.

23. Khare, P.; Singh, A.; Verma, S.; Bhati, A.; Sonker, A. K.; Tripathi, K. M.; Sonkar, S. K., Sunlight-Induced Selective Photocatalytic Degradation of Methylene Blue in Bacterial Culture by Pollutant Soot Derived Nontoxic Graphene Nanosheets. *ACS Sustainable Chem. Eng.* **2018**, *6*, 579-589.

24. Singh, A.; Khare, P.; Verma, S.; Bhati, A.; Sonker, A. K.; Tripathi, K. M.; Sonkar, S. K., Pollutant Soot for Pollutant Dye Degradation: Soluble Graphene Nanosheets for Visible Light Induced Photodegradation of Methylene Blue. *ACS Sustain. Chem. Eng.* **2017**, *5*, 8860-8869.

25. Uchida, T.; Ohashi, O.; Kawamoto, H.; Yoshimura, H.; Kobayashi, K.; Tanimura, M.; Fujikawa, N.; Nishimoto, T.; Awata, K.; Tachibana, M.; Kojima, K., Synthesis of Single-Wall Carbon Nanotubes from Diesel Soot. *Jpn. J. Appl. Phys.* **2006**, *45*, 8027-8029.

26. Tripathi, K. M.; Singh, A.; Bhati, A.; Sarkar, S.; Sonkar, S. K., Sustainable Feasibility of the Environmental Pollutant Soot to Few-Layer Photoluminescent Graphene Nanosheets for Multifunctional Applications. *ACS Sustainable Chem. Eng.* **2016**, *4*, 6399-6408.

27. Posa, V. R.; Annavaram, V.; Koduru, J. R.; Bobbala, P.; V, M.; Somala, A. R., Preparation of Graphene-TiO$_2$ Nanocomposite and Photocatalytic Degradation of Rhodamine-B under Solar Light Irradiation. *J. Exp. Nanosci.* **2016**, *11*, 722-736.

28. Gao, L.; Wang, Y.; Yan, T.; Cui, L.; Hu, L.; Yan, L.; Wei, Q.; Du, B., A Novel Magnetic Polysaccharide-Graphene Oxide Composite for Removal of Cationic Dyes from Aqueous Solution. *New J. Chem.* **2015**, *39*, 2908-2916.

29. Jiao, T.; Liu, Y.; Wu, Y.; Zhang, Q.; Yan, X.; Gao, F.; Bauer, A. J. P.; Liu, J.; Zeng, T.; Li, B., Facile and Scalable Preparation of Graphene Oxide-Based Magnetic Hybrids for Fast and Highly Efficient Removal of Organic Dyes. *Sci. Rep.* **2015**, *5*, 12451-12460.

30. Putri, L. K.; Ong, W.-J.; Chang, W. S.; Chai, S.-P., Heteroatom Doped Graphene in Photocatalysis: A Review. *Appl. Surf. Sci.* **2015**, *358*, 2-14.

31. Shen, H.; Zhao, X.; Duan, L.; Liu, R.; Wu, H.; Hou, T.; Jiang, X.; Gao, H., Influence of Interface Combination of RGO-Photosensitized SnO$_2$@RGO Core-Shell Structures on their Photocatalytic Performance. *Appl. Surf. Sci.* **2017**, *391*, 627-634.

32. Xiang, Q.; Yu, J.; Jaroniec, M., Graphene-Based Semiconductor Photocatalysts. *Chem. Soc. Rev.* **2012**, *41*, 782-796.

33.   Han, C.; Zhang, N.; Xu, Y.-J., Structural Diversity of Graphene Materials and Their Multifarious Roles in Heterogeneous Photocatalysis. *Nano Today* **2016**, *11*, 351-372.

34.   Quan, Q.; Lin, X.; Zhang, N.; Xu, Y.-J., Graphene and Its Derivatives as Versatile Templates for Materials Synthesis and Functional Applications. *Nanoscale* **2017**, *9*, 2398-2416.

35.   Zhang, J.; Xiong, Z.; Zhao, X. S., Graphene-Metal-Oxide Composites for the Degradation of Dyes under Visible Light Irradiation. *J. Mater. Chem.* **2011**, *21*, 3634-3640.

36.   Gurushantha, K.; Anantharaju, K. S.; Renuka, L.; Sharma, S. C.; Nagaswarupa, H. P.; Prashantha, S. C.; Vidya, Y. S.; Nagabhushana, H., New Green Synthesized Reduced Graphene Oxide-ZrO_2 Composite as High Performance Photocatalyst under Sunlight. *RSC Adv.* **2017**, *7*, 12690-12703.

37.   Boruah, P. K.; Szunerits, S.; Boukherroub, R.; Das, M. R., Magnetic $Fe_3O_4@V_2O_5$/RGO Nanocomposite as a Recyclable Photocatalyst for Dye Molecules Degradation under Direct Sunlight Irradiation. *Chemosphere* **2018**, *191*, 503-513.

38.   Dong, S.; Cui, Y.; Wang, Y.; Li, Y.; Hu, L.; Sun, J.; Sun, J., Designing Three-Dimensional Acicular Sheaf Shaped $BiVO_4$/Reduced Graphene Oxide Composites for Efficient Sunlight-Driven Photocatalytic Degradation of Dye Wastewater. *Chem. Eng. J.* **2014**, *249*, 102-110.

39.   Tang, B.; Chen, H.; Peng, H.; Wang, Z.; Huang, W., Graphene Modified TiO_2 Composite Photocatalysts: Mechanism, Progress and Perspective. *Nanomaterials* **2018**, *8*, 105.

40.   Sharma, P.; Das, M. R., Removal of a Cationic Dye from Aqueous Solution Using Graphene Oxide Nanosheets: Investigation of Adsorption Parameters. *J. Chem. Eng. Data* **2013**, *58*, 151-158.

41.   Jiao, T.-F.; Zhao, H.; Zhou, J.; Zhang, Q.; Luo, X.; Hu, J.; Peng, Q.; Yan, X., The Self-Assembly Reduced Graphene Oxide Nanosheet Hydrogel Fabrication by Anchorage of Chitosan/Silver and Its Potential Efficient Application toward Dyes Degradation for Wastewater Treatments. *ACS Sustainable Chem. Eng.* **2015**, *3*, 3130-3139.

42.   Yoon, T. P.; Ischay, M. A.; Du, J., Visible Light Photocatalysis as a Greener Approach to Photochemical Synthesis. *Nat. Chem* **2010**, *2*, 527-532.

43.   Sreeprasad, T. S.; Gupta, S. S.; Maliyekkal, S. M.; Pradeep, T., Immobilized Graphene-Based Composite from Asphalt: Facile Synthesis and Application in Water Purification. *J. Hazard. Mater.* **2013**, *246-247*, 213-220.

44.   Sreeprasad, T. S.; Pradeep, T., Graphene for Environmental and Biological Applications. *Int. J. Mod. Phys. B* **2012**, *26*, 1242001-1242026.

45.   Ussia, M.; Bruno, E.; Spina, E.; Vitalini, D.; Pellegrino, G.; Ruffino, F.; Privitera, V.; Carroccio, S. C., Freestanding Photocatalytic Materials Based on 3D Graphene and Polyporphyrins. *Sci. Rep.* **2018**, *8*, 5001.

46.   Shanmugam, M.; Alsalme, A.; Alghamdi, A.; Jayavel, R., Photocatalytic Properties of Graphene-SnO$_2$-PMMA Nanocomposite in the Degradation of Methylene Blue Dye under Direct Sunlight Irradiation. *Mater. Express* **2015**, *5*, 319-326.

47.   Xu, S.; Fu, L.; Pham, T. S. H.; Yu, A.; Han, F.; Chen, L., Preparation of ZnO Flower/Reduced Graphene Oxide Composite with Enhanced Photocatalytic Performance under Sunlight. *Ceram. Int.* **2015**, *41*, 4007-4013.

48.   Giovannetti, R.; Rommozzi, E.; Zannotti, M.; D'Amato, C. A., Recent Advances in Graphene Based TiO$_2$ Nanocomposites (GTiO$_2$Ns) for Photocatalytic Degradation of Synthetic Dyes. *Catalysts* **2017**, *7* , 305.

49.   Nguyen, B. H.; Nguyen, V. H., Promising Applications of Graphene and Graphene-Based Nanostructures. *Adv. Nat. Sci: Nanosci. Nanotechnol.* **2016**, *7*, 023002.

50.   Zhang, N.; Zhang, Y.; Xu, Y.-J., Recent Progress on Graphene-Based Photocatalysts: Current Status and Future Perspectives. *Nanoscale* **2012**, *4*, 5792-5813.

51.   Zhang, L. L.; Xiong, Z.; Zhao, X. S., Pillaring Chemically Exfoliated Graphene Oxide with Carbon Nanotubes for Photocatalytic Degradation of Dyes under Visible Light Irradiation. *ACS Nano* **2010**, *4*, 7030-7036.

52.   Shen, Y.; Chen, B., Sulfonated Graphene Nanosheets as a Superb Adsorbent for Various Environmental Pollutants in Water. *Environ. Sci. Technol.* **2015**, *49*, 7364-7372.

53. Ren, L.; Qi, X.; Liu, Y.; Huang, Z.; Wei, X.; Li, J.; Yang, L.; Zhong, J., Upconversion-P25-Graphene Composite as an Advanced Sunlight Driven Photocatalytic Hybrid Material. *J. Mater. Chem.* **2012**, *22*, 11765-11771.

54. Ameen, S.; Shaheer Akhtar, M.; Seo, H.-K.; Shik Shin, H., Advanced ZnO-Graphene Oxide Nanohybrid and Its Photocatalytic Applications. *Mater. Lett.* **2013**, *100*, 261-265.

55. Hou, C.; Zhang, Q.; Li, Y.; Wang, H., P25-Graphene Hydrogels: Room-Temperature Synthesis and Application for Removal of Methylene Blue from Aqueous Solution. *J. Hazard. Mater.* **2012**, *205-206*, 229-235.

56. Zhang, H.; Lv, X.; Li, Y.; Wang, Y.; Li, J., P25-Graphene Composite as a High Performance Photocatalyst. *ACS Nano* **2010**, *4*, 380-386.

57. Moitra, D.; Chandel, M.; Ghosh, B. K.; Jani, R. K.; Patra, M. K.; Vadera, S. R.; Ghosh, N. N., A Simple 'in *situ*' Co-Precipitation Method for the Preparation of Multifunctional $CoFe_2O_4$-Reduced Graphene Oxide Nanocomposites: Excellent Microwave Absorber and Highly Efficient Magnetically Separable Recyclable Photocatalyst for Dye Degradation. *RSC Adv.* **2016**, *6*, 76759-76772.

58. Sahoo, P. K.; Thakur, D.; Bahadur, D.; Panigrahy, B., Highly Efficient and Simultaneous Catalytic Reduction of Multiple Dyes Using Recyclable RGO/Co Dendritic Nanocomposites as Catalyst for Wastewater Treatment. *RSC Adv.* **2016**, *6*, 106723-106731.

59. Gupta, A. K.; Pal, A.; Sahoo, C., Photocatalytic Degradation of a Mixture of Crystal Violet (Basic Violet 3) and Methyl Red Dye in Aqueous Suspensions Using Ag^+ Doped TiO_2. *Dyes Pigm.* **2006**, *69*, 224-232.

60. Mosleh, S.; Rahimi, M. R.; Ghaedi, M.; Dashtian, K.; Hajati, S., Photocatalytic Degradation of Binary Mixture of Toxic Dyes by HKUST-1 MOF and HKUST-1-SBA-15 in a Rotating Packed Bed Reactor under Blue LED Illumination: Central Composite Design Optimization. *RSC Adv.* **2016**, *6*, 17204-17214.

61. Sahel, K.; Perol, N.; Dappozze, F.; Bouhent, M.; Derriche, Z.; Guillard, C., Photocatalytic Degradation of a Mixture of Two Anionic Dyes: Procion Red MX-5B and Remazol Black 5 (RB5). *J. Photochem. Photobiol., A.* **2010**, *212*, 107-112.

62.   Chakraborty, S.; Basu, J. K.; De, S.; DasGupta, S., Adsorption of Reactive Dyes from a Textile Effluent Using Sawdust as the Adsorbent. *Ind. Eng. Chem. Res.* **2006**, *45*, 4732-4741.

63.   Zhao, Z.; Ge, G.; Zhang, D., Heteroatom-Doped Carbonaceous Photocatalysts for Solar Fuel Production and Environmental Remediation. *ChemCatChem* **2018**, *10*, 62-123.

64.   Ma, H.-Y.; Zhao, L.; Wang, D.-B.; Zhang, H.; Guo, L.-H., Dynamic Tracking of Highly Toxic Intermediates in Photocatalytic Degradation of Pentachlorophenol by Continuous Flow Chemiluminescence. *Environ. Sci. Technol.* **2018**, *52*, 2870-2877.

65.   Scott, J. P.; Ollis, D. F., Integration of Chemical and Biological Oxidation Processes for Water Treatment: Review and Recommendations. *Environ. Prog. Sustain. Energy* **1995**, *14*, 88-103.

66.   Jardim, W. F.; Moraes, S. G.; Takiyama, M. M. K., Photocatalytic Degradation of Aromatic Chlorinated Compounds Using TiO_2: Toxicity of Intermediates. *Wat. Res.* **1997**, *31*, 1728-1732.

67.   Rochkind, M.; Pasternak, S.; Paz, Y., Using Dyes for Evaluating Photocatalytic Properties: A Critical Review. *Molecules* **2014**, *20*, 88-110.

68.   Zhang, B.; Zhang, D.; Xi, Z.; Wang, P.; Pu, X.; Shao, X.; Yao, S., Synthesis of $Ag_2O/NaNbO_3$ P-N Junction Photocatalysts with Improved Visible Light Photocatalytic Activities. *Sep. Purif. Technol.* **2017**, *178*, 130-137.

69.   Yang, C.; Dong, W.; Cui, G.; Zhao, Y.; Shi, X.; Xia, X.; Tang, B.; Wang, W., Highly-Efficient Photocatalytic Degradation of Methylene Blue by PoPD-Modified TiO_2 Nanocomposites Due to Photosensitization-Synergetic Effect of TiO_2 with PoPD. *Sci. Rep.* **2017**, *7*, 3973.

70.   Tao, T.-X.; Dai, J.-S.; Yang, R.-C.; Xu, J.-B.; Chu, W.; Wu, Z.-C., Synthesis, Characterization and Photocatalytic Properties of BiOBr/ Amidoxime Fiber Composites. *Mater. Sci. Semicond. Process.* **2015**, *40*, 344-350.

71.   Rajendran, R.; Varadharajan, K.; Jayaraman, V.; Singaram, B.; Jeyaram, J., Photocatalytic Degradation of Metronidazole and Methylene Blue by PVA-Assisted Bi_2WO_6-CdS Nanocomposite Film under Visible Light Irradiation. *Appl. Nanosci.* **2018**, *8*, 61-78.

72. Bibi, R.; Shen, Q.; Wei, L.; Hao, D.; Li, N.; Zhou, J., Hybrid BiOBr/UiO-66-NH_2 Composite with Enhanced Visible-Light Driven Photocatalytic Activity toward RhB Dye Degradation. *RSC Adv.* **2018**, *8*, 2048-2058.

73. Xu, Y.; Xu, S.; Wang, S.; Zhang, Y.; Li, G., Citric Acid Modulated Electrochemical Synthesis and Photocatalytic Behavior of BiOCl Nanoplates with Exposed {001} Facets. *Dalton Trans.* **2014**, *43*, 479-485.

74. Bhati, A.; Anand, S. R.; Gunture, Garg, A. K.; Khare, P.; Sonkar, S. K. Sunlight-Induced Photocatalytic Degradation of Pollutant Dye by Highly Fluorescent Red-Emitting Mg-N-Embedded Carbon Dots. *ACS Sustainable Chem. Eng.* **2018**, *6*, 9246-9256.

75. Rajendran, R., Varadharajan, K., Jayaraman, V.; Singaram, B.; Jeyaram, J., Photocatalytic degradation of metronidazole and methylene blue by PVA-assisted Bi_2WO_6-CdS nanocomposite film under visible light irradiation. *Appl. Nanosci.* **2018**, *8*, 61.

76. Bibi, R.; Shen, Q.; Wei, L.; Hao, D.; Li, N.; Zhou, J. Hybrid BiOBr/UiO-66-NH_2 Composite with Enhanced Visible-Light Driven Photocatalytic Activity toward RhB Dye Degradation. *RSC Adv.* **2018**, *8*, 2048-2058.

77. Garg, S.; Yadav, M.; Chandra, A.; Sapra, S.; Gahlawat, S.; Ingole, P. P.; Todea, M.; Bardos, E.; Pap, Z.; Hernadi, K., Facile Green Synthesis of BiOBr Nanostructures with Superior Visible-Light-Driven Photocatalytic Activity. *Materials* **2018**, *11*, 1273.

78. Reheman, A.; Tursun, Y.; Dilinuer, T.; Halidan, M.; Kadeer, K.; Abulizi, A. Facile One-Step Sonochemical Synthesis and Photocatalytic Properties of Graphene/Ag_3PO_4 Quantum Dots Composites. *Nanoscale Res. Lett.* **2018**, *13*, 70-79.

79. Ramacharyulu, P. V. R. K.; Abbas, S. J.; Sahoo, S. R.; Ke, S.-C., Mechanistic Insights into 4-Nitrophenol Degradation and Benzyl Alcohol Oxidation Pathways over MgO/g-C_3N_4 Model Catalyst Systems. *Catal. Sci. Technol.* **2018**, *8*, 2825-2834.

80. Priac, A.; Badot, P.-M.; Crini, G., Treated Wastewater Phytotoxicity Assessment Using *Lactuca sativa*: Focus on Germination and Root Elongation Test Parameters. *C. R. Biologies* **2017**, *340*, 188-194.

Chapter - 6

Photocatalytic Dye Degradation and Detection of DNA by Multicoloured Fluorescent Carbon Nanorods from the Waste Soot of Castor Oil
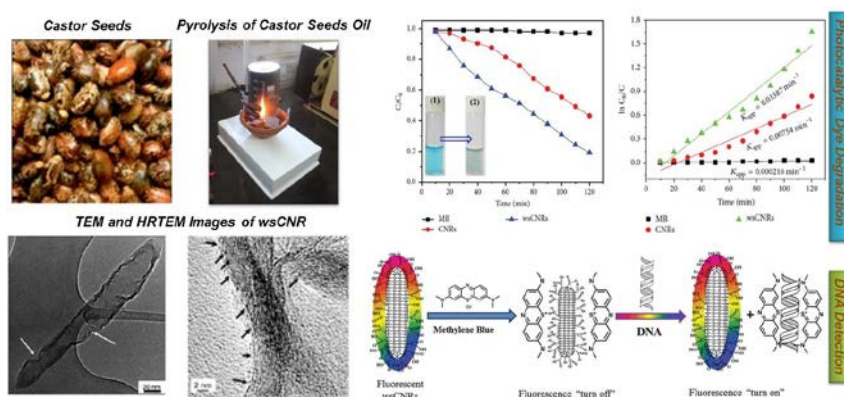
6.1   Introduction

Carbon nanorods (CNR) [1] are representing a unique class of one-dimensional carbon nanostructures, which may offer some advantageous properties in comparison with CNT [2, 3] since CNR offer straight, aligned, and hollow graphitic morphology. CNR are more or less similar to CNT, except their straightness. Spaghetti type arrangements of CNT restrict their many potential applications [4] that can be explored *via* the use of these CNR. Till now, CNR are the least explored in comparison with other members of nanocarbon family [2, 3, 5-16]. All these allotropic nanocarbons such as MWCNT [2], SWCNT [3], fullerenes [5], CNO [6-8], CND [9], graphene [10], carbon nanofibres (CNF) [15], carbon nanocubes [16], CD [13, 14, 17-19] and GQD [11] have attracted a great concern in the diverse fields of science and technology because of their potential applications [4, 8, 11, 12, 20-34]. Based on the few published reports, CNR exhibited impressive electrical, thermal, and mechanical properties and are promising for field emission devices [35], composite materials [36], lithium ion batteries [37], energy storage devices [38], electrochemical applications [39, 40]. The primary barrier for the successful commercialization of CNR is its typical synthetic procedures, such as CVD, arc discharge methods, solvothermal synthesis, electrodeposition, catalytic copyrolysis, and soft and hard template methods [41-51]. All these synthetic methods involve expensive instruments, metallic particles for growing the CNR, high-temperature, multistep fabrication protocols, and sophisticated techniques that notably restrict their economic viability. A metal-catalyst-free synthesis of CNR can be a significant approach.

Particularly for the biological application of CNR, aqueous solubility is the most important parameter, which requires the surface modifications like chemical functionalization with electrophilic groups (oxygen-rich species) [52] and bioactive groups [53]. The possible reasons for multicolored emissions from the single nanoparticle were attributed to the radiative recombination of photo-induced electrons and holes that present over the surface in the form of "surface defects" [8, 13, 33]. These surface defects can be confirmed *via* various microscopic and spectroscopic techniques. Recently, it has been demonstrated that the shape-

dependent photoluminescent CD relate "assemblies of fluorophores" [54] possibly located on the outer surface of nanocarbons. Phenomenologically these are similar as found in the case of semiconductors nanocarbons.

The simple synthesis of CNR at low cost without the use of a template or catalyst is reported in the present chapter by the pyrolysis of castor seeds oil (*Ricinus communis*) used as a green carbon precursor. The method could be used on a large scale. Castor oil is composed $\sim 87\%$ fatty acid (ricinoleic acid) and is extensively used in medicine as an antiviral, antibacterial, antifungal and analgesic agent; it is also used in cosmetics [55, 56]. The soot generated by burning castor oil in lamps was cleaned to remove any unburnt and volatile impurities. A simple HNO_3 treatment of the purified soot incorporated carboxylic acid and hydroxyl groups as surface defects [57, 58], introducing hydrophilicity that led to the formation of water soluble carbon nanorods (wsCNR). The high-density impregnation of these hydrophilic functional groups on the surface defects created by pyrolysis resulted in passivation of the surface [33, 59]. Such passivation in the presence of assorted sizes of wsCNR resulted in multicoloured PL over a broad range from green to red, with an extension into the NIR region. Such a simple catalyst-free method for the synthesis of fluorescent CNR at high yield from castor oil has not been reported previously.

6.2   Experimental Section
6.2.1   Materials and Reagents

Castor seed (*Ricinus communis*) oil used here for the synthesis of wsCNR was purchased from a local market in Jaipur, India. MB and nitro blue tetrazolium (NBT) chloride were procured from S.D. Fine-Chemicals, India. Solvents like acetone, methanol, ethanol, petroleum ether, HNO_3 and sodium nitrate are of analytical grade and procured from S.D. Fine-Chemicals, India. Sulfanilamide, N-(1-naphthyl) ethylenediamine, diformazan dye, carbon tetrachloride (CCl_4) and DNA were purchased from Sigma-Aldrich. All chemicals were of analytical grade and used without any further purification.

147

6.2.2 Instrumentation

FESEM analyses were carried using SUPRA 40VP, instrument operating under the high-vacuum mode at 10 kV (over the brass substrate (copper: 59.62 ± 0.15, zinc: 39.62 ± 0.50 %)). The sample for FESEM analysis was made by dropping a dilute droplet of sample onto brass substrate, followed by its drying at ambient temperature. AFM images were taken in tapping mode under ambient condition using Pico SPM (Molecular Imaging). AFM sample was prepared by placing a dilute solution of wsCNR on freshly cleaved, highly oriented pyrolytic graphite (HOPG) surface. TEM and HRTEM were carried over the Tecnai 20 G^2 200 kV, operating at 200 kV for studying the internal morphology. UV-Vis and PL spectroscopy were recorded with a Perkin Elmer, Lambda 35 and Perkin Elmer LS55 respectively. Raman spectra were recorded with WITEC model Raman spectrometer using Ar^+ laser (λ_{ex} = 532 nm) as an excitation source. The samples were taken in powdered form and analyzed over the glass holder. Zeta potential measurement was carried out in aqueous medium with the Beckman Coulter Delsa TM Nano. TGA were performed with Mettler Toledo Star System under the continuous flow of argon atmosphere, with the heating rate of 10˚C /min, with the temperature ranges from 25-1100 ˚C. FT-IR was recorded with a Bruker Fourier transform infrared spectrometer (Vector 22 model). p-XRD spectra of Soxhlet-purified soot and wsGNS were recorded at room temperature (Cu Kα radiation, scan rate of 3° min⁻¹) and recorded on a Bruker D8 Advance Series 2 powder X-ray diffractometer. XPS was recorded in omicron multiprobe system. Electron paramagnetic resonance (EPR) spectra of CNR and wsCNR were recorded on a Bruker-EMX EPR spectrometer. Quantum yield values calculations were made by following documented procedure [60]. Fluorescence studies were imaged with a Leica (Leica DM 2500, Leica microscopy system Ltd., CH- 9435, Heerbrugg) inverted microscope using 488 nm, 532 nm and 631 nm band pass filters.

6.2.3 Synthesis and Water Solubilization of CNR

Soot was collected from the top of the flame in a glowing castor oil lamp. The height of the cotton wick was adjusted to obtain a large yellow sooty flame so that a large amount of soot was formed. Soot was collected by covering the flame

from the top with an upturned earthenware pottery bowl to avoid metal contamination [67]. About 5.0 g of collected raw soot was placed in a paper thimble (Whatman-1) and washed in a Soxhlet extractor using PET-ether, toluene, acetonitrile and acetone solvents in sequence. This removed any unburnt oil and organic derivatives such as polyaromatic hydrocarbons deposited with the accumulated soot. The Soxhlet-purified soot was air-dried and then added in 3.0 g portions (to control the exothermic reaction) to 200 mL of concentrated HNO_3. The mixture was then refluxed for ~12 h to cause peripheral oxidation of the CNR and a large portion of the soot went into solution. The small amount of insoluble residue was separated by centrifugation and evaporated to dryness to give a solid black mass. This was repeatedly re-dissolved in minimum amounts of water and evaporated on a boiling water-bath until all traces of HNO_3 had been removed [57, 61]. The yield of the water-soluble product (as wsCNR) was ~80% based on the CNR.

6.2.4   Photochemical Experiment

A stock solution was prepared by dissolving 100 mg of wsCNR and CNR in 200 mL of 20 mg L^{-1} MB solution. CNR were dissolved in solution by sonication for 30 min and wsCNR just by shaking with hands. The aliquots were collected at the different time and then exposed to direct sunlight for 10 min. Aliquots of MB for photochemical degradation was analysed using UV-Vis spectrophotometer. The kinetic rate constant for the degradation of MB with wsCNR under visible light was analysed using the Langmuir-Hinshelwood model:

$$\ln (C_o/C) = K_{app} \times t, \tag{1}$$

where K_{app} represents the apparent kinetic rate constant and C_o and C are the initial concentration and concentration at time, respectively, and is the irradiance time.

6.2.5   Deoxyribose Nucleic Acid (DNA) Sensing

PL studies for DNA sensing were carried out at room temperature at an excitation wavelength of 460 nm. MB solution (6.25×10^{-4} M) was added stepwise at increments of 0.1 mL until a total of 1 mL had been added into 2 mL of an aqueous solution of wsCNR (2×10^{-5} g mL^{-1}). The solutions were finally made up to a constant volume of 3mL. The fluorescence intensity of wsCNR was slowly

quenched by the addition of MB solution within 10 min. A 0.01 mL volume of DNA solution (8×10^{-3} mg mL^{-1}) was then added to the quenched solution (wsCNR + MB) and restored the fluorescence within 2 min.

6.3   Results and Discussion

A simple, convenient and economic route has been developed for the synthesis of multicoloured fluorescent wsCNR without the use of a template or metallic catalyst; an almost quantitative (~80%) yield of CNR was obtained. The CNR were directly synthesized *via* the pyrolytic graphitization of castor oil. The high yield synthesis of CNR was repeated several times with castor oil from different geographical locations in India and each time a homogenous distribution of rod-like morphologies was obtained. The wsCNR were characterized by various spectroscopic and microscopic techniques and used for photochemical degradation of MB along with this their fluorescent properties were used in a sensor based on a fluorescent turn-off/turn-on mechanism for the selective and specific determination of DNA.

6.3.1   Spectroscopic Characterization

The as-obtained wsCNR had excellent solubility in water without the need for sonication as a result of high-density surface functionalization [16, 34, 62-65]. Figure 6.1(a) shows the solubility of the wsCNR at various concentrations from 0.1 to 1 mg mL^{-1}. The wsCNR remained in aqueous solution without any precipitation for several months. The UV-visible absorption spectrum (Figure 6.1(b)) shows an absorption band at 208 nm and a shoulder at 260 nm attributed to the π- π* transition of aromatic C=C bonds and the n-π* transition of the C=O bonds, respectively [57, 61]. Figure 6.1(c) and (d) show optical photographic images of the wsCNR illuminated under ordinary (Figure 6.1(c)) and UV irradiation (Figure 6.1(d)). Excitation with UV light gave an intense green fluorescence that can be seen with the naked eye.
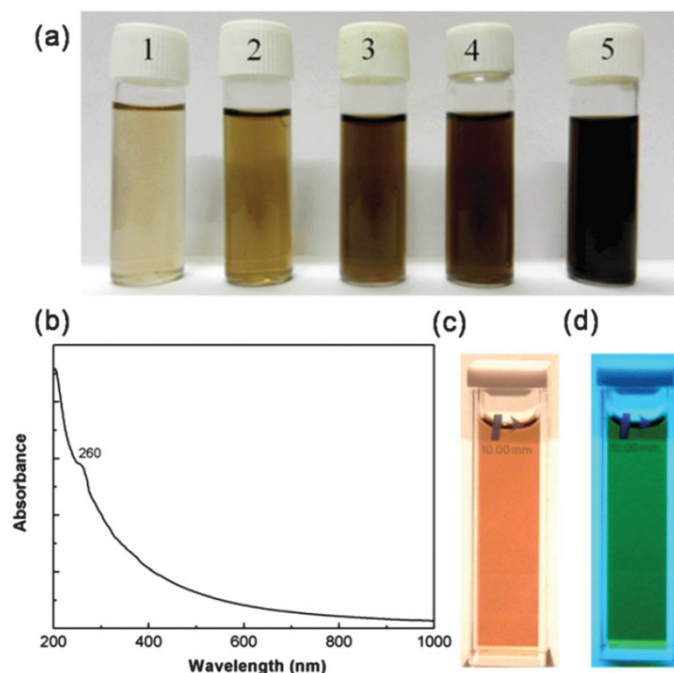
Figure 6.1. (a) Solubility of wsCNR immediately on adding the solid sample to water at concentrations of (1) 0.1, (2) 0.2, (3) 0.3, (4) 0.4 and (5) 1 mg mL^{-1}; (b) UV-visible absorption spectra of wsCNR; Optical images of wsCNR excited under (c) ordinary; and (d) UV light.

The FT-IR and Raman spectra [8, 23-25, 66] clearly show the presence of C=C and C-C bonds and the related stretching vibrations of sp^2 and sp^3 hybridized carbons. The FT-IR spectrum of the CNR shows a sharp peak around 2942 cm^{-1} due to the presence of sp^3 C-H stretching vibrations (Figure 6.2(a), solid line). A strong peak around 1620 cm^{-1} appears due to the presence of C=C stretching vibrations. A sharp peak around 1370 cm^{-1} represents sp^3 C-H bending vibrations and the peak around 607 cm^{-1} indicates sp^2 C-H bending vibrations, confirming the presence of the basic C=C structure with the sp^3 carbon atoms. The FT-IR spectrum of the wsCNR (Figure 6.2(a), dotted line) show a very broad band around 3430 cm^{-1} due to the presence of O-H stretching vibrations originating from the hydroxyl group of the carboxylate groups and the hydroxyl group attached to the carbon atom. A strong peak at 1715 cm^{-1} is due to the presence of the C=O stretching vibration of the carboxylate group and a peak around 1638 cm^{-1} confirms the presence of C=C stretching. The peak around 1230 cm^{-1} represents the C-O stretching of graphitic carbon and a low intensity peak at 2942 cm^{-1} is due to the sp^3 -C-H stretching

vibrations. Almost all these functional groups are missing in the CNR, suggesting a dominantly carbon-based material, but careful study showed the presence of weak vibrations due to -CH and C=O vibrations.

Raman spectroscopy showed the extent of derivatization (Figure 6.2(b)). The I_G/I_D ratio before (solid line) and after (dashed line) derivatization clearly show the enhancement in derivatization. The G-band originated from the sp^2 hybridized carbon atoms of the graphitic pool and the D-band arose from the disordered induced sp^3 hybridized carbon atoms (mostly formed through oxidative treatment) [66]. The reduction in the I_G/I_D ratio of the CNR after derivatization indicated the decrease in the amount of sp^2 graphitic carbon at the expense of sp^3 hybridized graphitic carbon. The I_G/I_D ratio of the peak area of the wsCNR was reduced to 0.26 from 0.36, confirming the increase in the surface defects of the CNR after derivatization. To confirm the presence of negatively charged surface functional groups, we determined the zeta potential of the wsCNR. The negative zeta potential of -35.88 mV confirmed the presence of carboxylate ions [8, 33, 67] on the surface of the wsCNR. To further quantify the sum of the carboxyl groups introduced onto the surface of the wsCNR, we used a simple acid-base titration to determine the weight percentage of carboxylic acid groups to be in the range 18-21% (this varied from batch to batch) [68]. The thermal stability of the surface carboxylic groups was investigated by TGA [8, 33] under an inert atmosphere. This was possible because the temperature required for the decomposition of the surface functional groups is much lower than that required to change the graphitic structure of the wsCNR. The selective removal of surficial -COOH (and C-OH) groups has been reported previously [69]. The TGA measurements were carried out in an inert atmosphere up to $1100°C$ at a heating rate of $10°C \ min^{-1}$. Figure 6.2(c) shows the weight loss *versus* temperature plots for the CNR (solid line) and wsCNR (dotted line). The CNR were comparatively more stable than the wsCNR and lost only ~12.38% of their weight up to a temperature of $1100°C$; the wsCNR lost weight progressively from $35°C$ and by $1100°C$ had lost ~54.57% of their total weight.
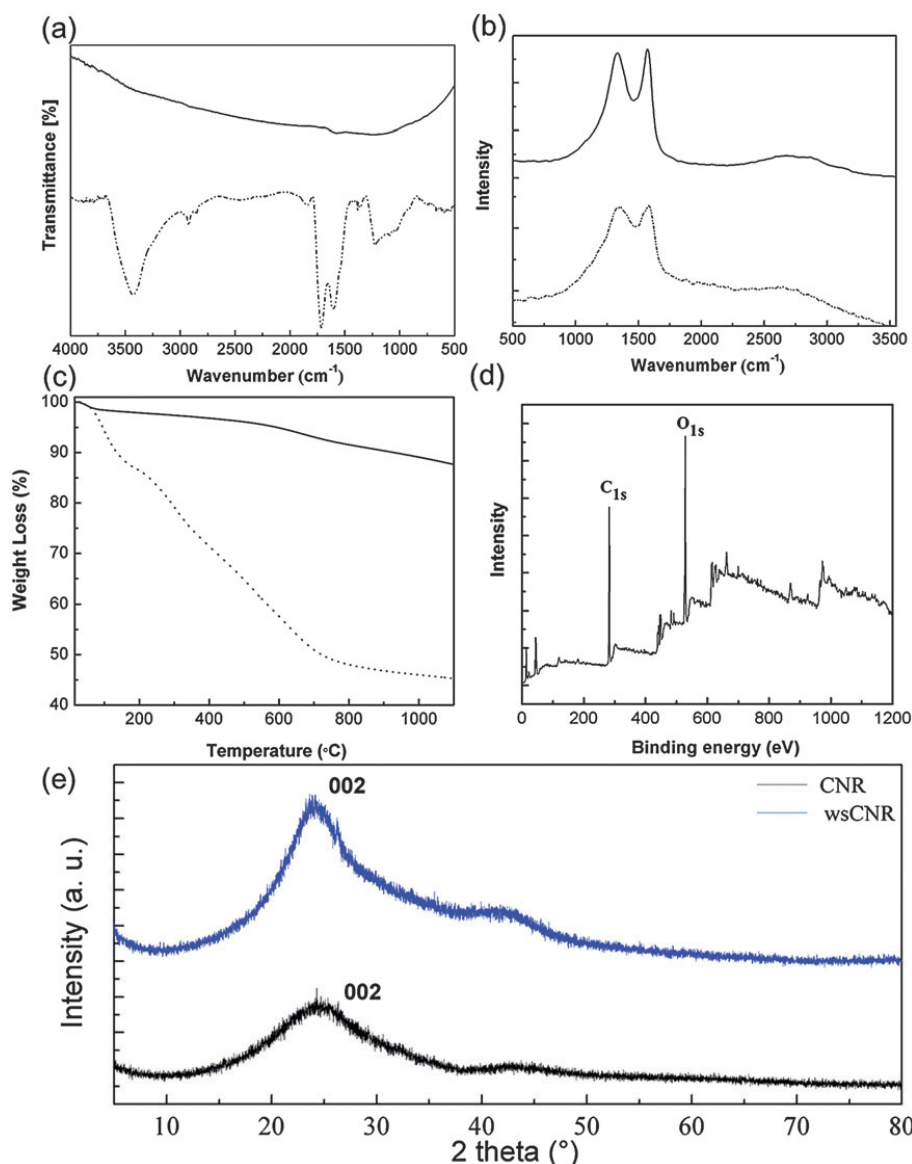
Figure 6.2 (a) FT-IR; and (b) Raman spectra of CNR before (solid line) and after (dashed line for wsCNR) derivatization; (c) TGA analysis of CNR (solid line) and wsCNR (dotted line) up to 1100°C; (d) XPS of wsCNR; (e) XRD patterns for the CNR (black line) and wsCNR (blue line).

The weight loss of the CNR is related to the removal of trace amounts of C-H and C=O functional groups at increased temperatures. The weight loss was more prominent in the wsCNR as a result of the presence of -COOH and -OH groups, which made up almost half of the total mass in the TGA study. At lower temperatures the gradual weight loss may be attributed to the release of adsorbed moisture, which is difficult to remove even under vacuum conditions.

The composition was further corroborated by a qualitative XPS analysis. Figure 6.2(d) shows a prominent peak for graphitic C_{1s} at 282 eV and another for O_{1s} at 530 eV [70, 71]. The relative intensity of these two peaks supports the presence of oxygen in atomic percent compared with carbon. This reflects the high-density surface functionalization in the carbogenic wsCNR by the presence of a large number of carboxylic acid and hydroxyl groups. Figure 6.2(e) shows the powder XRD patterns of the CNR and wsCNR. The crystal plane diffraction peak of the CNR at a 2θ value of ~24° (0 0 2) was small compared with that of the wsCNR. Another diffraction peak started to appear at 2θ value of 42° (1 0 0) in the wsCNR, indicating that the wsCNR were more crystalline graphitic carbon [16, 61] than the CNR. This could be attributed to the removal of amorphous carbon-like impurities during the oxidative process.

6.3.2 Microscopic studies

The surface morphology, topography and internal structure of the wsCNR were studied by FESEM, AFM and TEM/HRTEM. Figure 6.3(a and b) show the FESEM images of the wsCNR under low and high resolution, indicating the presence of homogeneous wsCNR with negligible contamination by amorphous carbon.

The length of the wsCNR ranged from several nanometers to micrometres and their diameter was in the nanometer range. The distribution in diameter was evaluated statistically and the histogram in Figure 6.3(c) shows that the diameter mainly ranged from 30 nm to 80 nm. The AFM image (Figure 6.3(d)) and its height profile analysis (Figure 6.3(e)) clearly show the non-uniform topographic surface of the wsCNR.
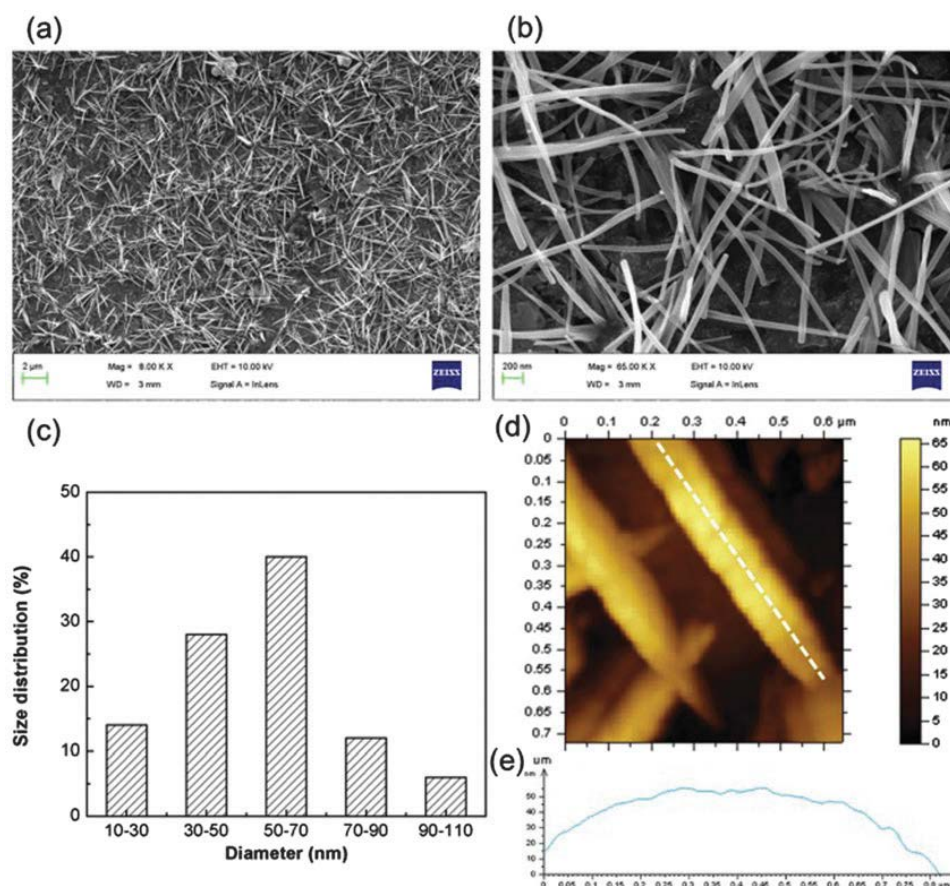
Figure 6.3. (a) Low- and (b) high-magnification FESEM images of wsCNR; (c) Histogram showing the distribution of diameters of the wsCNR; (d) High magnification AFM image; and (e) line profile (white dashed line) showing the irregular surface of the wsCNR.

Figure 6.4(a and b) are low-resolution TEM images of the wsCNR showing the hollow graphitic nature of the nanorods with defective tips and surface walls and a large number of surface defects and irregularities (marked by white arrows) that are suitable for decoration with other molecules. Figure 6.4(c-f) are HRTEM images showing the crystalline multilayered graphitic structures and outer surface walls with interlayer graphitic planes of wsCNR at a spacing of 0.33 nm [8, 23-25, 34, 62, 63].
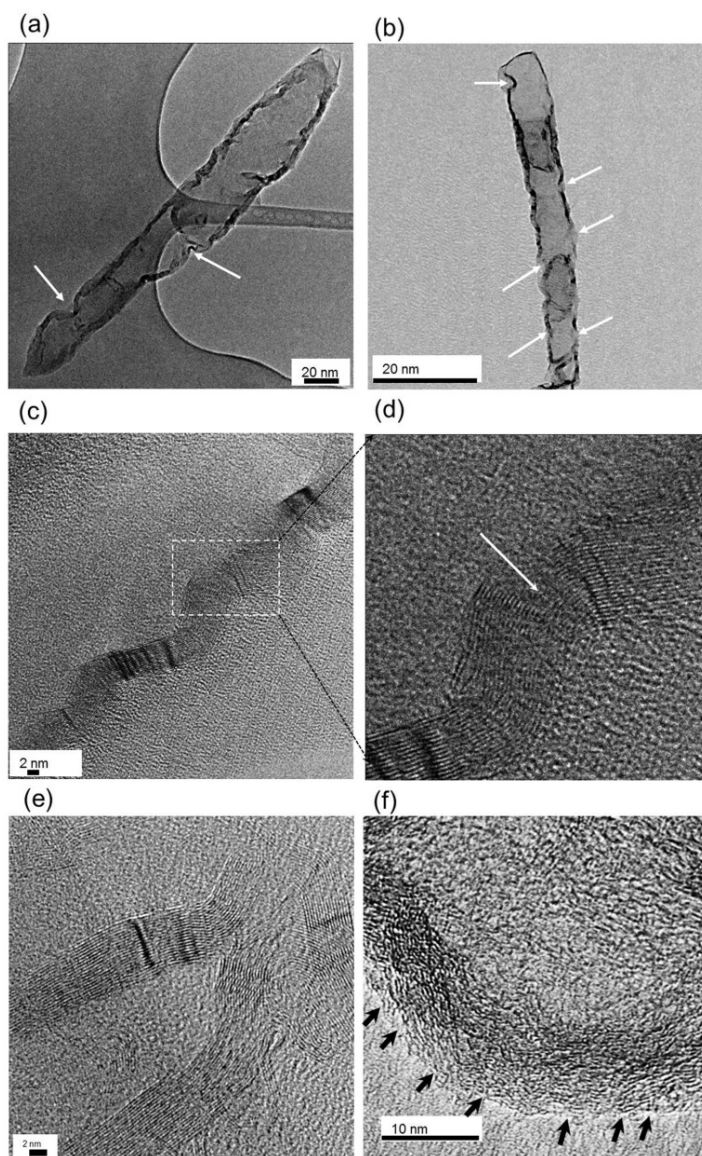
Figure 6.4. (a and b) Low magnification TEM images showing the defects on the surface of the wsCNR (white arrows); (c-f) HRTEM images showing the interlayer graphitic planes; (d) Magnified image of (c) (white box) showing the missing (broken) graphitic planes of wsCNR (white arrow); (e) HRTEM image of fused wsCNR with $d_{002} = 0.33$ nm; (f) HRTEM image focused on the outer wall of a wsCNR showing many surface defects (black arrows).

Figure 6.4 (c) shows a HRTEM image with missing graphitic planes over the continuous wall of a nanorod (magnified image in Figure 6.4 (d)) Figure 6.4 (e) shows the hollow space in the centre of the nanorod and figure 6.4 (f) reveals the high-density surface defects over the multi-layered structure (marked with black arrows).

156

The surface defects could be used to tune the physical and optical properties of the nanocarbons [72]. A comparative HRTEM analysis of the as-produced Soxhlet purified CNR *versus* wsCNR was carried out. Figure 6.5(a) is a HRTEM image of the outer surface of the CNR (marked by the black bracket) showing the presence of an even wall with few surface defects and wavy graphitic planes. In comparison, the wsCNR (Figure 6.5(b)) showed a high degree of surface defects (marked by black arrows) that originated during the oxidative process.
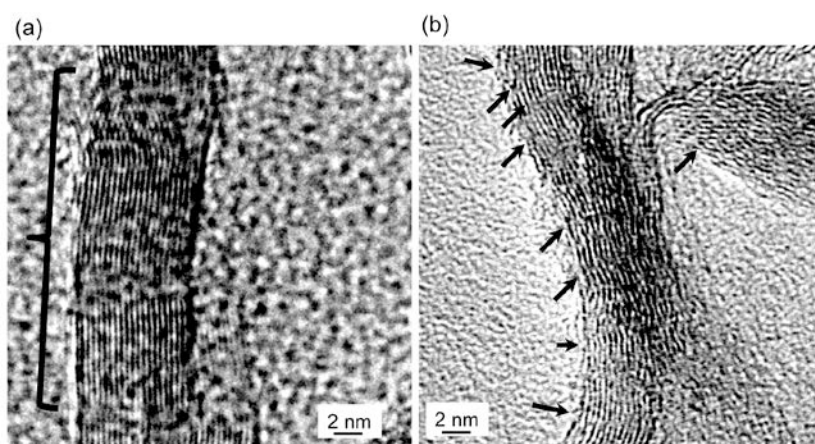
Figure 6.5. High-magnification TEM images of wsCNR (a) before and (b) after derivatization showing the incorporation of a high degree of surface defects (black arrows). Soxhlet-purified soot marked by black bracket.

6.3.3 Photoluminescence (PL) Emission-Excitation Study and Fluorescence Microscopy

The wsCNR exhibited PL properties even in the absence of any external surface passivating agents such as oligomeric [73] and monomeric amines [74]. The fluorescence appeared in the green to red region of the visible spectrum and extended to the NIR. Figure 6.6(a) shows the tunable excitation dependent PL spectra of wsCNR at different excitation wavelengths (400-660 nm) with a specified increment of 20 nm towards the longer wavelength region. Figure 6.6(b-c) show the magnified image of NIR emissions and the normalized intensities of PL.

The fluorescence of the wsCNR was highly photo-stable and did not bleach when continuously irradiated at 460 nm for 5 h (Figure 6.6(d)). More significantly, the photo-stability of the wsCNR remained unaffected even in the presence of high

ionic strength NaNO$_3$ (1 ×10^{-5} to 0.1 M; Figure 6.7 which is shown below). The wsCNR showed three PLE bands at 322 nm (3.85 eV), 340 nm (3.64 eV) and 390 nm (3.17 eV) (Figure 6.6(e)), confirming the presence of multiple types of emitting centres [8, 23-25]. Figure 6.6(f) shows the relationship between different excitation and emission wavelength profiles. Figure 6.6(g-i) show the optical microscopic images of wsCNR placed on freshly cleaned glass slides under different bandpass filters at 488 nm, 532 nm and 562 nm. The precise mechanism for the excitation-dependent PL of the carbon nanomaterials is still not clearly understood.
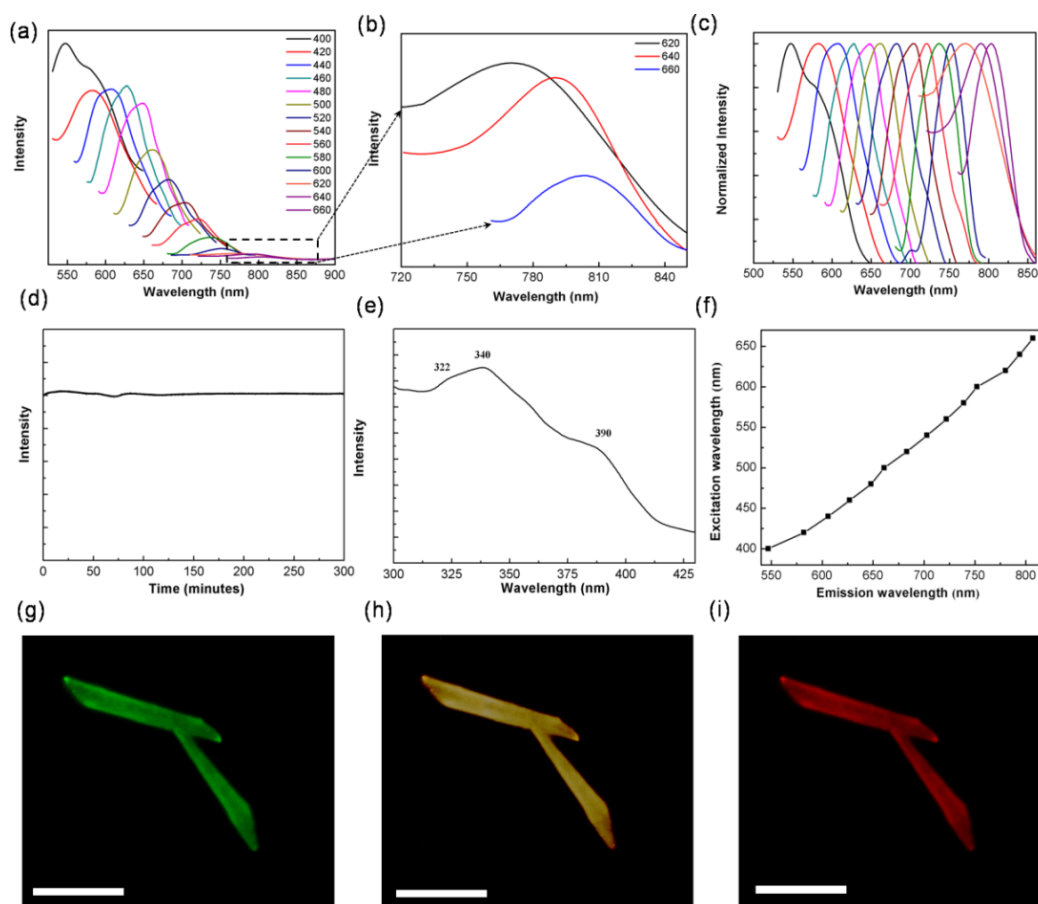
Figure 6.6. (a) Fluorescence spectra of wsCNR at different excitation wavelengths from 400 nm to 660 nm at increments of 20 nm; (b) Magnified image of (a) showing emission profiles from the red to NIR regions; (c) Normalized emission profiles of (a); (d) Photo-stability of wsCNR at an excitation wavelength of 460 nm with continuous excitation for 5 h; (e) PL excitation spectra of wsCNR at an emission wavelength of 626 nm; (f) Relationship between excitation and emission wavelengths; (g) Fluorescence images of the wsCNR over a glass slide imaged under different bandpass filters of 488 nm, 532 nm and 562 nm.
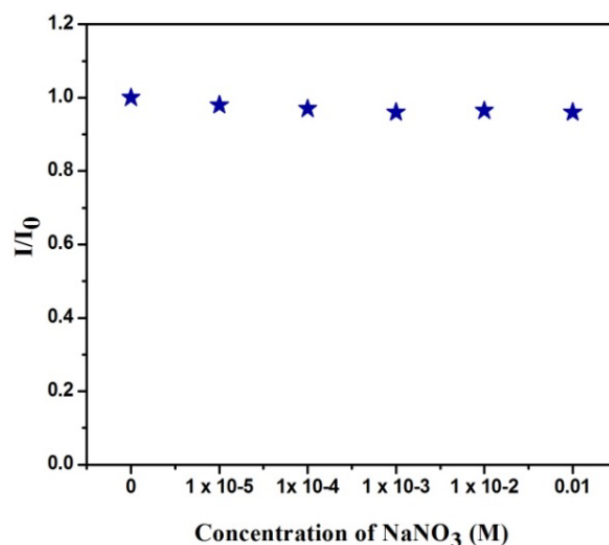
Figure 6.7. Change in the fluorescence intensity of wsCNR upon addition of 100 µL of NaNO₃ solutions of different concentration.

The excitation dependent emissive behaviour may be due to the diversity of surface energy traps between the π and π^* orbitals of the C-C bonds. The radiative recombination of both photo-induced electrons and holes present on the surface of the wsCNR in the shape of defects may be similar to the effect reported for CD [75]. It has also been shown that the shape-dependent photoluminescent CD resemble "assemblies of fluorophores" [54]. Strong oxidative treatment results in the surface carbon framework becoming impregnated with high-density oxygen-rich species in the form of carboxylate and hydroxyl-type functional groups [75]. High-density irregular surface defects impose a high degree of asymmetrical self-passivation effects, resulting in quantum confinement capable of inducing tunable fluorescence emissions. The fluorescence quantum yield of the aqueous solution of wsCNR was measured as ~1.1% (with quinine sulfate as a standard) [60] on excitation at 400 nm, with the emission peak centred at 548 nm. The carboxylation step has been shown to further functionalize the wsCNR with amine-terminated polymers via carbodiimide chemistry [76-78] to achieve a better solubility in water; however, in this instance only carboxylation resulted in the wsCNR becoming freely soluble in water. This is helpful and could be used in biomedical applications.

Application of wsCNR has been divided into two sections, Section A is photochemical degradation of MB by wsCNR and Section B is application of wsCNR for sensing and detection of DNA molecules.

SECTION A

6.3.4   Photochemical degradation of MB

Being concerned about the safety of ecosystem, especially the aquatic ecosystem, degradation of water-soluble contaminants in shapes of organic dyes via a simpler and viable approach is necessary and needs to be addressed with full attentions. In the present finding, wsCNR were explored for the visible light-induced photochemical degradation of MB in direct sunlight. For the production of many valuable products fabricated in textile, paper, and plastics industries/laboratories, we need to consume a lot of water-soluble organic dyes. These soluble dyes are further discharged with wastewater, where they are forming toxic complexes coupling with metal ions already present in aqueous system. Not only limited to the contamination of water, these are significantly hammering the photosynthetic activity of aquatic plants. Presently, various biological, chemical, and physical methods are available for the degradation of dye from sewage, like absorption, adsorption, flocculation, coagulation, ultrafiltration, and reverse osmosis, but unable to degrade properly as the transformation from one organic phase into another. To avoid this shortcoming of dye degradations, chemical oxidation, surface modifications [19], and Advanced Oxidation Process (AOP) are commonly used [79]. Still the existing methods could not be used potentially because of their high cost and incomplete degradation.

To overcome this, photocatalysis emerged as one of the most significant and economically viable methods that only require the irradiation of light without the usage of any additional chemicals [80, 81] [82]. Till now, many nanoparticles such as anatase TiO_2 [80], $Fe_2(WO_4)_3$ [81], ZnS, and CdS [82], are in use for dye degradation. But being composed of metallic in nature, their consequent toxicity is always the serious concern. Along with metallic nanoparticles, nanocarbons [19] were also explored for the dye degradation purposes. For example, doped CNT, CD, GO, graphdiyne, and graphene were used to degrade MB photochemically. Doping of nanocarbons with TiO_2 [83], Fe and Cu [84], N [85], zinc ferrite ($ZnFe_2O_4$) [86], zinc oxide (ZnO) [87, 88], MnO_2 [89], Gd [90] is a common practice but still fabrication is a tedious process. Herein, we reported a simple and viable method for the synthesis of undoped nanocarbons as wsCNR for the degradation of MB with more reliable and convenient route. To the best of our knowledge, the photochemical applications of wsCNR are not investigated till now.

6.3.4.1 Evaluation of Visible Light-Induced Photochemical Activity.

Solid-state EPR spectra of CNR (red line) and wsCNR (black line) at room temperature are shown in Figure 6.8(a). The EPR of CNR and wsCNR virtually showed the presence of very similar carbon radical signals. The average value of 1.99 in both is due to the presence of stable carbon radicals in the singly occupied orbital of carbon in their ground state. Singly occupied orbital reveals the electron donor nature of both [65]. Electron transfer properties of these CNR and wsCNR would be an advantage for a broad range of photochemical reactions.
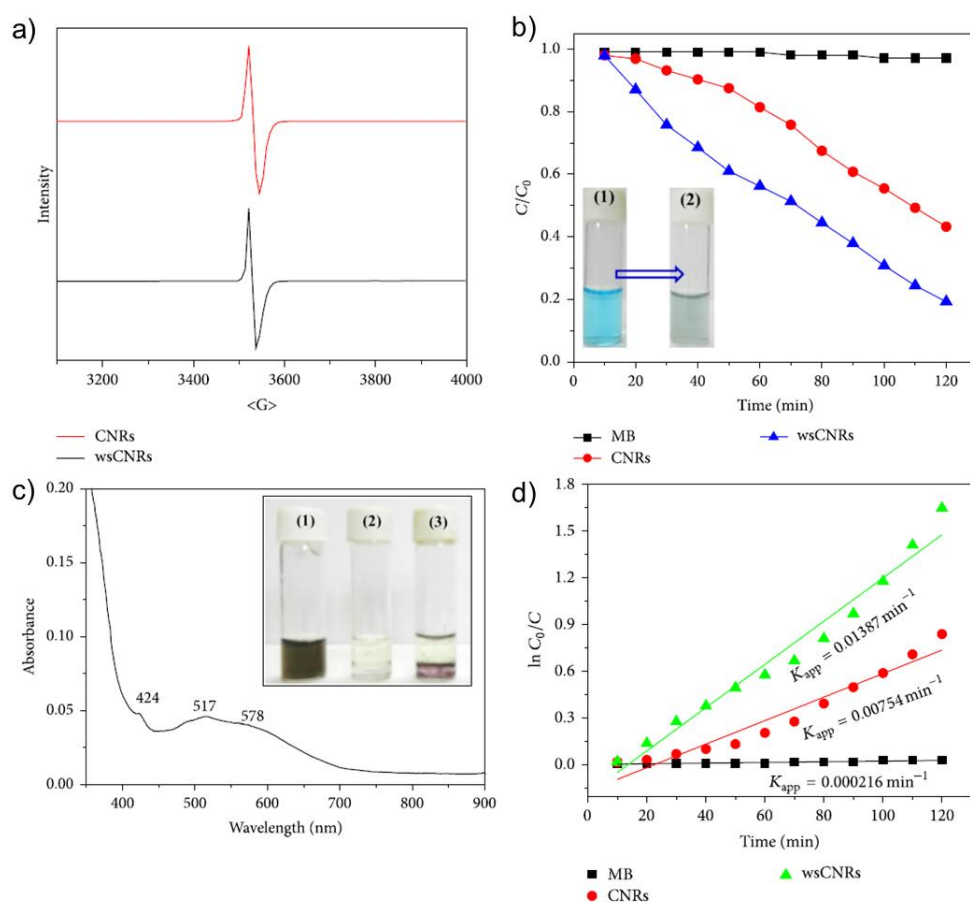
Figure 6.8. (a) EPR spectra of CNR and wsCNR showing the presence of high intensity carbon radical peak only; (b) photochemical degradation of MB in presence of only MB, CNR, and wsCNR under sunlight (inset photographs of (**1**) aqueous solution of MB); (**2**) complete photochemical degradation of MB after the addition of wsCNR (120 min) to colorless solution; (c) UV-visible spectrum of the generation of ROS by wsCNR showing the formation of diformazan dye (inset change in color of wsCNR solution (**1**) before (**2**) and after (**3**) the addition of NBT upon photoirradiation); (d) corresponding plot of $\ln(C_o/C)$ *versus* time for photochemical degradation of MB dye using only MB, CNR, and wsCNR.

161

The degradation of MB by CNR and wsCNR was carried out at room temperature with irradiation of visible photons under direct sunlight. For the homogenous photochemical degradation of MB, the higher aqueous solubility of wsCNRs is an advantageous property. An aqueous solution of MB was taken in a quartz cuvette, and degradation of MB was monitored with the UV-visible spectrometer at time intervals of 10 min. An aqueous solution of MB was light blue in color as shown in the inset of Figure 6.8(b)(**1**). After the addition of wsCNR (100 mg 200 mL^{-1}), absorption intensity of MB (20 mg L^{-1}) solution decreases gradually with time and finally the color of solution become colorless (inset of Figure 6.8(b)(**2**)) and corresponding degradation efficiency (C/C$_o$) *versus* irradiance time is illustrated in Figure 6.8(b). Spectra were measured at a time span of 10 min with the irradiation of direct sunlight. After 120 min, blue colored solution turned colorless that confirms the maximum achieved removal of MB. wsCNR generate ROS on exposure to aerial oxygen in aqueous solution on irradiation of visible photons in day light. The generation of ROS was confirmed by the NBT test (Figure6.8(c)) [65, 91, 92]. NBT was added in an aqueous solution of wsCNRs (inset of Figure 6.8(c)(**1**)) with few drops of CCl$_4$ and photoirradiated with visible photons. The change in color of CCl$_4$ layer from being colorless (inset of Figure 6.8(c)(**2**)) to being of pink color (inset of Figure 6.8(c)(**3**)) in solution indicated the reduction of NBT and hence the formation of diformazan dye.

The rate constant of MB degradation was calculated using ln(C$_o$/C) *versus* time plot as demonstrated in Figure 6.8(d) and was found to be 0.01387 min^{-1}. MB (control) exposed to direct sunlight without the addition of wsCNR did not show any significant photochemical degradation under identical conditions (Figure 6.8(b)). We did analyse the photochemical degradation of MB exposed to irradiation of visible photons under direct sunlight in the presence of CNR and found less degradation in comparison to wsCNR as illustrated in Figure 6.8(b). Oxidation of CNR introduces surface defects which enhance the photochemical activity of wsCNR. The rate constant of wsCNR is approximately two times higher in comparison to the CNR as illustrated in Figure 6.8(d).

Zeta potential confirms the negative surface charge of wsCNR (-33.4 mV) and hence facilitates the adsorption of positively charged MB over wsCNR surface via ion-pair interaction [19, 33]. Paramagnetic nature of wsCNR (presence of high-density unpaired electrons) facilitates the electron transfer between wsCNR and MB that would be the advantage of visible light-induced photochemical degradation of MB. Generation of singlet oxygen ($^1O_2$) occurred by energy transfer from wsCNR excited by visible photons to triplet oxygen ($^3O_2$) at the initial stage of photoreaction. Then reactive hydroxyl radical was formed and finally leads to superoxide anion radical ($O_2^{\cdot-}$). ROS abstracted proton from water and react with NBT [93]. The possible overall reactions[93] are illustrated in Scheme 6.1. wsCNR-MB complex was isolated to analyse its interactive surface modification during the photochemical degradation process.

$$\text{wsCNRs} \xrightarrow{h\nu} \text{wsCNRs}^*$$

$$^3O_2 \xrightarrow{\text{wsCNRs}^*} {}^1O_2$$

$$^1O_2 + \text{wsCNRs}^* \longrightarrow {}^1O_2^- + \text{wsCNRs}^+$$

$$\text{NBT} + O_2^- + H_2O \longrightarrow \text{Diformazan} + {}^-OH + O_2$$

$$\text{wsCNRs}^+ + OH^- \longrightarrow \text{wsCNRs}$$
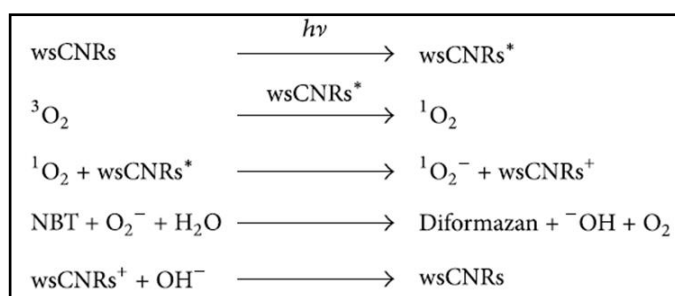
Scheme 6.1. A schematic illustration for the generation of reactive oxygen species and hence reduction of NBT induced by visible photon.

FT-IR analysis of wsCNR-MB composite was done. FT-IR spectrum of the wsCNR-MB composite is shown in Figure 6.9(a). The presence of characteristic absorption bands at 2880 cm^{-1}, 2984 cm^{-1}, and 2829 cm^{-1} confirmed the presence of -CH$_3$ and terminal N(CH$_3$)$_2$ groups. The degradation process can easily be monitored via FESEM analysis. Figure 6.9(b) shows the image of MB-interacting wsCNRs that reveals the adsorption of MB on wsCNR surface.
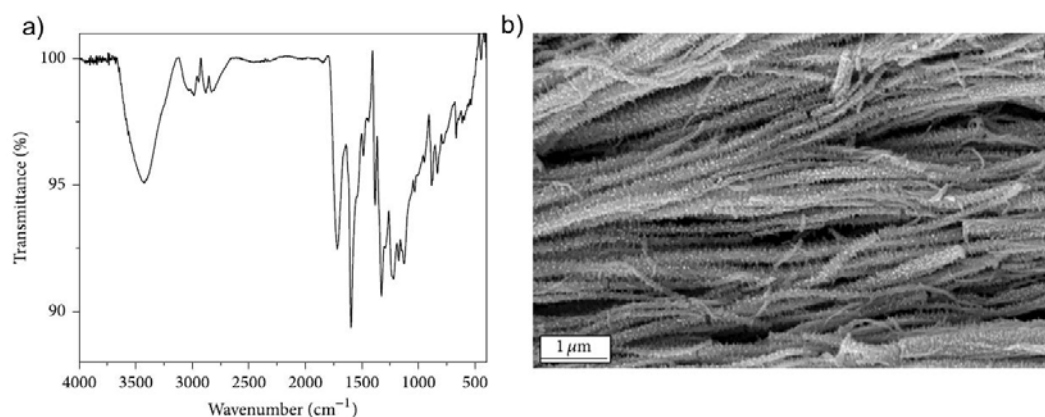
Figure 6.9. (a) FT-IR spectrum of wsCNR and MB composites isolated from the system. (b) FESEM image of wsCNR after adsorption of MB confirming its interactions.

6.3.4.2 Conclusion

In summary, wsCNR are produced by the conventional method of pyrolysis using castor oil as carbon precursor, followed by washing and oxidative treatment of as-collected soot. Because of the presence of high-density defective surfaces, carbon radicals are trapped here. Carbon radicals present over the nanocarbon surfaces are capable enough of generating ROS under irradiation of visible photons in direct sunlight via singlet oxygen-superoxide anion pathway. The wsCNR interacting with MB lead to the decolorization of MB in the presence of light through photochemical degradation reactions. This work is expected to open a new method for the preparation of wsCNR based nanohybrids/nano-composites for their practical application related to solving/minimizing the various environmental issues such a wastewater treatment to remove the organic pollutants and sensing of toxic metals. Moreover, in comparison with CNT due to their straightness, these may also be used for drug delivery purposes in future.

SECTION B

6.3.5 Sensing of DNA Molecules

The fluorescence of the synthesized wsCNR was used to determine DNA from calf thymus via a simple fluorescent switch-off/switch-on mechanism involving MB. Sensors for DNA are very important in diagnostic testing because the detection of disordered DNA is a powerful tool in the early diagnosis of disease, in the detection of genetic disorders and in the analysis of forensic samples [94-97]. Traditional DNA detection techniques use expensive instruments [96, 98]. Electrochemical methods [99, 100] for sensing of DNA require an additional reference electrode and there are difficulties associated with integration. Electrochemical DNA sensors are label-free, but have low sensitivity. Photochemical biosensors [101] have the disadvantages of photo-bleaching, a narrow excitation range and non-tunable emission spectra. Zhao *et al*. have reported the detection of zeptomolar amounts of DNA based on a polymerase chain reaction using metallic nanoparticles (an Au nanoparticle heterodimer covered with Ag or Au shells) [102]. DNA has been determined using optical techniques based on the use of a labeling molecule attached to the target DNA, although this method is costly, time-consuming and too bulky for use in portable devices [103].

A few nanocarbon materials [104,105] such as CD [106-111], GO [112,113], and SWCNT [114-117] have been used for the detection of DNA, these have lower detection limits than with the system reported here. The fabrication and use of wsCNR is a new approach for such sensing applications. Our method uses wsCNR to determine DNA with an efficient detection limit and response time. We describe here the solubility of wsCNR in aqueous media, their stability towards photo-bleaching during the experiment and their tunable PL emission properties. We have developed a rapid and cost-efficient nanocarbon-based sensor for the determination of DNA at low concentrations. This method could be used for the routine, low-cost determination of DNA in pathology laboratories.

6.3.5.1 Sensing DNA

The PL properties of the wsCNR were exploited to determine DNA molecules via a fluorescence-based turn-off/ turn-on mechanism. The fluorescence properties of the wsCNR were efficiently quenched by the addition of MB [106, 118]. A schematic representation of the plausible mechanism of the fluorescence turn-off/turn-on mechanism is shown in Figure 6.10(a). Figure 6.10(b) shows the effect of the gradual addition of MB to a solution of wsCNR. The PL properties of the wsCNR were quenched to a maximum, resulting in the fluorescence turn-off [119] of the wsCNR. The addition of DNA to the completely quenched sample solution restored the fluorescent properties, resulting in a turn-on mechanism. The fluorescence emission peak centred at ~626 nm showed a gradual decrease in intensity with the stepwise addition of 0.1 mL of MB solution (6.25×10^{-4} M) to a 2 mL volume of wsCNR (2×10^{-5} g mL^{-1}) up to a total of 1 mL (in each case the solutions were finally made up to a constant volume of 3 mL).
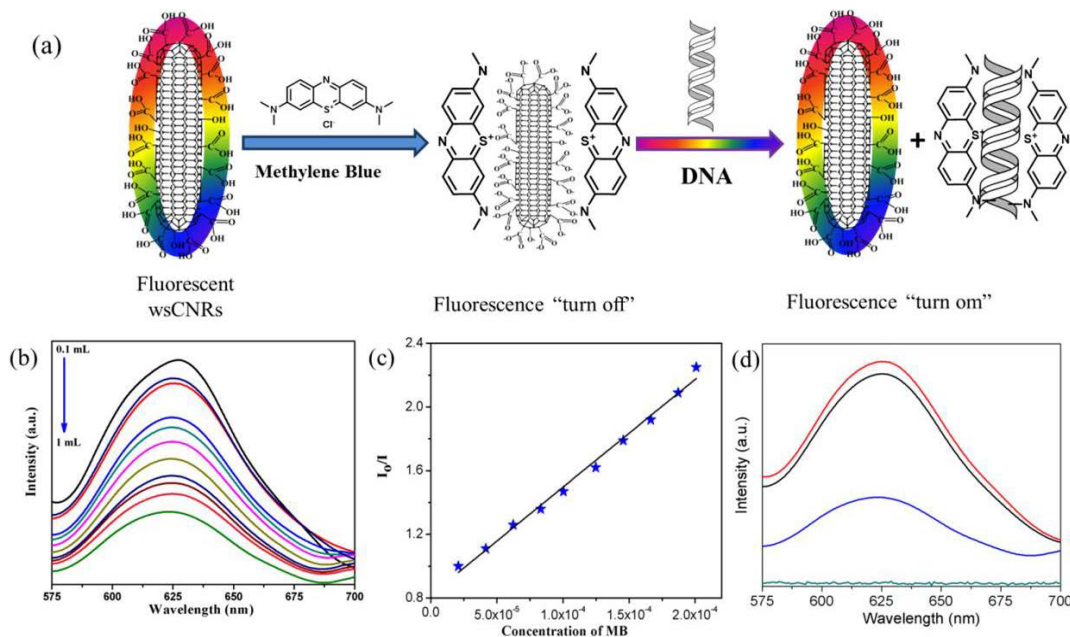
Figure 6.10. (a) Schematic representation for the fluorescence turn-off/turn-on mechanism of the DNA detection method; (b) Fluorescence spectra showing maximum quenching with the stepwise addition of 0.1 mL of aqueous solutions of MB to the wsCNR; (c) Relationship between I_o/I of wsCNR with various concentrations of MB; (d) Fluorescence turn-on (black trace) from maximally quenched sample (blue trace) after the release of surfacial MB molecules from the wsCNR after the addition of DNA and the fluorescence spectra of DNA as a control sample (cyan trace).

A 1 mL volume of MB quenched the fluorescence intensity to a maximum (Figure 6.10(b)). Figure 6.10(c) shows Stern-Volmer plots for the quenching of the wsCNR solution via the addition of MB, where I_o is the fluorescence intensity of the wsCNR solution and I is the fluorescence intensity after the addition of MB. The plot of I_o/I *versus* the concentration of MB shows a linear relationship, suggesting a dynamic and highly sensitive quenching process for the turn-off mechanism of the fluorescent properties [120-123]. Limit of detection (LOD) was determined using following equation:

$$LOD = 3SD/K$$

Where SD is the standard deviation of the blank measurements and K is the slope of the curve. The estimated detection limit was 1.14 nM, which is better than previously reported values [76,101,106,124]. Table 6.1 compares the sensing performance of various fluorescence sensors towards DNA. The positively charged MB molecules are adsorbed on the negatively charged wsCNR surface to create ion pairs. This results in the quenching of the fluorescent properties, as shown by the turn-off (blue) trace in Figure 6.10(d) [33]. After the addition of DNA, the MB molecules selectively attached to the DNA molecules by ion pair formation, removing them from the surface of the wsCNR. This resulted in fluorescence turn-on (black trace in Figure 6.10(d)). The restoration of fluorescence resulted from the association of DNA with MB *via* electrostatic interactions between the DNA and MB molecules [124]. As illustrated in Figure 6.10(d) (cyan trace), a control fluorescence spectrum of DNA was obtained to check for the presence of any intrinsic fluorescence.

Table 6.1. Performance comparison between various fluorescence sensors toward DNA molecule.

Methods	Response Time	Detection Limit	Ref.
CdTe NCs-MB	5 min	4.23×10^{-8} M	[101]
CD-MB	15 min	1×10^{-6} mol L^{-1}	[106]
GO-organic dye	NA	1nM	[112]
GO	30 min	10 nM	[113]
SWCNT	13h	6 nM	[114]
SWCNT	several h	4nM	[115]
CdTe-TGA QDs-Porphyrin	NA	2.72×10^{-9} M	[124]
wsCNR	2 min	1.14 nM	Present study

Figure 6.10(d) (cyan trace) shows the absence of any auto-fluorescence caused by the DNA itself. The effect of DNA concentration on the fluorescence intensity of the wsCNR was investigated. The gradual addition of DNA resulted in a gradual increase in the fluorescence intensity of the wsCNR in a linear relationship (Figure 6.11) The emission wavelength remained unchanged even at a relatively higher concentration of DNA. An enhancement in relative fluorescence intensity was observed on adding 0.33-3.3 µM amounts of DNA; this could be used to monitor the concentration of DNA. The LOD of the wsCNR-DNA system was 151.5 µM.
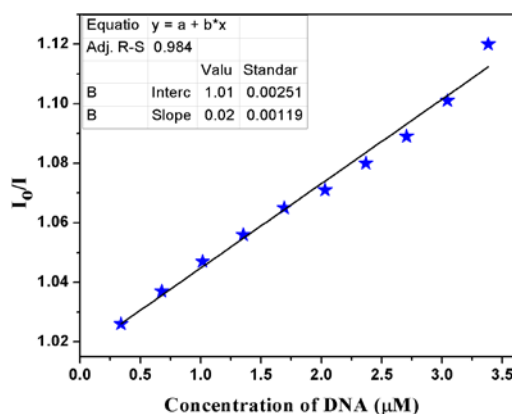
Figure 6.11. Relationship between changes in fluorescence intensity of wsCNR upon addition of 10 µL of ct-DNA solutions of different concentration.

The selective detection of DNA inside cellular systems is still challenging because of the presence of complex intracellular interactions. Our approach towards the detection of DNA is not only important with respect to its sensitivity, but also because of its selectivity suggests that it could be used for the specific determination of DNA among other biologically related molecules (e.g. amino acids, RNA) present in living organisms. The selectivity of the wsCNR towards DNA present with other biomolecules such as amino acids (aspartic acid, valine, methionine, tryptophan, cysteine), glucose and dopamine was investigated. We performed a similar set of experiments to those as carried out for DNA with these molecules. Figure 6.12 shows that restoration of the fluorescence intensity of an MB-quenched wsCNR solution reached a maximum (~95%) with DNA. Glucose showed a tiny inter-phase, whereas the other biomolecules did not affect the fluorescence turn-on. The turn-on mechanism was more sensitive than the turn-off mechanism. Therefore, the wsCNR-MB solution could function as a sensitive and selective fluorescence turn-on sensor for DNA present in mixtures of biological molecules. A linear relationship was observed between the amount of DNA added and the intensity of the fluorescence turn-on.
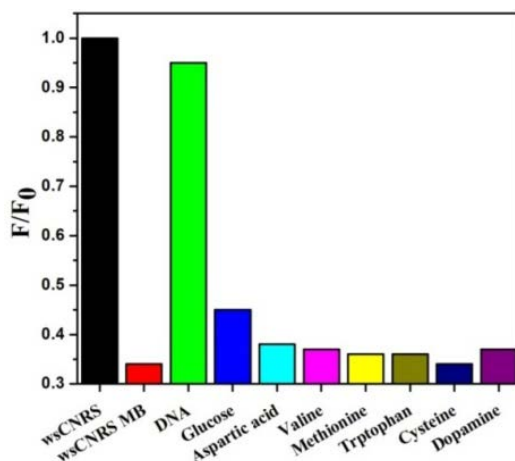
Figure 6.12. Maximum quenching of PL intensity of wsCNR at λ ~626 nm (black) after the addition of 1 mL of MB solution (red). Restoration of PL intensity of maximally quenched sample in the presence of different biomolecules (2 x 10^{-3} mg mL^{-1}). λ_{ex} = 460 nm.

6.3.5.2 Responses with Different DNA Systems

The fluorescence quenching of a wsCNR-MB solution significantly responded only to a calf thymus DNA system. The restoration of fluorescence was less effective for DNA extracted from *E. coli* plasmid and genomic DNA (Figure 6.13). This can be explained by strong ion pair interactions [106] between the calf thymus DNA and the wsCNR. The fluorescence turn-on was more prominent for calf thymus DNA under the same experimental conditions.
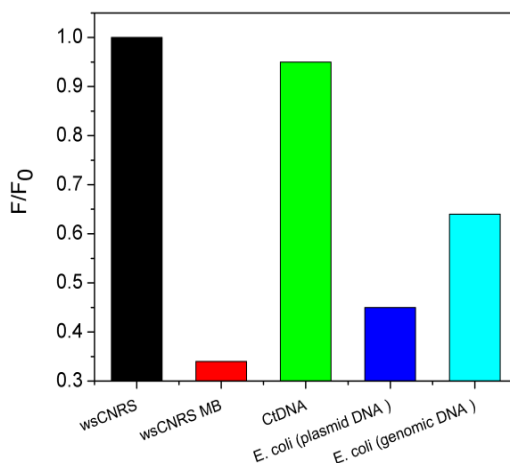
Figure 6.13. Maximum quenching of PL intensity of wsCNR ~ 626 nm (black) after addition of 1 mL MB solution (red). Restoration of PL intensity of maximum quenched sample in the presence of different types of DNA (0.01 mL, 8x10^{-3} mg mL^{-1}). λ_{ex} = 460 nm.

169

6.3.5.3 Conclusion

The physical and optical properties of CNT are not typically coupled because of their spaghetti-like structure with numerous turns and kinks. This lack of straightness limits their potential applications in the biomedical sciences. CNR are similar to CNT, but have a straight alignment; they are, however, the least explored of all the carbon nanomaterials, probably due to their poor availability. We developed a straightforward method for the synthesis of CNR and their water-soluble derivatives from castor oil seeds in nearly quantitative yields. With their extensive self-surface passivation, the wsCNR produced multicoloured emissions in the visible region and extending into the NIR. The wsCNR selectively sensed trace amounts of DNA and displayed a fluorescence turn-off/turn-on mechanism. This method could be used for the fast and low-cost determination of DNA at the nano level and could be used in diagnostic forensic kits. The possibility of using wsCNR as a Trojan horse to carry drug molecules is currently being explored.

6.4   References

1. Chang, Y.-H.; Chiu, H.-T.; Wang, L.-S.; Wan, C.-Y.; Peng, C.-W.; Lee, C.-Y., Synthesis of sp^2 Carbon Nano- and Microrods with Novel Structure and Morphology. *J. Mater. Chem.* **2003**, *13*, 981-982.

2. Iijima, S., Helical Microtubules of Graphitic Carbon. *Nature* **1991**, *354*, 56-58.

3. Iijima, S.; Ichihashi, T., Single-Shell Carbon Nanotubes of 1-nm Diameter. *Nature* **1993**, *363*, 603-605.

4. Lin, Y.; Taylor, S.; Li, H.; Fernando, K. A. S.; Qu, L.; Wang, W.; Gu, L.; Zhou, B.; Sun, Y.-P., Advances toward Bioapplications of Carbon Nanotubes. *J. Mater. Chem.* **2004**, *14*, 527-541.

5. Kroto, H. W.; Sheath, J. R.; O'Brien, S. C.; Curl, R. F.; Smalley, R. E., C60 - Buckminsterfullerene. *Nature* **1985**, *318*, 162-163.

6. Ugarte, D., Curling and Closure of Graphitic Networks under Electron-Beam Irradiation. *Nature* **1992**, *359*, 707-709.

7. Tripathi, K. M.; Bhati, A.; Singh, A.; Gupta, N. R.; Verma, S.; Sarkar, S.; Sonkar, S. K., From the Traditional Way of Pyrolysis to Tunable Photoluminescent Water Soluble Carbon Nano-Onions for Cell Imaging and Selective Sensing of Glucose. *RSC Adv.* **2016**, *6*, 37319-37329.

8. Dubey, P.; Tripathi, K. M.; Sonkar, S. K., Gram Scale Synthesis of Green Fluorescent Water-Soluble Onion-Like Carbon Nanoparticles from Camphor and Polystyrene Foam. *RSC Adv.* **2014**, *4*, 5838-5844.

9. Chang, Y.-R.; Lee, H.-Y.; Chen, K.; Chang, C.-C.; Tsai, D.-S.; Fu, C.-C.; Lim, T.-S.; Tzeng, Y.-K.; Fang, C.-Y.; Han, C.-C.; Chang, H.-C.; Fann, W., Mass Production and Dynamic Imaging of Fluorescent Nanodiamonds. *Nat. Nanotechnol.* **2008**, *3*, 284-288.

10. Geim, A. K.; Novoselov, K. S., The Rise of Graphene. *Nat. Mater.* **2007**, *6*, 183-191.

11. Shen, J.; Zhu, Y.; Yang, X.; Li, C., Graphene Quantum Dots: Emergent Nanolights for Bioimaging, Sensors, Catalysis and Photovoltaic Devices. *Chem. Commun.* **2012**, *48*, 3686-3699.

12. Luo, P. G.; Sahu, S.; Yang, S.-T.; Sonkar, S. K.; Wang, J.; Wang, H.; LeCroy, G. E.; Cao, L.; Sun, Y.-P., Carbon "Quantum" Dots for Optical Bioimaging. *J. Mater. Chem. B* **2013**, *1*, 2116-2127.

13. Dubey, P.; Tripathi, K. M.; Mishra, R.; Bhati, A.; Singh, A.; Sonkar, S. K., A Simple One-Step Hydrothermal Route Towards Water Solubilization of Carbon Quantum Dots from Soya-Nuggets for Imaging Applications. *RSC Adv.* **2015**, *5*, 87528-87534.

14. Saxena, M.; Sonkar, S. K.; Sarkar, S., Water Soluble Nanocarbons Arrest the Growth of Mosquitoes. *RSC Adv.* **2013**, *3*, 22504-22508.

15. Jiang, J.; Zhu, J.; Ai, W.; Fan, Z.; Shen, X.; Zou, C.; Liu, J.; Zhang, H.; Yu, T., Evolution of Disposable Bamboo Chopsticks into Uniform Carbon Fibers: A Smart Strategy to Fabricate Sustainable Anodes for Li-Ion Batteries. *Energy Environ. Sci.* **2014**, *7*, 2670-2679.

16. Sonkar, S. K.; Manav Saxena; Saha, M.; Sarkar, S., Carbon Nanocubes and Nanobricks from Pyrolysis of Rice. *J. Nanosci. Nanotechnol.* **2010**, *10*, 4064-4067.

17. Sun, Y.-P.; Zhou, B.; Lin, Y.; Wang, W.; Fernando, K. A. S.; Pathak, P.; Meziani, M. J.; Harruff, B. A.; Wang, X.; Wang, H.; Luo, P. G.; Yang, H.; Kose, M. E.; Chen, B.; Veca, L. M.; Xie, S.-Y., Quantum-Sized Carbon Dots for Bright and Colorful Photoluminescence. *J. Am. Chem. Soc.* **2006**, *128*, 7756-7757.

18. Babar, D. G.; Sonkar, S. K.; Tripathi, K. M.; Sarkar, S., P_2O_5 Assisted Green Synthesis of Multicolor Fluorescent Water Soluble Carbon Dots. *J. Nanosci. Naotechnol.* **2014**, *14*, 2334-2342.

19. Tripathi, K. M.; Gupta, N. R.; Sonkar, S. K., Nano-Carbons from Pollutant Soot: A Cleaner Approach toward Clean Environment. In *Smart Materials for Waste Water Applications*, **2016**, *1*, 127-153.

20. Guldi, D. M.; Illescas, B. M.; Atienza, C. M.; Wielopolski, M.; Martin, N., Fullerene for Organic Electronics. *Chem. Soc. Rev.* **2009**, *38*, 1587-1597.

21. Tyagi, A.; Tripathi, K. M.; Gupta, R. K., Recent Progress in Micro-Scale Energy Storage Devices and Future Aspects. *J. Mater. Chem. A* **2015**, *3*, 22507-22541.

22. Fushen, L.; Lingrong, G.; J., M. M.; Xin, W.; G., L. P.; Monica, V. L.; Li, C.; Ya-Ping, S., Advances in Bioapplications of Carbon Nanotubes. *Adv. Mater.* **2009**, *21*, 139-152.

23. Sonkar, S. K.; Ghosh, M.; Roy, M.; Begum, A.; Sarkar, S., Carbon Nano-Onions as Nontoxic and High-Fluorescence Bioimaging Agent in Food Chain-an *in vivo* Study from Unicellular *E. coli* to Multicellular *C. elegans*. *Mater. Express* **2012**, *2*, 105-114.

24. Ghosh, M.; Sonkar, S. K.; Saxena, M.; Sarkar, S., Carbon Nano-Onions for Imaging the Life Cycle of *Drosophila melanogaster*. *Small* **2011**, *7*, 3170-3177.

25. Sonkar, S. K.; Roy, M.; Babar, D. G.; Sarkar, S., Water Soluble Carbon Nano-Onions from Wood Wool as Growth Promoters for Gram Plants. *Nanoscale* **2012**, *4*, 7670-7675.

26. Saito, N.; Aoki, K.; Usui, Y.; Shimizu, M.; Hara, K.; Narita, N.; Ogihara, N.; Nakamura, K.; Ishigaki, N.; Kato, H.; Haniu, H.; Taruta, S.; Ahm Kim, Y.; Endo, M., Application of Carbon Fibers to Biomaterials: A New Era of Nano-Level Control of Carbon Fibers after 30-Years of Development. *Chem. Soc. Rev.* **2011**, *40*, 3824-3834.

27. Chang, H.; Wu, H., Graphene-Based Nanocomposites: Preparation, Functionalization, and Energy and Environmental Applications. *Energy Environ. Sci.* **2013**, *6*, 3483-3507.

28. McGuinness, L. P.; Yan, Y.; Stacey, A.; Simpson, D. A.; Hall, L. T.; Maclaurin, D.; Prawer, S.; Mulvaney, P.; Wrachtrup, J.; Caruso, F.; Scholten, R. E.; Hollenberg, L. C. L., Quantum Measurement and Orientation Tracking of Fluorescent Nanodiamonds inside Living Cells. *Nat. Nanotechnol.* **2011**, *6*, 358-363.

29. Luo, P. G.; Yang, F.; Yang, S.-T.; Sonkar, S. K.; Yang, L.; Broglie, J. J.; Liu, Y.; Sun, Y.-P., Carbon-Based Quantum Dots for Fluorescence Imaging of Cells and Tissues. *RSC Adv.* **2014**, *4*, 10791-10807.

30. Zhang, Z.; Zhang, J.; Chen, N.; Qu, L., Graphene Quantum Dots: An Emerging Material for Energy-Related Applications and Beyond. *Energy Environ. Sci.* **2012**, *5*, 8869-8890.

173

31.   Mendes, R. G.; Bachmatiuk, A.; Buchner, B.; Cuniberti, G.; Rummeli, M. H., Carbon Nanostructures as Multi-Functional Drug Delivery Platforms. *J. Mater. Chem. B* **2013**, *1*, 401-428.

32.   Wei, D.; Kivioja, J., Graphene for Energy Solutions and Its Industrialization. *Nanoscale* **2013**, *5*, 10108-10126.

33.   Tripathi, K. M.; Sonker, A. K.; Sonkar, S. K.; Sarkar, S., Pollutant Soot of Diesel Engine Exhaust Transformed to Carbon Dots for Multicoloured Imaging of *E. coli* and Sensing Cholesterol. *RSC Adv.* **2014**, *4*, 30100-30107.

34.   Roy, M.; Sonkar, S. K.; Tripathi, S.; Saxena, M.; Sarkar, S., Non-Toxicity of Water Soluble Multi-Walled Carbon Nanotube on *Escherichia-coli* Colonies. *J. Nanosci. Nanotechnol.* **2012**, *12*, 1754-1759.

35.   Che, R.; Takeguchi, M.; Shimojo, M.; Furuya, K., Field Electron Emission from Single Carbon Nanorod Fabricated by Electron Beam Induced Deposition. *J. Phys. Conf. Ser.* **2007**, *61*, 200-204.

36.   Wong, E. W.; Sheehan, P. E.; Lieber, C. M., Nanobeam Mechanics: Elasticity, Strength, and Toughness of Nanorods and Nanotubes. *Science* **1997**, *277* , 1971-1975.

37.   Zhu, T.; Chen, J. S.; Lou, X. W., Glucose-Assisted One-Pot Synthesis of FeOOH Nanorods and Their Transformation to Fe_3O_4@Carbon Nanorods for Application in Lithium Ion Batteries. *J. Phys. Chem. C* **2011**, *115*, 9814-9820.

38.   Yu, H.; Zhang, Q.; Joo, J. B.; Li, N.; Moon, G. D.; Tao, S.; Wang, L.; Yin, Y., Porous Tubular Carbon Nanorods with Excellent Electrochemical Properties. *J. Mater. Chem. A* **2013**, *1*, 12198-12205.

39.   Orikasa, H.; Akahane, T.; Okada, M.; Tong, Y.; Ozaki, J.-i.; Kyotani, T., Electrochemical Behavior of Carbon Nanorod Arrays Having Different Graphene Orientations and Crystallinity. *J. Mater. Chem.* **2009**, *19*, 4615-4621.

40.   Bo, X.; Zhu, L.; Wang, G.; Guo, L., Template-Free Synthesis of Rectangular Mesoporous Carbon Nanorods and Their Application as a Support for Pt Electrocatalysts. *J. Mater. Chem.* **2012**, *22*, 5758-5763.

41. Liu, Y.; Hu, W.; Wang, X.; Long, C.; Zhang, J.; Zhu, D.; Tang, D.; Xie, S., Carbon Nanorods. *Chem. Phys. Lett.* **2000**, *331*, 31-34.

42. Li, Y.; Qiu, J.; Wang, Y.; Zhang, H., Novel Iron-Decorated Carbon Nanorods from Fullerene Soot. *Chem. Commun.* **2004**, 656-657.

43. Thiên-Nga, L.; Hernadi, K.; Forró, L., Catalytic Growth of Carbon Nanorods on a High-Tc Substrate. *Adv. Mater.* **2001**, *13*, 148-150.

44. Liu, Y.; Hu, W.; Wang, X.; Long, C.; Zhang, J.; Zhu, D.; Tang, D.; Xie, S., Carbon Nanorods. *Chem. Phys. Lett.* **2000**, *331*, 31-34.

45. Wang, B. B.; Ostrikov, K.; van der Laan, T.; Zheng, K.; Wang, J. J.; Yan, Y. P.; Quan, X. J., Carbon Nanorods and Graphene-Like Nanosheets by Hot Filament CVD: Growth Mechanisms and Electron Field Emission. *J. Mater. Chem. C.* **2013**, *1*, 7703-7708.

46. Woo, Y. S.; Jeon, D. Y.; Han, I. T.; Park, Y. J.; Kim, H. J.; Jung, J. E.; Kim, J. M.; Lee, N. S., Structural Characteristics of Carbon Nanorods and Nanotubes Grown Using Electron Cyclotron Resonance Chemical Vapor Deposition. *J. Appl. Phys.* **2003**, *94*, 6789-6795.

47. Ritikos, R.; Rahman, S. A.; Gani, S. M. A.; Muhamad, M. R.; Yap, Y. K., Catalyst-Free Formation of Vertically-Aligned Carbon Nanorods as Induced by Nitrogen Incorporation. *Carbon* **2011**, *49*, 1842-1848.

48. Wang, X.; Lu, J.; Xie, Y.; Du, G.; Guo, Q.; Zhang, S., A Novel Route to Multiwalled Carbon Nanotubes and Carbon Nanorods at Low Temperature. *J. Phys. Chem. B* **2002**, *106*, 933-937.

49. Xia, Y.; Yang, Z.; Mokaya, R., Simultaneous Control of Morphology and Porosity in Nanoporous Carbon: Graphitic Mesoporous Carbon Nanorods and Nanotubules with Tunable Pore Size. *Chem. Mater.* **2006**, *18*, 140-148.

50. Wan, S.; Wang, L.; Xue, Q., Electrodeposition of Nitrogenated Carbon Nanorods by a Facile Electrochemical Method: Microstructure and the Growing Process. Electrochem. *Solid-State Lett.* **2010**, *13*, K89-K92.

51. Zou, G.; Lu, J.; Wang, D.; Xu, L.; Qian, Y., High-Yield Carbon Nanorods Obtained by a Catalytic Copyrolysis Process. *Inorg. Chem.* **2004**, *43*, 5432-5435.

52. Tripathi, K. M.; Tyagi, A.; Ashfaq, M.; Gupta, R. K., Temperature Dependent, Shape Variant Synthesis of Photoluminescent and Biocompatible Carbon Nanostructures from Almond Husk for Applications in Dye Removal. *RSC Adv.* **2016**, *6*, 29545-29553.

53. Huang, W.; Taylor, S.; Fu, K.; Lin, Y.; Zhang, D.; Hanks, T. W.; Rao, A. M.; Sun, Y.-P., Attaching Proteins to Carbon Nanotubes via diimide-Activated Amidation. *Nano Lett.* **2002**, *2*, 311-314.

54. Dekaliuk, M. O.; Viagin, O.; Malyukin, Y. V.; Demchenko, A. P., Fluorescent Carbon Nanomaterials: "Quantum Dots" or Nanoclusters? *Phys. Chem. Chem. Phys.* **2014**, *16*, 16075-16084.

55. Achaya, K. T.; Craig, B. M.; Youngs, C. G., The Component Fatty Acids and Glycerides of Castor Oil. *J. Am. Oil Chem. Soc.* **1964**, *41*, 783-784.

56. Okullo, A. A.; Temu, A. K.; Ogwok, P.; Ntalikwa, J. W., Physico-Chemical Properties of Biodiesel from Jatropha and Castor Oils. *IJRER* **2012**, *2*, 47-52.

57. Dubey, P.; Sonkar, S. K.; Majumder, S.; Tripathi, K. M.; Sarkar, S., Isolation of Water Soluble Carbon Nanotubes with Network Structure Possessing Multipodal Junctions and Its Magnetic Property. *RSC Adv.* **2013**, *3*, 7306-7312.

58. Begum, A.; Sonkar, S. K.; Saxena, M.; Sarkar, S., Nanocomposites of Carbon Quantum Dots-Nickel(III) dithiolene as Nanolights. *J. Mater. Chem.* **2011**, *21*, 19210-19213.

59. Tang, L.; Ji, R.; Cao, X.; Lin, J.; Jiang, H.; Li, X.; Teng, K. S.; Luk, C. M.; Zeng, S.; Hao, J.; Lau, S. P., Deep Ultraviolet Photoluminescence of Water-Soluble Self-Passivated Graphene Quantum Dots. *ACS Nano* **2012**, *6*, 5102-5110.

60. Wang, J.; Sahu, S.; Sonkar, S. K.; (II), K. N. T.; Sun, K. W.; Liu, Y.; Maimaiti, H.; Anilkumar, P.; Sun, Y.-P., Versatility with Carbon Dots - from Overcooked BBQ to Brightly Fluorescent Agents and Photocatalysts. *RSC Adv.* **2013**, *3*, 15604-15607.

61. Dubey, P.; Muthukumaran, D.; Dash, S.; Mukhopadhyay, R.; Sarkar, S., Synthesis and Characterization of Water-Soluble Carbon Nanotubes from Mustard Soot. *Pramana* **2005**, *65*, 681-697.

62.   Tripathi, S.; Sonkar, S. K.; Sarkar, S., Growth Stimulation of Gram (*Cicer arietinum*) Plant by Water Soluble Carbon Nanotubes. *Nanoscale* **2011**, *3*, 1176-1181.

63.   Tripathi, K. M.; Begum, A.; Sonkar, S. K.; Sarkar, S., Nanospheres of Copper(III) 1,2-dicarbomethoxy-1,2-dithiolate and its Composite with Water Soluble Carbon Nanotubes. *New J. Chem.* **2013**, *37*, 2708-2715.

64.   Sonkar, S. K.; Tripathi, K. M.; Sarkar, S., Ferromagnetic Behaviour of Anthropogenic Multi-Walled Carbon Nanotubes Trapped in Spider Web Indoor. *J. Nanosci. Nanotechnol.* **2014**, *14*, 2532-2538.

65.   Sonkar, S. K.; Tripathi, S.; Sarkar, S., Activation of Aerial Oxygen to Superoxide Radical by Carbon Nano Tube of Aerosol Trapped in Indoor Spider Web. *Curr. Sci.* **2009**, *97*, 1227-1230.

66.   Saito, R.; Hofmann, M.; Dresselhaus, G.; Jorio, A.; Dresselhaus, M. S., Raman Spectroscopy of Graphene and Carbon Nanotubes. *Adv. Phys.* **2011**, *60*, 413-550.

67.   White, B.; Banerjee, S.; O'Brien, S.; Turro, N. J.; Herman, I. P., Zeta-Potential Measurements of Surfactant-Wrapped Individual Single-Walled Carbon Nanotubes. *J. Phys. Chem. C* **2007**, *111*, 13684-13690.

68.   Hu, H.; Bhowmik, P.; Zhao, B.; Hamon, M. A.; Itkis, M. E.; Haddon, R. C., Determination of the Acidic Sites of Purified Single-Walled Carbon Nanotubes by Acid-Base Titration. *Chem. Phys. Lett.* **2001**, *345*, 25-28.

69.   Rettenbacher, A. S.; Elliott, B.; Hudson, J. S.; Amirkhanian, A.; Echegoyen, L., Preparation and Functionalization of Multilayer Fullerenes (Carbon Nano-Onions). *Chem. Euro. J.* **2006**, *12*, 376-387.

70.   Yang, X.; Zhuo, Y.; Zhu, S.; Luo, Y.; Feng, Y.; Dou, Y., Novel and Green Synthesis of High-Fluorescent Carbon Dots Originated from Honey for Sensing and Imaging. *Biosens. Bioelectron.* **2014**, *60*, 292-298.

71.   Sevilla, M.; Fuertes, A. B., Chemical and Structural Properties of Carbonaceous Products Obtained by Hydrothermal Carbonization of Saccharides. *Chem. Euro. J.* **2009**, *15*, 4195-4203.

177

72. Cao, L.; Meziani, M. J.; Sahu, S.; Sun, Y. P., Photoluminescence Properties of Graphene Versus Other Carbon Nanomaterials. *Acc. Chem. Res.* **2013**, *46*, 171-80.

73. Wang, X.; Cao, L.; Yang, S. T.; Lu, F.; Meziani, M. J.; Tian, L.; Sun, K. W.; Bloodgood, M. A.; Sun, Y. P., Bandgap-Like Strong Fluorescence in Functionalized Carbon Nanoparticles. *Angew Chem. Int. Ed.* **2010**, *49*, 5310-5314.

74. LeCroy, G. E.; Sonkar, S. K.; Yang, F.; Veca, L. M.; Wang, P.; (II), K. N. T.; Yu, J. J.; Vasile, E.; Qian, H.; Liu, Y.; Luo, P. G.; Sun, Y. P., Toward Structurally Defined Carbon Dots as Ultracompact Fluorescent Probes. *ACS Nano* **2014**, *8*, 4522-4529.

75. Wang, X.; Cao, L.; Lu, F.; Meziani, M. J.; Li, H.; Qi, G.; Zhou, B.; Harruff, B. A.; Kermarrec, F.; Sun, Y. P., Photoinduced Electron Transfers with Carbon Dots. *Chem. Commun.* **2009**, 3774-3776.

76. Chandra, S.; Das, P.; Bag, S.; Laha, D.; Pramanik, P., Synthesis, Functionalization and Bioimaging Applications of Highly Fluorescent Carbon Nanoparticles. *Nanoscale* **2011**, *3*, 1533-1540.

77. Dahoumane, S. A.; Nguyen, M. N.; Thorel, A.; Boudou, J. P.; Chehimi, M. M.; Mangeney, C., Protein-Functionalized Hairy Diamond Nanoparticles. *Langmuir* **2009**, *25*, 9633-9338.

78. Huang, L. C. L.; Chang, H.-C., Adsorption and Immobilization of Cytochrome C on Nanodiamonds. *Langmuir* **2004**, *20*, 5879-5884.

79. Lachheb, H.; Puzenat, E.; Houas, A.; Ksibi, M.; Elaloui, E.; Guillard, C.; Herrmann, J.-M., Photocatalytic Degradation of Various Types of Dyes (Alizarin S, Crocein Orange G, Methyl Red, Congo Red, Methylene Blue) in Water by UV-Irradiated Titania. *Appl. Catal. B.* **2002**, *39*, 75-90.

80. Bubacz, K.; Choina, J.; Dolat, D.; Morawski, A. W., Methylene Blue and Phenol Photocatalytic Degradation on Nanoparticles of Anatase TiO_2. *Polish J. Environ. Stud.* **2010**, *19*, 685-691.

81. Ameta, A.; Ameta, R.; Ahuja, M., Photocatalytic Degradation of Methylene Blue over Ferric Tungstate. *Sci. Rev. Chem. Commun.* **2013**, *3*, 172-180.

82.   Soltani, N.; Saion, E.; Hussein, M. Z.; Erfani, M.; Abedini, A.; Bahmanrokh, G.; Navasery, M.; Vazir, P., Visible Light-Induced Degradation of Methylene Blue in the Presence of Photocatalytic ZnS and CdS Nanoparticles. *Int. J. Mol. Sci.* **2012**, *13*, 12242-12258.

83.   Zhao, D.; Yang, X.; Chen, C.; Wang, X., Enhanced Photocatalytic Degradation of Methylene Blue on Multiwalled Carbon Nanotubes-TiO$_2$. *J. Colloid Interface Sci.* **2013**, *398*, 234-239.

84.   Rodríguez, A.; Ovejero, G.; Mestanza, M.; Callejo, V.; García, J., Degradation of Methylene Blue by Catalytic Wet Air Oxidation with Fe and Cu Catalyst Supported on Multiwalled Carbon Nanotubes. *Chem. Eng. Trans.* **2009**, *17*, 145-150.

85.   Zhang, W.; Zhang, X.; Zhang, Z.; Wang, W.; Xie, A.; Xiao, C.; Zhang, H.; Shen, Y., A Nitrogen-Doped Carbon Dot-Sensitized TiO$_2$ Inverse Opal Film: Preparation, Enhanced Photoelectrochemical and Photocatalytic Performance. *J. Electrochem. Soc.* **2015**, *162*, H638-H644.

86.   Singhal, S.; Sharma, R.; Singh, C.; Bansal, S., Enhanced Photocatalytic Degradation of Methylene Blue Using/MWCNT Composite Synthesized by Hydrothermal Method. *Indian J. Mater. Sci.* **2013**, *2013*, 356025.

87.   Lv, T.; Pan, L.; Liu, X.; Sun, Z., Enhanced Photocatalytic Degradation of Methylene Blue by ZnO-Reduced Graphene Oxide-Carbon Nanotube Composites Synthesized *via* Microwave-Assisted Reaction. *Catal. Sci. Technol.* **2012**, *2*, 2297-2301.

88.   Thangavel, S.; Krishnamoorthy, K.; Krishnaswamy, V.; Raju, N.; Kim, S. J.; Venugopal, G., Graphdiyne-ZnO Nanohybrids as an Advanced Photocatalytic Material. *J. Phys. Chem. C* **2015**, *119*, 22057-22065.

89.   Qu, J.; Shi, L.; He, C.; Gao, F.; Li, B.; Zhou, Q.; Hu, H.; Shao, G.; Wang, X.; Qiu, J., Highly Efficient Synthesis of Graphene/MnO$_2$ Hybrids and their Application for Ultrafast Oxidative Decomposition of Methylene Blue. *Carbon* **2014**, *66*, 485-492.

90.   Mamba, G.; Mbianda, X. Y.; Mishra, A. K., Gadolinium Nanoparticle-Decorated Multiwalled Carbon Nanotube/Titania Nanocomposites for Degradation of Methylene Blue in Water under Simulated Solar Light. *Environ. Sci. Pollut. Res.* **2014**, *21*, 5597-5609.

91.   Bhattacharya, D.; Maji, S.; Pal, K.; Sarkar, S., Formation of Superoxide
       Anion on Aerial Oxidation of Cu(II)-Porphyrinogen in the Synthesis of
       Tetrakis(cyclohexyl)porphyrinogenCu(III) Anion. *Inorg. Chem.* **2008**, *47* ,
       5036-5038.

92.   Bhattacharya, D.; Maji, S.; Pal, K.; Sarkar, S., Oxygen-Cobalt Chemistry
       Using a Porphyrinogen Platform. *Inorg. Chem.* **2009**, *48*, 6362-6370.

93.   Dutta, T.; Sarkar, R.; Pakhira, B.; Ghosh, S.; Sarkar, R.; Barui, A.; Sarkar,
       S., Ros Generation by Reduced Graphene Oxide (RGO) Induced by Visible
       Light Showing Antibacterial Activity: Comparison with Graphene Oxide
       (GO). *RSC Adv.* **2015**, *5*, 80192-80195.

94.   Nakayama, S.; Sintim, H. O., Colorimetric Split G-Quadruplex Probes for
       Nucleic Acid Sensing: Improving Reconstituted Dnazyme's Catalytic
       Efficiency *via* Probe Remodeling. *J. Am. Chem. Soc.* **2009**, *131*, 10320-
       10333.

95.   Ferguson, B. S.; Buchsbaum, S. F.; Wu, T. T.; Hsieh, K.; Xiao, Y.; Sun, R.;
       Soh, H. T., Genetic Analysis of H1N1 Influenza Virus from Throat Swab
       Samples in a Microfluidic System for Point-of-Care Diagnostics. *J. Am.
       Chem. Soc.* **2011**, *133*, 9129-9135.

96.   Xu, W.; Xue, X.; Li, T.; Zeng, H.; Liu, X., Ultrasensitive and Selective
       Colorimetric DNA Detection by Nicking Endonuclease Assisted
       Nanoparticle Amplification. *Angew Chem. Int. Ed.* **2009**, *48*, 6849-6852.

97.   Brown, P. O.; Botstein, D., Exploring the New World of the Genome with
       DNA Microarrays. *Nature Genet.* **1999**, *21*, 33-37.

98.   Makrigiorgos, G. M.; Chakrabarti, S.; Zhang, Y.; Kaur, M.; Price, B. D., A
       PCR-Based Amplification Method Retaining the Quantitative Difference
       between Two Complex Genomes. *Nature Biotechnol.* **2002**, *20*, 936-939.

99.   Christine, B.; Per, S.; Jan, B.; Gillis, J., A Feasibility Study of a Capacitive
       Biosensor for Direct Detection of DNA Hybridization. *Electroanalysis* **1999**,
       11, 156-160.

100.   Degefa, T. H.; Kwak, J., Electrochemical Impedance Sensing of DNA at Pna
       Self Assembled Monolayer. *J. Electroanal. Chem.* **2008**, *612*, 37-41.

101. Shen, J.-S.; Yu, T.; Xie, J.-W.; Jiang, Y.-B., Photoluminescence of Cdte Nanocrystals Modulated by Methylene Blue and DNA. A Label-Free Luminescent Signaling Nanohybrid Platform. *Phys. Chem. Chem. Phys.* **2009**, *11*, 5062-5069.

102. Zhao, Y.; Xu, L.; Ma, W.; Wang, L.; Kuang, H.; Xu, C.; Kotov, N. A., Shell-Engineered Chiroplasmonic Assemblies of Nanoparticles for Zeptomolar DNA Detection. *Nano Lett.* **2014**, *14*, 3908-3913.

103. Moore, S. K., Making Chips to Probe Genes. *IEEE Spectrum* **2001**, *38*, 54-60.

104. Sun, H.; Ren, J.; Qu, X. Carbon Nanomaterials and DNA: from Molecular Recognition to Applications. *Acc. Chem. Res.* **2016**, *49*, 461-470.

105. Zhu, Z. An Overview of Carbon Nanotubes and Graphene for Biosensing Applications. *Nano-Micro Lett.* **2017**, *9*, 25-48.

106. Bai, W.; Zheng, H.; Long, Y.; Mao, X.; Gao, M.; Zhang, L., A Carbon Dots-Based Fluorescence Turn-on Method for DNA Determination. *Anal. Sci.* **2011**, *27*, 243-246.

107. Liu, L.; Zhang, C.; Yu, Y.; Chen, Y. F. Determination of DNA Based on Fluorescence Quenching of Terbium Doped Carbon Dots. *Microchim. Acta.* **2018**, *185*, 514-520.

108. Pramanik, S.; Chatterjee, S.; Kumar, G. S.; Devi, P. S. Egg-Shell Derived Carbon Dots for Base Pair Selective DNA Binding and Recognition. *Phys. Chem. Chem. Phys.* **2018**, *20*, 20476-20488.

109. Loo, A. H.; Sofer, Z.; Bousa, D.; Ulbrich, P.; Bonanni, A.; Pumera, M., Carboxylic Carbon Quantum Dots as a Fluorescent Sensing Platform for DNA Detection. *ACS Appl. Mater. Interfaces* **2016**, *8*, 1951-1957.

110. Jin, M.; Liu, X.; Zhang, X.; Wang, L.; Bing, T.; Zhang, N.; Zhang, Y.; Shangguan, D., Thiazole Orange-Modified Carbon Dots for Ratiometric Fluorescence Detection of G-Quadruplex and Double-Stranded DNA. *ACS Appl. Mater. Interfaces.* **2018**, *10*, 25166-25173.

111. Kumari, S.; Solanki, A.; Mandal, S.; Subramanyam, D.; Das, P., Creation of Linear Carbon Dot Array with Improved Optical Properties through Controlled Covalent Conjugation with DNA. *Bioconjugate Chem.* **2018**, *29*, 1500-1504.

181

112. Balapanuru, J.; Yang, J.-X.; Xiao, S.; Bao, Q.; Jahan, M.; Polavarapu, L.; Wei, J.; Xu, Q.-H.; Loh, K. P., A Graphene Oxide-Organic Dye Ionic Complex with DNA-Sensing and Optical-Limiting Properties. *Angew. Chem. Int. Ed.* **2010**, *122*, 6699-6703.

113. Lu, C. H.; Yang, H. H.; Zhu, C. L.; Chen, X.; Chen, G. N., A Graphene Platform for Sensing Biomolecules. *Angew. Chem. Int. Ed.* **2009**, *48*, 4785-4787.

114. Jeng, E. S.; Moll, A. E.; Roy, A. C.; Gastala, J. B.; Strano, M. S., Detection of DNA Hybridization Using the Near-Infrared Band-Gap Fluorescence of Single-Walled Carbon Nanotubes. *Nano Lett.* **2006**, *6*, 371-375.

115. Yang, R.; Jin, J.; Chen, Y.; Shao, N.; Kang, H.; Xiao, Z.; Tang, Z.; Wu, Y.; Zhu, Z.; Tan, W., Carbon Nanotube-Quenched Fluorescent Oligonucleotides: Probes that Fluoresce upon Hybridization. *J. Am. Chem. Soc.* **2008**, *130*, 8351-8358.

116. Tang, X.; Bansaruntip, S.; Nakayama, N.; Yenilmez, E.; Chang, Y. L.; Wang, Q., Carbon Nanotube DNA Sensor and Sensing Mechanism. *Nano Lett.* **2006**, *6*, 1632-1636.

117. Wang, J.; Liu, G.; Jan, M. R., Ultrasensitive Electrical Biosensing of Proteins and DNA: Carbon-Nanotube Derived Amplification of the Recognition and Transduction Events. *J. Am. Chem. Soc.* **2004**, *126*, 3010-3011.

118. Hu, Y. J.; Li, W.; Liu, Y.; Dong, J. X.; Qu, S. S., Fluorometric Investigation of the Interaction between Methylene Blue and Human Serum Albumin. *J. Pharma. Biomed. Anal.* **2005**, *39*, 740-745.

119. Gallagher, S. A.; Comby, S.; Wojdyla, M.; Gunnlaugsson, T.; Kelly, J. M.; Gun'ko, Y. K.; Clark, I. P.; Greetham, G. M.; Towrie, M.; Quinn, S. J., Efficient Quenching of TGA-Capped CdTe Quantum Dot Emission by a Surface-Coordinated Europium(III) Cyclen Complex. *Inorg. Chem.* **2013**, *52*, 4133-4135.

120. Song, Y.; Zhu, S.; Xiang, S.; Zhao, X.; Zhang, J.; Zhang, H.; Fu, Y.; Yang, B., Investigation into the Fluorescence Quenching Behaviors and Applications of Carbon Dots. *Nanoscale* **2014**, *6*, 4676-4682.

121. Zu, F.;Yan, F.; Bai, Z.; Xu, J.; Wang, Y.; Huang, Y.; Zhou, X. The Quenching of the Fluorescence of Carbon Dots: A Review on Mechanisms and Applications. *Microchim. Acta.* **2017**, *184*, 1899-1914.

122. Pereira da Silva Neves, M.M.; González-García, M.B.; Pérez-Junquera, A.; Hernández-Santos, D.; Fanjul-Bolado, P., Quenching of Graphene Quantum Dots Fluorescence by Alkaline Phosphatase Activity in the Presence of Hydroquinone Diphosphate. *Luminescence.* **2018**, *33*, 552-558.

123. Das, R.; Rajendera, G.; Giri, P. K., Anomalous Fluorescence Enhancement and Fluorescence Quenching of Graphene Quantum Dots by Single Walled Carbon Nanotubes. *Phys. Chem. Chem. Phys.* **2018**, *20*, 4527-4537.

124. Vaishnavi, E.; Renganathan, R., "Turn-on-off-on" Fluorescence Switching of Quantum Dots-Cationic Porphyrin Nanohybrid: A Sensor for DNA. *Analyst* **2014**, *139*, 225-234.

Chapter -7

Conclusion and Future Scope

7.1   Conclusion

The thesis explains a simple and sustainable methodology for the exploitation of dirty dangerous pollutant black carbon and waste soot of castor oil and exploration of their potential perspectives. This pollutant black carbon has been used as a sustainable source for destroying and degrading other pollutant materials. The environmental practicalities of black carbon soot for the isolation of nanosized graphene sheets and fabricate the tunable photoluminescent wsGNS. After simple oxidation of black carbon soot and waste soot of castor oil provides a suitable technique for the large-scale synthesis of carbon nanoparticles such as few-layer wsGNS and wsCNR) respectively. wsGNS being tunable in photoluminescence emissions covering the green and red regions with a slight extension in the near infra-red region. This high degree of passivation with negative surface functional moieties imparts the aqueous solubility along with excellent stability for its long-term imaging purposes. In addition, wsGNS was used as fluorescence nanoprobes for the selective and sensitive detection of toxic and carcinogenic Cr(VI) in an aqueous solution and for the imaging of HeLa cells.

The substantial prospective of hazardous pollutant soot as an effective material for water remediation is further explored. Freely available pollutant petrol soot used for simplistic isolation of wsGNS which exhibited huge potential for the photocatalytic degradation of pollutant organic dyes. In comparison to GNS, presence of large amount of surface defects in wsGNS are efficaciously used for the artificial-light-induced (60 W tungsten bulb) photodegradation of MB and exhibited a higher rate of photocatalytic degradation.

Further, sunlight was used as a most promising sustainable light source. Photocatalytic dye degradation under artificial light and natural light was compared and found that sunlight induced photocatalytic dye degradation rate of methylene blue is greater than artificial light. wsGNS are being used here for the selective photodegradation of pollutant dye without harming the bacterial balance. wsGNS are nontoxic on the tested *E. coli* and *S. aureus* cells. This would sustain the environmental outlook and the sustainability of the overall described procedure.

Conclusively, reusability, recyclability and stability made this pollutant soot derived water soluble graphene nanosheets as a future alternative material which could be further employed in real applications of biomedical and biological sciences. Nontoxicity along with photocatalytic properties marks wsGNS as a potential material, which could be utilized thoroughly as a photocatalytic material for the photodegradation purposes.

Moreover, free of cost available photocatalytic materials (wsGNS) for the complete photodegradation of three individual dyes like crystal violet, rhodamine B and methylene blue and their mixture under the sunlight irradiation. The most probable photocatalytic mechanism is proposed based upon the trapping of active-reactive species responsible for photodegradation and analysis of the photodegraded products with various spectroscopic techniques and exhibits that photodegraded products after the degradation of dyes are confirming the breaking of the organic complex aromatic framework of the dyes into their smaller non-toxic forms. The ability of water soluble graphene nanosheets were further studied under the presence of common interfering ions/substances. The complete photodegradation of the mixture of dyes was achieved within ~ 225 min of the sunlight exposure. By radical trapping experiments, reactive oxygen species which were responsible for the photodegradation processes identified as holes and hydroxide radicals. Further to endure the overall sustainability of the whole process the photodegraded wastewater from the pollutant dyes is being used for growth of wheat plants, which shows the remarkable results compared to the dye treated plants. Further, the use of wastewater for growing the wheat plants could relate to with the practical sustainability of the treated water for its use in real-life applications.

Apart from pollutant petrol soot, waste soot of castor oil has been used for the synthesis of carbon nanorods and their water-soluble derivatives in nearly quantitative yields. wsCNR produced multicoloured emissions in the visible region and extends into the near infra-red region due to extensive self-surface passivation. A viable approach is taken for the visible light-induced photochemical degradation of MB in direct sunlight by wsCNR. wsCNR selectively sensed trace amounts of DNA and displayed a fluorescence turn-off/turn-on mechanism involving MB.

Sensors for DNA are very important as in diagnostic testing since the recognition of disordered DNA is a powerful tool in the early diagnosis of disease and in the detection of genetic disorders. DNA detection by wsCNR is easily and economically viable as compared to traditionally used expensive instruments. This method could be used for the fast and low-cost determination of DNA at the nano level. Thus, such water-soluble versions in form of wsGNS and wsCNR are made to being used for the explorations of wet side applications of waste derived nanocarbons in the field of aqueous phase photocatalysis and in the biological sciences.

7.2   Future Scope

This presented thesis followed a simple and realistic approach for the exploitation of dirty, dangerous pollutant BC soot as the freely available carbon precursor for the isolation/synthesis of nanocarbons for multiple applications. A simple oxidative treatment is followed to achieve the water-soluble versions of wsGNS and wsCNR. Such water-soluble versions are made to being used for the explorations of wet side applications of waste derived nanocarbons in the field of aqueous phase photocatalysis and in the biological sciences:

❖   The present research offers the possibility for use of nanocarbons derived from pollutant soot as future alternative material that could be further employed in real-world applications.

❖   wsGNS has been chiefly used for photodegradation of some other dyes cationic and anionic dyes. Additionally, higher instability and reusability, make wsGNS a strong photocatalyst material in wastewater treatment. Especially for the photoreduction of the toxic metal ions to their respective non-toxic oxidation states. There lies a scope where wsGNS could be used as a sensor for detecting and eliminating toxic ions from the wastewater.

❖   The treated wastewater after the photodegradations of organic dyes can further lessen the overexploitation of natural water and could promote the reuse of treated wastewater to at least irrigate the playgrounds, parks, and gardens.

❖   GNS from the BC could also be used to fabricate graphene-metal composite which finds their application as an active material for the electrode. This area

of research opens way for various applications like energy storage devices, electrochemical sensing, and as composite materials.

❖ wsCNR can be used for drug delivery purposes in future. Fast and low-cost determination of DNA at nano-level could be used in diagnostic, forensic kits. CNR-composites can be manufactured for various electrochemical applications.

SCIENTIFIC REPORTS

OPEN

Soluble Graphene Nanosheets for the Sunlight-Induced Photodegradation of the Mixture of Dyes and its Environmental Assessment

Gunture Kumar[1], Anupriya Singh [iD][1], Anshu Bhati [iD][1], Prateek Khare[1], Kumud Malika Tripathi[2] & Sumit Kumar Sonkar [iD][1]

Currently, the air and water pollutions are presenting the most serious global concerns. Despite the well known tremendous efforts, it could be a promising sustainability if the black carbon (BC) soot can be utilized for the practical and sustainable applications. For this, the almost complete aqueous phase photodegradation of the three well-known organic pollutant dyes as crystal violet (CV); rhodamine B (RhB); methylene blue (MB) and their mixture (CV + RhB + MB), by using water-soluble graphene nanosheets (wsGNS) isolated from the BC soot under the influence of natural sunlight is decribed. The plausible mechanism behind the photocatalytic degradation of dyes and their mixture has been critically analyzed via the trapping of active species and structural analysis of photodegraded products. The impact of diverse interfering ions like Ca^{2+}, Fe^{3+}, SO_4^{2-}, HPO_4^{2-}, NO_3^-, and Cl^- on the photodegradation efficiency of wsGNS was also investigated. Importantly, the environmental assessment of the whole process has been evaluated towards the growth of wheat plants using the treated wastewater. The initial studies for the fifteen days confirmed that growth of wheat plants was almost the same in the photodegraded wastewater as being noticed in the control sample, while in case of dyes contaminated water it showed the retarded growth. Using the natural sunlight, the overall sustainability of the presented work holds the potential for the utilization of pollutant soot in real-practical applications related to the wastewater remediation and further the practical uses of treated water.

The ever-growing desire to improve the quality of human lifestyle significantly promoted the rapid industrialization and urbanization[1–3]. Primarily, associated with the accelerating advancement of the automotive industrialization, which can directly link to the release of dirty-dangerous pollutant black soot as black carbon (BC)[4–7] particulate matter in the environment. BC is closely related with global warming and at present is continuously deteriorating the environmental and human health[7,8]. Along with air pollutions, industrialization have also brought the another important concern related to the water pollutions[9]. So, the most demanding aggravated concerns of the present world is to significantly reuse the waste products (it could also be the dangerous-dirty-BC)[10] and the treatment of wastewater[11,12]. From the standpoint of the overall environmental health, the discharge of the BC[7] in air and the effluents of industrial wastewater[13–15] (containing hazardous, carcinogenic and non-biodegradable organic dyes) in the water-bodies are unceasingly deteriorating the ecological balance[16,17], and causes many serious diseases[18–20]. At present, few groups have explored the recent-promising approaches related to the adaptation of pollutant soot as freely avilable carbon precursor for the synthesis/isolation of the valued-added nano-carbons[21–29]. Such as carbon dots (CD)[23], graphene nanosheets (GNS)[24,25,27], single-walled carbon nanotubes (SWCNT)[26], carbon nanoparticles[22] for the diverse applications[22,23,27] including the photodegradation of the

[1]Department of Chemistry, Malaviya National Institute of Technology, Jaipur, Jaipur, 302017, India. [2]Department of Bio-nanotechnology, Gachon University, Gyeonggi-do, South Korea. Gunture Kumar and Anupriya Singh contributed equally. Correspondence and requests for materials should be addressed to K.M.T. (email: kumud20010@gmail.com) or S.K.S. (email: sksonkar.chy@mnit.ac.in)

NJC

PERSPECTIVE

Exploration of nano carbons in relevance to plant systems

Anshu Bhati, [a] Gunture,[a] Kumud Malika Tripathi, [b] Anupriya Singh,[a] Sabyasachi Sarkar [c] and Sumit Kumar Sonkar *[a]

The effects of nano-carbon interactions on plant growth have recently been the subject of much scientific research. In the past, the use of insoluble nano-carbons on plants led to physical damage to the plant cells due to biochemical incompatibility; at present, the availability of dispersible or soluble forms of several nano-carbons avoids unnecessary physical damage, which could be a possible solution to the continuous increase in the demand for food. These interactions provide a feasible approach that is backed by the long-known results from age-old practices related to the simple addition of charred bio-waste as a carbon source, known as "biochar," to the soil as a promoter of nutrients. The purposeful use of biochar significantly increases the rate of development of the next generation crop along with the retention of soil fertility. It is known that biochar contains a significant amount of nano-carbons along with micro carbon with oxo-functionality; these are hydrophilic and are readily passed through the plant roots. As such, the potential application of charred carbons/biochar in the growth of plant systems is a time-tested process, and the same can be expected with the nano-carbons. This perspective article provides a summary of the recent advances in the agricultural applications of nano-carbons. In particular, the cellular uptake, translocation, and accumulation of nano-carbons inside the plant, and their significant impacts on the plant physiological parameters are studied. Like plant growth, water uptake and protein expression properties, increasing crop productivity and disease prevention are correlated. The present perspective article also addresses the negative aspects that arise, based on a few reports showing the toxicity of nano-carbons; most of these are physical in nature and care is needed to determine the quality of the nano-carbons, which should be biocompatible.

[a] Department of Chemistry, Malaviya National Institute of Technology, Jaipur, Jaipur-302017, India. E-mail: sksonkar.chy@mnit.ac.in
[b] Department of Chemistry, Indian Institute of Technology, Kanpur, Kanpur-208016, India
[c] Department of Chemistry, Indian Institute of Engineering Science and Technology, Shibpur, Howrah-711103, India

Anshu Bhati

Anshu Bhati received her BSc degree (2005) from Maharani Girls College, Bikaner, and MSc Degree in Chemistry (2007) from Dr Tanveer Malawat College of Biosciences, Bikaner, Rajasthan, India. She is currently a PhD student in the Chemistry department, Malaviya National Institute of Technology, Jaipur, Rajasthan, India. She has been doing her research work under the supervision of Dr Sumit Kumar Sonkar. Her research work is focused on the synthesis of doped fluorescent nano-carbons for multifunctional uses like imaging, and sunlight induced-photocatalysis for water treatment.

Gunture

Gunture is a PhD student at the Malaviya National Institute of Technology Jaipur, India, working under the supervision of Dr Sumit Kumar Sonkar, in the Chemistry department, Malaviya National Institute of Technology. He received his BSc degree (2011) from Raj Rishi College, Alwar, India, and obtained his MSc degree (2014) from University of Rajasthan, India. His research interest is focused on the fabrication of carbon nano-onions for bio-imaging, sensing and energy applications.

1. Introduction

The ever-increasing food shortage due to the continuous growth of the human and animal population has been the most serious concern to mankind. The increment in the growth rate in food production requires the use of newer techniques, in addition to the already existing techniques,[1] based on sustainable and economically viable resources in the field of agriculture,[2–5] such as the utilisation of the newer nano-materials,[6–11] especially, nano-carbons.[12–16] Nano-carbons possess a very high aspect ratio;[17,18] they have always inspired innovative solutions to existing challenges and are explored worldwide.[13,19–37] The family of nano-carbons is comprised of fullerenes,[38] multi-walled carbon nanotubes (MWCNTs),[39] single-walled carbon nanotubes (SWCNTs),[40] carbon nano-onions (CNOs),[41] carbon nano-fibres,[6,42] graphene,[43] carbon-nanorods (CNRs),[44] carbon dots (CDs)[45,46] and graphene quantum dots (GQDs).[47] This is corroborated by the substantial number of findings,[6,12–16,48–93] which are consistently producing significant and encouraging outcomes in the plant systems. Nano-carbons indubitably have considerable potential to bring lasting solutions to the present challenges in the field of agriculture,[14,91,94] and can also be used as a nano-fertilizer.[67,68,95]

Recent findings show the tremendous effects of nano-carbons on the growth of plants; they are primarily used to augment crop production,[13,16,57] in seed germination,[12,48,52,54,70–72,96] cell division,[96] protein expressions,[54,71,72,96] water uptake[12,13,15] and photosynthesis,[52] as a fluorescent marker,[14,58] molecular

Kumud Malika Tripathi

Kumud Malika Tripathi is an Assistant Professor in the Department of Bionanotechnology, Gachon University, South Korea. She has received her PhD in Chemistry from Indian Institute of Technology, Kanpur in 2013. Before joining Gachon University, she held several positions including postdoctoral fellow at the University of South Brittany, Lorient, France, IIT Kanpur, India, and Gachon University. Her research activities include the green synthesis of multifunctional nanomaterials for energy and environmental applications. Kumud works at the interface of chemistry, material science and biology, exploring nanomaterial-based new strategies for environmental monitoring and remediation, energy storage devices and photocatalytic water splitting.

Anupriya Singh

Anupriya Singh received her BSc degree (2008) from the University of Jammu, Jammu & Kashmir and MSc degree in Chemistry (2010) from Maharishi Dayanand University, Ajmer, Rajasthan. She received her MPhil (2011) from Mewar University, Gangrar, Rajasthan. Since 2014, she has been working as a PhD scholar at the Malaviya National Institute of Technology, Jaipur, Rajasthan, India. Her PhD research focuses on the synthesis of pollutant soot derived carbon nanoparticles for environmental assessment, especially with photocatalytic applications.

Sabyasachi Sarkar

Prof. Sabyasachi Sarkar is interested in chemistry closely related to the natural set up of functional models of hyperthermophilic to mesophilic metalloproteins, with emphasis on the enzymatic oxo transfer reactions of Eyring activated complex-based chemical oxo transfer reactions. He has demonstrated CO_2 bound magnesium in chlorophyll in photosynthesis as thought by Willstätter. He was the first to explore water-soluble nanocarbons made from cheap sources to demonstrate their use in plant growth, and as a drug carrier to cross the blood–brain barrier. He is involved in the non-invasive bioimaging of living animals via nanocarbons. He also showed that non-toxic nano carbons induce anoxia in mosquito larvae (http://home.iitk.ac.in/~abya/).

Sumit Kumar Sonkar

Sumit Kumar Sonkar received his BSc (2003) and MSc (2005) from the Christ Church College, Kanpur. He earned his PhD (2012) in Chemistry from the Indian Institute of Technology Kanpur, Kanpur, India, under the supervision of Prof. Sabyasachi Sarkar. After his postdoctoral training at Clemson University, at South Carolina with Prof. Ya-Ping Sun, he joined the Malaviya National Institute of Technology, Jaipur, India in 2013. His research interest is focused on carbon-based materials.

Sunlight-Induced Selective Photocatalytic Degradation of Methylene Blue in Bacterial Culture by Pollutant Soot Derived Nontoxic Graphene Nanosheets

Prateek Khare,[†] Anupriya Singh,[†] Sankalp Verma,[‡] Anshu Bhati,[†] Amit Kumar Sonker,[‡] Kumud Malika Tripathi,*[,§] and Sumit Kumar Sonkar*[,†]

[†]Department of Chemistry, Malaviya National Institute of Technology, Jaipur, Jaipur 302017, India
[‡]Department of Materials Science & Engineering, Indian Institute of Technology, Kanpur, Kanpur 208016, India
[§]Department of Bio-nanotechnology, Gachon University, Gyeonggi-do, South Korea

Ⓢ *Supporting Information*
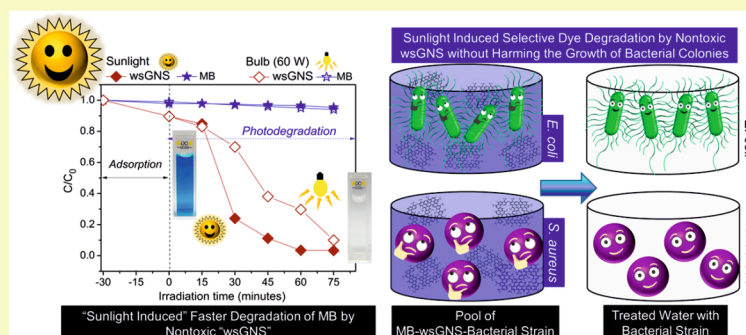
ABSTRACT: Herein, a potential approach is described for assessing the ecological importance of the graphitic nanocarbons isolated from dirty, dangerous black pollutant particulate material. A simple experiment of photodegradation and a toxicological test were done using the natural sunlight as a source of energy and the pollutant petrol soot derived water-soluble graphene nanosheets (wsGNS) as photocatalyst to achieve complete degradation of pollutant organic dye as methylene blue (MB). Compared to the artificial source of visible light (60W tungsten bulb), the sunlight-induced photodegradation using wsGNS show ∼1.5 times higher rate of photodegradation. The toxicological test confirmed the nontoxic behavior of wsGNS against the two different types of bacterial strains: Gram-negative and Gram-positive cells, *Escherichia coli* and *Staphylococcus aureus*, respectively. Moreover, wsGNS are precisely used for the selective photodegradation of MB without harming the bacterial growth from the pool of MB-bacterial strains. Nontoxicity and selectivity along with the improved in photodegradation efficiencies by wsGNS under the influence of sunlight are the most significant and sustainable perspectives of the present finding.

KEYWORDS: Pollutant soot, Toxic dye, Water-soluble graphene nanosheets, Methylene blue, Nontoxic, Selective photodegradation, Dye degradation

■ INTRODUCTION

Advances in the field of light-induced photocatalysis,[1,2] particularly in aqueous-phase photocatalytic degradation[3,4] of various toxic and hazardous water-soluble organic pollutant dyes have shown tremendous development.[5,6] The prime focus for the aqueous-phase photodegradation of organic dyes is associated with their partial or complete degradation to relatively nontoxic constituents such as low molecular weight hydrocarbons that can ultimately end up to carbon dioxide and water.[7−10] Moreover, the use of sunlight as a freely available renewable light source under the natural conditions can offer an additional advantage for searching the newer sustainable alternatives of water remediation.[11,12] In the recent past years, the extent of the use of pollutant dyes like methylene blue (MB) in different industrial applications[13,14] followed by their

subsequent discharge as a waste in water stream is continuously increasing. Once released into the water bodies as contaminants, these were causing serious issues for both humans and the environment such as heart disease, lung and urinary bladder cancer, chromosomal fractures, mutagenesis, and respiratory toxicity in humans.[15−18] From the environmental perspective, organic dyes are well-known for their ability to significantly damage the aquatic biota of the water system.[19] So tremendous effort for the photodegradation of these pollutant dyes,[20] especially using metal-based nanomaterials, are gained a lot attention[21−23] because of their higher photodegradation

Edited by
Chaudhery Mustansar Hussain and Ajay Kumar Mishra

Nanotechnology in Environmental Science

Volume 1 & 2

6

Nanocarbons in Agricultural Plants: Can be a Potential Nanofertilizer?

Anupriya Singh,[1] Anshu Bhati,[1] Gunture,[1]
Kumud Malika Tripathi,[2] and Sumit Kumar Sonkar[1]

[1]*Malaviya National Institute of Technology, Department of Chemistry, Jaipur, Rajasthan 302017, India*
[2]*Gachon University, Department of Bionanotechnology, Seongnam, Gyeonggi-do 13120, South Korea*

6.1 Introduction

At present, the need of opting for sustainable materials such as organic-based fertilizers is of great interest because of their better efficiencies [1–8] and biocompatibility [9–11], which makes them suitable for long-term use in agricultural sciences, compared to synthetic fertilizers [12–18]. The present situation demands [19–26] sustainable and newer techniques [2,27–32] that can be employed for increasing crop/plant productivity to meet the future challenges of global food crises. Owing to concerns about the toxicity issues and the long-term sustainable uses, switching from the synthetic fertilizers [12–18] to organic [33,34], carbon-based [28,35–41], and nanocarbon-based fertilizers [2,42–48] could be a worthy option. The increase in productivity [2,29,43] associated with growing food requirements using environment-friendly and simpler methods should be free from toxicity issues. We have been using synthetic fertilizers for decades to increase agricultural production [12–18], but they have brought on us adverse outcomes in the long run [16–18,49–53], such as destruction of valuable microorganisms [12,13,54] (responsible for conversion of plant and animal remains into nutrient-rich organic matter), water pollution [49], methemoglobinemia [49], soil contaminations [50], and so on, and significantly disturbing the natural constitution of soil [50–53]. Among all other types of organic fertilizers, charred carbon-based fertilizers deal with both the classical (additions of black carbon as biochar) and the modern techniques (applications of nanocarbons) used for increasing the crop productivity. This is very simple to understand based on the important and precise information taken from the long-known ancient practice in agricultural sciences, concerned with the deliberate additions of biochar [7,8,35–37] to the soil for increasing fertility [55–57], sequestration [56–58], restoration [59] of soil

NANOTECHNOLOGY FOR SUSTAINABLE WATER RESOURCES

Edited By

Ajay Kumar Mishra and
Chaudhery Mustansar Hussain

Sustainable Nanocarbons as Potential Sensor for Safe Water

Kumud Malika Tripathi[1], Anupriya Singh[2], Yusik Myung[1],
TaeYoung Kim[1]*, and Sumit Kumar Sonkar[2]*

[1]*Department of Bionanotechnology, Gachon University, Seongnam,
Gyeonggi-do, Korea*
[2]*Department of Chemistry, Malaviya National Institute of Technology, Jaipur, India*

Abstract

Currently, the scarcity of safe water is the top concern with the rise in global population and exploitation of water resources. Sensitive and selective evaluation of chemical contaminations is a crucial step for water remediation. Nanocarbon-based sensors have emerged as significant potentials for the detection and monitoring of toxins, microbes, heavy metal ions, inorganic and organic pollutants in water, with the expectations that they can play a significant role in the development of next generation water remediation techniques and devices. To support the sustainable concern for developments of water remediation technologies, nanocarbons from greener route are evaluated by all relevant aspects. These sustainable nanocarbons are gradually moving out from the experimental side to practical regime and emphasis on the detection and discrimination of chemical pollutant in water system.

Keywords: Nanocarbons, green synthesis, waste management, sensing, water remediation

5.1 Introduction

Protecting the quality of water is crucial for both the human and the ecosystem [1]. Rapid industrialization and unplanned urbanization with

---

Corresponding authors: taeykim@gachon.ac.kr; sksonkar.chy@mnit.ac.in

Pollutant Soot for Pollutant Dye Degradation: Soluble Graphene Nanosheets for Visible Light Induced Photodegradation of Methylene Blue

Anupriya Singh,[†] Prateek Khare,[†] Sankalp Verma,[‡] Anshu Bhati,[†] Amit Kumar Sonker,[‡] Kumud Malika Tripathi,*,[§] and Sumit Kumar Sonkar*,[†] [ID]

[†]Department of Chemistry, Malaviya National Institute of Technology Jaipur, Jaipur−302017, India

[‡]Department of Materials Science & Engineering and [§]Department of Chemistry, Indian Institute of Technology Kanpur, Kanpur−208016, India

Ⓢ Supporting Information

ABSTRACT: The findings presented here offer a new approach for the environmental application of pollutant soot somewhat like utilizing a pollutant material for degrading the other pollutant material. Herein, a simpler approach is described for the isolation of two-dimensional graphitic materials as water-soluble graphene nanosheets (wsGNS) from the globally identified dirty−dangerous black pollutant particulate matter as black carbon (BC) from the petrol soot. The as-isolated wsGNS are further employed for the photocatalytic degradation of toxic dye such as methylene blue (MB) under the influence of visible light irradiation. The photodegradation performance of wsGNS compared to insoluble graphene nanosheets (GNS) showed ~11 times faster degradation rate within ~90 min of visible light exposure (60 W tungsten bulb). The insights of the aqueous phase photodegradation of MB by the system of MB-wsGNS were studied by different chemical characterization techniques including nuclear magnetic resonance spectroscopy, high-performance liquid chromatography, Raman, and fourier transform infrared spectroscopy. Furthermore, we have checked the regeneration efficiency of wsGNS, which was still at its higher value even after five cycles of recycling testing.

KEYWORDS: Pollutant soot, Toxic dye, Water-soluble graphene nanosheets, Methylene Blue, Photodegradation, Dye degradation
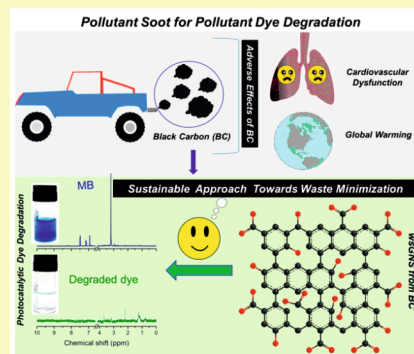
■ INTRODUCTION

The globally generated black particulate matter black carbon (BC) soot has, at present, shown dramatic negative impacts on human and environmental health. These include cancer,[1] dysfunctions of heart and lungs,[2] and mental retardation that are consequently responsible for the loss of millions of lives every year as well as significantly contributing toward global warming.[3] Similarly, like BC for air pollution, the contamination of water bodies arising from the discharge of water-soluble organic dyes[4] from various textiles and printing industries has also become a crucial environmental issue due to the fast growth in industrialization.[5] The considerable sources of nonaesthetic pollutants in water are potentially damaging the aquatic biota and life.[6] In reaction to the overall concern related to water pollution,[7] different techniques (adsorption, advanced oxidation process, flocculation, ultrafiltration, coagulation by chemical agents, etc.) have been employed in the past,[8] for the remediation of soluble toxic dyes.[9] From all the techniques, photocatalysis is very attractive and currently in high demand, since it provides a clean and cost-effective method for water purification. Additionally, visible light driven photocatalysis employs renewable and abundant energy to promote dye degradation under mild conditions. It can be a sustainable approach if we could utilize

the nanocarbons derived from the pollutant BC[10−15] for the photocatalytic removal of organic dyes from wastewater via a single step that resolves two contaminant issues at the same time. The idea is very simple and purely based on the age-old practice of using carbon for water filtration because of its high adsorption efficiency.[16] The scientific insights about the conversion of pollutant soots into nanocarbons could open a new sustainable and potential window to mitigate climate change to some extent. Few groups have already been reported[11−15] the isolation (via the simplest processes from the bulk) of nanocarbons of different shapes from BC as carbon dots (CDs), single walled carbon nanotubes (SWCNT), and graphene nanosheets (GNS) for their multiple applications in the field of bioimaging,[11,15] sensing of heavy metal ions,[13] and sensing biomolecules.[11] Composition-wise (graphitic/amorphous structures) nanocarbons isolated from BC[11−15] and from other black charred carbonaceous materials[17−22] are similar to the nanocarbons fabricated from sophisticated instruments.[23−27]

Sustainable Changes in the Contents of Metallic Micronutrients in First Generation Gram Seeds Imposed by Carbon Nano-onions: Life Cycle Seed to Seed Study

Kumud Malika Tripathi,[†,‡] Anshu Bhati,[§,‡] Anupriya Singh,[§] Amit Kumar Sonker,[○] Sabyasachi Sarkar,[†,⊥] and Sumit Kumar Sonkar*,[§]

[†]Department of Chemistry and [○]Department of Materials Science & Engineering, Indian Institute of Technology, Kanpur, Kanpur—208016, India

[§]Department of Chemistry, Malaviya National Institute of Technology, Jaipur, Jaipur—302017, India

[⊥]Department of Chemistry, Indian Institute of Engineering Science and Technology, Shibpur, Howrah—711103, India

ABSTRACT: Plant−nanocarbon interactions have been mostly explored for enhanced germination, cell growth, and plant growth, with a limited study on the productivity of seeds under controlled conditions. The present finding reports the sustainable impacts of biowaste (wood wool) derived nanocarbons as carbon nano-onions (CNOs) on the entire life cycle of gram plants to obtain the first generation seeds (FGSs) as "seed to seed". A water-soluble version of CNOs as water-soluble carbon nano-onions (wsCNOs) at 0 (control), 10, 20, and 30 μg mL^{-1} were used for the germination of gram seeds, for the initial 10 days only. Followed by transferring of 10 days old baby plants into the soil to complete their natural life cycle (~4 months). FGSs harvested from the wsCNOs treated plants showed a significant increase in their yield and health with respect to their individual weight, overall dimensions, enhanced protein, stored electrolytes and metallic micronutrient contents. The protein content increased from 96 to 170 μg mL^{-1}, and the level of electrolytic conductivity increased from 2.2 to 3.4 mS in the FGSs, harvested from the plants treated with 0 (control) to 30 μg mL^{-1} of wsCNOs, respectively. wsCNOs used here were presumably acting as a stimulant to increase the contents of metallic micronutrients (Mn, Mo, Cu, Zn, Fe, and Ni) in FGSs without showing its inside accumulations as a contaminant examined by transmission electron microscope (TEM) and Raman spectral analysis. In the future, a sustainable approach for the utilization of wood waste as a nanofertilizer could provide a possible approach in agricultural science to overcome the shortage of stored nutrients inside the seeds and also to limit the excessive use of fertilizers.

KEYWORDS: Waste wood wool, Water-soluble carbon nano-onions, First generation seeds, Micronutrients, Protein content, Conductivity, Enhanced productivity, Nanofertilizer
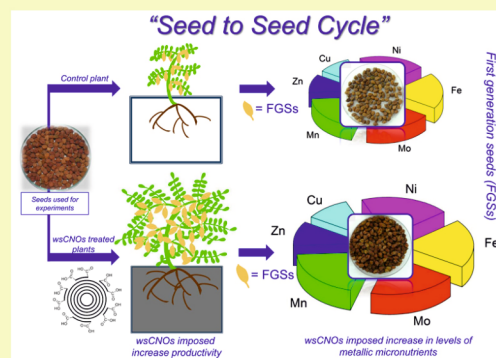
INTRODUCTION

Presently agricultural science need to adopt the sustainable strategies concerning the most serious global issue of continuously increasing food demand.[1,2] Related to boosting the crop productivity, along with preserving the nutritional values of food.[1,3−5] As a possible measure to increase the crop productivity, exploration of diverse nanoparticles as fertilizers/nanofertilizers in plants has increased in recent years.[6−11] To stimulate physiological and biochemical changes in plants. The long term and safer use of nanoparticles in agricultural science, requires the adaptation of sustainable strategies,[3,12] precisely related with improved productivity.That directly depends on the nutrition's provided to the plants and can help to resolve the problem of increased food demand.[7,13,14] To be prepared in advance, we need to explore and optimize the use of advanced organic based fertilizers like sustainable nanocarbons,[3,12,15−17] compared to synthetic chemical fertilizers. For increasing the productivity and nutrient contents in plants. Stimulating the healthier makeup of micronutrients contents in plants in an environmentally friendly manner could hold great future promises. Because of the significant role of micronutrients in all the metabolic and cellular functions of plants.[18] Such as in plant growth, production of chlorophyll, synthesis of growth hormones, gene expressions, cell division, photosynthetic activities, root development, N_2 and CO_2 fixation, etc.[19,20] Deficiency of micronutrients in plant lead to retarded growth, deferred flowering, chlorosis of matured leaves, reduction in protein expressions, total protein synthesis, and, consequently, decrease in productivity.[19−22] However, the accumulation of nanoparticle/nanocarbons mainly in edible parts (seeds) of plants is a major concern and needs in-depth and detailed analysis.[23]

Sustainable Feasibility of the Environmental Pollutant Soot to Few-Layer Photoluminescent Graphene Nanosheets for Multifunctional Applications

Kumud Malika Tripathi,[†] Anupriya Singh,[‡] Anshu Bhati,[‡] Sabyasachi Sarkar,[§] and Sumit Kumar Sonkar[*,‡]

[†]Department of Chemistry, Indian Institute of Technology Kanpur, Kanpur 208016, India

[‡]Department of Chemistry, Malaviya National Institute of Technology, Jaipur, Jaipur 302017, India

[§]Department of Chemistry, Indian Institute of Engineering Science and Technology, Shibpur, Howrah 711103, India

Ⓢ Supporting Information

ABSTRACT: A simple and realistic approach to the utilization of waste "black carbon particulates of petrol soot" for the fabrication of few-layer water-soluble photoluminescent graphene nanosheets (wsGNS) is described herein. Direct transformation of pollutant soot to fluorescent nanocarbons can be a promising approach for providing some economic benefits along with a clean atmosphere. Oxidation of petrol soot resulted in the isolation of the water-soluble version of graphene nanosheets (GNS). Oxidative treatment is a key step in preventing the aggregation of the GNS and rendering them water-soluble. A high degree of "self-passivation" on wsGNS provides evidence of the tunable photoluminescent emissions over a broad range of the visible spectrum with slight extension in the near-infrared region. The photoluminescent properties of wsGNS are used here for the selective detection of hexavalent chromium ions with a detection limit of 0.51 μM and for imaging HeLa cells.

KEYWORDS: Pollutant soot, Water-soluble, Few-layer graphene nanosheets, Self-passivation, Photoluminescent, Chromium sensing
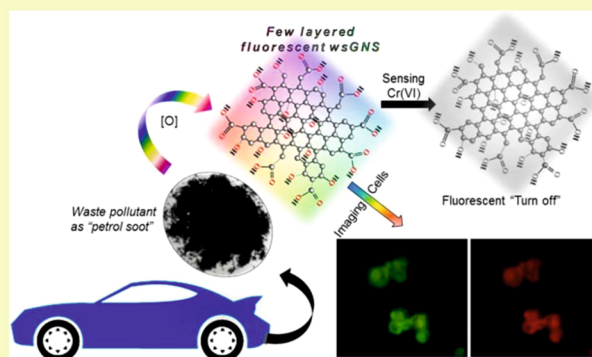
1. INTRODUCTION

Globally generated black particulate matter, known as black carbon (BC), is recognized as a major air pollutant. Alternatively, this BC holds significant potential to be used as a free carbon precursor for the synthesis of valuable nanocarbons.[1−3] Considerable efforts and evidence of the role of air pollution caused by BC and its adverse impacts on the radiation budget of Earth have been documented.[4] To prevent its negative impacts, the quantity of BC should be decreased alternatively by its utilization in value-added products. To provide a clean environment along with some economic benefits, waste management of BC and identifying its second-life uses can be a possible approach to the synthesis of well-developed nanocarbons.[5−7] Recently, a few groups reported the presence of graphitic nanoparticles in the pollutant waste soot of diesel[5,6,8,9] and petrol engines,[7] along with the prospects of its application.[5,6,9] For example, Uchida et al. synthesized single-walled carbon nanotubes from diesel soot using a laser vaporization technique.[9] Tripathi et al. used diesel soot for the practical isolation of multiemissive water-soluble carbon dots (wsCD)[5] for multicolored imaging of *Escherichia coli* and sensing cholesterol. Wang et al. reported the synthesis of fluorescent water-soluble carbon nanoparticles (wsCNP)[6] for the selective sensing of Mn(II). Remarkably, Tripathi et al.[5] and Wang et al.[6] did not synthesize any nanocarbons. In contrast,

they synthesized only the soluble version of nanocarbons that was routinely manufactured during the burning process inside the engine chambers and discharged globally into the atmosphere as BC.[6,9,10] On the basis of these findings, we need to use these "freely available carbon precursors"[5−9] for the isolation of nanocarbons from pollutant soot. A few reports about the structural or nanostructural characterization of pollutant soot are also available.[7,11,12] The burning process in a diesel engine is very much similar to the burning of conventional hydrocarbon flames, whereas petrol engines typically need a "spark" for the ignition of fuel, which is premixed with atmospheric air.[7] Therefore, differences in morphologies of synthesized nanocarbons are expected.[5,6,8] Like diesel soot particulates, petrol soot particulates also cause environmental pollution,[10,13] but in comparison to diesel particulates, petrol soot particulates are a bit less harmful when they interact with the proteins of the cell membranes[10] but still cause several cardiopulmonary diseases.[14]

The findings presented in this paper are associated with the isolation of graphene nanosheets (GNS) from the petrol soot to provide some commercial and environmental benefits. GNS

Research Article

Sunlight-Induced Photochemical Degradation of Methylene Blue by Water-Soluble Carbon Nanorods

Anshu Bhati,[1] Anupriya Singh,[1] Kumud Malika Tripathi,[2] and Sumit Kumar Sonkar[1]

[1]*Department of Chemistry, Malaviya National Institute of Technology Jaipur, Jawaharlal Nehru Marg, Jaipur 302017, India*
[2]*Department of Chemistry, Indian Institute of Technology Kanpur, Kanpur 208016, India*

Correspondence should be addressed to Kumud Malika Tripathi; kumud20010@gmail.com and
Sumit Kumar Sonkar; sksonkar.chy@mnit.ac.in

Water-soluble graphitic hollow carbon nanorods (wsCNRs) are exploited for their light-driven photochemical activities under outdoor sunlight. wsCNRs were synthesized by a simple pyrolysis method from castor seed oil, without using any metal catalyst or template. wsCNRs exhibited the light-induced photochemical degradation of methylene blue used as a model pollutant by the generation of singlet oxygen species. Herein, we described a possible degradation mechanism of methylene blue under the irradiation of visible photons via the singlet oxygen-superoxide anion pathway.

1. Introduction

Carbon nanorods (CNRs) [1, 2] are representing a unique class of one-dimensional carbon nanostructures, which may offer some advantageous properties in comparison with carbon nanotubes (CNTs) [3, 4] since CNRs offer straight, aligned, and hollow graphitic morphology [2]. CNRs are more or less similar to CNTs, except their straightness. Spaghetti type arrangements of CNTs restrict their many potential applications [5] that can be explored via the use of these CNRs. Till now, CNRs are the least explored in comparison with other members of nanocarbon family [3, 4, 6–17]. All these allotropic nanocarbons such as multiwalled CNTs [3]/ single-walled CNTs [4], fullerenes [6], carbon nanoonions [7–9], carbon nanodiamonds [10], graphene [11], graphene quantum dots [12], carbon dots [13–15], carbon nanofiber [16], and carbon nanocubes [17] have attracted a great concern in the diverse fields of science and technology because of their potential applications [5, 18–21]. Based on the few published reports, CNRs exhibited impressive electrical, thermal, and mechanical properties and are promising for field emission devices [22], energy storage devices [23], composite materials [24], and sensing applications [2]. The primary barrier for the successful commercialization of CNRs is its

typical synthetic procedures, such as chemical vapor deposition (CVD), arc discharge methods, solvothermal synthesis, electrodeposition, catalytic copyrolysis, and soft and hard template methods [2]. All these synthetic methods involve expensive instruments, metallic particles for growing the CNRs, high-temperature, multistep fabrication protocols, and sophisticated techniques that notably restrict their economic viability. A metal-catalyst-free synthesis of CNRs can be a significant approach.

Particularly for the biological application of CNRs [2], aqueous solubility is the most important parameter, which requires the surface modifications like chemical functionalization with electrophilic groups (oxygen-rich species) [25] and bioactive groups [26]. Tripathi et al. [2] described a new viable method for the catalyst-free synthesis of multicolored emissive wsCNRs from the pyrolysis of castor seed oil. The as-synthesized CNRs after Soxhlet purification were oxidized via simple oxidative method yielded photoluminescent water-soluble form as wsCNRs. The photoluminescent properties of wsCNRs were further utilized to construct a selective, specific, and active sensor for DNA sensing based upon fluorescent "turn-off/turn-on" technique [2]. The possible reasons for multicolored emissions from the single nanoparticle were attributed to the radiative recombination of photoinduced

From the traditional way of pyrolysis to tunable photoluminescent water soluble carbon nano-onions for cell imaging and selective sensing of glucose†

Kumud Malika Tripathi,‡[a] Anshu Bhati,‡[b] Anupriya Singh,[b] Nidhi Rani Gupta,[c] Sankalp Verma,[d] Sabyasachi Sarkar*[e] and Sumit Kumar Sonkar*[b]

The traditional pyrolysis of vegetable ghee leads to the fabrication of graphitic photoluminescent, water soluble carbon nano-onions (wsCNO) with tunable photoluminescence without using any metal catalyst. Simple oxidative treatment by nitric acid fabricated a high density "self-passivated" water soluble version. As-synthesized wsCNO possessed tunable photoluminescence behavior from the visible-to-near infrared region. Further small sized wsCNO separated from the bulk as-synthesized wsCNO *via* gel filtration achieved a highly fluorescent colored fraction, used for cell imaging (*Escherichia coli* and *Pseudomonas putida*) and selective, immediate sensing of glucose molecules based upon a simple fluorescence "turn-off"/"turn-on" technique.

1. Introduction

Nano-sized fluorescent nanocrystals, generally referred as quantum dots (QDs), have attracted a lot of interest for imaging, especially in the biomedical sciences.[1,2] However, being metallic in nature their toxicity significantly challenges the excellent optical advantageous performances.[3–5] Tremendous efforts have been made to find a non-toxic alternative of QD-type photo-luminescent probe with comparable optical properties. The outcome of these significant efforts has resulted in the discovery of a new class of fluorescent nano-carbons (FNCs),[6–12] referred as a non-toxic fluorescent probe, having optical prop-erties comparable with QDs. FNCs predominantly consist of carbon dots (CD),[6,13,14] carbon nano-diamonds,[7] graphene quantum dots,[8,9,15] carbon nano rods[16,17] and carbon nano-onions (CNO).[10–12,18] Among all of these, the CD have been studied the most[6,14,19–24] as a fluorescent probe for non-toxic biological imaging purposes, whereas CNO have been

investigated least.[10,11,25–27] Because of the presence of a well-defined band gap, QDs shows quantum confinement effects as a result of which, its size dependent electronic and optical properties can easily be tuned. However, FNCs do not have any theoretically defined band gap based fluorescence color related size distributions of nanoparticles. Because of this, these are different from QDs and have the advantageous, significant properties of tunable photoluminescence from the single particle[10,11,28,29] together with high solubility, stability, and non-toxicity. Among the FNCs, CNO is an emerging class of quasi-spherical nano carbon, which typically consists of successive layer of graphene around a filled or hollow core and they offer a high aspect ratio and conductivity.[30] Morphologically, graphitic structures of CNO are in between fullerene and graphitic nanotubes having closed graphitic shells which are placed on one on another.[11,31,32] So far, less attention have been given to CNO even though the prospective applications have already discussed. CNO exhibited the characteristic, onion-like morphology and small domains of graphitic sp² carbons with localization of the π electrons and dangling bond defects in the periphery.[30] As a consequence, it could be envisioned as an enclosed graphitic shell with excellent optical and electro-chemical properties that render them a potential nanomaterial for industrial, biomedical and electronic applications.[33–36] From the time of their discovery[12] until the present date, only a limited number of synthetic methods for CNO have been available and it can be synthesized mainly by using high energy techniques. Such as the arc-discharge method, in which two graphite electrodes are arced under water for the synthesis of CNO on the water surface.[32] Annealing of nano-diamond for

[a]Department of Chemistry, Indian Institute of Technology Kanpur, Kanpur-208016, India

[b]Department of Chemistry, Malaviya National Institute of Technology, Jaipur-302017, India. E-mail: sumitsonkar@gmail.com; Tel: +91-9415594017

[c]Department of Chemistry, GSSDGS Khalsa College, Patiala-147001, India

[d]Department of Materials Science & Engineering, Indian Institute of Technology Kanpur, Kanpur-208016, India

[e]Department of Chemistry, Indian Institute of Engineering Science and Technology, Shibpur, Howrah-711103, India. E-mail: abya@iitk.ac.in

† Electronic supplementary information (ESI) available. See DOI: 10.1039/c6ra04030f

‡ Both the authors contributed equally.

ROYAL SOCIETY
OF CHEMISTRY

PAPER

CrossMark
← click for updates

Large-scale synthesis of soluble graphitic hollow carbon nanorods with tunable photoluminescence for the selective fluorescent detection of DNA†

Kumud Malika Tripathi,[a] Amit Kumar Sonker,[b] Anshu Bhati,[c] Jagannath Bhuyan,[a] Anupriya Singh,[c] Ajay Singh,[a] Sabyasachi Sarkar*[d] and Sumit Kumar Sonkar*[c]

Photoluminescent water-soluble hollow carbon nanorods were synthesized by the pyrolysis of castor oil seeds (*Ricinus communis*) without the use of a catalyst. Oxidation of the pyrolysed soot produced a water-soluble form of graphitic hollow carbon nanorods. These showed excitation-dependent multicoloured photoluminescent emission from the green to red region of the visible spectrum and extending to the near-infrared region. This photoluminescent behaviour was used to produce a fluorescent turn-off/turn-on sensor for the specific, sensitive and rapid determination of DNA with a detection limit of ∼1.14 nM.

Introduction

Many different types of nanocarbon have been reported in recent years, such as fullerenes,[1] multiwalled carbon nanotubes,[2] single-walled carbon nanotubes,[3] carbon nano-onions,[4] carbon nanorods (CNRs),[5] carbon nanofibres,[6] graphene,[7] carbon nano-diamonds,[8] and the recently discovered photoluminescent carbon dots (CDs)[9,10] and graphene quantum dots.[11] These have attracted much interest as a result of their diverse applications.[11–25] Morphologically, CNRs are similar to 1D, multiwalled carbon nanotubes except they show less bundling and aggregation as a result of their linear shape and aligned graphitic inter-planar structure.[26–31] However, CNRs have not been studied very much because of the lack of a simple and reproducible method for synthesis. CNRs have potential applications in various field such as lithium ion batteries,[32] supercapacitors,[33] electrochemical applications[34,35] and in biologically important reactions like the electrocatalytic oxidation of NADH, uric acid[36] and dopamine.[37] Conventional synthetic procedures such as arc discharge,[38] chemical vapour deposition,[39–42] solvothermal methods,[32,43] template-assisted synthesis,[33,34,44,45] electrodeposition[46] and catalytic co-pyrolysis[47] have been used to

obtain CNRs. Li *et al.*[38b] synthesized CNRs in an arc discharge experiment using an anode made from fullerene soot and iron particles. Wang *et al.*[39] fabricated plasma-enhanced CNRs with Au nanoparticles as a catalyst using hot filament chemical vapour deposition. Thién-Nga *et al.*[40] used BSYCO (Bi, Sr, Y, Cu, O) as a substrate for the synthesis of CNRs by chemical vapour deposition. Wang *et al.*[43] synthesized CNRs at low temperatures using tetrachloroethylene and potassium to obtain a C_2 infrastructure. An Ag catalyst has been used to synthesize CNRs *via* calcination.[43] Li *et al.*[44] synthesized CNRs using a soft template (a tri-block polymer) and phenolic resin by the combination of a hydrothermal method and annealing. Yu *et al.*[33] and Orikasa *et al.*[34] synthesized template-assisted CNRs using an Ni–hydrazine complex and aluminium substrate, respectively. Zou *et al.*[47] fabricated CNRs *via* pyrolysis using C_6H_6 and C_5H_6 with Fe and Mg catalysts in an autoclave. All these synthetic approaches required multi-step fabrication protocols, expensive instruments, high-temperature synthetic conditions, toxic chemicals, metallic particles and sophisticated techniques that restricted their economic viability. In contrast, the method reported here is an economically viable and catalyst-free process for the synthesis of CNRs in an almost quantitative yield.

We report the simple synthesis of CNRs at low cost without the use of a template or catalyst by the pyrolysis of castor seeds oil (*Ricinus communis*) used as a green carbon precursor. The method could be used on a large scale. Castor oil is composed ∼87% fatty acid (ricinoleic acid) and is extensively used in medicine as an antiviral, antibacterial, antifungal and analgesic agent; it is also used in cosmetics.[48,49] The soot generated by burning castor oil in lamps was cleaned to remove any unburnt and volatile impurities. A simple nitric acid treatment of the

[a] *Department of Chemistry, Indian Institute of Technology Kanpur, Kanpur-208016, India*
[b] *Department of Materials Science & Engineering, Indian Institute of Technology Kanpur, Kanpur-208016, India*
[c] *Department of Chemistry, Malaviya National Institute of Technology, Jaipur, Jaipur-302017, India. E-mail: sksonkar.chy@mnit.ac.in*
[d] *Department of Chemistry, Indian Institute of Engineering Science and Technology, Shibpur, Howrah-711103, India. E-mail: abya@iitk.ac.in*
† Electronic supplementary information (ESI) available. See DOI: 10.1039/c5nj02037a

A simple one-step hydrothermal route towards water solubilization of carbon quantum dots from soya-nuggets for imaging applications

Prashant Dubey,*[a] Kumud Malika Tripathi,[b] Ragini Mishra,[a] Anshu Bhati,[c] Anupriya Singh[c] and Sumit Kumar Sonkar*[c]

A simple and low-cost pyrolytic carbonization method has been performed for the easy synthesis of carbon quantum dots from soya-nuggets under an insufficient amount of oxygen. Furthermore, hydrothermal functionalization of the carbonized black material after Soxhlet purification with nitric acid leads to the formation of its quantum sized water soluble version. The hydrothermally functionalized, water soluble carbon quantum dots (wsCQDs) are highly fluorescent and self-passivated, having a quantum yield value of ∼3%, with a small range of size distribution. High photostability with high solubility makes these potential candidates for imaging purposes, and we used these for the fluorescent labeling of *Escherichia coli* cells.

Introduction

In the past few years, fluorescent nano-carbons (FNCs),[1–9] comprising carbon dots (CDs),[1–4] carbon nano-diamonds (CNDs),[5] carbon nano-onions (CNOs),[6,7] and graphene quantum dots (GQDs),[8,9] have drawn immense interest, particularly for biological cell imaging[3,4,10–12] with several benefits in comparison with conventional metal-based quantum dots (QDs).[13–15] In terms of bio-compatibility (non-toxic nature),[4,12,16,17] their high values of quantum yield,[4,12,18] combined with their excellent solubility and stability,[1,3,4] make these QDs an effective fluorescent probe for long-term use for biological purposes.[3,4] FNCs are mostly composed of spherical nano-carbon possessing a high surface area to volume ratio, and have further been utilized for surface passivation purposes *via* simple surface modification (attaching surface functionalities). Surface modification is mainly achieved *via* the simple organic chemistry of oxidation, followed by the addition of polymeric[2,10] and monomeric amines[19] to achieve high quantum yield values,[4,12,18] comparable with those of conventional metal-based QDs.[13–15] Metal-based QDs show classical quantum confinement effects[1] in their size-dependent multi-colored emission. Theoretically, in comparison with QDs, FNCs do not have any defined band gap for fluorescence emission,[19] and

this is an advantageous property for multi-colored emission from the same nano-carbon.[20–22]

Among the FNCs, CDs are widely used fluorescent nano-carbons because of their simpler synthetic methodologies with easy reproducibility. It has been widely accepted that the presence of high density surfacial defects (defective centers) on FNCs is responsible for their tunable multi-colored emission profiles.[12] Emission from the defective centers of surfacial defects was first noticed from the surfacial defects of single-walled and multi-walled carbon nanotubes passivated with polymeric amines.[23,24] Since the first report of CDs from laser ablation of a graphitic target,[1] many more top-down[10–12,25–32] and bottom-up[33–40] synthetic techniques have been explored for their easy production. Along with exciting sophisticated techniques, such as arc-discharge,[41] abundant progress has been reported in the past few years for the cost-effective green synthesis of photoluminescent CDs by using bio-mass/waste bio-mass as a low-cost, compatible and easily available carbon precursor material, including ascorbic acid,[42] banana juice,[43] candle soot,[35] chicken eggs,[44] citrate,[45] chitosan,[46] diesel soot,[47] gelatin,[48] glucosamine,[49] saccharides,[50] juices (orange, sugar cane, and strawberry),[51–53] pomelo,[54] and watermelon peel.[55] Because of their simplicity and straightforward synthesis, most of the synthetic approaches involve either hydrothermal or microwave-assisted green methods. As synthesized, CDs and their functionalized versions have shown immense potential for a wide variety of applications, such as bio-imaging agents,[12,56] biosensors,[47,57] chemical sensors,[58] drug delivery,[59] electro-catalysts,[60] photo-catalysts,[61] and photodynamic therapy.[62] Low-cost synthetic protocols with easy reproducibility and bio-compatibility make these CDs best suited for imaging purposes.[3,12,62,63]

[a]Centre of Material Sciences, Institute of Interdisciplinary Studies (IIDS), University of Allahabad, Allahabad, 211002, India. E-mail: pdubey.au@gmail.com

[b]Laboratory of Materials Engineering of Brittany (LIMATB), University of South Brittany (UBS), 56321 Lorient Cedex, France

[c]Department of Chemistry, Malaviya National Institute of Technology (MNIT), Jaipur, 302016, India. E-mail: sksonkar.chy@mnit.ac.in

ANUPRIYA SINGH

Department of Chemistry,
Malaviya National Institute of Technology - Jaipur
JLN Marg, Jaipur - 302017,
Rajasthan-INDIA
E-mail: anupriyasingh709@gmail.com, 2013rcy9571@mnit.ac.in
Mob. No: (+91) – 8875811759, 9887495502

Education Qualification:

Degree	Institute/University	Year	Percentage/ CGPA
Ph. D. (Chemistry)	Malaviya National Institute of Technology, Jaipur, India	2018	8.42
M. Phil. (Chemistry)	Mewar University, Chittorgarh, Rajasthan, India	2011	9.0
M. Sc. (Chemistry)	Government College Ajmer, Ajmer, Rajasthan, India	2010	69%
B. Sc. (Chemistry/Botany/Zoology)	Government College, Kathua, Jammu-Kashmir, India	2008	74%

Research Interest:

- Synthesis of Carbon Nanoparticles for Environmental Assessment.
- Isolation and synthesis of Graphene Nanomaterials for photocatalytic applications.
- Synthesis and characterization of Carbon Nanorods, Carbon Nano-Onions, Carbon Dots for Imaging and Sensing applications.
- Carbon nanomaterials for heavy metal ions Sensing applications.
- Nanocarbons for waste-water treatment.

Academic Achievements:

- **GATE 2014** with score 377 and 87.40 percentile.
- Best Poster at **National conference** on Green chemistry- Bridge between Energy and Environment (NCGC-Dausa-2014)
- Second Prize in the poster presentation in **National Symposium** on Water Purification & Reject Management (WPRM-2016).

- **Institute Doctoral Fellowship** in Malaviya National Institute of Technology, Jaipur-Rajasthan-India.

Professional Skills & Experiences:
- Synthesis and characterization of Nanocarbons from primitive Chemical Vapor Deposition Method, Hydrothermal and Microwave methods.
- SEM, TEM, HRTEM, AFM, RAMAN, and XRD.
- NMR, EPR, UV–Vis, FT-IR, fluorescence, mass specrometric and Cyclic Voltammetry.

Teaching and Research Experience

- As an Assistant Professor in the department of chemistry for two years in Mewar University, Chittorgarh, Rajasthan.

- As spoken English Trainer at Indian Institute of Investment Finance and Accounts (I3FA) for four months.

Publications/Book-chapters

1. Gunture Kumar, **Anupriya Singh**, Anshu Bhati, Prateek Khare, Kumud Malika Tripathi, and Sumit Kumar Sonkar, Soluble Graphene Nanosheets for the Sunlight-Induced Photodegradation of the Mixture of Dyes and its Environmental Assessment. *Sci. Rep.* **2018**, DOI:10.1038/s41598-019-38717-1.

2. Anshu Bhati, Gunture Kumar, Kumud Malika Tripathi, **Anupriya Singh**, Sabyasachi Sarkar and Sumit Kumar Sonkar, Exploration of Nano-carbons in Relevance to Plant Science. *New J. Chem.* **2018**, 42, 16411-16427.

3. Prateek Khare,[†] **Anupriya Singh**,[†] Sankalp Verma, Anshu Bhati, Amit Kumar Sonker, Kumud Malika Tripathi and Sumit Kumar Sonkar, Sunlight-Induced Selective Photocatalytic Degradation of Methylene Blue in Bacterial culture by Pollutant Soot Derived Nontoxic Graphene Nanosheets, *ACS Sustainable Chem. Eng.* **2018,** *6*, 579-589. ([†]=equal contribution)

4. **Anupriya Singh**, Anshu Bhati, Gunture, Kumud Malika Tripathi, and Sumit Kumar Sonkar, Nanocarbons in Agricultural Plants: Can be a Potential

Nanofertilizer? In *Nanotechnology in Environmental Science*, (153-190), **2018** First Edition. Wiley-VCH Verlag GmbH & Co. KGaA.

5. Kumud Malika Tripathi, **<u>Anupriya Singh</u>**, Yusik Myung, TaeYoung Kim and Sumit Kumar Sonkar, Sustainable Nanocarbons as Potential Sensor for Safe Water. In *Nanotechnology for Sustainable Water Resources*, (141-176) © **2018** Scrivener Publishing LLC.

6. **<u>Anupriya Singh</u>,** Prateek Khare, Sankalp Verma, Anshu Bhati, Amit Kumar Sonker, Kumud Malika Tripathi and Sumit Kumar Sonkar, Pollutant Soot for Pollutant Dye Degradation: Soluble Graphene Nanosheets for Visible Light Induced Photodegradation of Methylene Blue, *ACS Sustainable Chem. Eng.* **2017**, *5*, 8860-8869

7. Kumud Malika Tripathi, Anshu Bhati, **<u>Anupriya Singh</u>**, Amit Kumar Sonker, Sabyasachi Sarkar, and Sumit Kumar Sonkar, Sustainable Changes in the Contents of Metallic Micronutrients in First Generation Gram Seeds Imposed by Carbon Nano-Onions: Life Cycle Seed to Seed Study. *ACS Sustainable Chem. Eng.* **2017**, *5*, 2906-2916.

8. Kumud Malika Tripathi,[†] **<u>Anupriya Singh</u>**,[†] Anshu Bhati, Sabyasachi Sarkar, and Sumit Kumar Sonkar, Sustainable Feasibility of the Environmental Pollutant Soot to Few-Layer Photoluminescent Graphene Nanosheets for Multifunctional Applications, *ACS Sustainable Chem. Eng.* **2016**, *4*, 6399-6408. ([†]=equal contribution)

9. Anshu Bhati,[†] **<u>Anupriya Singh</u>**,[†] Kumud Malika Tripathi, Sumit Kumar Sonkar, Sunlight-Induced Photochemical Degradation of Methylene Blue by Water-Soluble Carbon Nanorods. *Int. J. Photoenergy*, **2016**, *2016*, 2583821. ([†]=equal contribution)

10. Kumud Malika Tripathi, Anshu Bhati, **<u>Anupriya Singh</u>**, Nidhi Rani Gupta, Sabyasachi Sarkar, and Sumit Kumar Sonkar, From the Traditional Way of Pyrolysis to Tunable Photoluminescent Water Soluble Carbon Nano-Onions for Cell Imaging and Selective Sensing of Glucose, *RSC Adv.*, **2016**, *6*, 37319-37329.

11. Kumud Malika Tripathi, Amit Kumar Sonker, Anshu Bhati, Jagannath Bhuyan, **<u>Anupriya Singh</u>**, Ajay Singh, Sabyasachi Sarkar, and S. K. Sonkar,

Large-Scale Synthesis of Soluble Graphitic Hollow Carbon Nanorods with Tunable Photoluminescence for the Selective Fluorescent Detection of DNA. *New J. Chem.*, **2016**, *40*, 1571-1579.

12. Prashant Dubey, Kumud Malika Tripathi, Anshu Bhati, **<u>Anupriya Singh</u>**, and Sumit Kumar Sonkar, A Simple One-Step Hydrothermal Route towards Water Solubilization of Carbon Quantum Dots from Soya-Nuggets for Imaging Applications. *RSC Adv.*, **2015**, *5*, 87528-87534.

Conferences/Seminar/Symposium:

1. Participated in National Seminar on Recent Trends & Advances in Chemical Science and their Impact on Environment (RTACIE-2018) organized by department of chemistry, Amity University, Jaipur on 13th April, 2018.

2. Participated in five days short-term course on Nano Forms of Carbon organized by Materials Research Centre, MNIT, Jaipur, Rajasthan from 19th March - 23rd March, 2018.

3. Presented in poster presentation in three days International Conference on Nano and Functional Materials (NFM-2017) organized by chemistry department at BITS, Pilani, Rajasthan from 16th Nov - 18th Nov, 2017.

4. Oral presentation in two days National conference on Desalination and Water Purification for Defence and Civil Applications organized by Defence Laboratory, Jodhpur (DRDO) & Indian Desalination Association (InDA) Jodhpur, Rajasthan from 22nd - 23rd March, 2017.

5. Poster presentation in National Symposium on Water purification & Reject Management (WPRM-2016) organized by Department of Chemical Engineering, MNIT Jaipur in association with WWSO, PHED Rajasthan, Indian Desalination Association (InDA) & Jaipur Regional Center of IIChE on 12th November, 2016 and got second prize in poster competition.

6. Poster presentation in two days International conference on Advances in Nanomaterials and Nanotechnology (ICANN-2016) organized by Centre for Nanoscience and Nanotechnology, Jamia Milia Islamia, New Delhi, India from 4th - 5th November, 2016.

7. Oral presentation in three days National conference on Advanced Materials and Processing (CAMP-2015) organized by physics, chemistry and metallurgy department, MNIT, Jaipur from 2nd - 4th December, 2015

8. Poster presentation in three days National conference on Recent Advancement in Chemical Sciences (RAICS-2015) from 21st-23rd August, 2015 organized by department of chemistry, MNIT Jaipur.

9. Participated in poster presentation in three days National conference on Frontiers at the Chemistry - Allied Sciences Interface (FCASI-2015), Rajasthan University, Jaipur from 10th - 12th March, 2015.

10. Participated in poster presentation in two days National conference on Green chemistry- Bridge between Energy and Environment (NCGC-Dausa-2014) from 15th - 16th December, 2014 and got the Best Poster Award.

Declaration:

I hereby declare that the information given above is true to the best of my knowledge and belief.

Place: MNIT Jaipur   Sincerely Yours

                                                        Anupriya Singh